TECHNICAL REPORT N-72-2

OPERATION PRAIRIE FLAT, PROJECT LN 302: EARTH MOTION AND STRESS MEASUREMENTS

by

D. W. Murrell

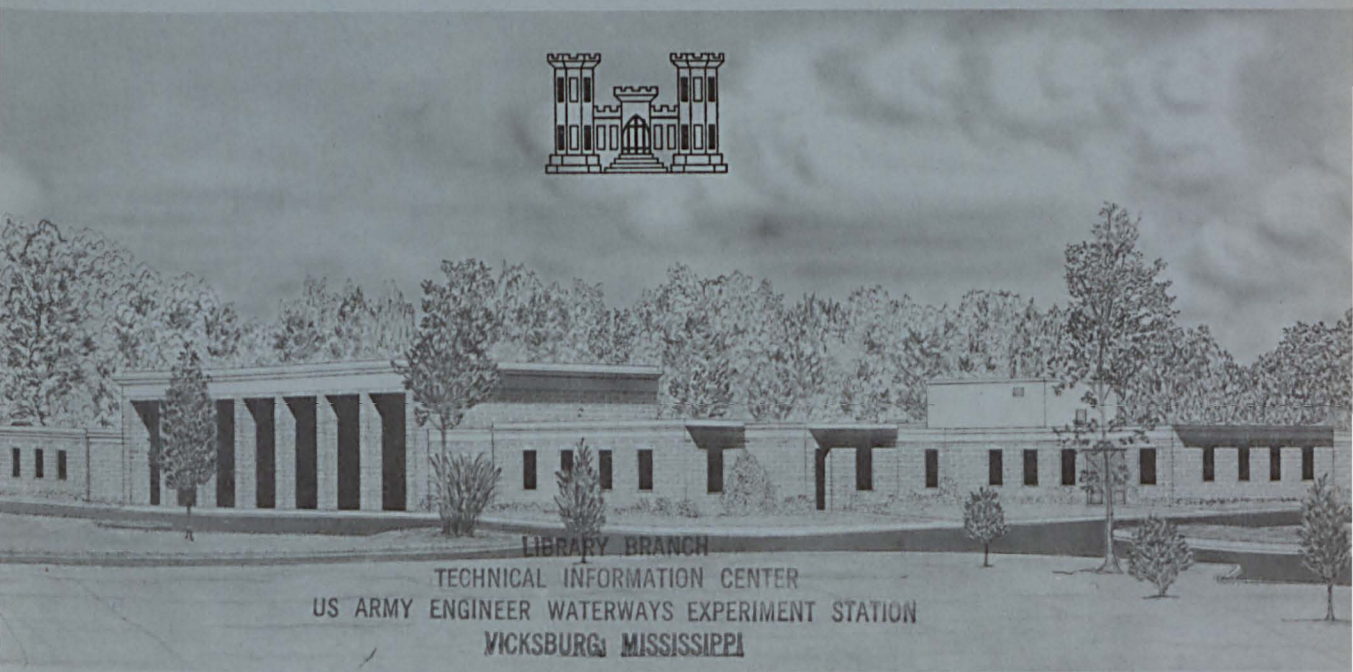

February 1972

Sponsored by Defense Nuclear Agency

Conducted by U. S. Army Engineer Waterways Experiment Station, Vicksburg, Mississippi

TECHNICAL REPORT N-72-2

OPERATION PRAIRIE FLAT, PROJECT LN 302: EARTH MOTION AND STRESS MEASUREMENTS

by

D. W. Murrell

February 1972

Sponsored by Defense Nuclear Agency

Conducted by U. S. Army Engineer Waterways Experiment Station, Vicksburg, Mississippi

ARMY-MRC VICKSBURG, MISS.

THE CONTENTS OF THIS REPORT ARE NOT TO BE USED FOR ADVERTISING, PUBLICATION, OR PROMOTIONAL PURPOSES. CITATION OF TRADE NAMES DOES NOT CONSTITUTE AN OFFICIAL ENDORSEMENT OR APPROVAL OF THE USE OF SUCH COMMERCIAL PRODUCTS.

ABSTRACT

The objectives of this study were to measure and interpret the earth motions and stresses produced by the Prairie Flat 500-ton TNT detonation.

Acceleration, particle velocity, and soil stress gages were installed to measure the ground motions and stresses encompassed by the 2,000- to 10-psi predicted airblast overpressure region (84 to 1,150 feet from ground zero) and depths below the ground surface of 1.5 to 30 feet. Time histories of all successful measurements are included in Appendixes A and B.

Ground shock arrival times indicated the occurrence of outrunning ground motion at a distance of about 560 feet, or the 35-psi pressure level. Peak vertical particle accelerations varied from 1,200 to 1.9 g's at the extremes of the instrumented region, attenuating sharply with both distance and depth. Peak acceleration to peak overpressure ratios, used as a basis for correlation, were observed to be both pressure and yield dependent, increasing with lower pressures and higher yields.

Vertical particle velocities varied from 84 to 0.33 ft/sec over the area instrumented, also attenuating rapidly with distance and depth. Vertical velocities were also correlated on the basis of velocity to pressure ratios, and the ratios were again observed to be pressure and yield dependent.

Peak horizontal velocities were found to vary from about 20 to 0.3 ft/sec over the same region, with little or no attenuation with depth. These velocities were compared with those obtained on Distant Plain Event 6 by means of cube-root scaling, and excellent comparability was noted.

Both horizontal and vertical displacements were calculated from measured accelerations and velocities. Peak transient displacements were 20 feet upward and 20 feet outward at the 84-foot range and 1.5-foot depth. The upward displacement attenuated more rapidly with distance, so that at 400 feet it was only one-half of the outward displacement.

Soil stress measurements were generally of poor quality from a signal-to-noise standpoint. Data at the 1.5- and 30-foot depths, where good measurements resulted, were exceptions. Vertical stresses at the 1.5-foot depth averaged 40 percent of the surface overpressure.

PREFACE

This report describes an experiment conducted by the U. S. Army Engineer Waterways Experiment Station (WES) as a part of Operation Prairie Flat. The study was sponsored by the Defense Nuclear Agency (formerly Defense Atomic Support Agency).

The work was conducted during March-August 1968 by the Nuclear Weapons Effects Division under the direction of Messrs. G. L. Arbuthnot, Jr., Division Chief, L. F. Ingram, Chief, Physical Sciences Branch, and J. D. Day, Chief, Blast and Shock Section. Project personnel were Messrs. D. W. Murrell, Project Officer and author of this report, M. A. Vispi, Field Operations Officer, and C. M. Wright, all of the Blast and Shock Section, and Messrs. L. T. Watson, G. P. Bonner, G. H. Williams, and C. E. Tompkins of the WES Instrumentation Branch.

COL Levi A. Brown, CE, and COL Ernest D. Peixotto, CE, were Directors of WES during this experiment and the preparation of this report. Messrs. J. B. Tiffany and F. R. Brown were Technical Directors.

CONTENTS

FIGURES

CONVERSION FACTORS, BRITISH TO METRIC UNITS OF MEASUREMENT

British units of measurement used in this report can be converted to metric units as follows.

Multiply	By	To Obtain
inches	25.4	millimeters
feet	0.3048	meters
tons (2,000 pounds)	0.907185	megagrams
pounds per square inch	6.894757	kilonewtons per square meter
pounds per cubic foot	16.0185	kilograms per cubic meter
feet per second	0.3048	meters per second

CHAPTER 1

INTRODUCTION

1.1 OBJECTIVES

The objectives of Project LN302 were to measure the earth motions and stresses on the Prairie Flat Event and to analyze and correlate the results with those obtained on other pertinent detonations, such as Snow Ball, Flat Top, and several events of the Distant Plain Series.

1.2 BACKGROUND

Operation Prairie Flat, conducted at the Defence Research Establishment, Suffield (DRES), Alberta, Canada, during August 1968, was a continuation of a high explosive test program at DRES planned under the auspices of the Tripartite Technical Cooperation Program (TTCP). The primary purpose of the Prairie Flat Event was to obtain loading and response data for a variety of military targets, since knowledge of free-field ground motions and stresses is essential for analysis of such target response. In addition, experimental data are needed for verifying and improving calculational techniques for ground shock prediction.

The charge size (500 tons[1]) and geometry (tangent sphere) for the Prairie Flat Event were such that measurements of ground shock were feasible up to an airblast overpressure of 2,000 psi. Substantial outrunning ground motion was anticipated based on results of the Snow Ball and Distant Plain Event 6 detonations; therefore, documentation of earth motion in this region, i.e., 10 to 50 psi, was desired in order to assess responses of various structural systems.

1.3 GROUND MOTION AND STRESS PREDICTIONS

Estimated peak values of ground motions and stresses are necessary for selecting proper gage ranges and making recording system gain settings.

---

[1] A table of factors for converting British units of measurement to metric units is given on page 8.

For the Prairie Flat Event, ground motion predictions (Reference 1) were made by the Technical Director's staff and are presented in Table 1.1 Predictions of soil stress were based on relative attenuations with depth observed on Operation Upshot-Knothole (Reference 2). Attenuation of vertical earth stress as a function of depth, at least to a depth of 10 feet, was determined to be

$$P = P_1\left(\frac{d}{d_1}\right)^{-0.37} \qquad (1)$$

which describes the vertical stress P at a depth d in terms of stress P_1 at a depth d_1 (Reference 2). For the Prairie Flat Event, P_1 and d_1 were arbitrarily fixed to be the surface overpressure and 0.5 foot, respectively, thus allowing calculation of expected pressures at any desired depth. Stress predictions are listed in Table 1.2.

All stresses in directions other than vertical were taken as two-thirds of the vertical for the upper 10 feet of soil. For the 17- and 30-foot depths, no further attenuation with depth was assumed, and all components were taken to be equal due to the increasingly saturated nature of the soil.

TABLE 1.1 PREDICTED GROUND MOTION PARAMETERS

For the values above the line, airblast-induced motion predominates; for those below the line, cratering-induced motion predominates.

Depth	Maximum Value at Indicated Range								
	70 ft	84 ft	105 ft	140 ft	170 ft	220 ft	280 ft	330 ft	400 ft
feet									
Maximum Vertical Acceleration, g's:									
1.5	750	720	720	700	660	580	430	320	220
5	180	180	180	180	180	180	160	130	100
10	80	85	80	80	90	80	80	70	60
17	80	45	45	45	45	40	45	40	35
24	80	45	30	30	30	30	30	30	25
30	80	45	25	25	25	25	25	25	20
Maximum Horizontal Acceleration, g's:									
1.5	120	120	120	110	110	100	75	60	40
5	80	45	30	30	30	30	25	25	20
10	80	45	25	15	15	15	15	15	10
17	80	45	25	10	10	7	8	7	7
24	80	45	25	10	6	5	5	6	5
30	80	45	25	10	6	4	4	5	4
Maximum Vertical Velocity, ft/sec:									
1.5	40	40	35	35	30	30	20	15	11
5	40	40	25	15	15	15	15	10	9
10	40	35	15	10	10	10	10	9	8
17	35	20	10	7	7	7	7	7	6
24	35	20	10	6	6	6	6	5	5
30	35	20	10	5	5	5	5	5	5
Maximum Horizontal Velocity, ft/sec:									
1.5	70	40	20	8	5	4	3	2	2
5	70	40	20	8	5	3	3	2	2
10	65	40	20	8	5	3	3	3	2
17	60	35	20	8	5	3	3	3	3
24	60	35	20	8	5	3	3	3	3
30	50	30	15	8	4	3	3	3	3

TABLE 1.2 PREDICTED EARTH STRESSES

PV--vertical stress; PH--horizontal stress; PS--stress at 45 degrees to horizontal; PT--tangential stress.

Range	Depth	Maximum Stress			
		PV	PH	PS	PT
feet	feet	psi	psi	psi	psi
84	1.5	1,200	--	--	--
	5	800	533	533	533
	10	700	467	467	467
	17	500	500	--	--
	30	--	500	--	--
140	1.5	670	--	--	--
	5	420	270	270	270
	10	350	233	233	233
	17	270	270	270	270
	30	--	270	--	--
220	1.5	330	--	--	--
	5	200	133	133	133
	10	175	117	117	117
	17	150	150	150	150
	30	--	150	--	--
330	1.5	130	--	--	--
	5	85	57	57	57
	10	70	47	47	47
400	1.5	80	--	--	--
	5	50	33	33	33

CHAPTER 2

PROCEDURE

2.1 DESCRIPTION OF TEST SITE

The Prairie Flat Event was detonated on the Watching Hill Blast Range of DRES. Over the area instrumented for this project, the ground surface was essentially flat, with an elevation of approximately 2,160 feet above mean sea level. Geologically, the test site lies in the southern end of the Ross Depression, which apparently was once covered by a large lake. The soils to a depth of 200 feet are lacustrine deposits consisting of fairly uniform beds of clays and silts with occasional sand lenses (Reference 3).

Detailed accounts of the soil survey and testing for the Distant Plain Series are given in References 4 and 5. Briefly, Project 3.10, Soil Sampling and Testing (References 4 and 5), reported the upper 5.5 feet of soil at the Watching Hill Range to be a tan, sandy, silty clay. From this point to a depth of about 30 feet, the soil was sandy silt. The upper 30 feet of soil (both layers) was about 40 percent air by volume, resulting in a high compressibility. For example, a dynamic uniaxial strain test on a sample taken from the upper 5 feet produced a 23 percent vertical strain at 4,000 psi. Upon unloading, the material recovered only about 2 percent of this strain (Reference 5).

2.2 INSTRUMENTATION LAYOUT

A total of 129 earth motion and stress gages were installed for this project, which included 51 accelerometers, 30 particle velocity gages, and 48 earth stress gages. One hundred and eleven gages, including all of the particle velocity and stress gages, were installed in the region of superseismic ground shock, between the 125- and 2,000-psi predicted overpressure levels. Twenty-four locations were instrumented in this region at depths of 1.5, 5, 10, 17, and 30 feet below ground surface. The remaining 18 accelerometers were installed in the region of anticipated outrunning ground shock, at pressure levels of 10, 20, and 50 psi, and at depths of 1.5, 5, and 10 feet.

At 12 of the locations instrumented in the superseismic region, multiple stress gages were installed, oriented to sense vertical stress, horizontal stress, stress at an angle of 45 degrees with the horizontal, and, at four of these locations, tangential stress. By using the multiple gages and assuming spherical symmetry, it is theoretically possible to calculate the principal stresses, their directions, and the shear stress component in the plane of the sensors.

The total gage array for this project is listed in Tables 2.1 and 2.2.

2.3 INSTRUMENTATION

2.3.1 Gages and Calibration. All particle motion gages used on this project were commercially available units which have proved reliable in numerous field or laboratory soil motion experiments. The particle velocity gages were the Sparton Southwest, Inc., Model 601. This gage was developed under a Defense Atomic Support Agency contract by Stanford Research Institute and modified by Sandia Corporation. The Model 601 is a variable reluctance gage of the highly overdamped accelerometer design.

Two different types of accelerometers were used. Pace Model A18 variable reluctance gages were installed at the 17- and 30-foot depths, and in the outrunning region, while Endevco Corporation semiconductor strain gage accelerometers were used at the remaining locations.

The soil stress gages were constructed by the Waterways Experiment Station (WES) using our own design. Basically, the gage is a dual-diaphragm gage with two arms of a full semiconductor strain gage bridge bonded to each diaphragm. Reference 6 gives a detailed account of the development and testing of this gage.

All velocity gages were calibrated by using the free fall of the pendulum method. The variable reluctance accelerometers were statically calibrated on a rotary accelerator (spin table), while the strain gages were dynamically calibrated with a dynamic shock calibrator of the impacting ball type. The soil stress gages were calibrated statically in a small pressure chamber.

All gages were electrically calibrated just prior to shot time by shunting a resistor across one arm of the bridge circuit, producing a

circuit imbalance of a known motion or stress equivalence.

2.3.2 Gage Canisters and Placement. All motion gages installed at a particular location were mounted in a single aluminum canister along with associated calibration and line-matching electronics. Figure 2.1 shows a typical canister with mounted gages. All canisters were potted with paraffin in order (1) to resist water leakage and (2) to damp high-frequency vibrations. The final density of the assembled canister was about 100 pcf, which provided a good match with the in situ soil. Stress gages placed at the 1.5-foot depth were placed by hand, and soil was hand tamped around them. The stress gages at depths of 5 feet and below were cast in soil-cement plugs consisting of native soil, about 3 percent portland cement, and about 10 percent water to enable compaction.

In all cases, the instrument holes were backfilled with the same soil-cement mixture used for the stress gage plugs. This mixture, though perhaps slightly stiffer than the in situ soil, provided a good density match and was considered to be a significant improvement over dry sand or cement grout for matching alluvial soils.

Instrument cables were protected downhole by heavy-duty reinforced rubber hose, and in the main cable trench were fed into a 3-inch-diameter plastic pipe. This method proved satisfactory since the few cables which broke did so well after significant motion peaks had occurred.

2.3.3 Recording System. Signal conditioning and recording equipment was housed in a wooden bunker located about 3,800 feet southwest of ground zero (GZ).

The basic signal conditioning equipment for all variable reluctance gages was the CEC Model 113-B (System D) 3-kHz carrier-demodulator amplifier. Outputs from this system were recorded on CEC 5-119 oscillographs. The strain gage transducer outputs were fed into an operational amplifier system designed and constructed by WES, and all but four stress gage outputs were recorded on CEC VR-3300 FM magnetic tape recorders. Those four were recorded on oscillographs.

Calibration and recorder start signals were produced by a cam-type timing device which was triggered by the -30-second signal from DRES Control. The -2-second signal from Control was used as a backup to shift all

recorders to operating speed. The zero time pulse from Control (DET ZERO) was recorded directly on all oscillographs and was superimposed on the 1-kHz timing channel on magnetic tape.

TABLE 2.1 SUMMARY OF MOTION GAGE INSTALLATION

+ = Vertical velocity, horizontal velocity, vertical acceleration.
Y = Vertical acceleration, horizontal acceleration.

Pressure	Distance	Gage Array at Depths of				
		1.5 ft	5 ft	10 ft	17 ft	30 ft
psi	feet					
2,000	84	+	+	+	Y	Y
1,000	140	+	+	+	Y	Y
500	220	+	+	+	Y	Y
200	330	+	+	+	Y	Y
125	400	+	+	+	Y	--
50	560	Y	Y	Y	--	--
20	830	Y	Y	Y	--	--
10	1,150	Y	Y	Y	--	--

TABLE 2.2 SUMMARY OF STRESS GAGE INSTALLATION

X--three-component soil stress (PV, PH, PS); Z--four-component soil stress (PV, PH, PS, PT); PV--vertical soil stress; PH--horizontal soil stress; PS--soil stress at 45 degrees to horizontal; PT--tangential soil stress.

Pressure	Distance	Gage Array at Depths of				
		1.5 ft	5 ft	10 ft	17 ft	30 ft
psi	feet					
2,000	84	PV	Z	X	Z	PH
1,000	140	PV	Z	X	X	PH
500	220	PV	X	Z	X	PH
200	330	PV	X	X	--	--
125	400	PV	X	--	--	--

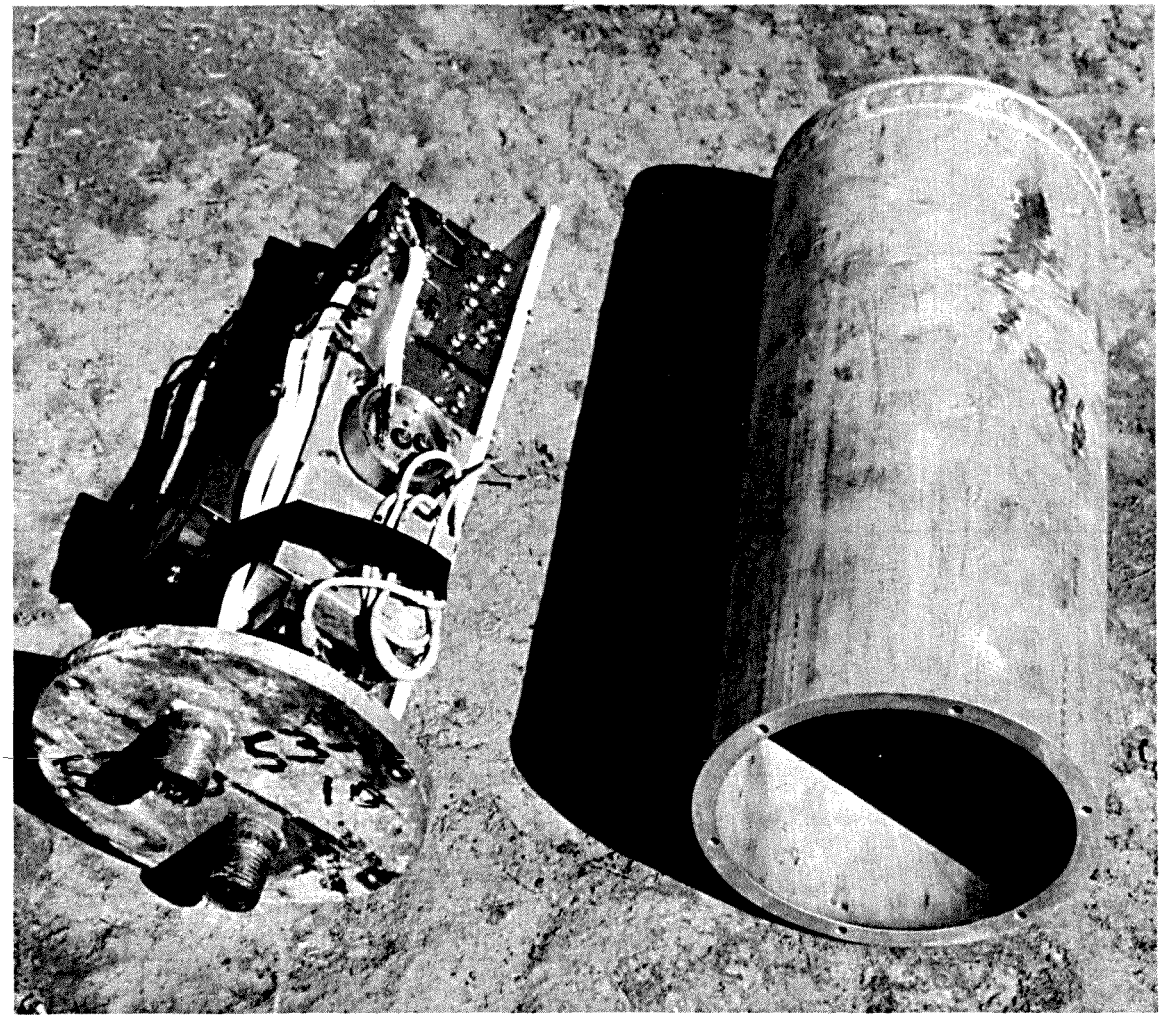

Figure 2.1 Typical gage canister.

CHAPTER 3

RESULTS AND DISCUSSION

3.1 INSTRUMENT PERFORMANCE

All of the 129 gages installed for Prairie Flat were operational at shot time, and all gages responded to shock arrival. Of the 81 motion gages installed, 72 yielded useful data of generally high quality from a signal-to-noise perspective. The eight accelerometers installed at the 30-foot depths were severely overranged, and no data other than arrival times were obtained from them. Stress gage outputs were consistently much lower than had been estimated preshot, except for the 1.5- and 30-foot depths. The four gages at the 220-foot range and 10-foot depth, which were recorded on oscillographs, produced no measurable trace deflection. Seven other stress gages produced either no usable output or outputs sufficiently low to render the data questionable.

The calibration and sequence initiating signals from DRES control were properly received and translated, and all equipment operated as programmed. A good DET ZERO signal was received and recorded.

3.2 DATA REDUCTION

Data recorded on oscillograph recorders were read on an electromechanical pencil follower unit. The output from this apparatus was in a computer-compatible digital magnetic tape format. Data recorded on magnetic tape were digitized on the WES high-speed analog-to-digital converter. All digitized records were then processed through a digital computer, where baseline corrections and integrations were performed. Computer outputs were then plotted to a report-size format.

The data were initially plotted to a time of 4 seconds after detonation. However, difficulties were encountered in making reasonable baseline corrections to the oscillograph records and their integrations when carried to the full 4 seconds. This problem arose, at least in part, from the large number of separate "setups" required in reading each record, since only 200 msec of record could be read at a time in the frame of the pencil follower. Thus slightly different baselines were possibly introduced at a

number of points on the record. Consequently, it was decided to alleviate, if not eliminate, the problem by processing data to only 2 seconds rather than 4 seconds, at the cost of not showing late-time motions on some records.

Data plots for all successful measurements and their integrals are presented in Appendixes A and B. Tables 3.1 and 3.2 summarize the absolute peak values and shock arrival times for these records. The location code used in the tables and the plots in the appendixes was simply a method for identifying a given gage or gage location and was developed to insure uniformity of designation between this project and others.

3.3 ARRIVAL TIMES

Shock arrival times were established for all successfully recorded gages. In addition, several of the channels which yielded no useful peak data gave arrival time information. Among these were the eight accelerometers at the 30-foot depth. For the most part, agreement of arrival times obtained from several gages installed at a point was only fair. Differences from gage to gage on the order of a millisecond were not uncommon, and several cases of as much as 5-msec difference were noted. Since the expanded-time oscillograms offered a time resolution of a fraction of a millisecond, the problem must lie with the slow rise times noted, particularly for horizontal velocity gages. These slow rise times made the selections of shock arrivals tenuous at best.

Shock propagation velocities for the upper soil layer were calculated using the earliest arrival times noted for the 1.5- and 10-foot depths. For the saturated material below the water table, shock arrivals at the 30-foot depth were used. Propagation velocities for the two layers were found to average 1,270 and 6,100 ft/sec, respectively. These values are 15 percent and 11 percent higher than were reported for Distant Plain Event 6 (Reference 7). No explanation for the difference is readily apparent, since it is unlikely that soil properties vary to that degree between the two sites. The lack of precision among the arrival times could account for some of the difference, but it is improbable that this is the only contributing factor.

Figure 3.1 is a shock front profile constructed from airblast arrival

time data (Reference 8), ground shock arrival times measured on this project, the calculated propagation velocities, and, importantly, the directions of initial motions for vertical measurements. The development of two distinct shock fronts is indicated by Figure 3.1. The first of these is the airblast-induced ground shock which trails behind the airblast wave. Motions generated by this pulse are downward and outward and are the initial motions in the superseismic region. The shock front is nearly horizontal near the source and becomes more nearly vertical as the airblast wave slows down. The second pulse identifiable from Figure 3.1 is a shock front refracted along the saturated layer. Energy from this wave is continuously fed back into the overburden as an upward-moving pulse. This refracted wave is seen to overtake the airblast, and at a ground range of about 560 feet, or about the 35-psi overpressure level, produces the initial motion at the ground surface. The onset of outrunning ground motion occurs at this approximate range, and at all points beyond this range, initial motions will be upward and outward due to the outrunning motion.

Not shown in Figure 3.1, but of great significance to a range of several hundred feet, is the directly induced, or cratering-induced, front in the upper soil layer. This shock front follows the airblast-induced motion at all locations, and, as will be discussed later, it is dominant in producing displacements.

3.4 PARTICLE ACCELERATION

3.4.1 Measurements. Peak airblast-induced downward accelerations are plotted versus horizontal distance in Figure 3.2. Data from the three shallowest depths (1.5, 5, and 10 feet) are shown. A rapid attenuation with both increasing range and depth is noted, with airblast-induced downward accelerations varying from 1,200 g's at the 84-foot range and 1.5-foot depth to 1.9 g's at the 1,150-foot range and 10-foot depth.

Figure 3.3 shows typical vertical acceleration records from the 220-foot range. The first three of these (1.5-, 5-, and 10-foot depths) are characteristic of near-surface accelerations in the superseismic region in that they are dominated by a sharp downward spike at air shock arrival followed by a lesser magnitude upward "rebound." Subsequent to

these peaks, upward cratering-induced motion occurs, also of less magnitude than the airblast motion but of considerably longer duration. The airblast-induced pulse is also noted to increase in duration with depth, from about 5 msec at the 1.5-foot depth to about 14 msec at the 10-foot depth. The record from the 17-foot depth also shows initially downward motion. However, at this point the downward pulse has attenuated to such a degree that subsequent upward motions are greater.

3.4.2 Discussion and Correlation. For airbursts, maximum near-surface vertical acceleration is caused by the airblast, and ratios of peak downward acceleration to overpressure have proved to be a useful tool for correlating motions. Figure 3.4 is a plot of the ratio of airblast-induced acceleration to overpressure (g's/psi) versus overpressure, which offers a means of predicting accelerations based on overpressure. Data from three events at DRES (Prairie Flat and Distant Plain Events 3 and 6) and two at NTS (Flat Top II and III) are included for comparison. Two well-defined trends in this data are apparent. First, there is an observable tendency toward smaller ratios at the higher pressures. This effect was predicted by Sauer (Reference 9) and is attributed to the more rapid rates of decay ("spikedness") of airblast at higher overpressures. The second noticeable trend is a yield dependency, as indicated by the generally higher Prairie Flat data. The difference, if any, between the Distant Plain Event 6 (100-ton yield) and the Distant Plain Event 3 and Flat Top events (20 tons) is less apparent, however, even though the fivefold difference in yield was the same as the Prairie Flat to Distant Plain Event 6 difference. The data scatter for all five sets of data plotted in Figure 3.4 is unfortunately too large to make reliable fits to the data. Therefore, the usefulness of Figure 3.4 is limited to showing the broad patterns of yield and pressure dependency of acceleration-to-pressure ratios.

For depths below the 1.5-foot level, a plot was constructed which normalized peak accelerations at the 5- and 10-foot depths to a depth of 1.5 feet. Figure 3.5 presents normalized data for Prairie Flat and Distant Plain Events 3 and 6. A large amount of scatter is readily apparent, being on the order of a factor of four for the extremes. To explain the

scatter, at least in part, the pressure levels for the Prairie Flat data are listed. With a few exceptions, notably the data at the 1,150-foot range (8-psi level), the most rapid attenuations, or lowest ratios on the ordinate of the graph, occur at the highest pressure levels. This, too, is in keeping with predictions, and again is due to the more rapid rate of decay of the pressure-time history at higher pressures. As a result, it appears that average attenuation rates would be meaningless without considering the pressure level of interest. Sauer (Reference 9) uses a correlation method which accounts for pressure effects and effectively reduces the scatter in a plot such as Figure 3.5.

3.4.3 Outrunning Effects. Figures 3.6 and 3.7 are comparisons of vertical and horizontal acceleration waveforms, respectively, for locations in the outrunning region. The first record on Figure 3.6, for the 560-foot range and 1.5-foot depth, still shows superseismic characteristics, i.e., an initially sharp downward airblast-induced spike. The remaining three records, however, show well developed outrunning motion waveforms, as demonstrated by the initially upward pulse, with the airblast-induced motion superimposed. Of interest here is the relationship between the outrunning and airblast-induced pulses. For the first record, the airblast-induced motion is dominant, being greater than the upward pulse by a factor of about seven. At the 10-foot depth, while the airblast-induced motion is still greater, its dominance has been reduced to a factor of less than two. For the shallow depth at the 1,150-foot range, the airblast-induced motion occurs well after onset of motion, and is still greater than the upward motions, although by a factor of only about three, in contrast to the 560-foot range. At the 10-foot depth, the trend toward lessening importance of the airblast-induced motion is continued, and in fact, outrunning motions are at this point three times greater than the airblast pulse. Thus the airblast-induced vertical motion is seen to decrease in significance relative to outrunning motion as the distance and depth increase.

For horizontal accelerations in the outrunning region (Figure 3.7) a somewhat similar pattern is observed, although at the 560-foot range the change with depth of the airblast to outrunning motion relationship was less pronounced than was noted for vertical measurements. At the

1,150-foot range, the airblast motion was greater than the outrunning by a factor of six at the 1.5-foot depth, but was only slightly greater at the 10-foot depth. Vertical motions from both sources were generally two to three times the associated horizontal motions.

3.5 VERTICAL PARTICLE VELOCITY

3.5.1 Measurements. Peak airblast-induced downward particle velocity is plotted versus distance in Figure 3.8. Very much the same pattern noted for accelerations is observed, that is, a rapid attenuation with both increasing depth and distance. Data plotted in Figure 3.8 are measured velocities out to a distance of 400 feet, and beyond that are integrals of accelerations. Peak vertical velocities ranged from 74 ft/sec at the 84-foot range and 1.5-foot depth to 0.33 ft/sec at the 1,150-foot range and 5-foot depth.

Measured velocity peaks were in reasonably good agreement with first integrals of accelerations, with generally less than 20 percent difference in the two methods. Waveforms were also observed to agree. Figure 3.9 shows time histories of vertical velocities at the 220-foot range. Both measured velocities and integrals of accelerations are shown for the first three depths, and excellent agreement is apparent. As with acceleration waveforms at the same distance (Figure 3.3), typical superseismic signatures are featured. These exhibit initial dominant downward peaks due to passage of the airblast, followed by an upward pulse. An exception is the measured velocity at the 1.5-foot depth, where a baseline shift has eliminated the upward motion; characteristics of the wave are still discernible, however, when compared with the acceleration integral.

3.5.2 Discussion and Correlation. As with accelerations, velocity to overpressure ratios are convenient for correlation. Figure 3.10 is a plot of vertical airblast-induced velocity to overpressure ratio versus overpressure for Prairie Flat, Distant Plain Events 3 and 6, and Flat Top II and III. There is again a trend toward smaller ratios at higher pressures, although the four points from Distant Plain Event 6 in the 10- to 50-psi region appear to counter the trend. The yield dependency of the velocity to overpressure ratio is obvious, and in this case the 100-ton

data (Distant Plain Event 6) fall clearly above the 20-ton data in the region above 200 psi. As a result, the scatter of data in Figure 3.10 is much less than it at first appears if yield dependency is considered.

Attenuation of vertical particle velocity with depth is plotted in Figure 3.11 using the normalizing method used in Figure 3.5. A great deal of scatter is again encountered, but is partially explainable on the basis of pressure dependency since the most rapid attenuation rates are associated with the higher pressures. The effect of yield, if any, on attenuation rates is not apparent from Figure 3.11, since data points over a 25-fold yield difference are well mixed. The rates of attenuation of vertical velocity with depth are somewhat less rapid than was found for accelerations, an effect which is more pronounced for the 10-foot depth than for the 5-foot depth. This can be attributed to the dependence of peak accelerations on both peak velocity and velocity rise times, which increase with distance traveled by the shock wave.

3.6 HORIZONTAL PARTICLE VELOCITY

3.6.1 Measurements. Horizontal particle velocities are characterized in the close-in region (out to several crater radii) by two distinct outward waves. The first of these is due to passage of the airblast. The second is caused by cratering-induced energy, and within roughly three crater radii is of paramount importance in producing displacements. These are clearly apparent in Figure 3.12, which shows three horizontal velocity-time histories at the 10-foot depths. The first of these, from the 84-foot range, shows a relatively small airblast-induced motion of about 3 ft/sec, followed by a very long cratering-induced pulse of 15 to 20 ft/sec. The next record, from the 220-foot range, shows both pulses reduced somewhat in magnitude, although the difference is not nearly so great, and at 330 feet, the airblast-induced motion is the greater.

Horizontal cratering-induced velocities are listed in the following tabulation, and are plotted versus distance in Figure 3.13. A rapid attenuation with distance is observed, as the -2.3 power of range. Very little scatter is present except at the 330-foot range, and although the 1.5-foot data are generally highest, the three data points at a common

Horizontal Cratering-Induced Particle Velocities			Horizontal Cratering-Induced Particle Velocities		
Range	Depth	Velocity	Range	Depth	Velocity
feet	feet	ft/sec	feet	feet	ft/sec
84	1.5	22	330	1.5	1.6
	5	19.2		5	0.72
	10	17.6		10	0.44
140	1.5	7.2	400	1.5	0.40
	5	6.2		5	0.32
	10	6.3		10	0.38
220	1.5	2.4			
	5	2.84			
	10	3.1			

distance are sufficiently close to preclude positive statements about attenuation with depth.

3.6.2 Discussion and Correlation. Since the cratering-induced velocities arise from a directly induced effect, somewhat analogous to that from contained detonations, cube-root scaling was applied to the data for correlative purposes. Figure 3.14 is a plot of peak cratering-induced velocities for the Prairie Flat and Distant Plain Event 6 data versus scaled range. Due to the above-mentioned lack of attenuation with depth, the data are not differentiated on this basis. Excellent agreement between the two events is noted, with neither being uniformly high nor low with respect to the fitted line. The decay power of -2.3 is the same as for the unscaled Prairie Flat data. The precision of the scaled data from the two events adds to its reliability, and probably points to horizontal velocity as the most predictable parameter measured.

3.7 DISPLACEMENT

Both vertical and horizontal displacements in the close-in region are dominated by the cratering-induced pulses. In the case of vertical displacements, the downward motion caused by the airblast is insignificant compared with the upward motion, at least at the closest stations, and is

quite possibly clipped short by arrival of the cratering pulse. For this reason, discussion of transient displacements is limited to the dominant upward motion.

Figure 3.15 is a plot of upward vertical displacements versus distance. The plot is marked by a very rapid attenuation as the -3.8 power of distance. Relatively little scatter is present considering the dependency of calculated displacements on measurement accuracy and data reduction techniques (e.g., baseline corrections). Of interest on this figure are the large ($\approx$20-foot) displacements observed at the 84-foot range. It is pointed out here that this location was in the lip of the crater, which accounts for the large motions upward.

Figure 3.16 is a similar plot for horizontal displacements. Here the decay rate is a slightly lower -3.1 power of distance. This accounts for somewhat larger horizontal than vertical displacements at the greater distances, even though upward and outward displacements at the 84-foot range were virtually identical.

3.8 SOIL STRESS

Soil stress data obtained by this project were unfortunately not of uniformly good quality. With the exception of data at the 1.5- and 30-foot depths, recorded signals were generally much lower than had been expected, resulting in poor signal-to-noise ratios. This precluded calculation of shear stresses, for example, which depends on three virtually ideal records with no negative (tensile) stresses to avoid extraneous results. In addition, attenuation patterns below the 1.5-foot depth were quite irregular, to the point of meaninglessness. Subsequent investigation of the problem points toward the extreme sensitivity of stress measurements to gage placement techniques. For example, in recent laboratory tests at WES it has been found that there is a tendency for the material in the soil plug to separate from the gage on curing, producing extremely small but significant voids. In addition, there is a possibility that the soil plugs were too stiff, allowing the arching effect to reduce load on the gage. This, too, has been suggested by laboratory tests.

Measurements at the 1.5- and 30-foot depths, however, were of good

quality. A partial explanation of the more successful measurements at these depths lies in the method of placement and coupling. For the 1.5-foot depths, placement of the gage and tamping of the backfill material was done by hand directly around the gage. This apparently led to greater uniformity and better coupling of the gage. At the 30-foot depth, the plug of soil containing the gage was located in saturated material, which in turn saturated the plug and filled any voids which may have opened. Improved methods of placement and development of better potting materials should alleviate stress gage coupling problems. Studies of this nature are under way at WES.

Figure 3.17 shows the vertical stress-time histories for the 1.5-foot depths. These are plotted on an expanded time scale in order to show detail of the stress pulses. All of the records show predominant single pulses which are associated with passage of the airblast. All of the stress records are marked by a fairly rapid rise to peak, which tends to increase at lower pressure. For example, the fastest rise was at the 140-foot range (2.4 msec) and the slowest at the 330-foot range (7.6 msec). The peaks are followed by a decay which in all cases is less rapid than the rise and takes on a semi-exponential form. The time required for decay to one-half of peak amplitude was taken as a correlating characteristic, and again increased for lower pressures. The most rapid decay was at the 140-foot range (2.4 msec), and the longest decay to one-half amplitude was at the 400-foot range (8.8 msec). At the same ranges, the airblast decay to one-half amplitude increased from 1.4 msec to 9 msec (Reference 8). It follows that the test site soil is better able to respond to stress waves as the stress level decreases and, more significantly, as the sharpness of airblast decay is reduced since at the 400-foot range decay rates of airblast and stress at the 1.5-foot depth were virtually identical. This reinforces the evidence cited previously that motion to overpressure ratios increase at decreasing pressure levels.

Figure 3.18 is a plot of vertical stresses measured at the 1.5-foot depths versus distance. Peak overpressures measured by Project LN101 (Reference 8) are also plotted for comparison purposes. With the exception of data at the 330-foot range, the data exhibit a uniform attenuation

with distance and are observed to maintain a nearly constant relation to the airblast overpressure. The ratio of vertical stress to overpressure of 0.4 is a more rapid attenuation with depth than the 0.67 which had been predicted. However, the prediction method used assumed an unattenuated overpressure at a depth of 0.5 foot, which accounts to some degree for the difference.

TABLE 3.1 SUMMARY OF MOTION MEASUREMENTS

Positive motion is upward or outward. AV--vertical acceleration; AH--horizontal acceleration; UV--vertical velocity; UH--horizontal velocity.

Range	Depth	Location Code	Gage Type and Orientation	Time of Arrival	Peak Acceleration		Peak Velocity		Peak Displacement	
					Positive	Negative	Positive	Negative	Positive	Negative
feet	feet			msec	g's	g's	ft/sec	ft/sec	feet	feet
84	1.5	1051	AV	8.4	580	1,200	45	51	36	0.4
			UV	8.2	--	--	32	74	14.4	1.2
			UH	7.2	--	--	22	[a]	21.2	[a]
	5	1052	AV	9.9	80	208	35	24	36	[b]
			UV	10.6	--	--	27.6	20.4	18.4	0.4
			UH	10.8	--	--	19.2	[a]	20.4	[a]
	10	1053	AV	13.9	86	84	27.6	14.4	24.0	0.5
			UV	14.3	--	--	27	13.0	21.2	0.45
			UH	18.8[c]	--	--	17.6	[a]	15.6	[a]
	17	1054	AV	21.7	46	37	15	[b]	[d]	[b]
			AH	22.2	94	32	19.8	[a]	[d]	[a]
	30	1056	AV	21.4	[e]	--	--	--	--	--
			AH	21.8	[e]	--	--	--	--	--
140	1.5	1071	AV	13.3	860	840	42	40	16.4	[b]
			UV	12.8	--	--	26	62	12.6	0.2
			UH	12.8	--	--	7.2	[a]	6.0	[a]
	5	1072	AV	14.6	56	101	10.0	14.4	3.04	0.12
			UV	16.0	--	--	8.2	12.8	4.2	0.14
			UH	20.3[c]	--	--	6.2	[a]	3.9	[a]
	10	1073	AV	18.1	22	64	9.0	9.8	4.1	[b]
			UV	21.7[c]	--	--	7.2	8.6	4.2	0.1
			UH	23.0[c]	--	--	6.3	[a]	3.9	[a]
	17	1074	AV	25.3	24	12	7.2	2.3	3.1	[b]
			AH	26.7	9.8	5.6	7.1	[a]	4.8	[a]
	30	1076	AV	32.2	[e]	--	--	--	--	--
			AH	33.1	[e]	--	--	--	--	--
220	1.5	1091	AV	26.8	230	560	4.8	39	2.23	0.31
			UV	25.0	--	--	4.0	32.4	0.40	0.32
			UH	25.6	--	--	2.4	[a]	0.92	[a]
	5	1092	AV	27.3	56	122	3.5	17.8	0.38	0.32
			UV	27.0	--	--	3.6	19.2	0.37	0.30
			UH	26.8	--	--	2.84	[a]	0.96	[a]
	10	1093	AV	31.3	17	55	3.1	10.0	[f]	0.18
			UV	30.5	--	--	2.0	10.8	0.16	0.17
			UH	29.0	--	--	3.1	[a]	1.14	[a]
	17	1094	AV	36.2	29	16	2.64	4.96	[f]	0.08
			AH	35.0	3.3	7.4	2.08	[a]	0.78	[a]
	30	1096	AV	41.7	[e]	--	--	--	--	--
			AH	41.1	[e]	--	--	--	--	--
330	1.5	1121	AV	48.7	24	190	5.4	11.0	1.41	0.2
			UV	47.5	--	--	4.4	21.2	0.064	0.38
			UH	47.9	--	--	3.68	[a]	0.65	[a]
330 (Cont'd)	5	1122	AV	52.0	15.2	36.4	2.2	9.1	[f]	0.25
			UV	51.3	--	--	3.0	8.5	0.088	0.21
			UH	50.6	--	--	1.68	[a]	0.32	[a]
	10	1123	AV	55.0	11.2	29.6	1.6	8.0	[f]	0.21
			UV	55.7	--	--	1.3	4.8	[f]	0.11
			UH	61.0[c]	--	--	0.80	[a]	0.17	[a]
	17	1124	AV	59.5	8.8	6.2	2.2	1.8	0.36	[b]
			AH	59.0	2.5	4.0	0.80	[a]	0.24	[a]
	30	1126	AV	60.8	[e]	--	--	--	--	--
			AH	61.3	[e]	--	--	--	--	--
400	1.5	1151	AV	66.0	12	152	3.5	8.2	0.96	0.18
			UV	66.5	--	--	3.1	8.5	0.06	0.18
			UH	67.8	--	--	1.28	[a]	0.22	[a]
	5	1152	AV	69.0	18	42	2.0	6.2	0.18	0.15
			UV	68.1	--	--	1.8	4.5	[f]	0.12
			UH	69.0	--	--	0.54	[a]	0.11	[a]
	10	1153	AV	72.0	9.2	22.4	1.92	5.52	0.18	0.11
			UV	73.3	--	--	1.28	3.80	[f]	0.084
			UH	74.0	--	--	0.84	[a]	0.13	[a]
	17	1154	AV	78.0	5.0	3.1	1.4	0.9	0.40	0.011
			AH	77.2	3.88	1.32	0.52	[a]	0.16	[a]
560	1.5	1181	AV	--	4.0	28	[f]	2.6	[f]	0.052
			AH	--	7.2	7.6	0.56	[a]	0.04	[a]
	5	1182	AV	--	3.4	13.4	0.88	1.6	[f]	0.028
			AH	--	1.32	2.8	0.80	[a]	0.15	[a]
	10	1183	AV	--	4.6	8.2	0.92	0.88	0.28	[b]
			AH	--	3.52	1.36	0.49	[a]	0.086	[a]
830	1.5	1211	AV	--	3.6	25.6	0.76	1.04	0.011	0.045
			AH	--	2.6	3.2	[g]	[g]	[g]	[g]
	5	1212	AV	--	2.4	10.2	0.52	0.64	0.034	[b]
			AH	--	2.8	2.2	0.52	[a]	0.062	[a]
	10	1213	AV	--	5.2	5.2	0.44	0.58	0.008	[b]
			AH	--	1.24	0.52	0.51	[a]	0.041	[a]
1,150	1.5	1231	AV	--	7.6	15.8	0.68	0.82	0.009	[b]
			AH	--	4.2	6.3	0.84	[a]	0.025	[a]
	5	1232	AV	--	8.3	3.2	0.57	0.33	0.011	[b]
			AH	--	1.9	1.2	0.35	[a]	0.029	[a]
	10	1233	AV	--	7.9	4.2	0.48	[b]	[f]	[b]
			AH	--	2.2	0.84	0.42	[a]	0.034	[a]

[a] Negative peaks not reported for horizontal velocity and acceleration.

[b] No reliable negative peak.

[c] Questionable arrival time due to slow initial rise.

[d] Displacement plot cut off before peak reached due to gage or cable damage.

[e] No peak data.

[f] No reliable positive peak.

[g] No reliable integrals.

TABLE 3.2 SUMMARY OF STRESS MEASUREMENTS

PV--vertical stress; PH--horizontal stress; PS--stress at 45 degrees to horizontal; PT--tangential stress.

Range	Depth	Location Code	Gage Type and Orientation	Time of Arrival	Peak Stress
feet	feet			msec	psi
84	1.5	1051	PV	7.9	680
	5	1052	PV	9.9	40
			PH	10.4	78
			PS	[a]	[a]
			PT	10.4	47
	10	1053	PV	17.2[b]	55
			PH	18.5[b]	46[c]
			PS	17.1[b]	90
	17	1054	PV	31.0[b]	132
			PH	29.4[b]	408
			PS	30.1[b]	140
			PT	30.1[b]	340
	30	1056	PH	21.8	1,040[a]
140	1.5	1071	PV	14.3	352
	5	1072	PV	21.0[b]	30[c]
			PH	20.6[b]	15
			PS	18.7[b]	73
			PT	20.6[b]	28
	10	1073	PV	[a]	[a]
			PH	19.0	13
			PS	21.1	3.4[c]
	17	1074	PV	28.0	24
			PH	27.4	30
			PS	27.5	50
	30	1076	PH	33.2	710
220	1.5	1091	PV	25.1	172
	5	1092	PV	30.7	4.0[c]
			PH	29.0	9.4[c]
			PS	28.5	14[c]
220	10	1093	PV	[d]	[d]
			PH	[d]	[d]
			PS	[d]	[d]
			PT	[d]	[d]
	17	1094	PV	49.1[b]	38
			PH	53.3[b]	14
			PS	48.5[b]	10
	30	1096	PH	48.0[b]	620
330	1.5	1121	PV	47.0	210
	5	1122	PV	53.0	9.5
			PH	54.3	11
			PS	53.8	19
	10	1123	PV	55.1	3.2
			PH	56.2	8
			PS	54.7	4.9
400	1.5	1151	PV	67.6	45
	5	1152	PV	67.5	4.5
			PH	66.5	6.8
			PS	67.1	14

[a] No data.

[b] Questionable arrival times due to very slow initial rise.

[c] Questionable data.

[d] Oscillogram traces too small to read peaks or arrival.

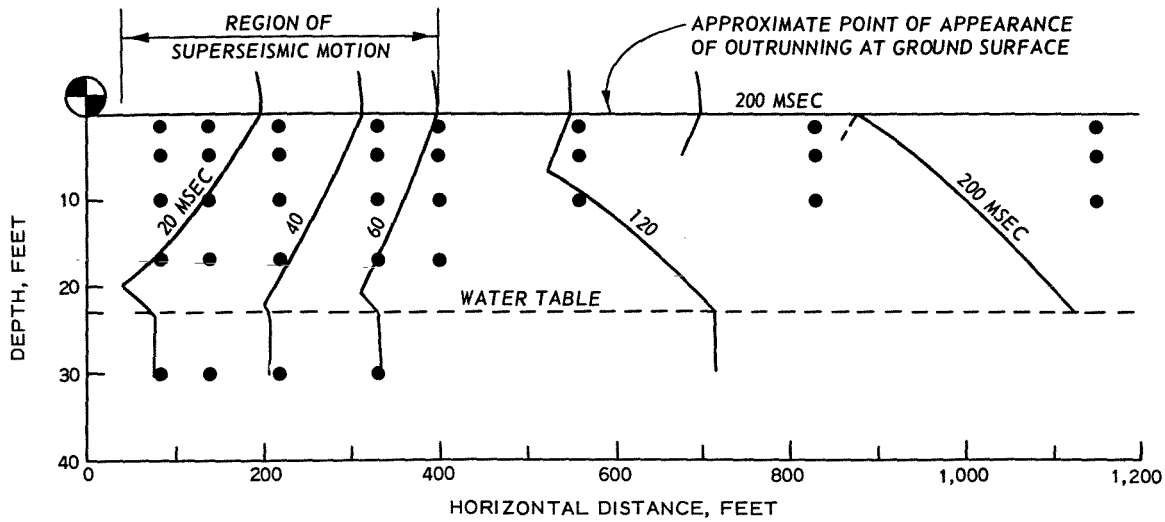

Figure 3.1 Ground shock profile.

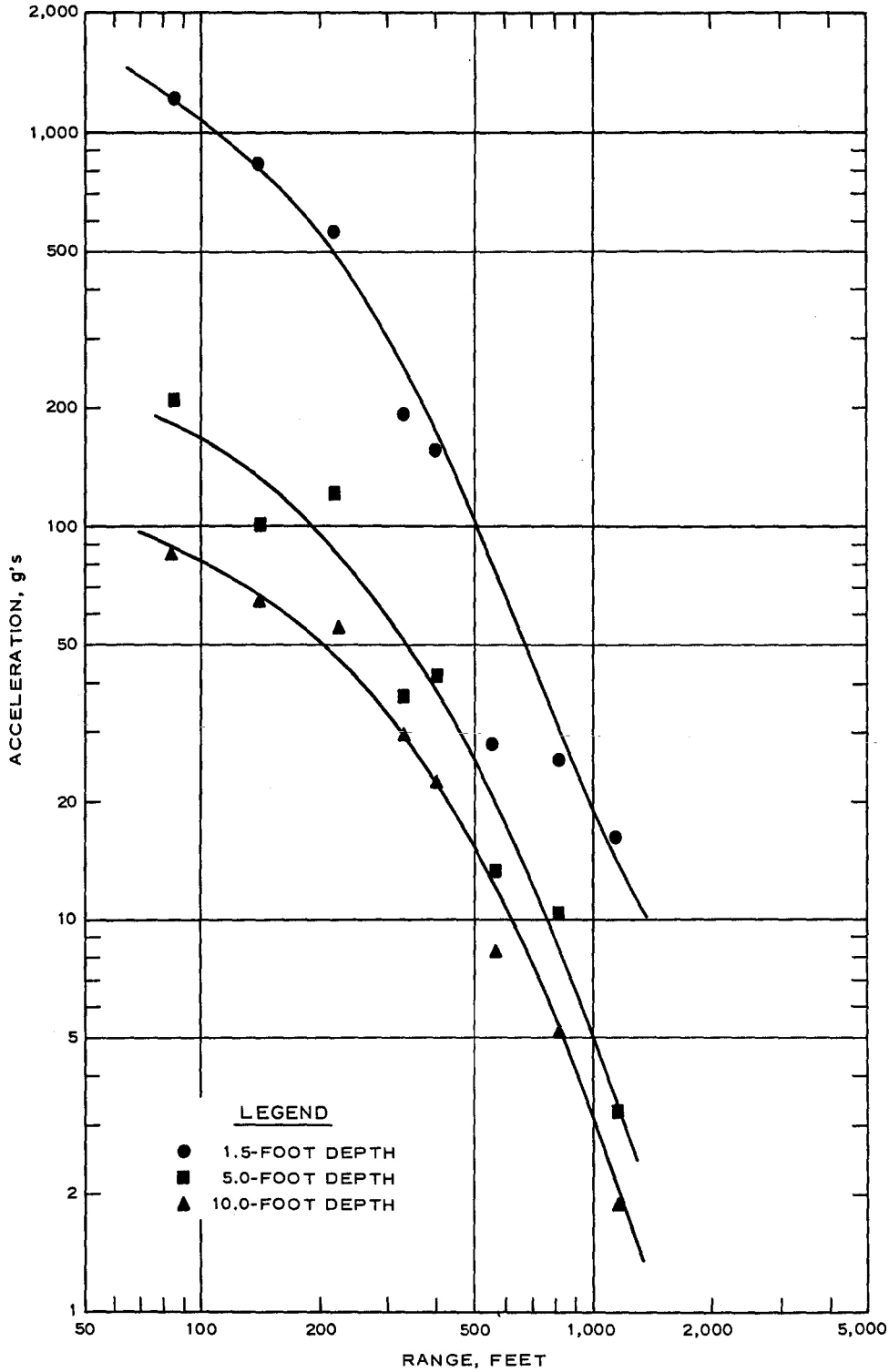

Figure 3.2 Peak airblast-induced (downward) vertical acceleration versus distance.

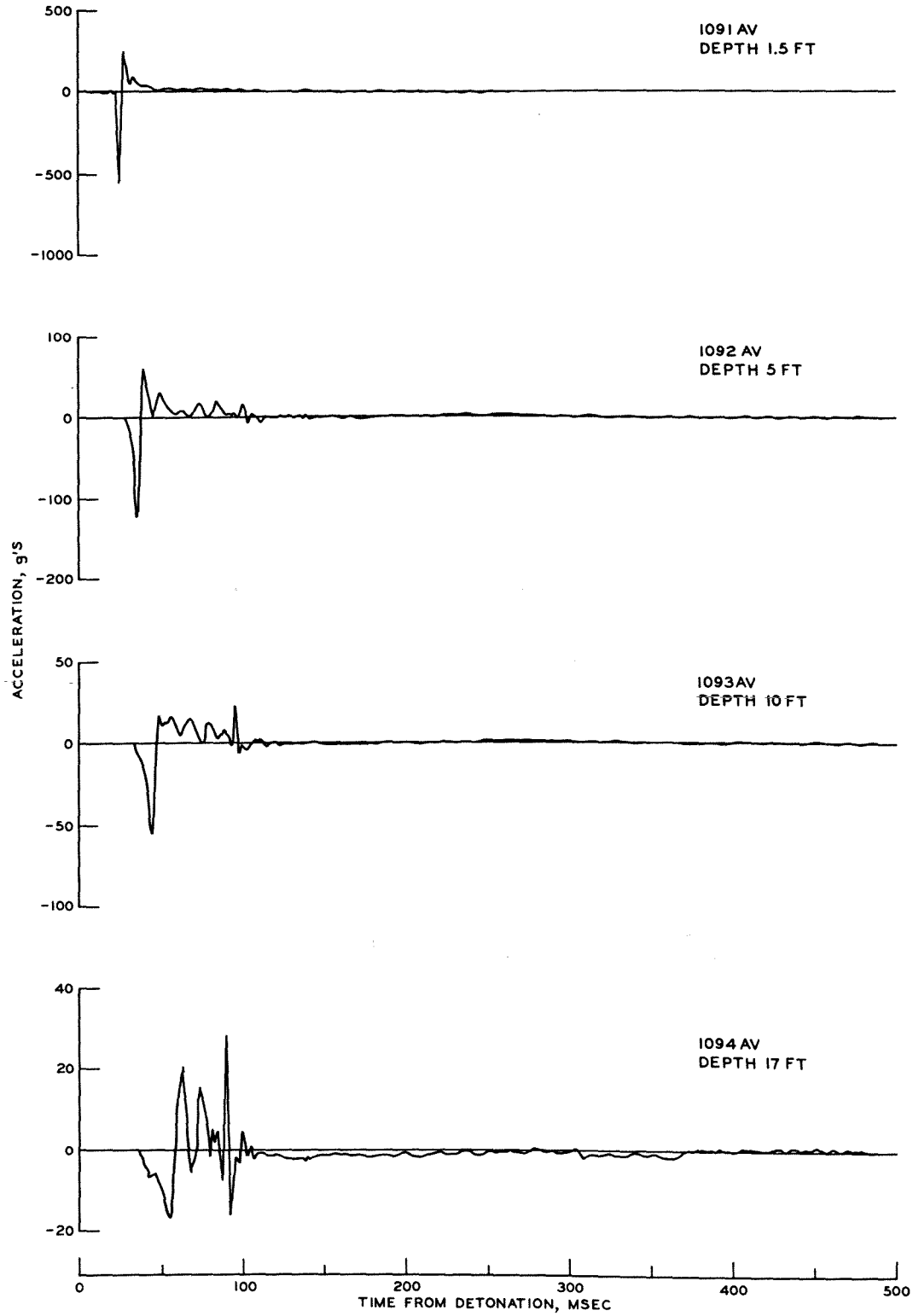

Figure 3.3 Vertical acceleration waveforms, 220-foot range.

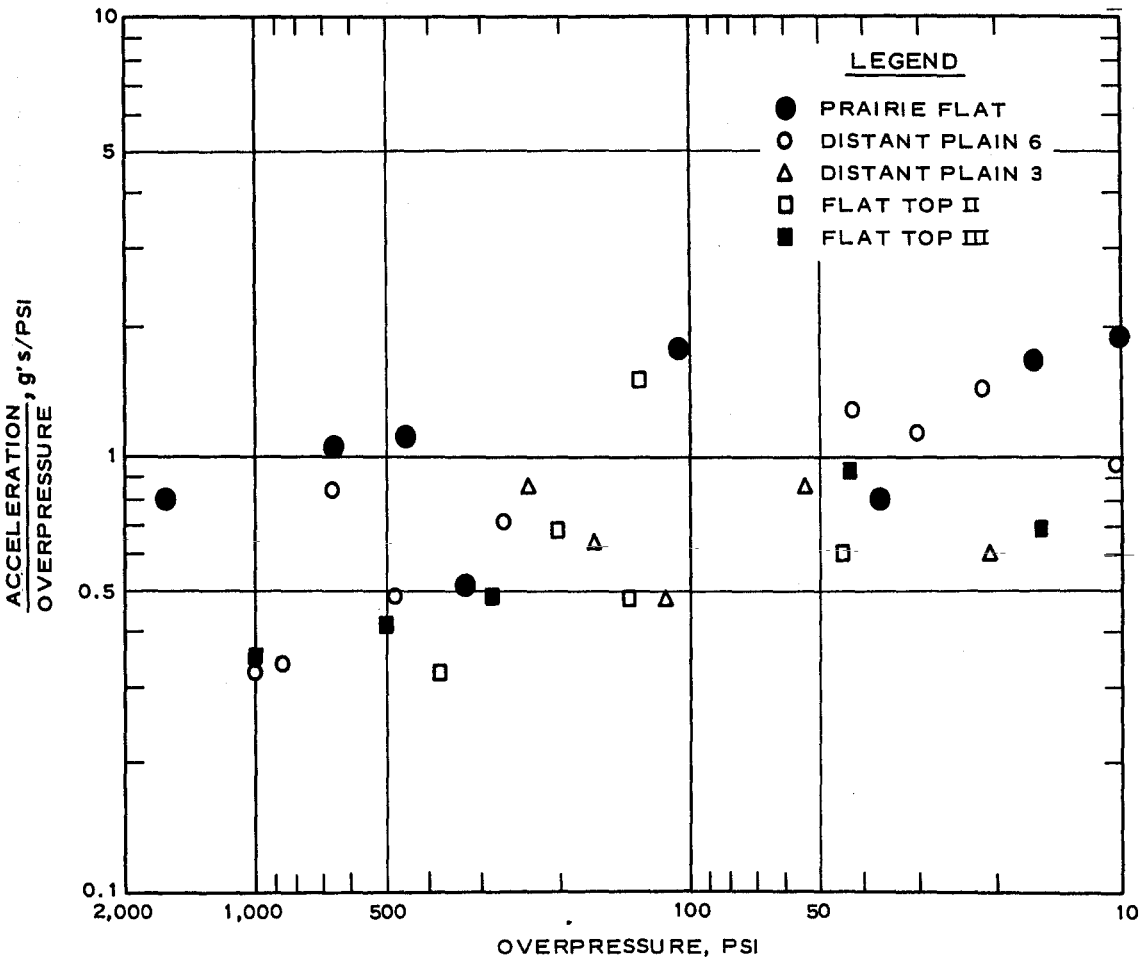

Figure 3.4 Correlation of vertical acceleration data with airblast, 1.5-foot depths.

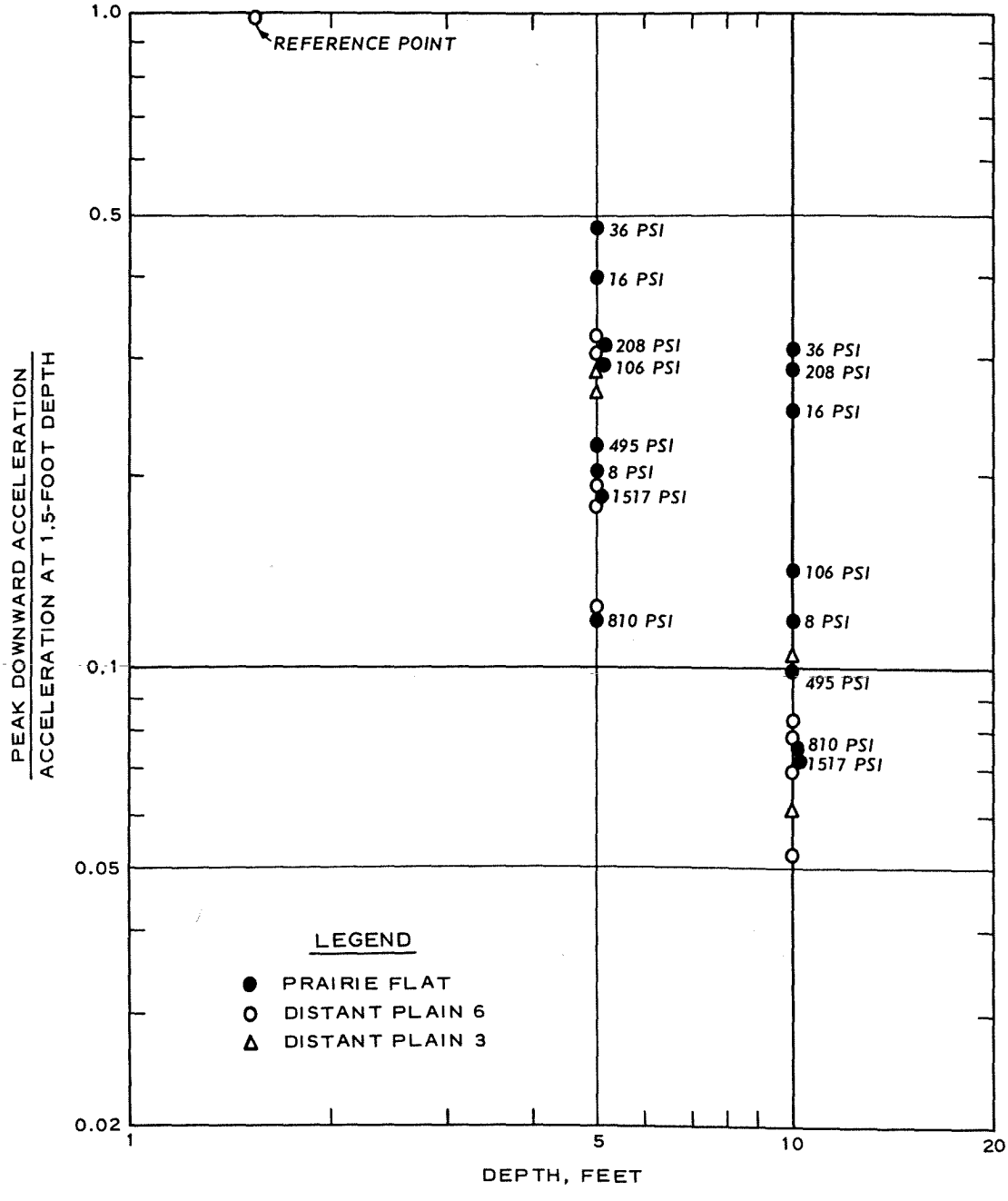

Figure 3.5 Vertical acceleration attenuation with depth.

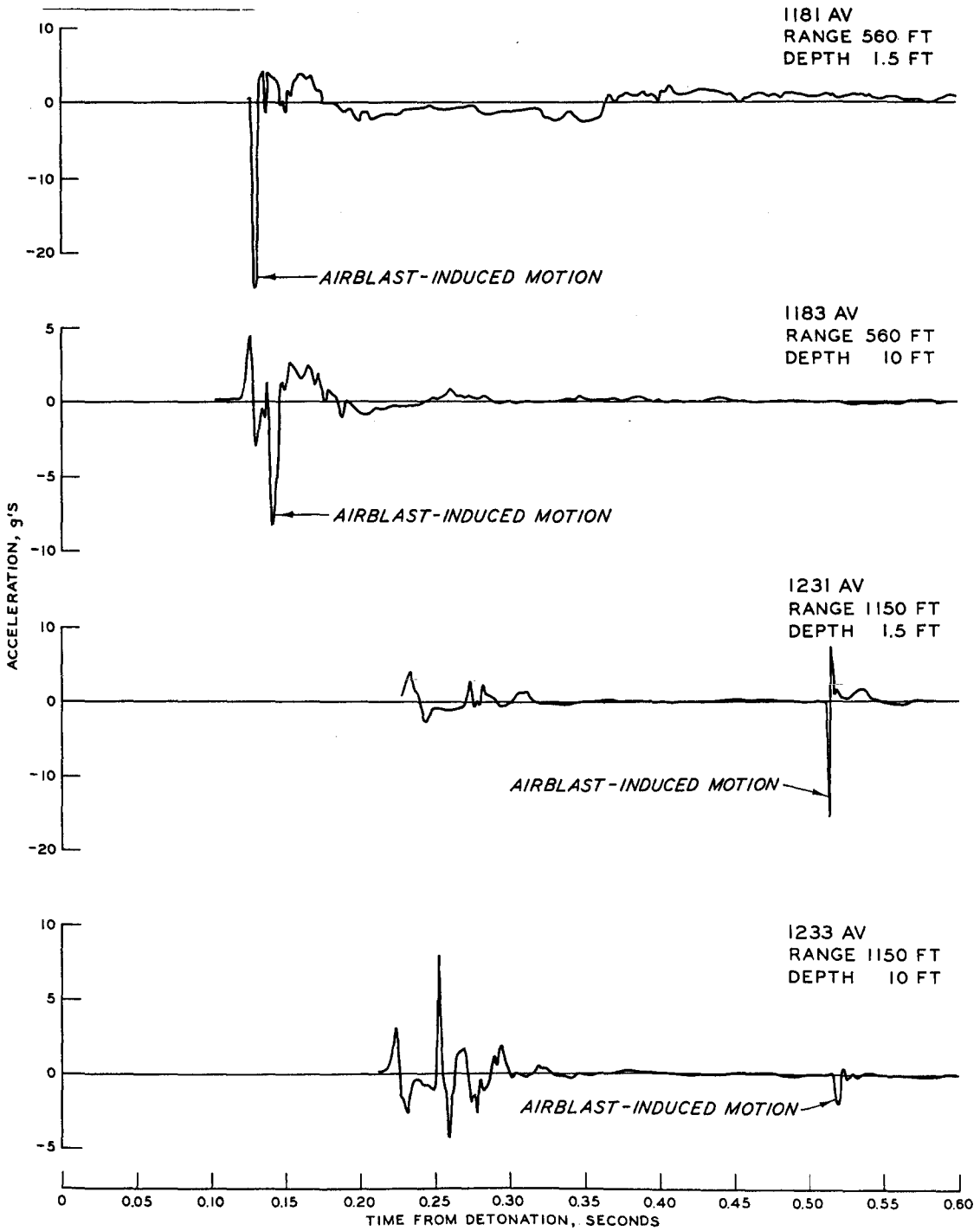

Figure 3.6 Vertical acceleration waveforms in outrunning region.

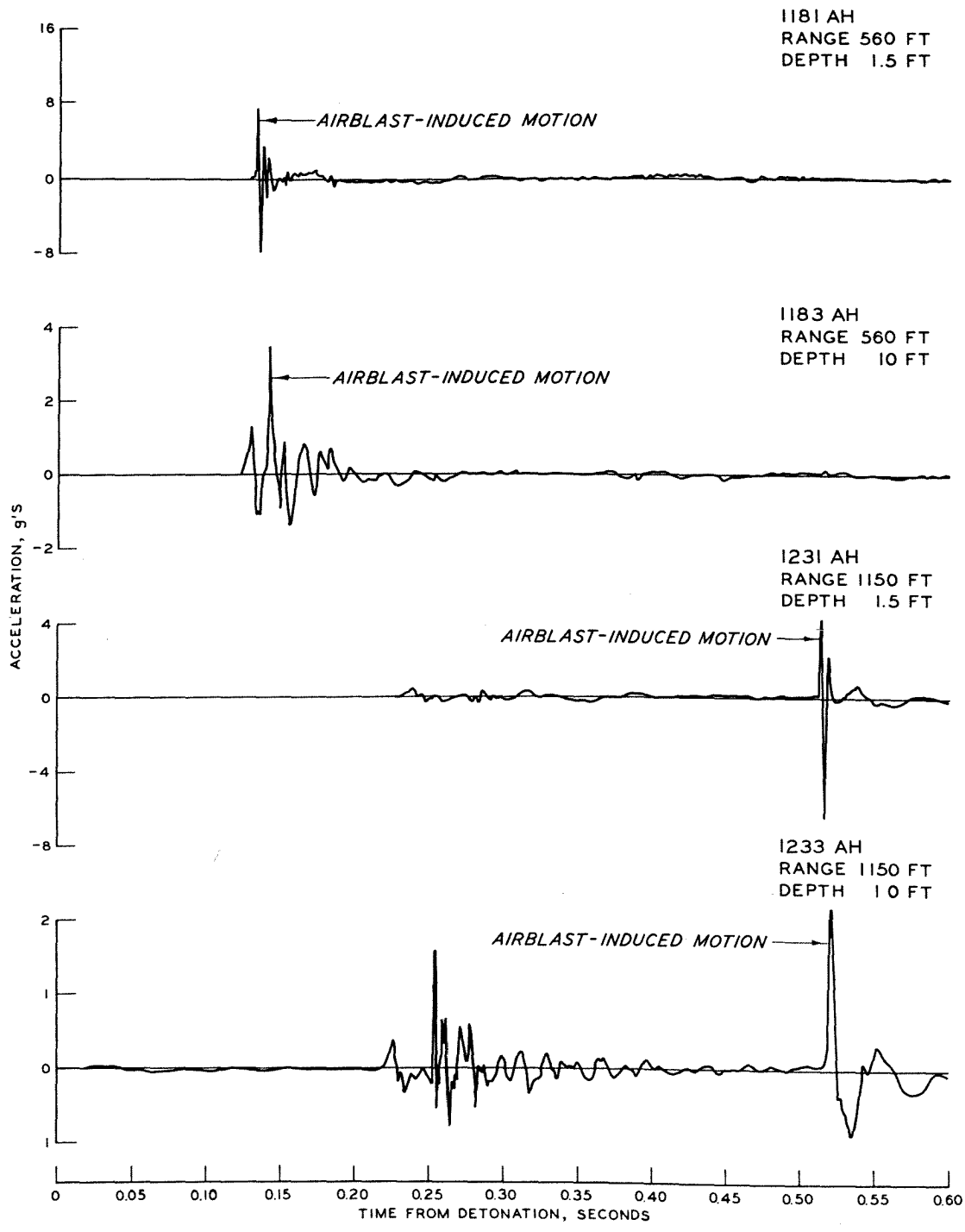

Figure 3.7 Horizontal acceleration waveforms in outrunning region.

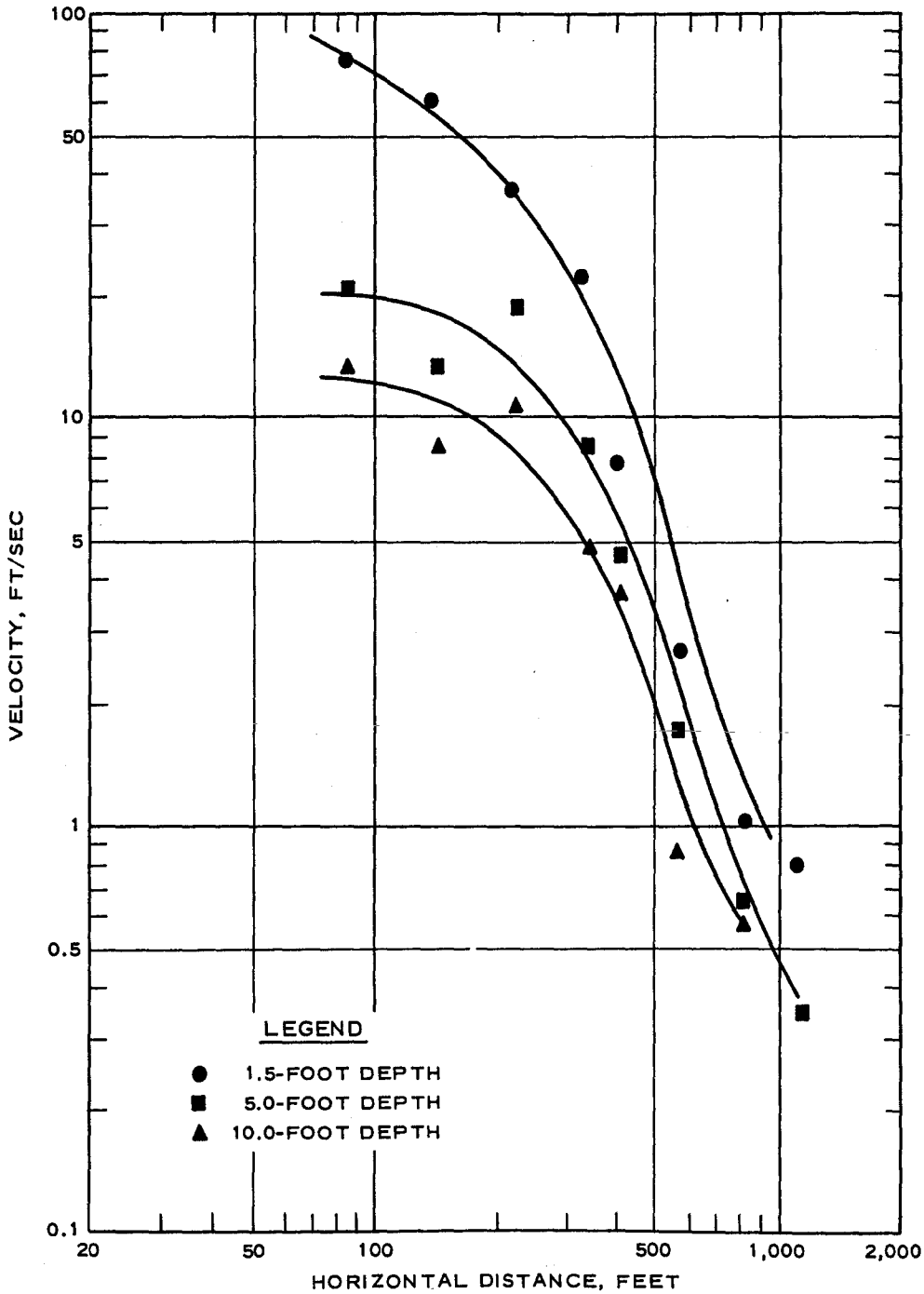

Figure 3.8 Peak airblast-induced (downward) vertical velocity versus distance.

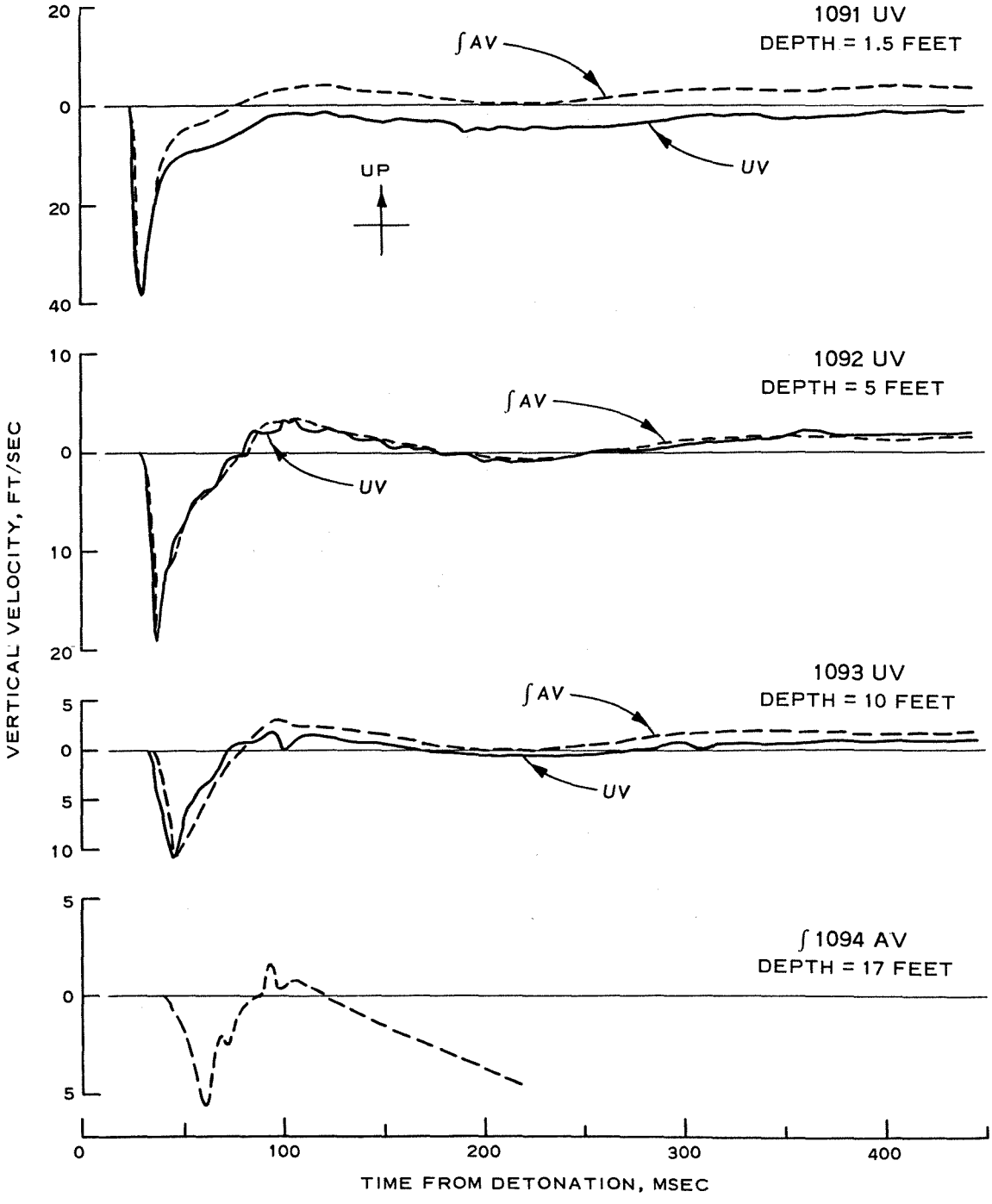

Figure 3.9 Vertical velocity waveforms, 220-foot distance.

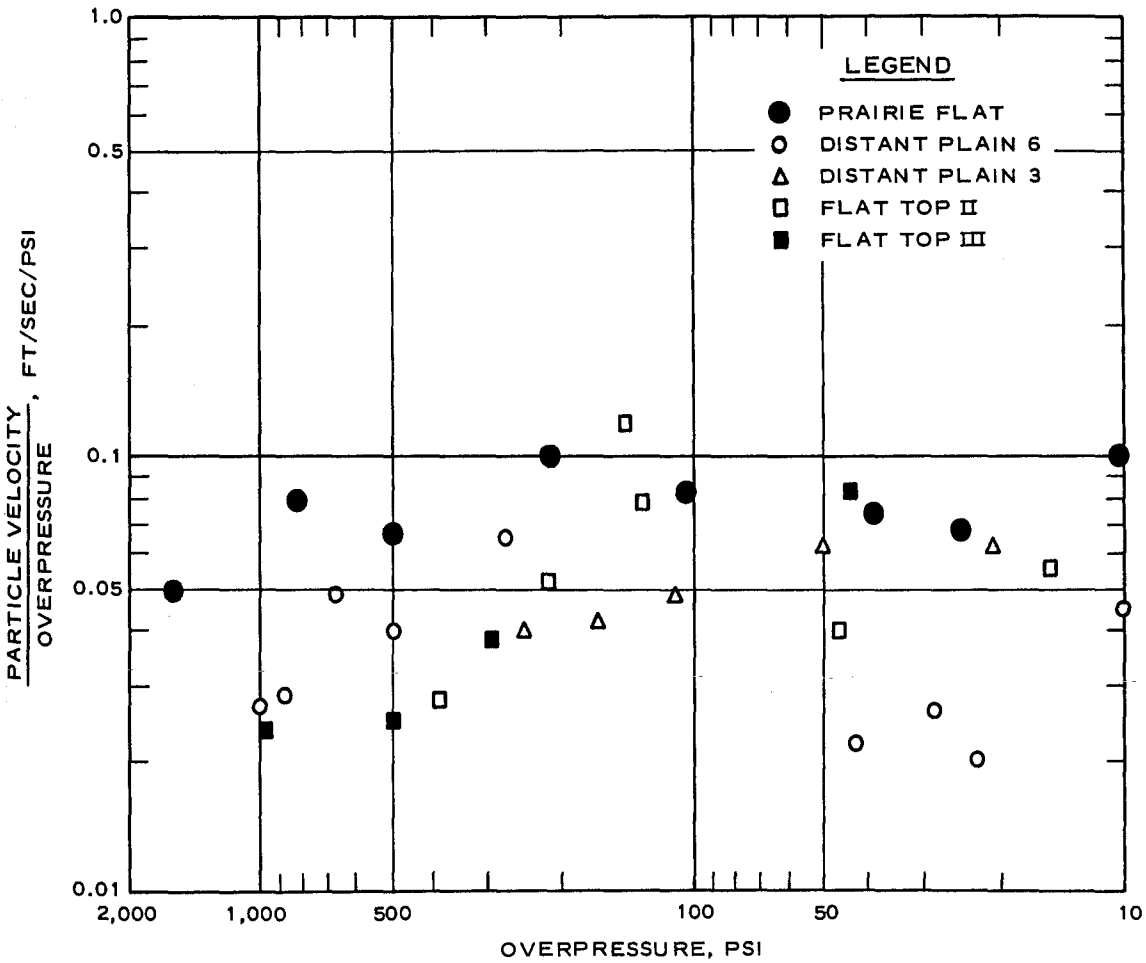

Figure 3.10 Correlation of vertical velocity with airblast, 1.5-foot depth.

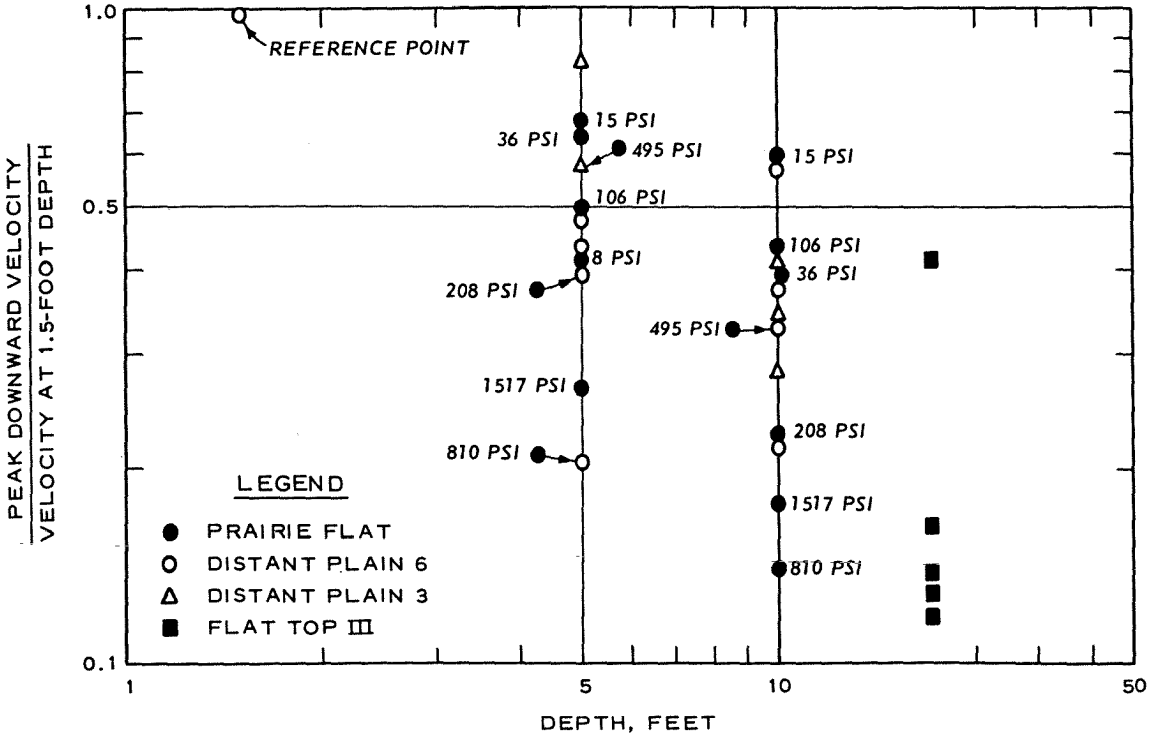

Figure 3.11 Vertical velocity attenuation with depth.

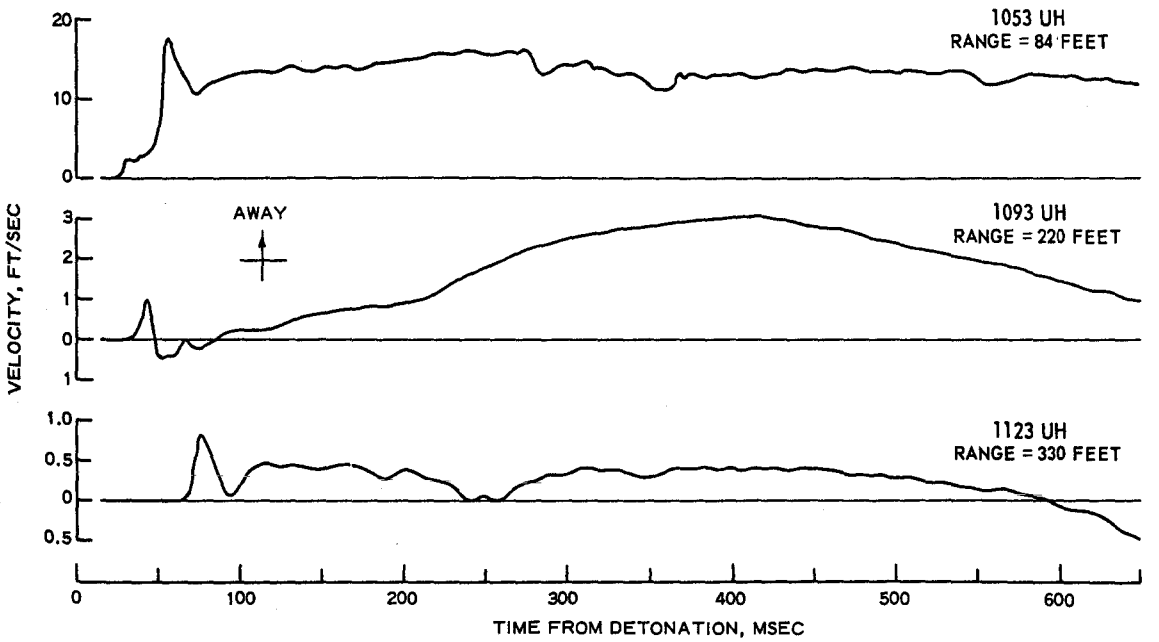

Figure 3.12 Horizontal velocity waveforms at 10-foot depth.

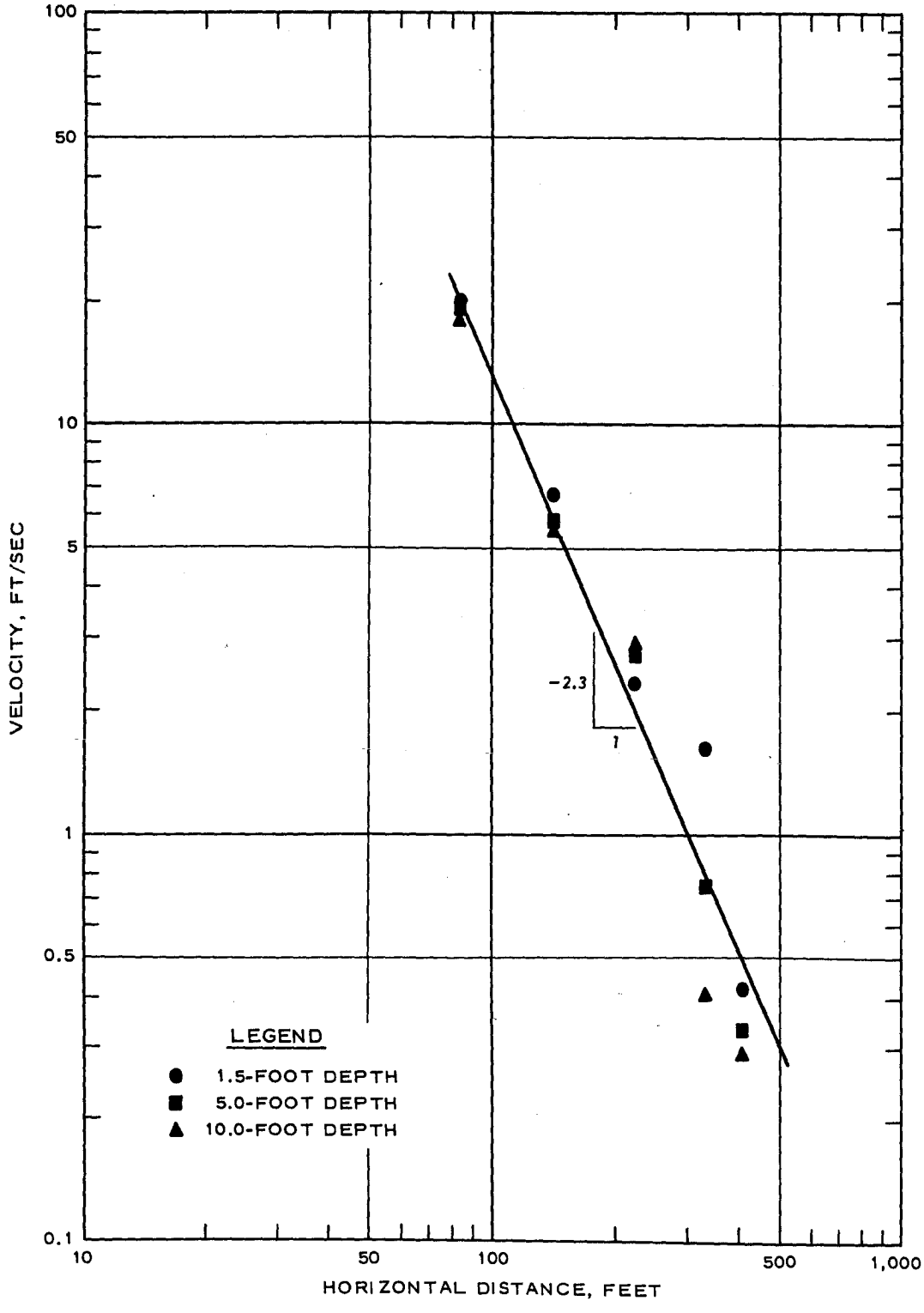

Figure 3.13 Peak horizontal cratering-induced (outward) velocity attenuation with distance.

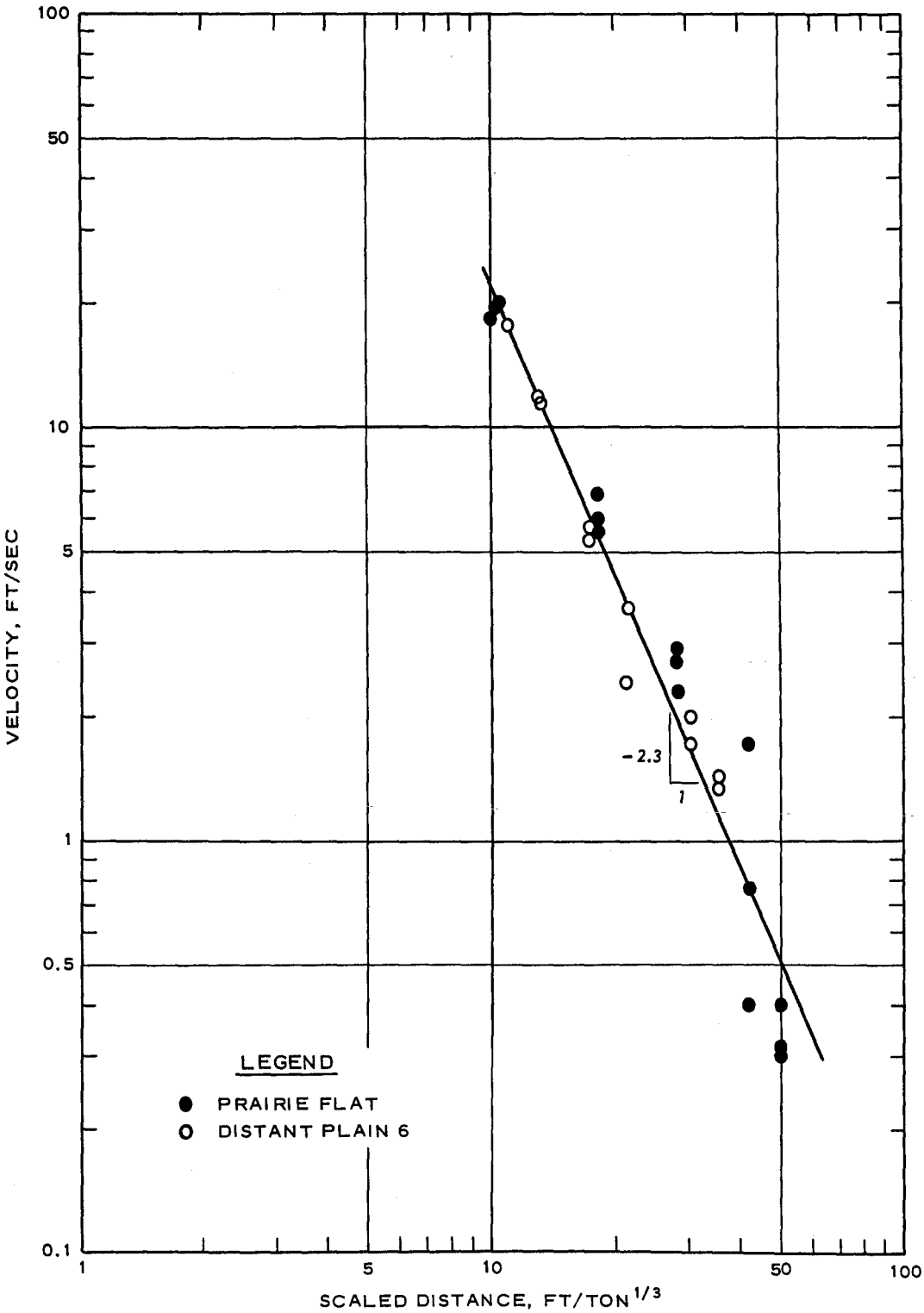

Figure 3.14 Peak cratering-induced (outward) horizontal velocity versus scaled distance.

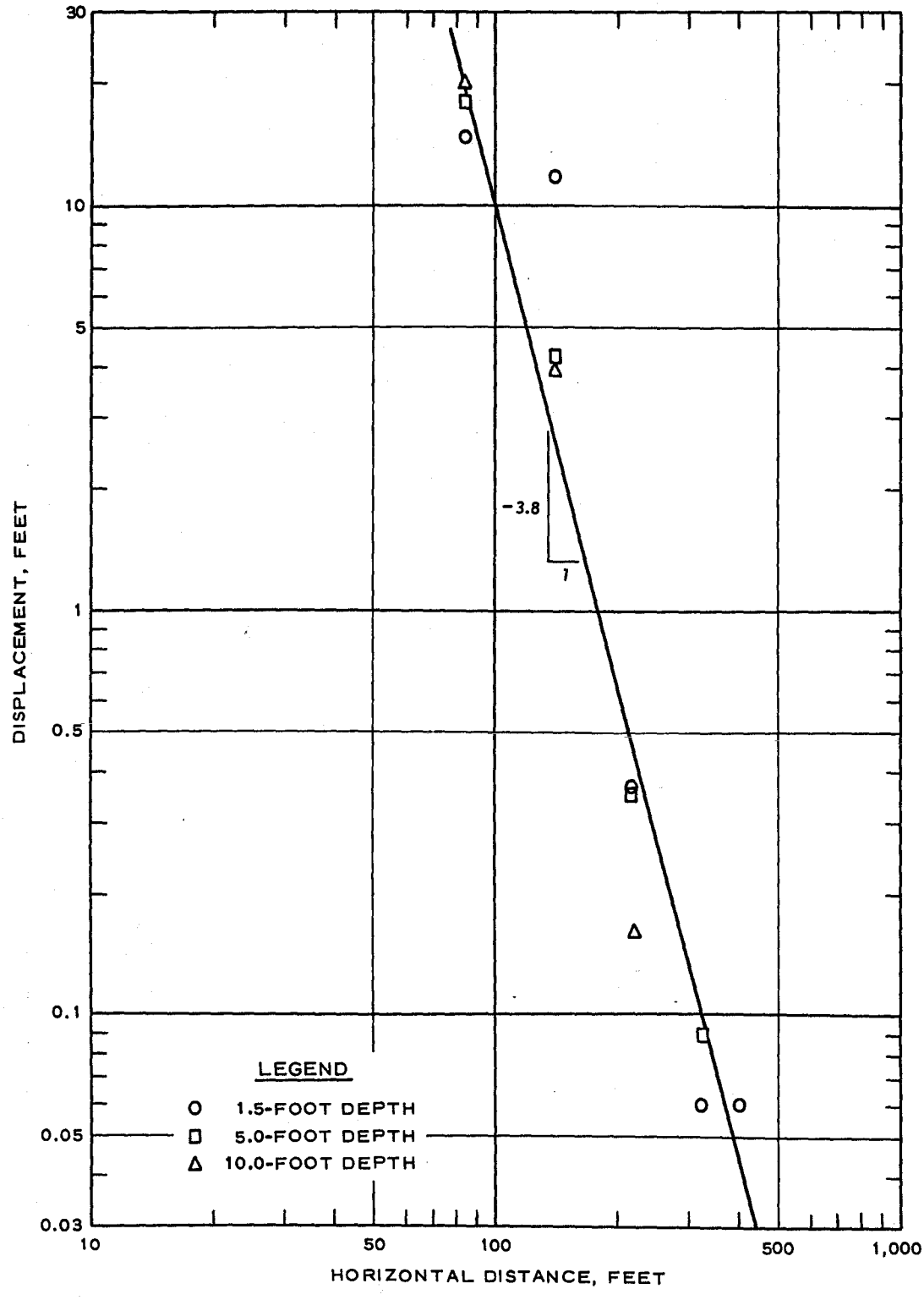

Figure 3.15 Peak transient upward displacement versus distance.

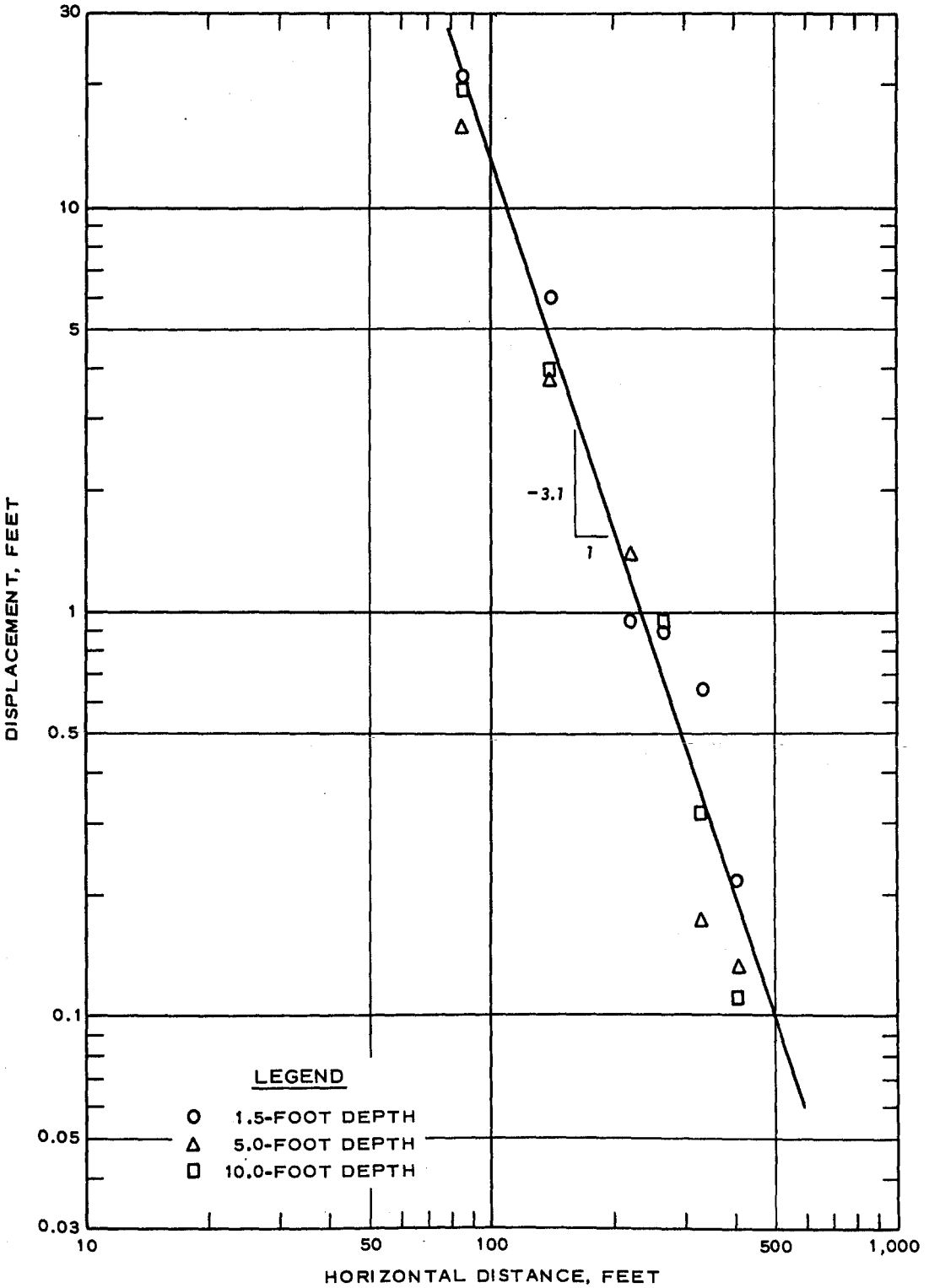

Figure 3.16 Peak transient outward displacement versus distance.

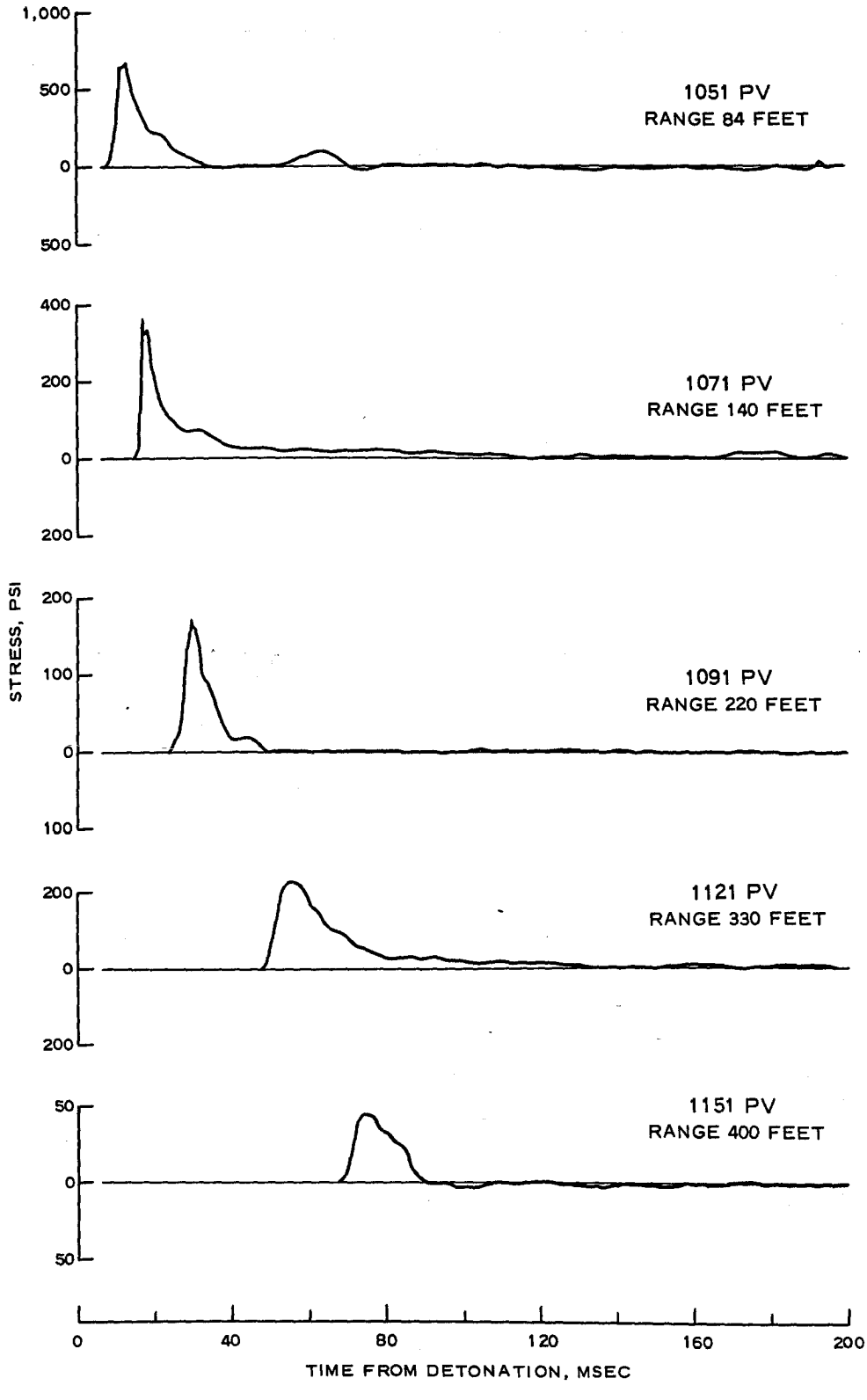

Figure 3.17 Vertical stress-time histories, 1.5-foot depth.

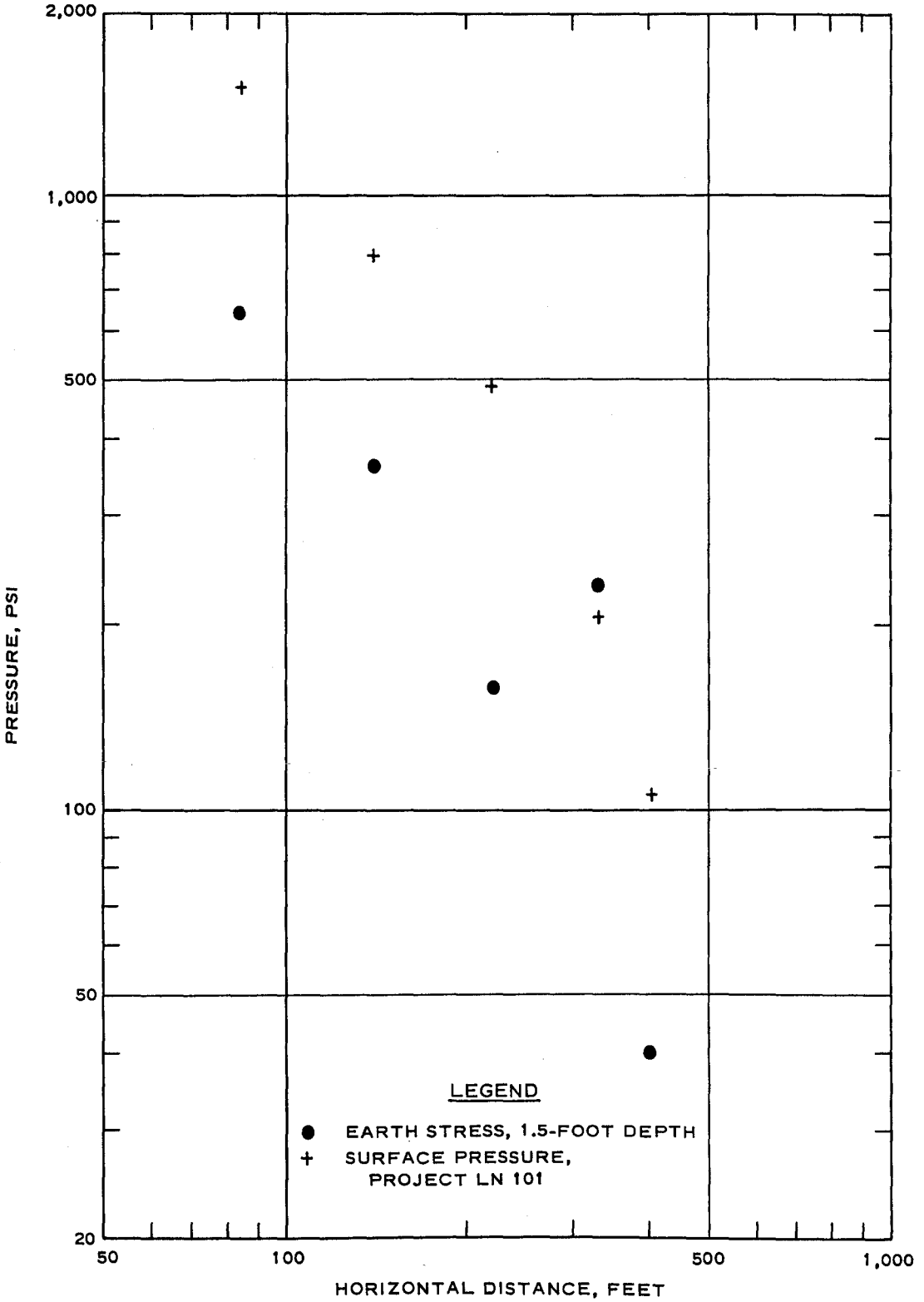

Figure 3.18 Vertical stress versus distance, 1.5-foot depth.

CHAPTER 4

CONCLUSIONS

Overall performance of motion gages for Prairie Flat was excellent. Stress gage performance was less satisfactory due to apparent placement or coupling problems, especially at intermediate depths.

Arrival times were obtained for nearly all gages installed. These were used primarily to construct a shock front profile. From this profile, the spatial development of outrunning ground motion was determined, and it was observed that outrunning conditions first appeared at the ground surface at a distance of about 560 feet, or the 35-psi overpressure level.

Peak vertical accelerations were found to attenuate sharply with both distance and depth, varying over the range of distances and depths instrumented from 1,200 to 1.9 g's. The ratio of acceleration to overpressure was used as a correlating factor for comparison with Distant Plain and Flat Top data. This ratio was noted to be both pressure and yield dependent, decreasing for both higher pressures and smaller yields. These effects had both been predicted. Attenuation of vertical acceleration was also found to be pressure dependent, with more rapid attenuation at higher pressures.

Peak vertical velocities also attenuated sharply with distance and depth, although to a somewhat lesser degree than did accelerations. Peak downward velocities varied from 84 to 0.33 ft/sec over the intervals instrumented. Peak vertical velocities were also correlated on the basis of motion to overpressure ratios, and again the ratios were observed to be pressure and yield dependent, decreasing for smaller yields and higher pressures. Attenuation with depth was also found to be dependent on pressure, being more rapid at higher pressures.

Peak horizontal velocities were compared with those measured on Distant Plain Event 6 by means of cube-root scaling. Excellent agreement, with little data scatter, was noted for the two events. These velocities varied from about 20 ft/sec at the 84-foot range to 0.3 ft/sec at the 400-foot range. There was essentially no attenuation with depth.

Both vertical and horizontal displacements were calculated from

velocity measurements. Peak transient displacements in both directions were 20 feet at the 84-foot range. The upward vertical displacement, however, attenuated more rapidly with distance so that at a range of 400 feet it was only one-half of the horizontal.

Soil stress measurements were generally of a mixed quality. Only at the 1.5- and 30-foot depths were the data of uniformly good quality. Data at the other locations were much lower than predicted, which degraded the data from a signal-to-noise standpoint. Peak vertical stresses at the 1.5-foot depth were, with one exception, consistent in averaging 40 percent of the applied overpressure.

APPENDIX A

MOTION-TIME HISTORIES

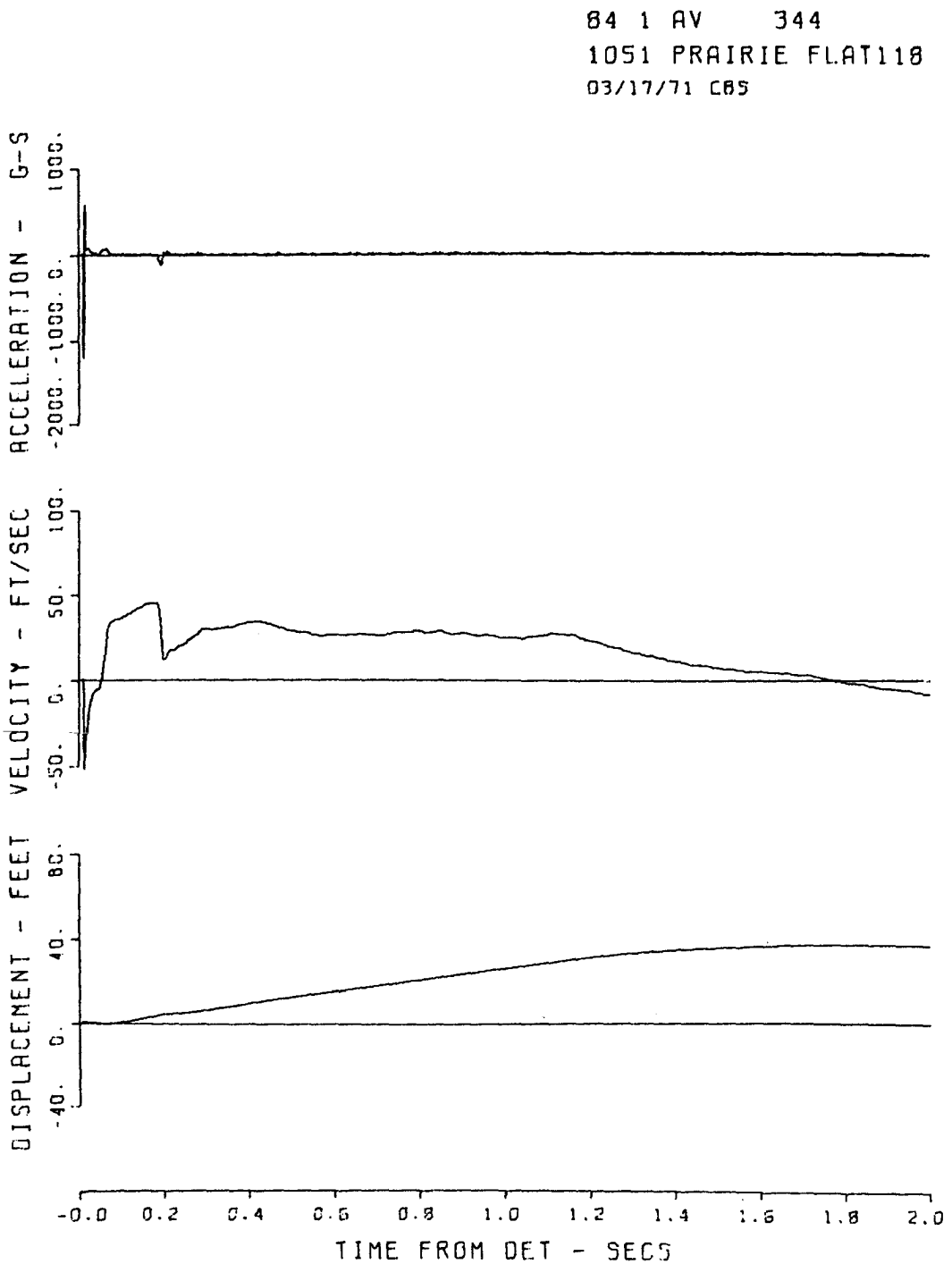

Figure A.1 Gage 1051 AV.

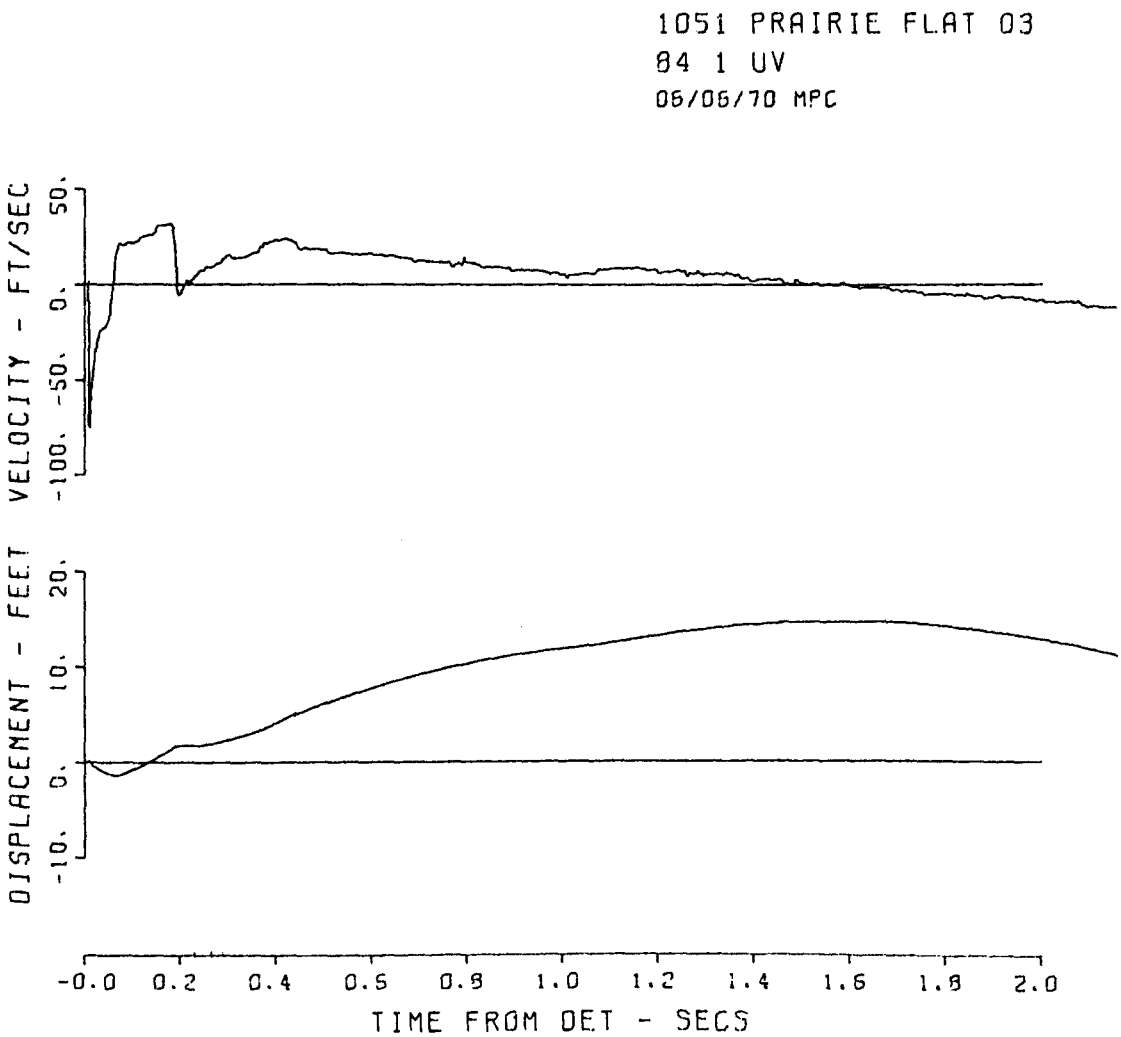

Figure A.2 Gage 1051 UV.

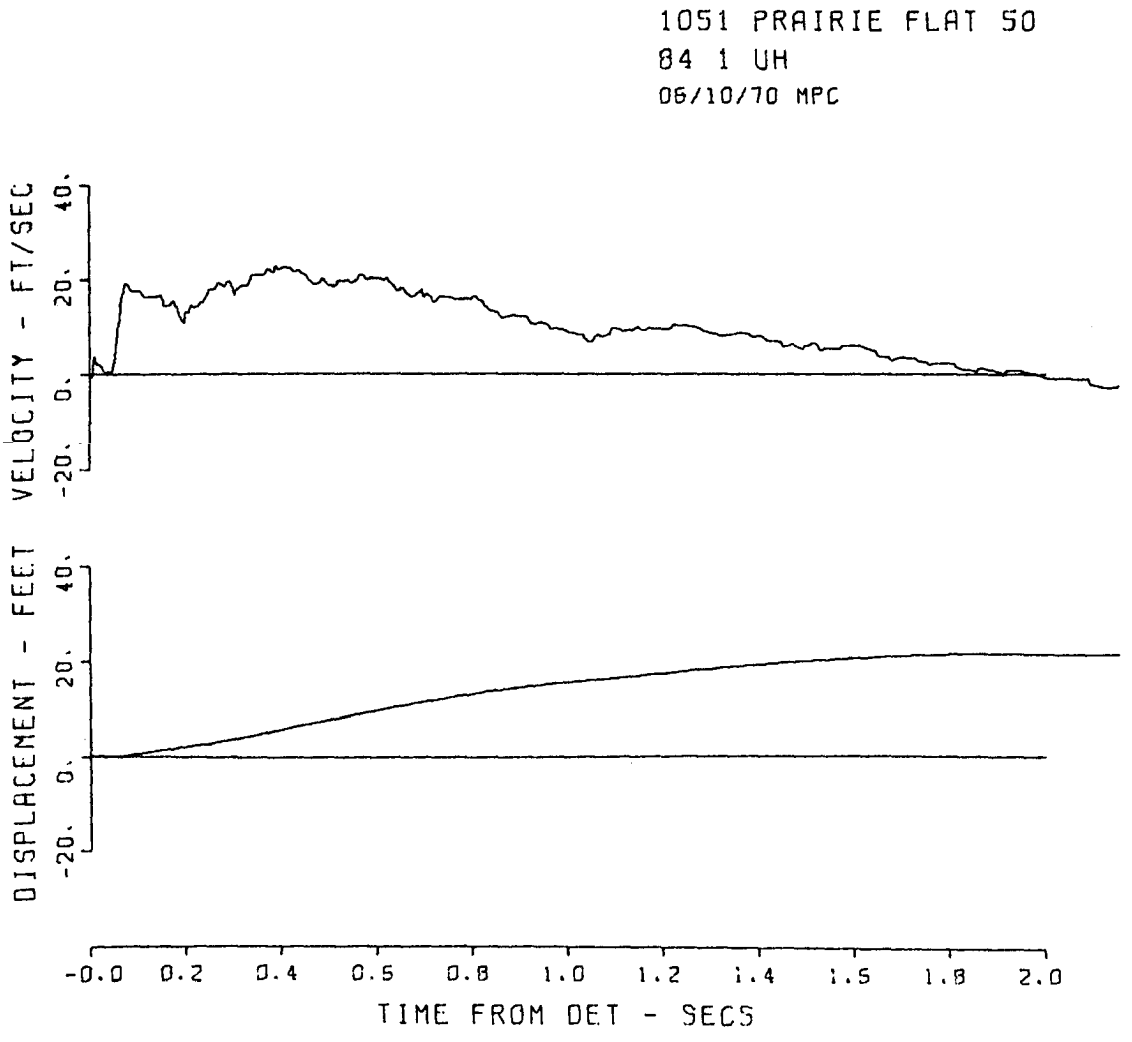

Figure A.3 Gage 1051 UH.

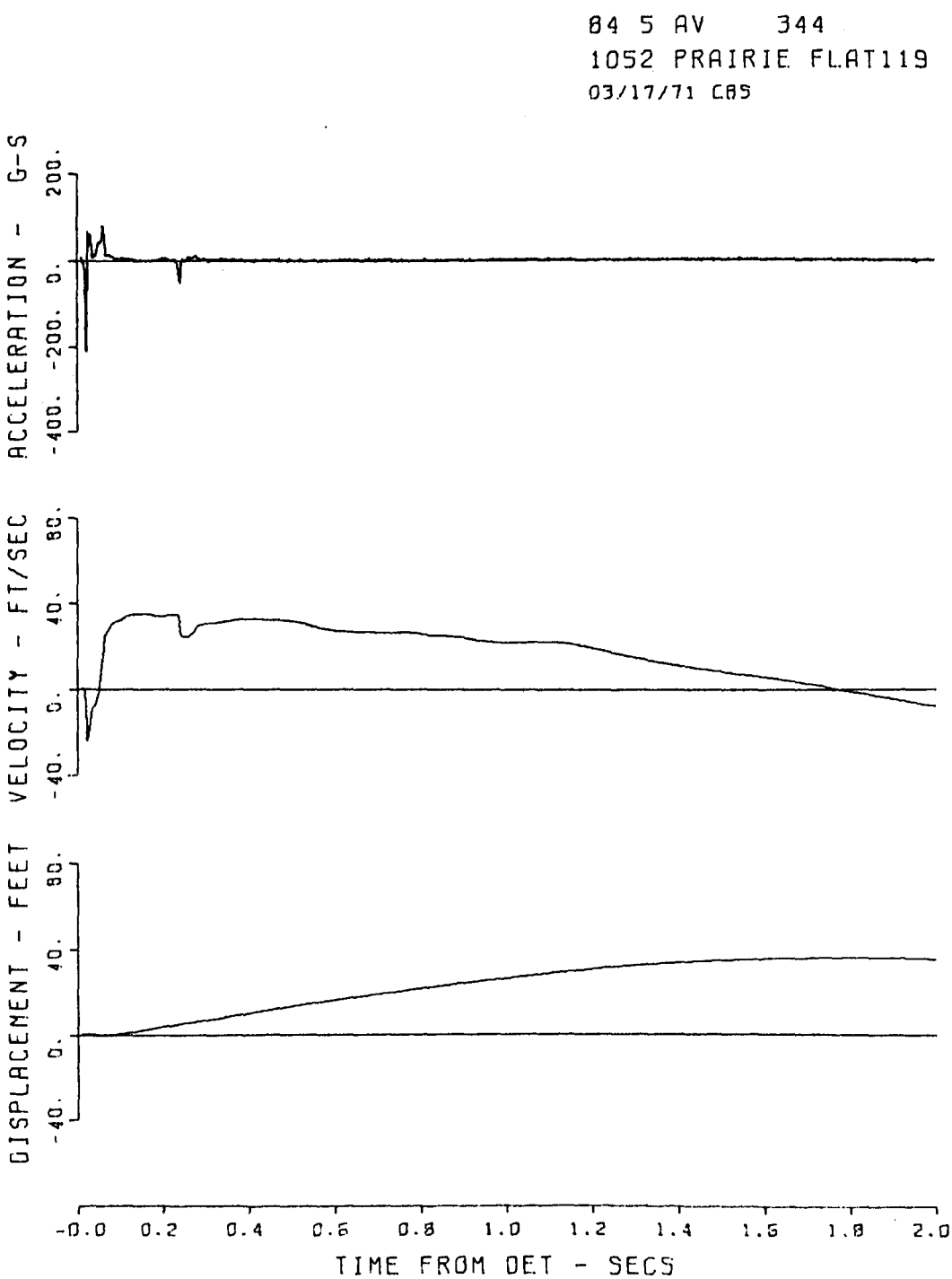

Figure A.4 Gage 1052 AV.

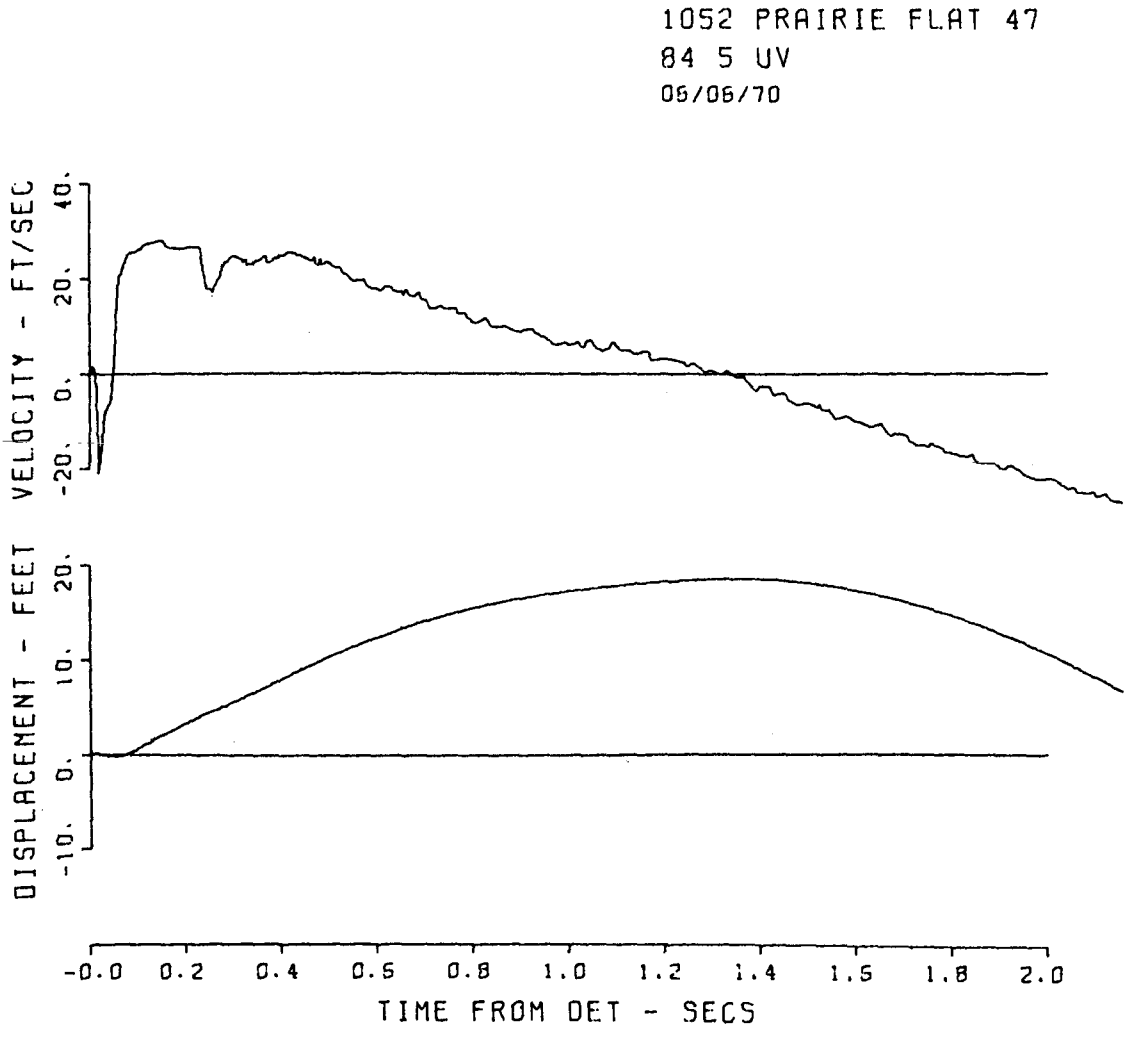

Figure A.5 Gage 1052 UV.

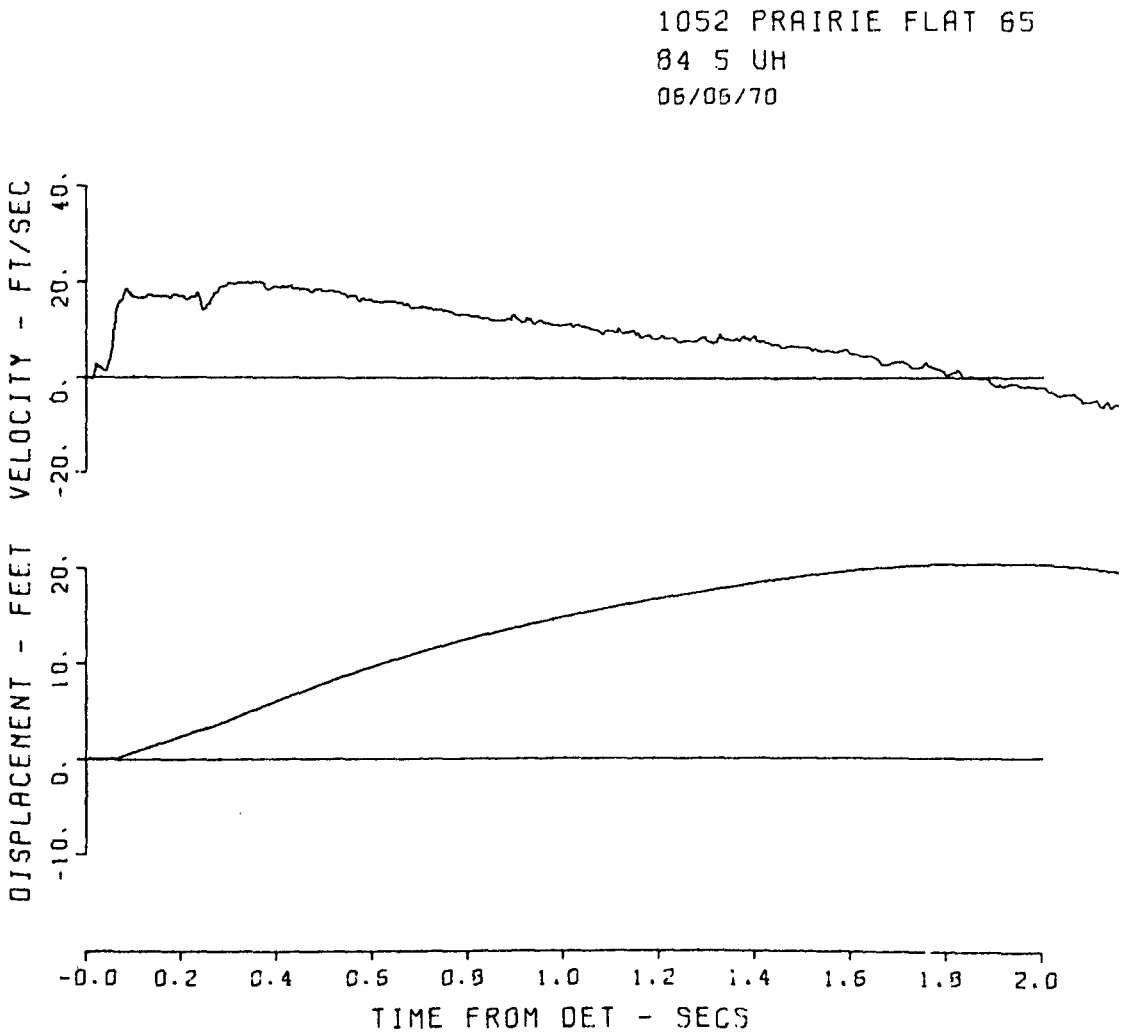

Figure A.6 Gage 1052 UH.

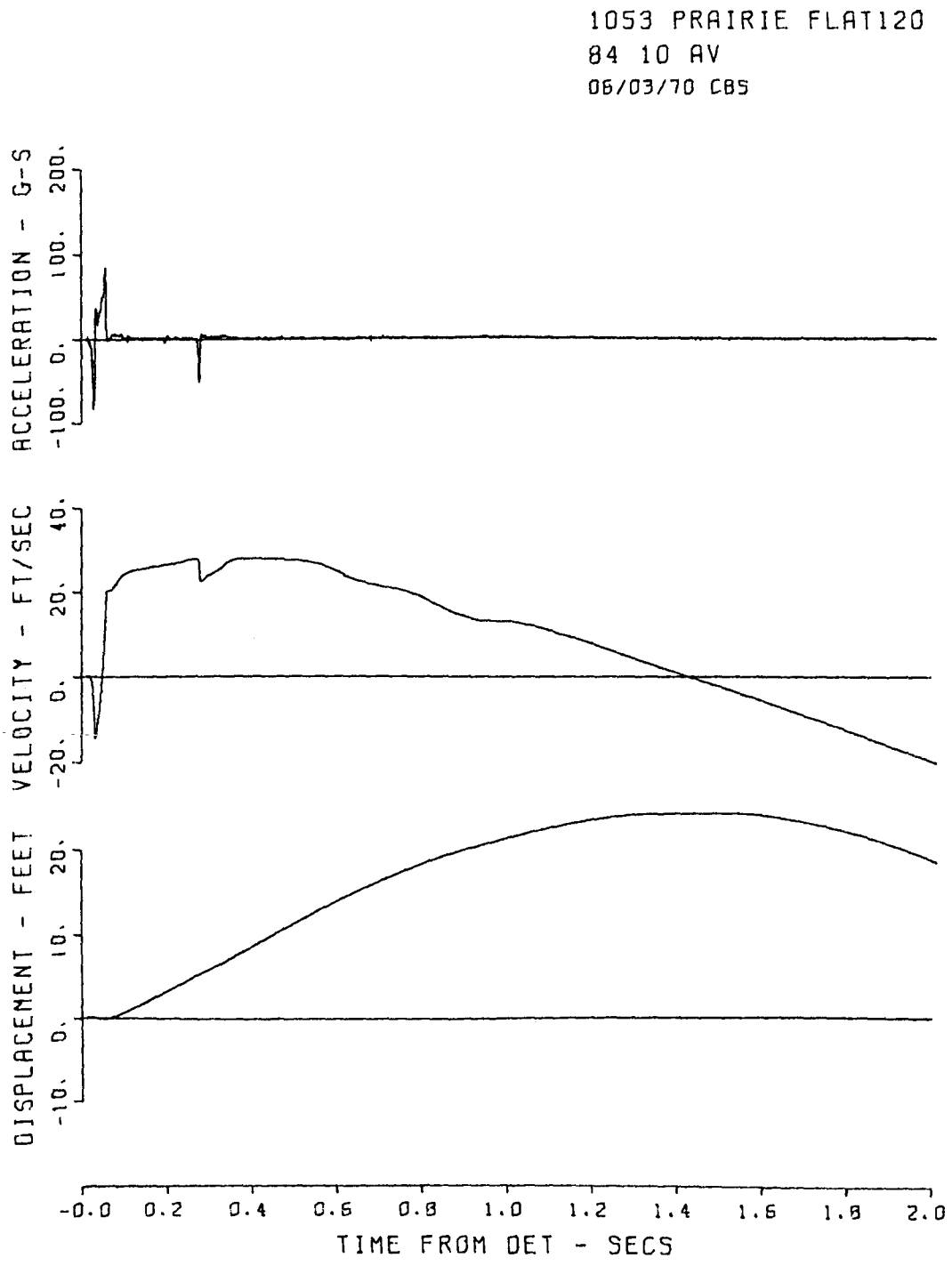

Figure A.7 Gage 1053 AV.

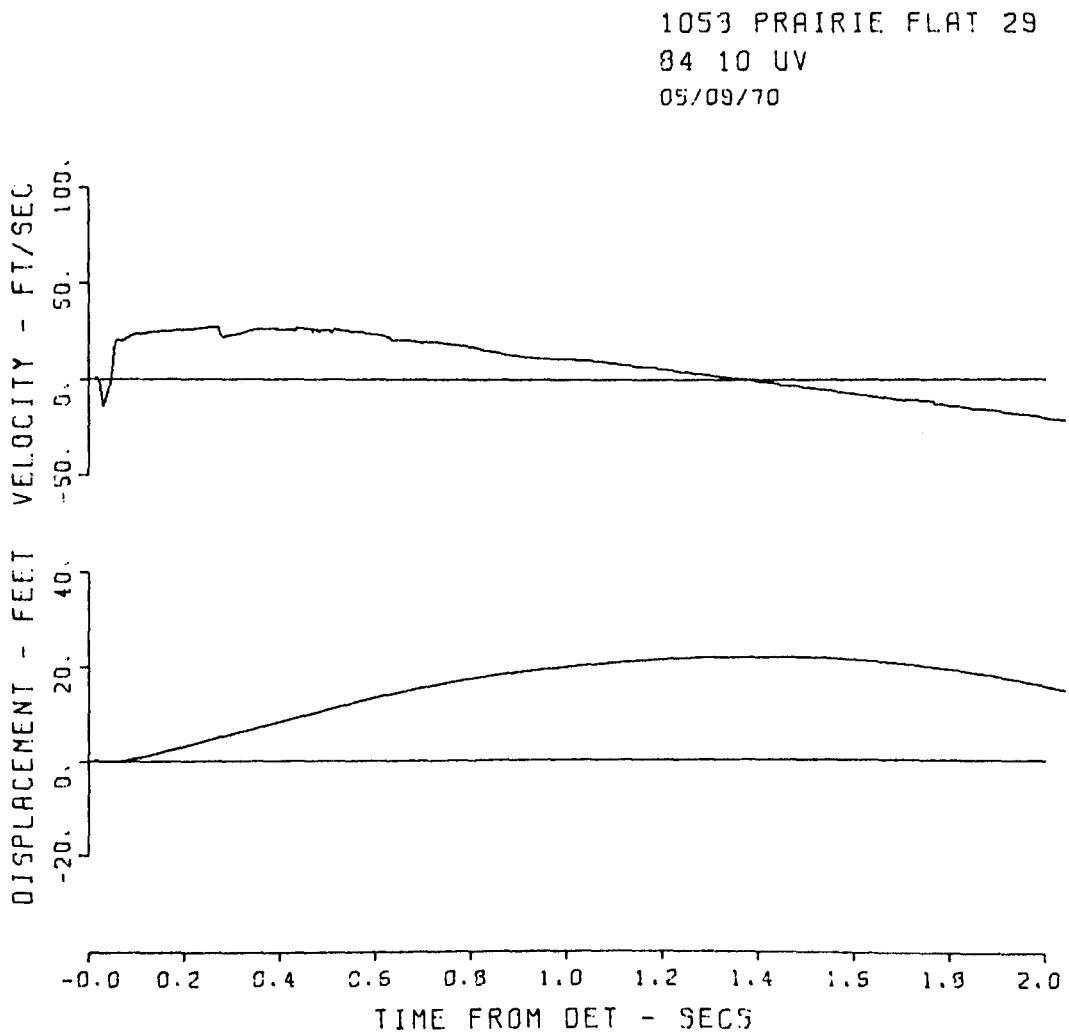

Figure A.8 Gage 1053 UV.

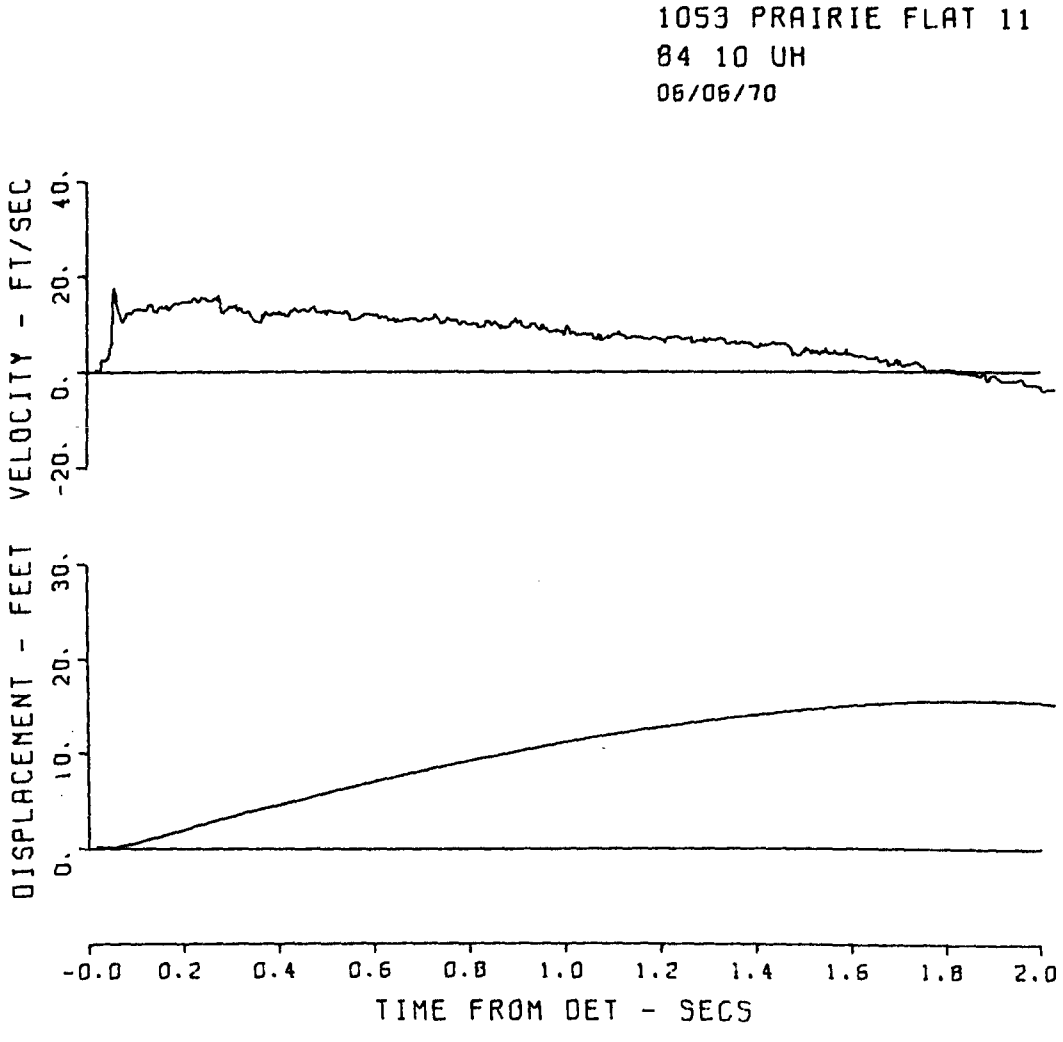

Figure A.9 Gage 1053 UH.

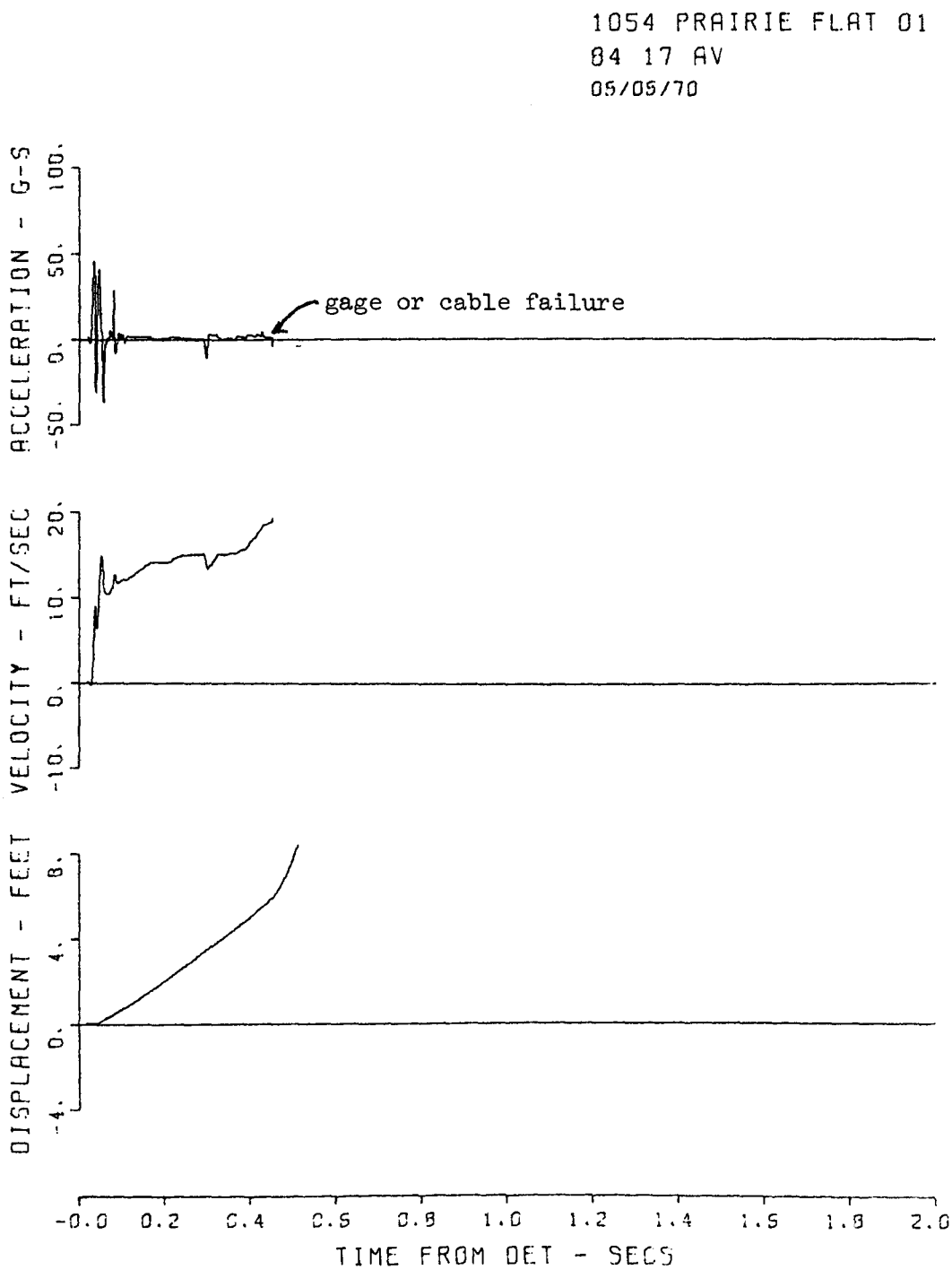

Figure A.10 Gage 1054 AV.

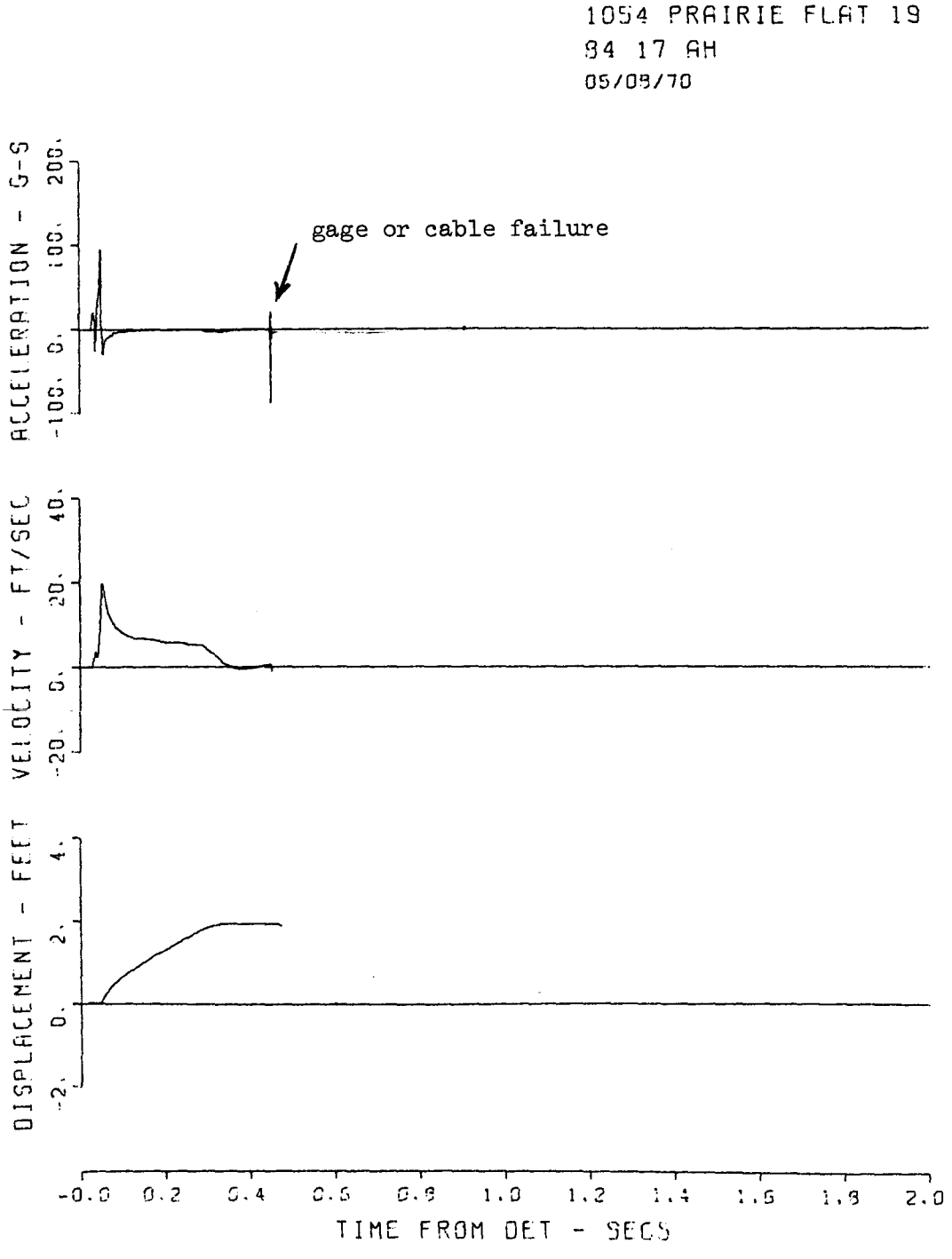

Figure A.11 Gage 1054 AH.

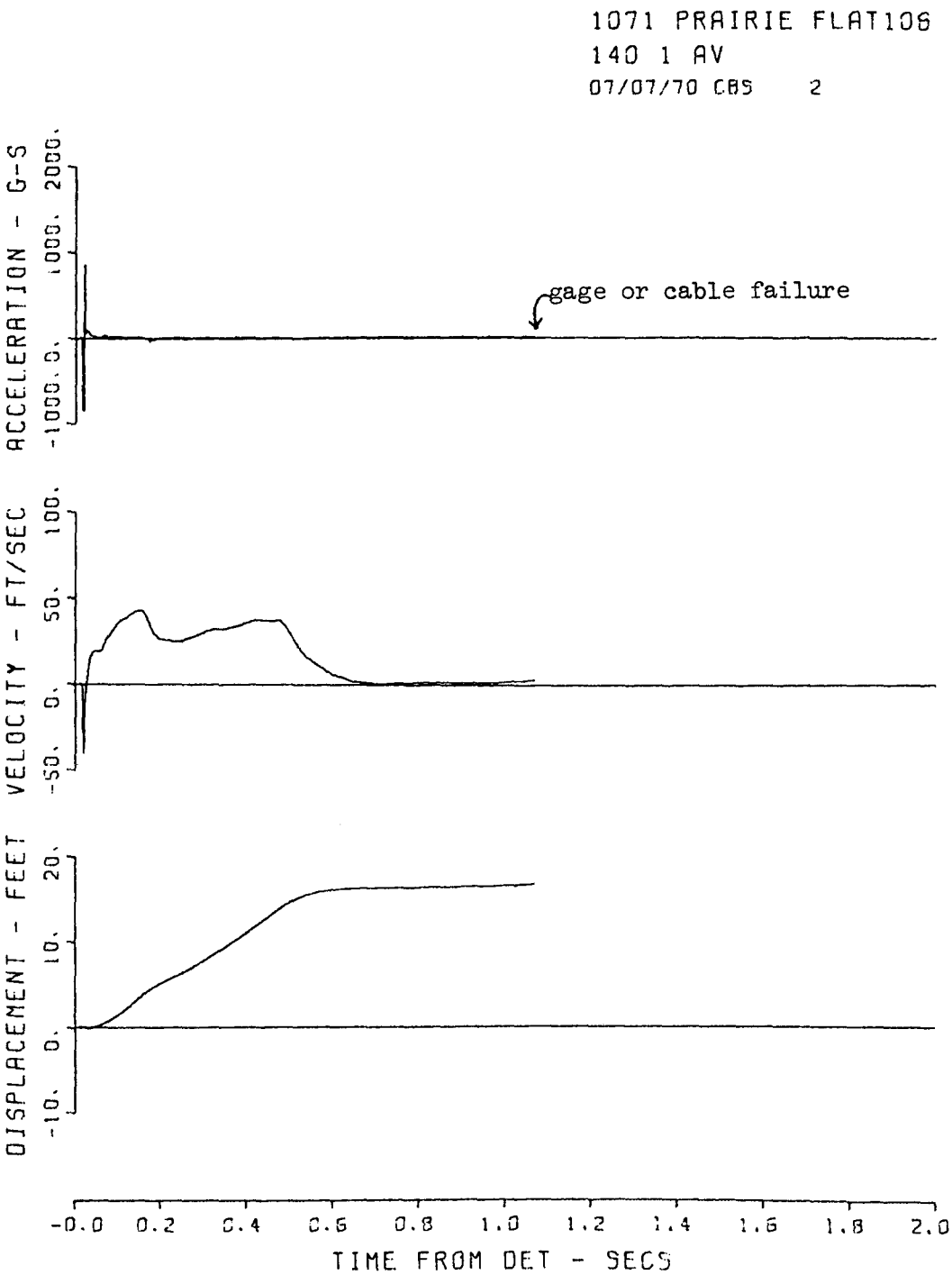

Figure A.12 Gage 1071 AV.

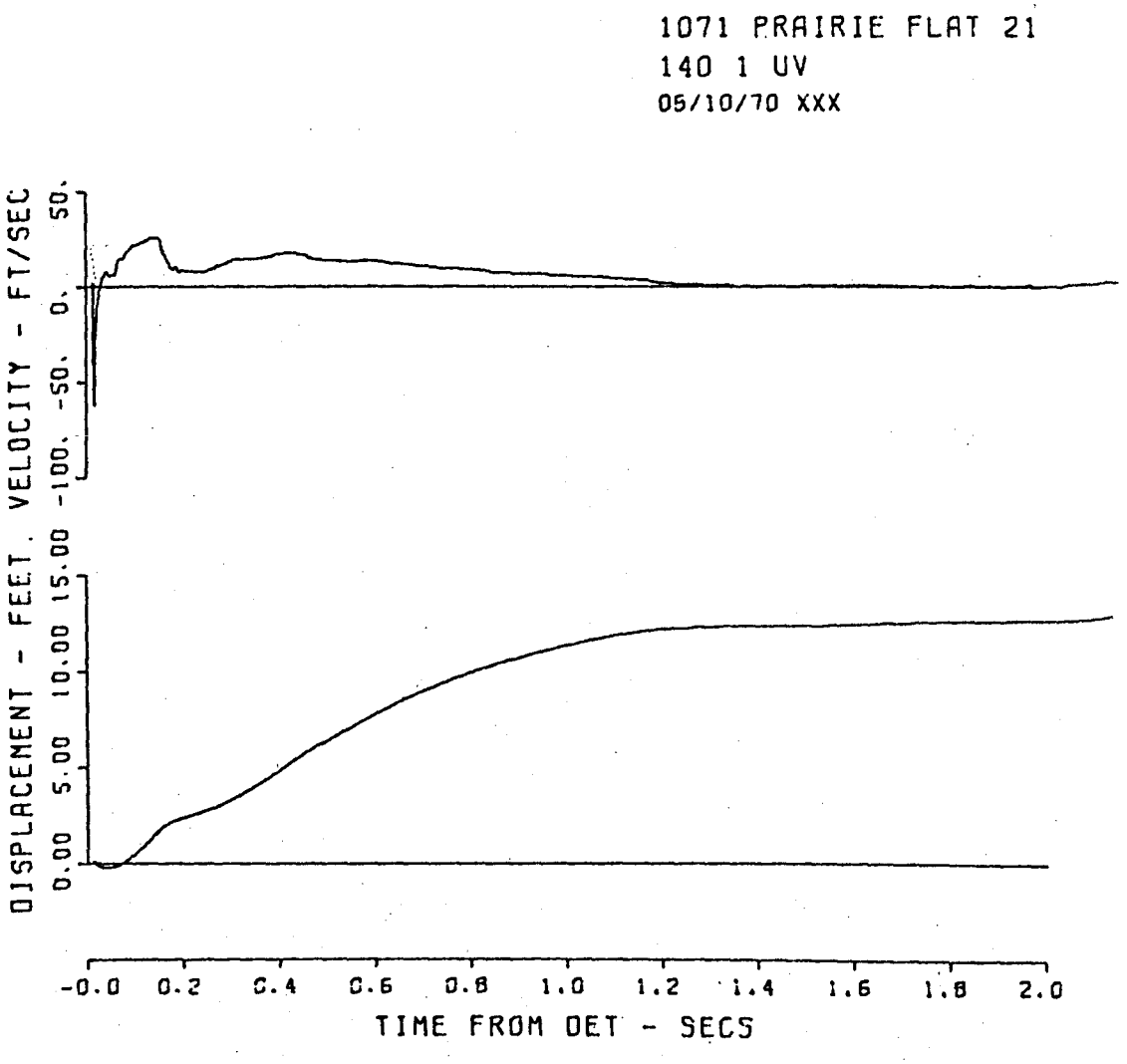

Figure A.13. Gage 1071 UV.

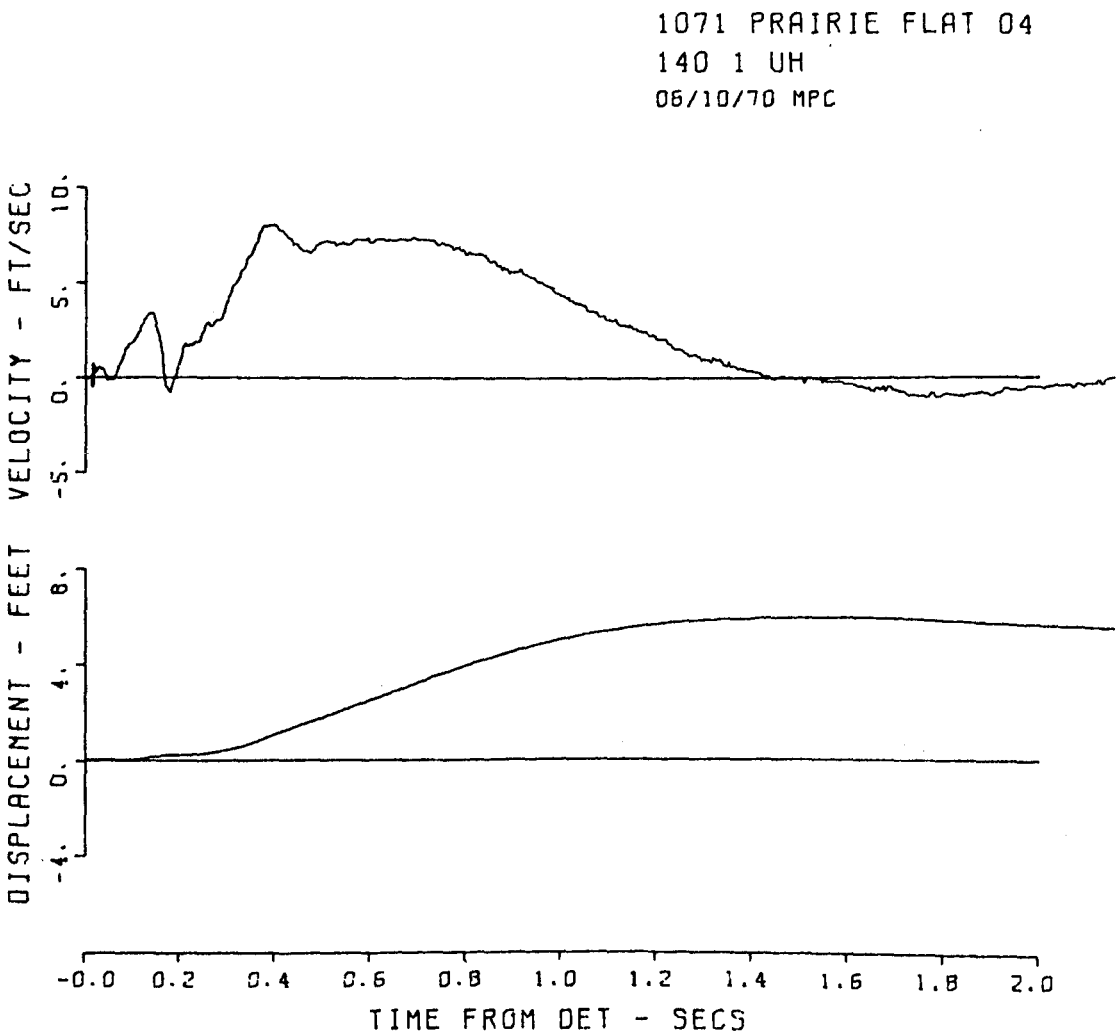

Figure A.14 Gage 1071 UH.

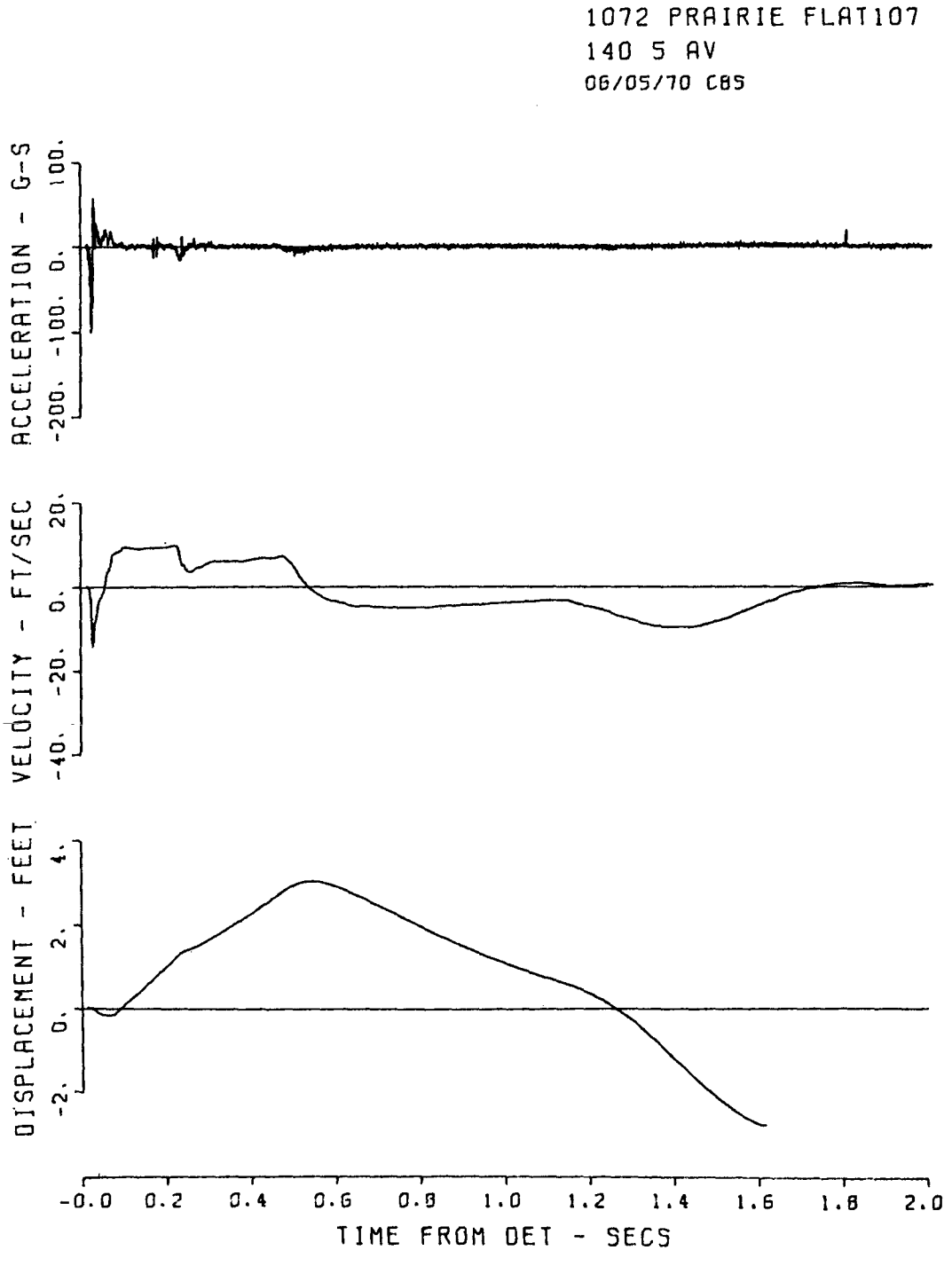

Figure A.15 Gage 1072 AV.

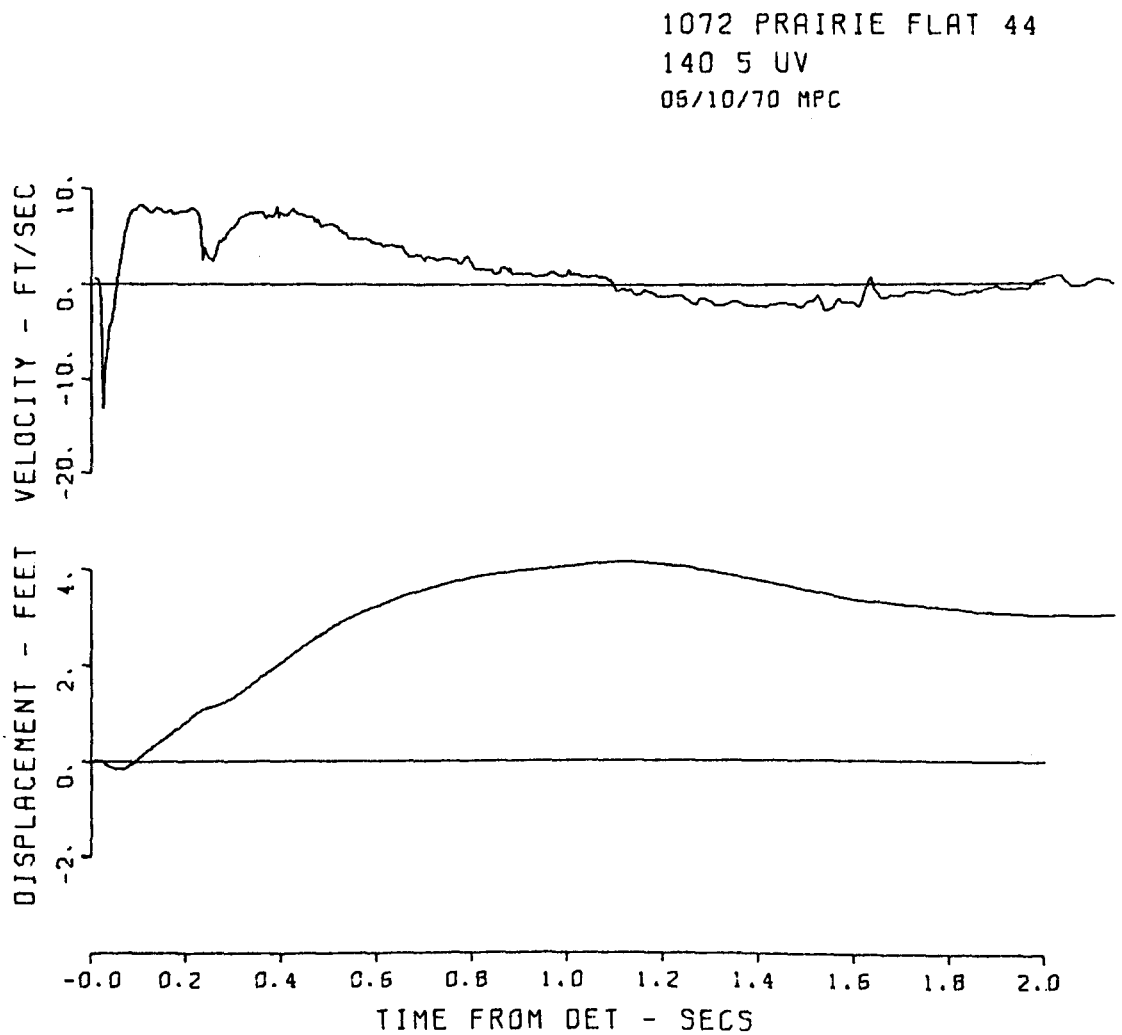

Figure A.16 Gage 1072 UV.

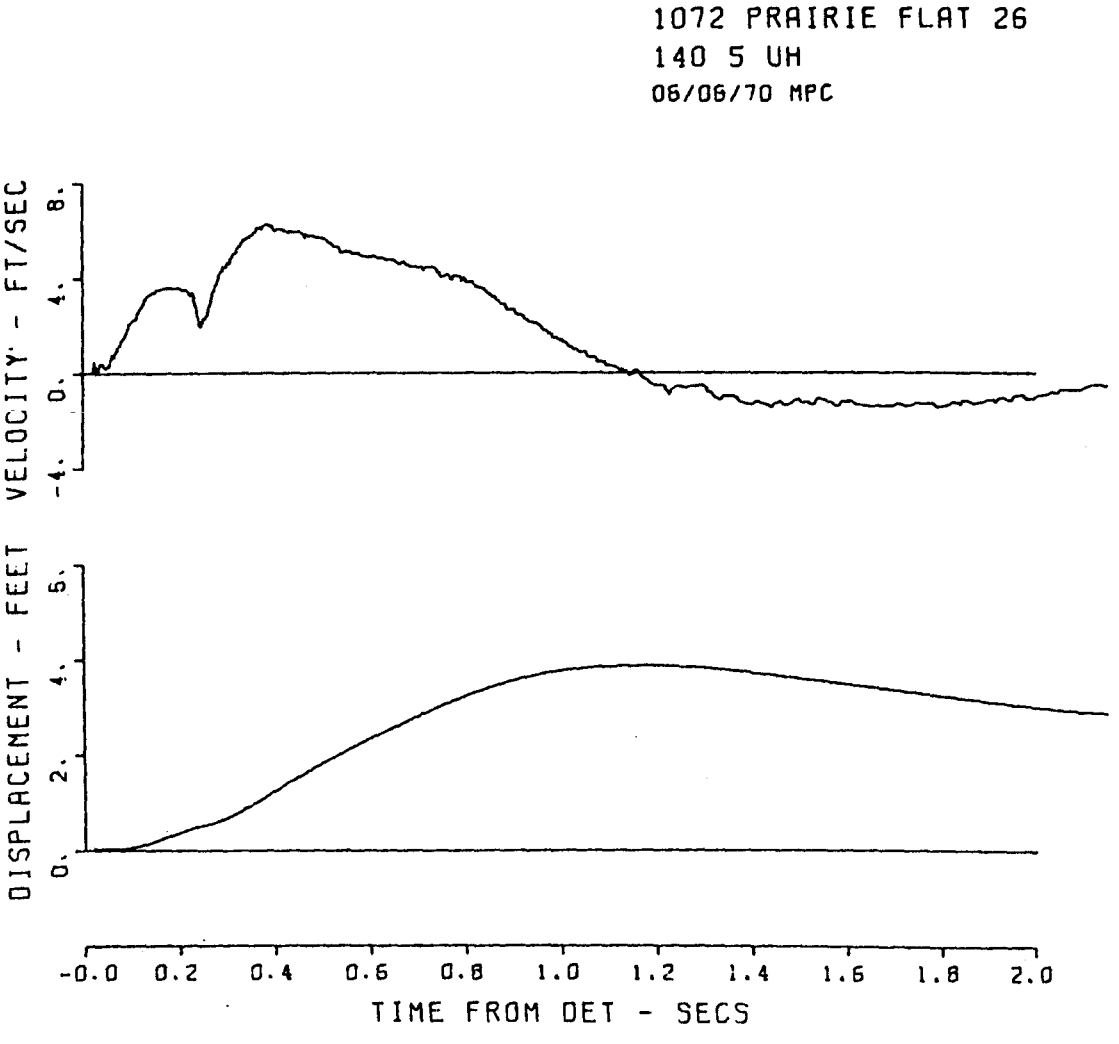

Figure A.17 Gage 1072 UH.

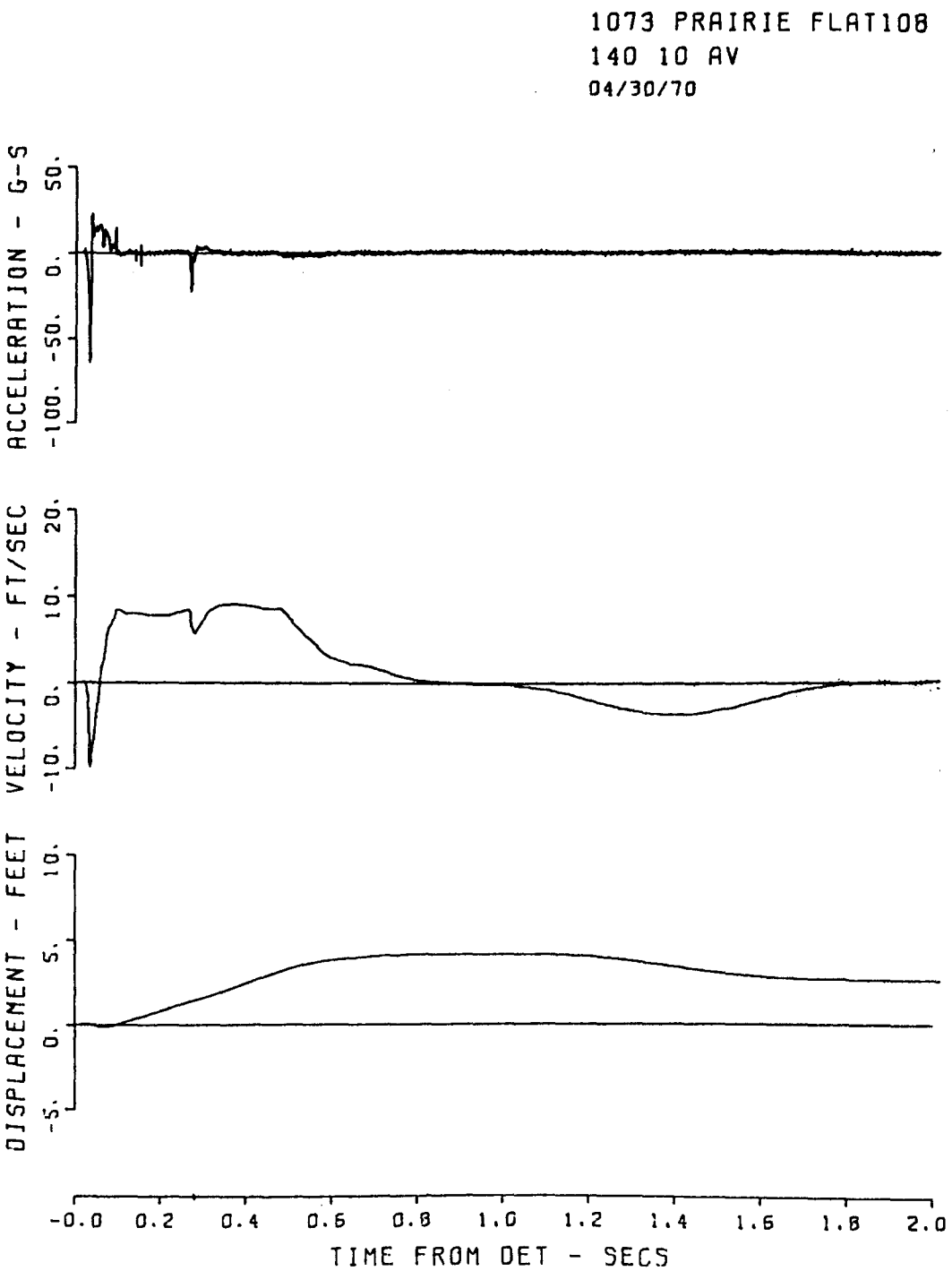

Figure A.18 Gage 1073 AV.

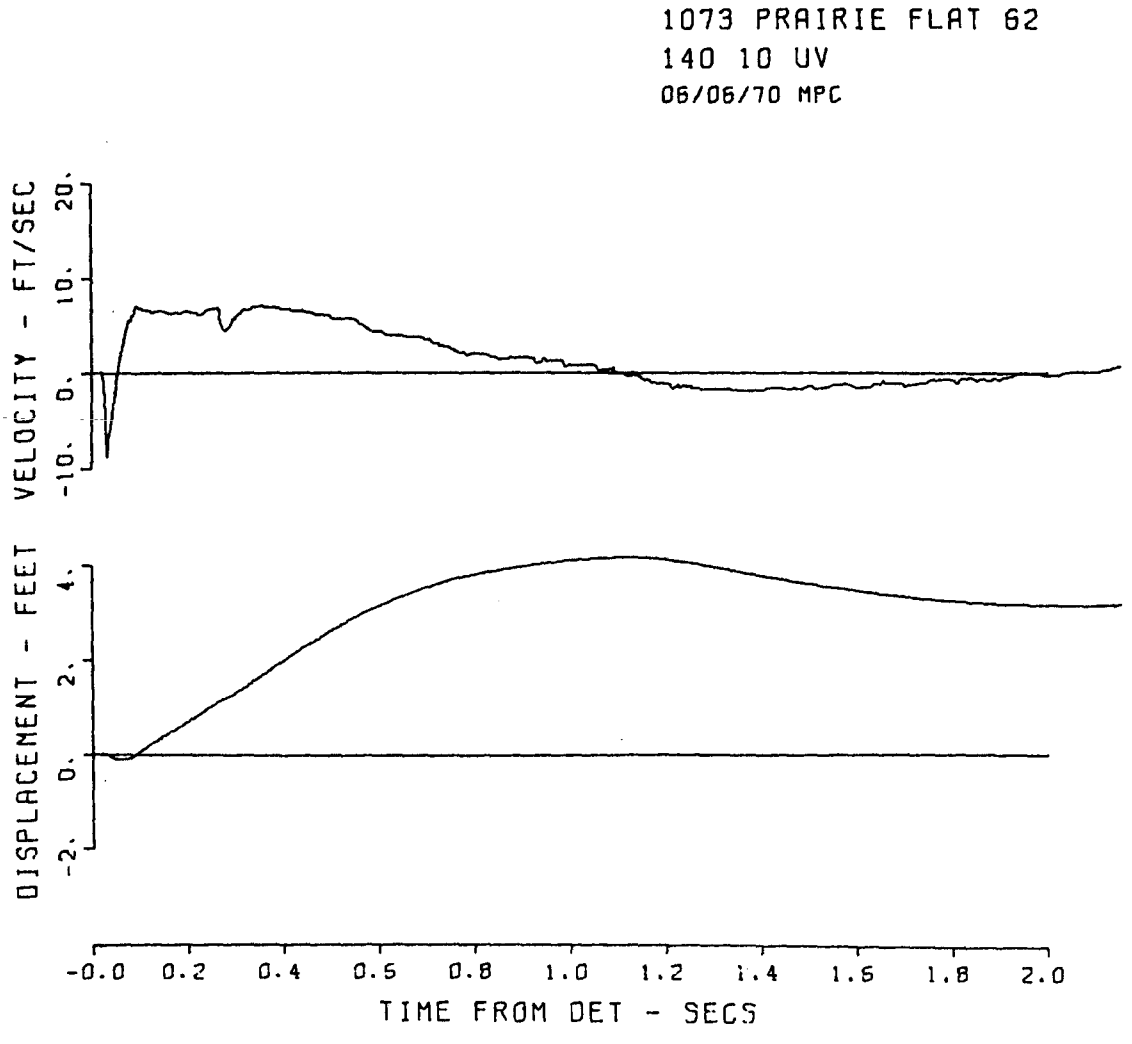

Figure A.19 Gage 1073 UV.

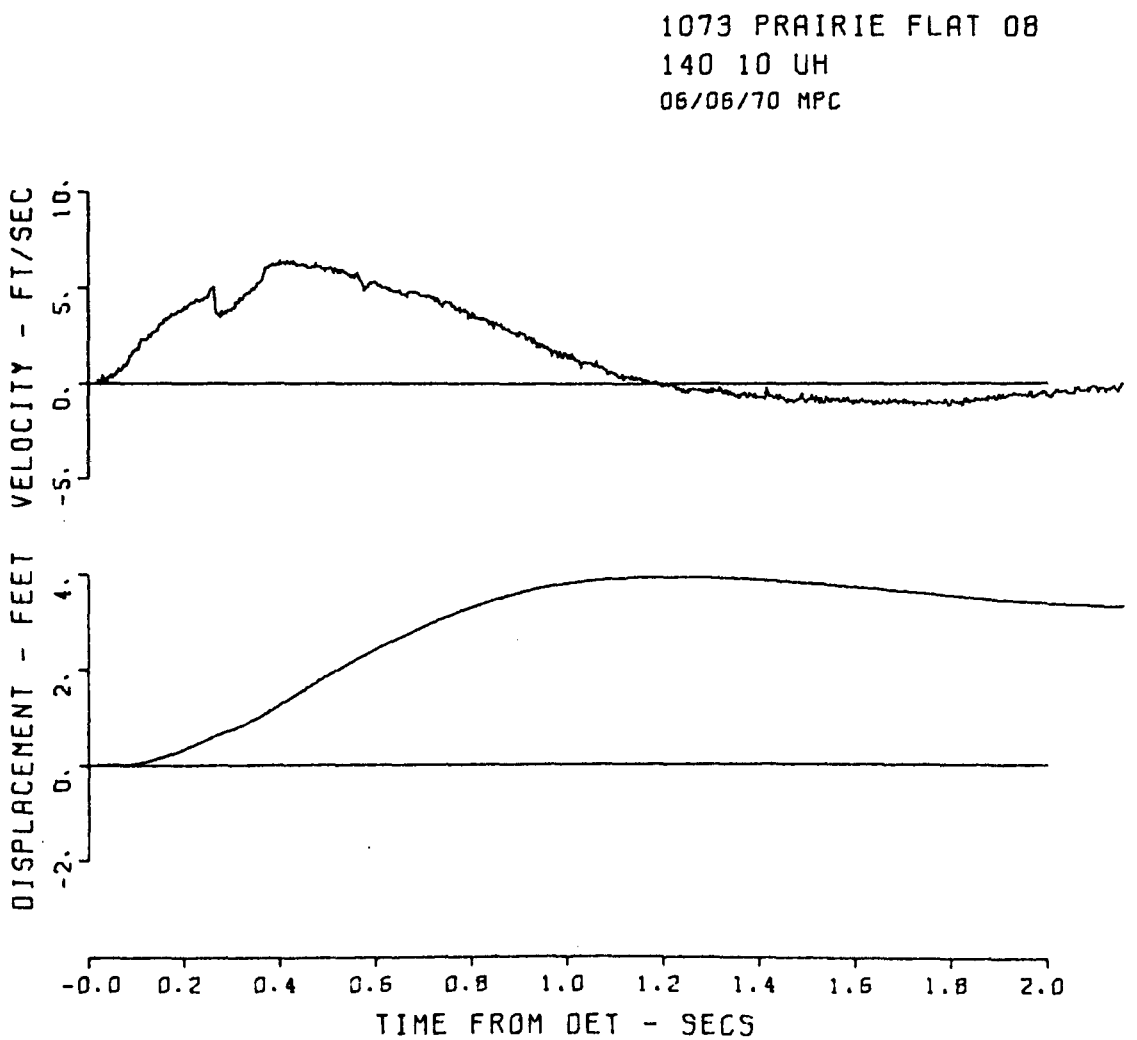

Figure A.20 Gage 1073 UH.

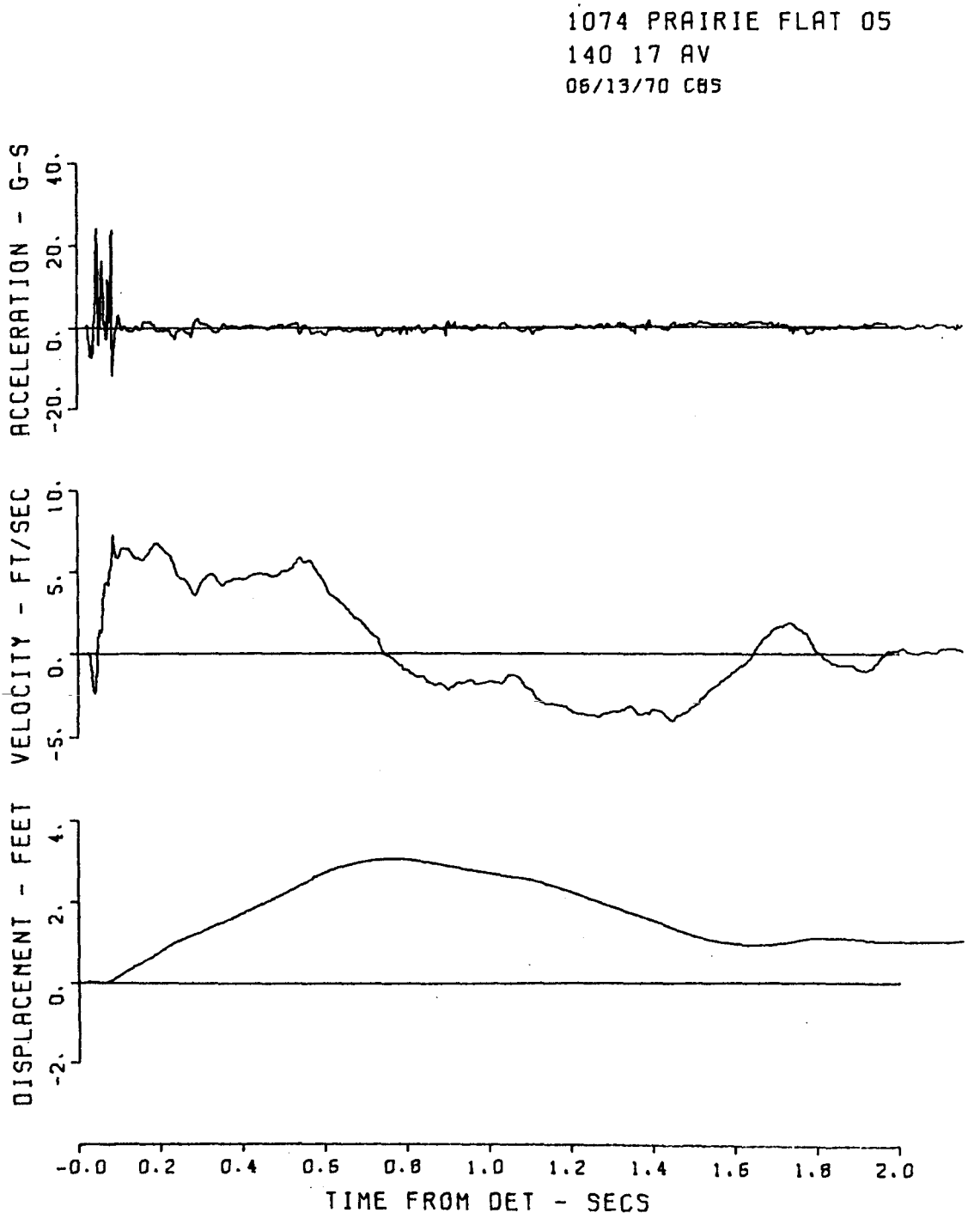

Figure A.21 Gage 1074 AV.

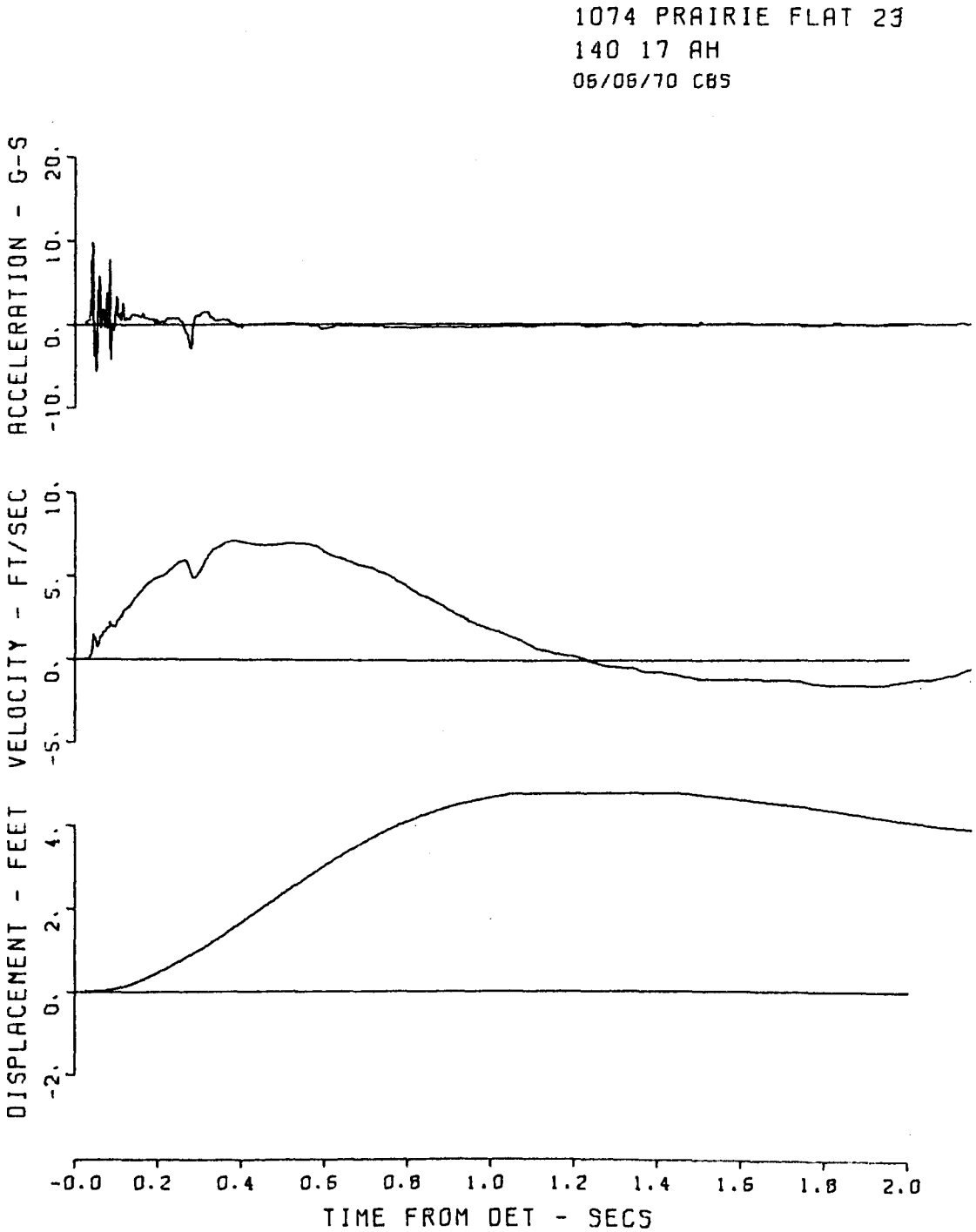

Figure A.22 Gage 1074 AH.

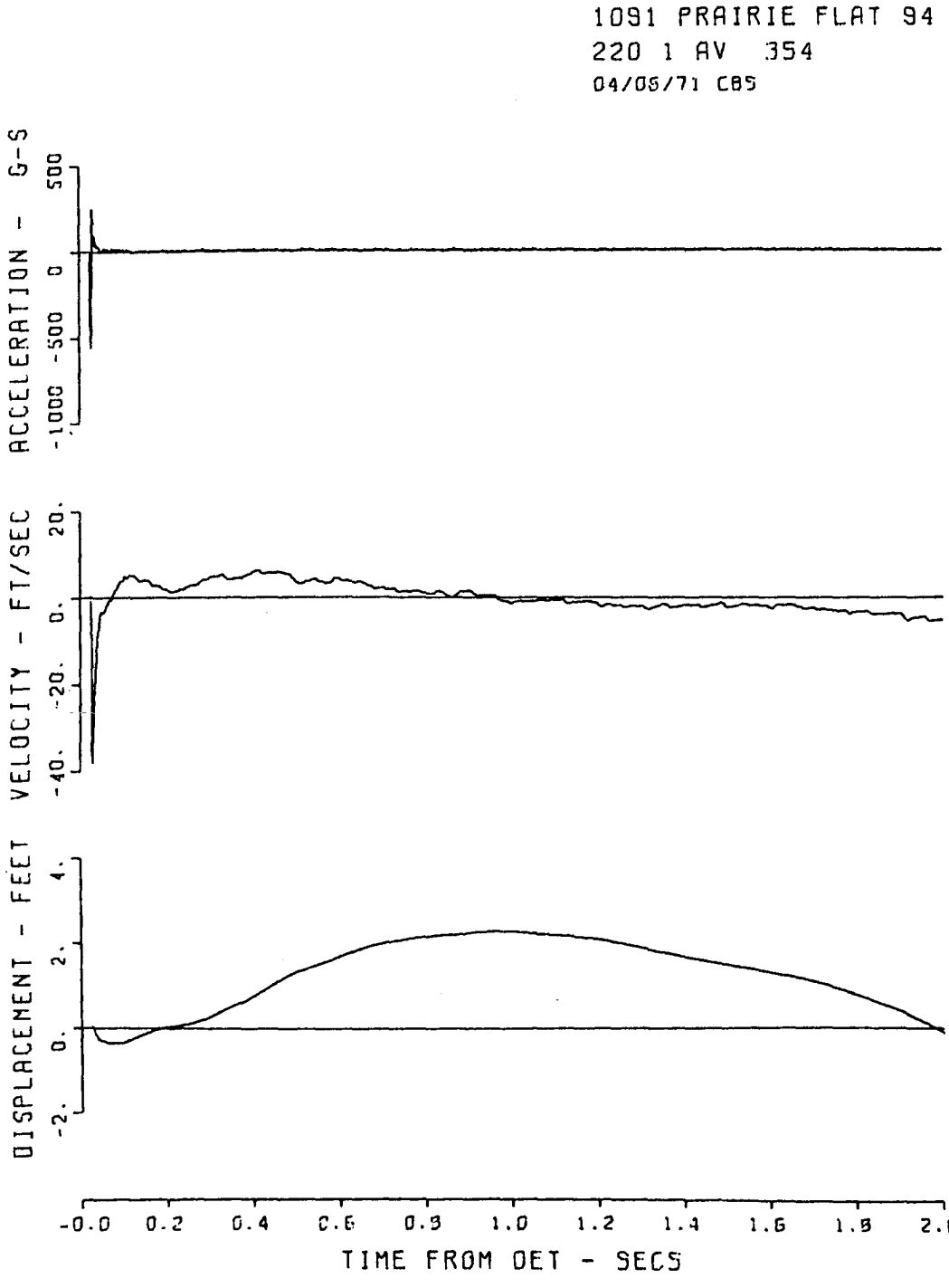

Figure A.23 Gage 1091 AV.

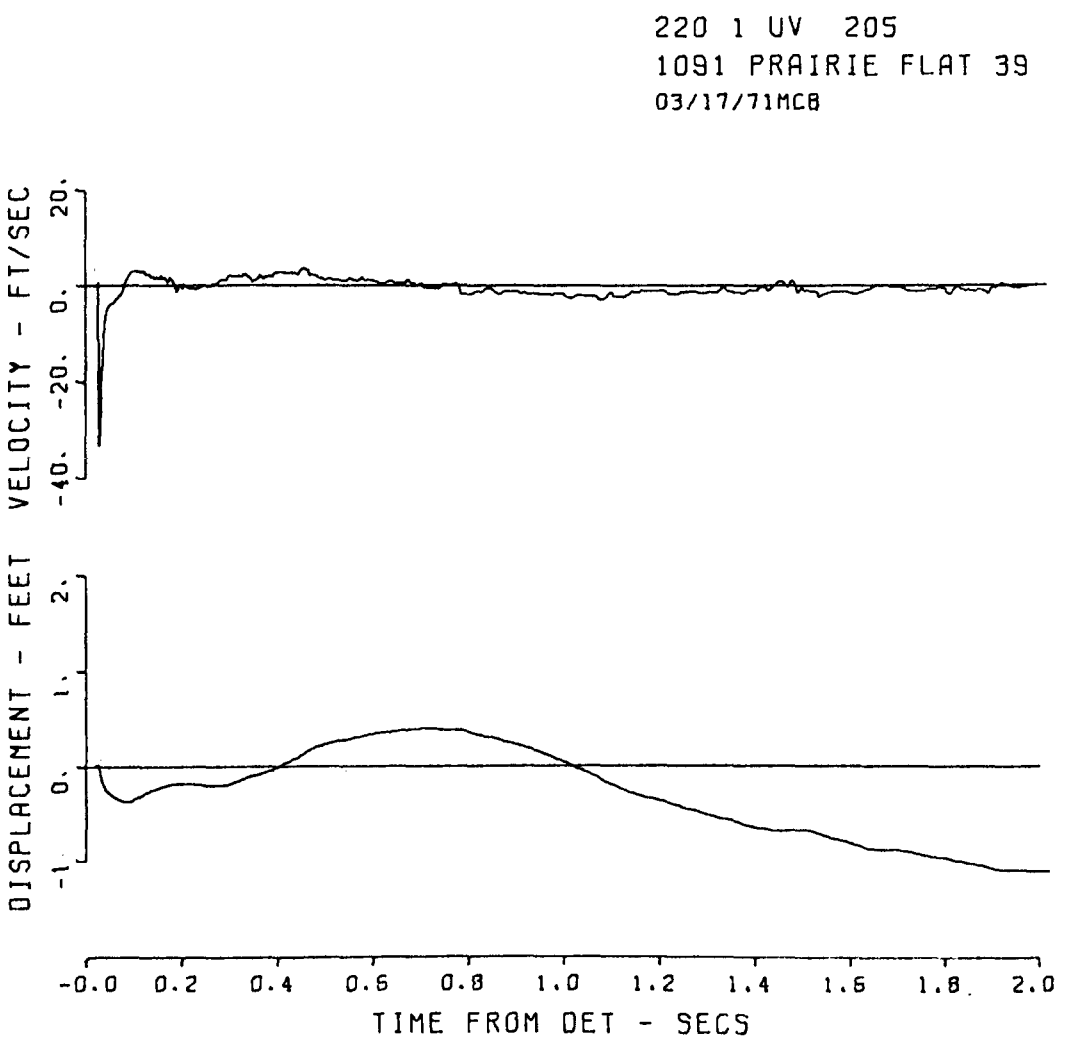

Figure A.24 Gage 1091 UV.

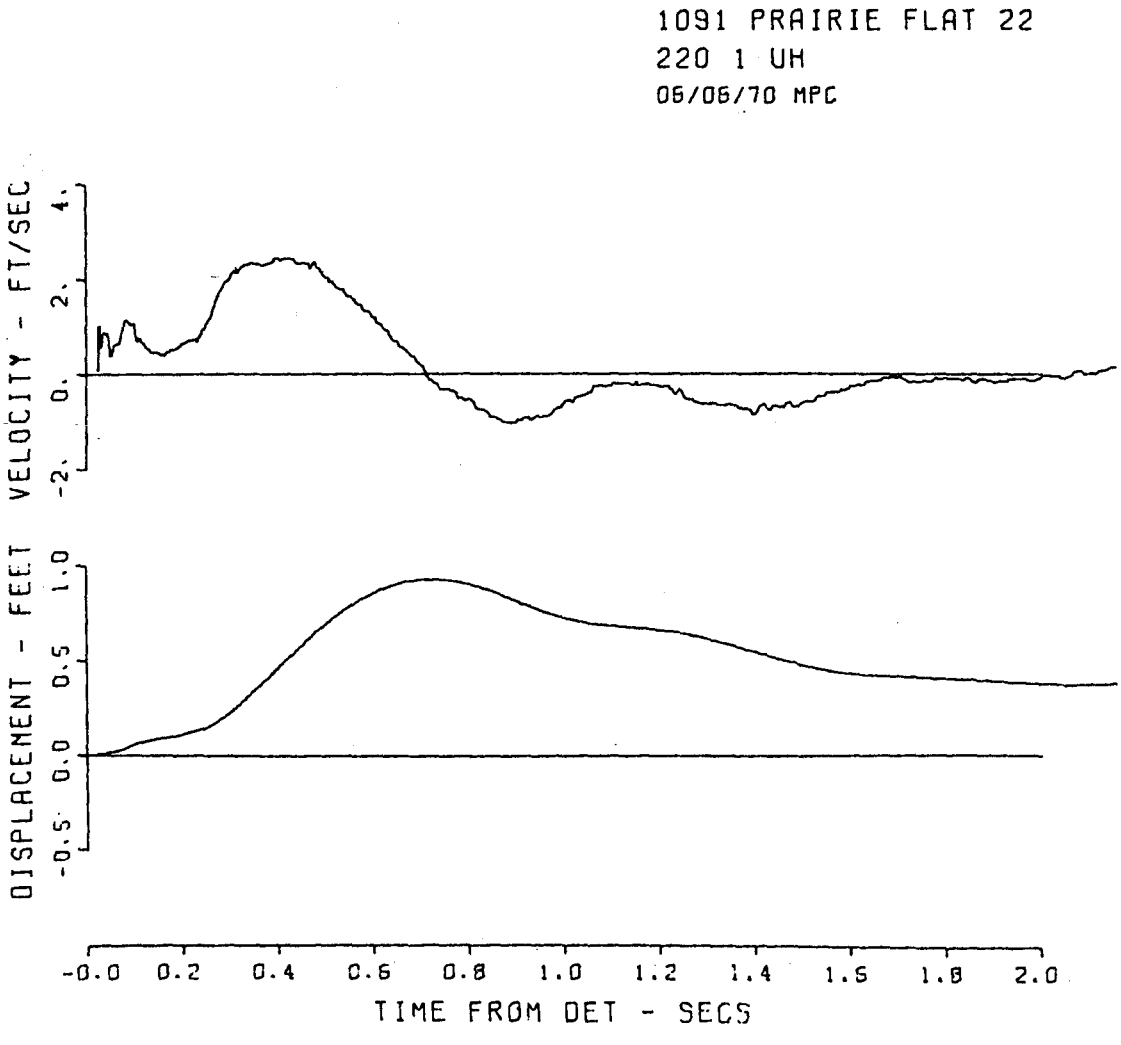

Figure A.25 Gage 1091 UH.

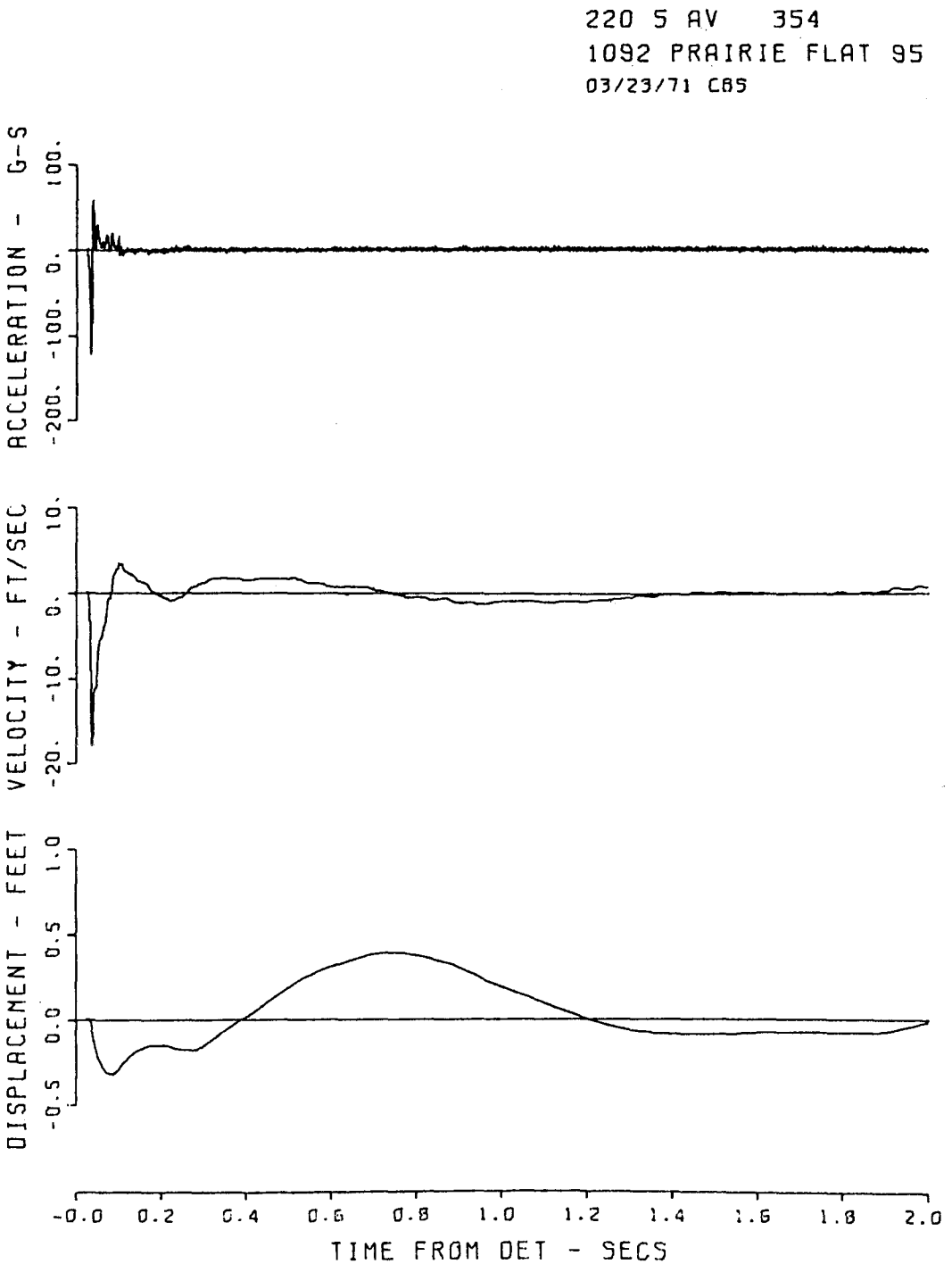

Figure A.26 Gage 1092 AV.

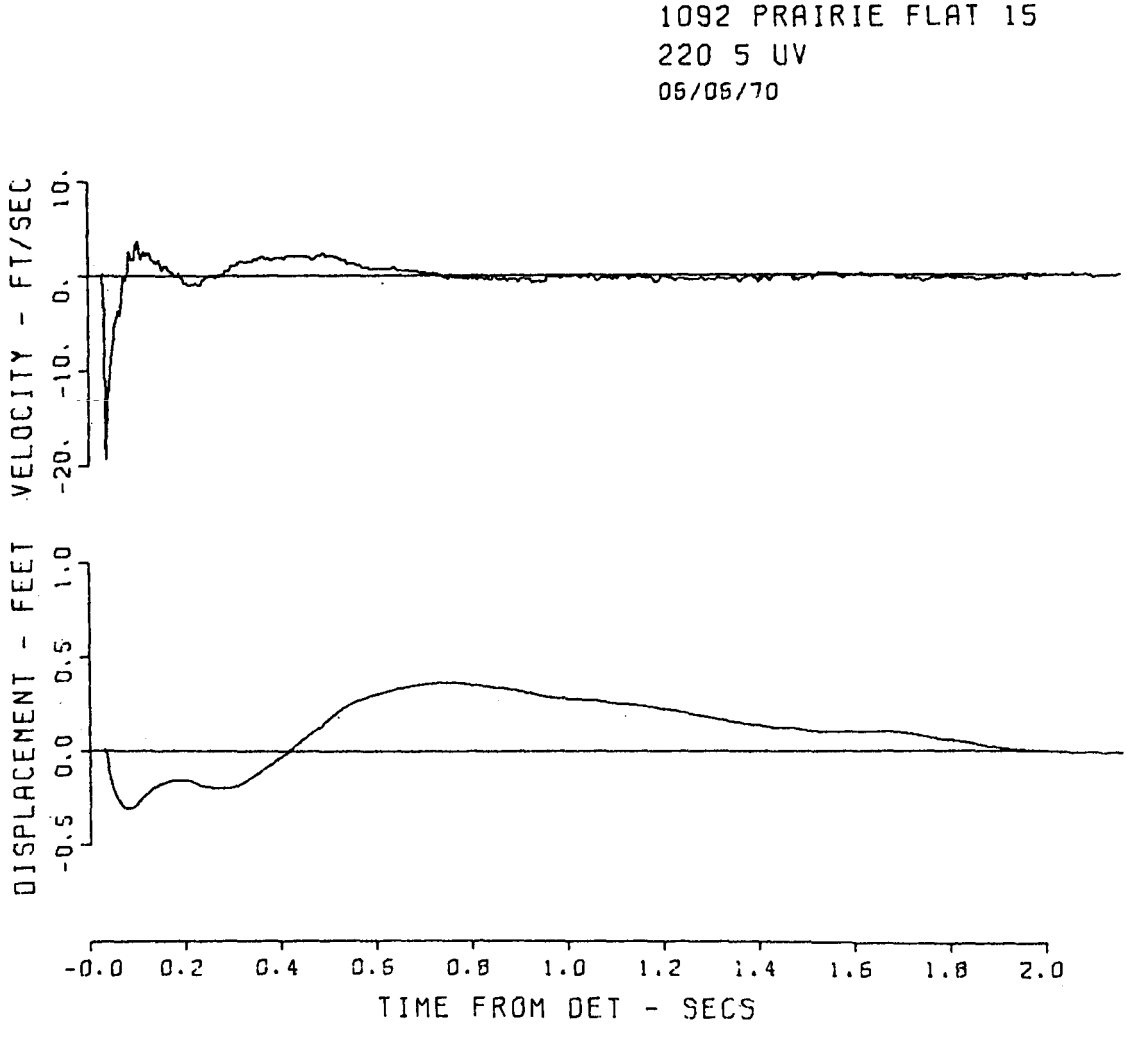

Figure A.27 Gage 1092 UV.

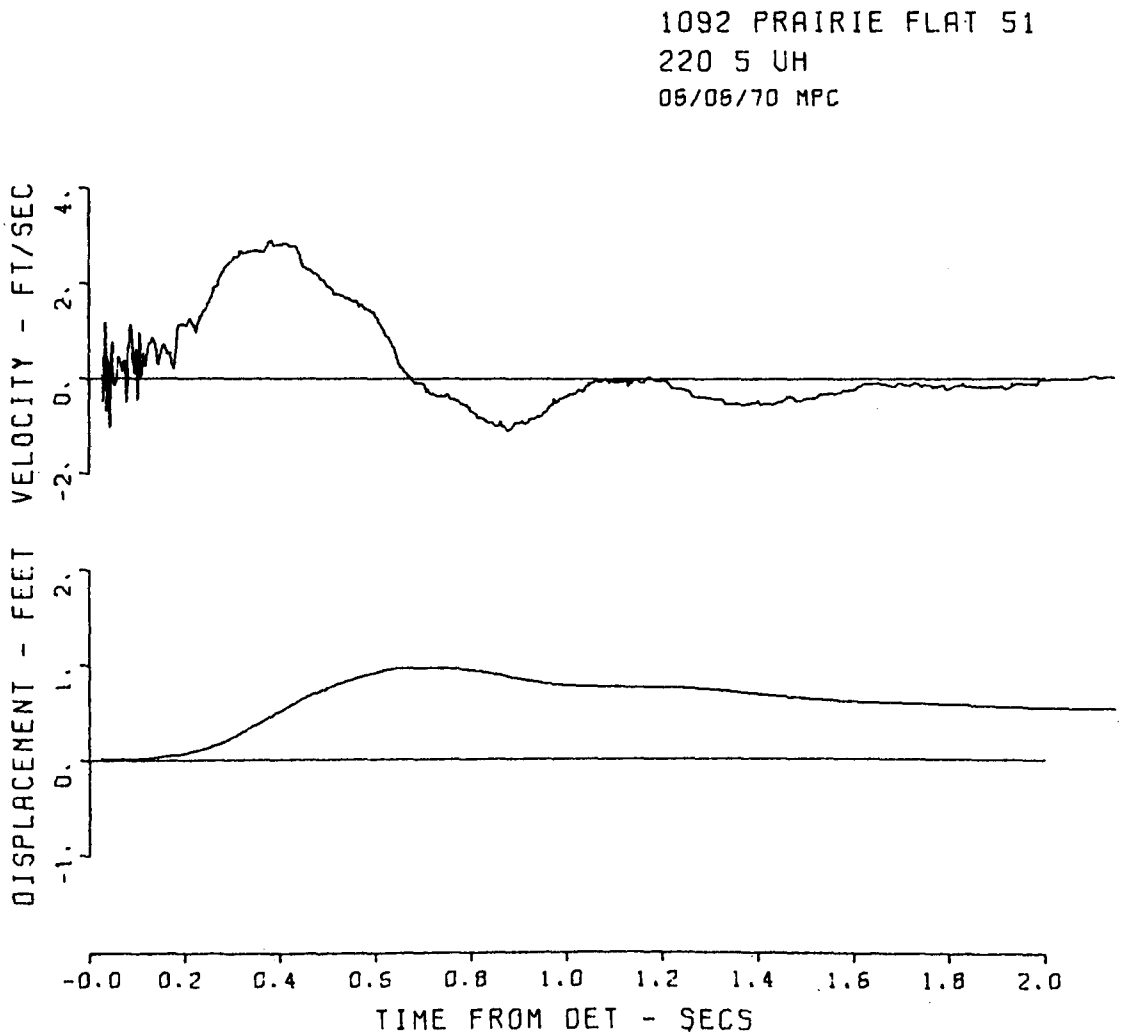

Figure A.28 Gage 1092 UH.

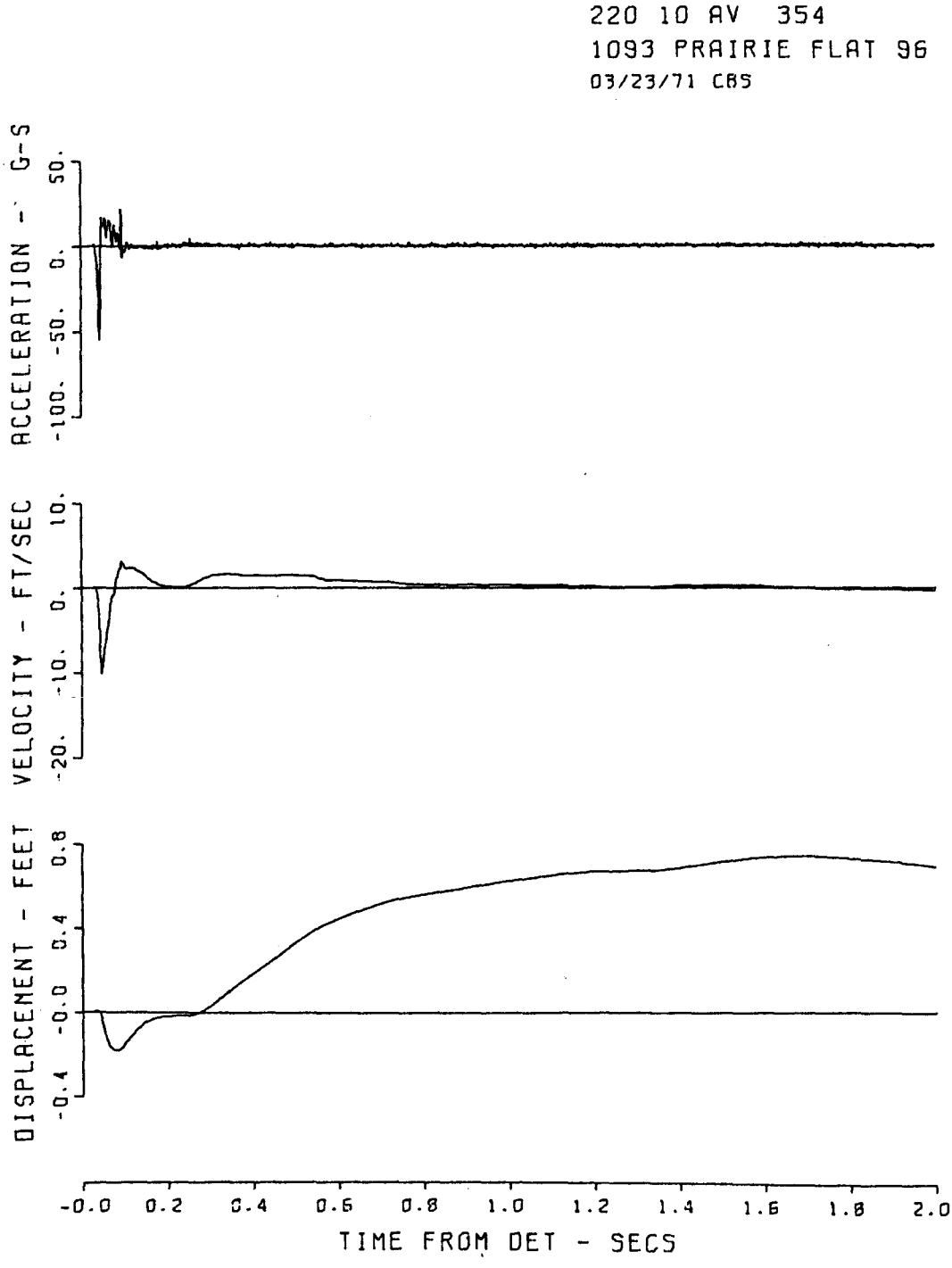

Figure A.29 Gage 1093 AV.

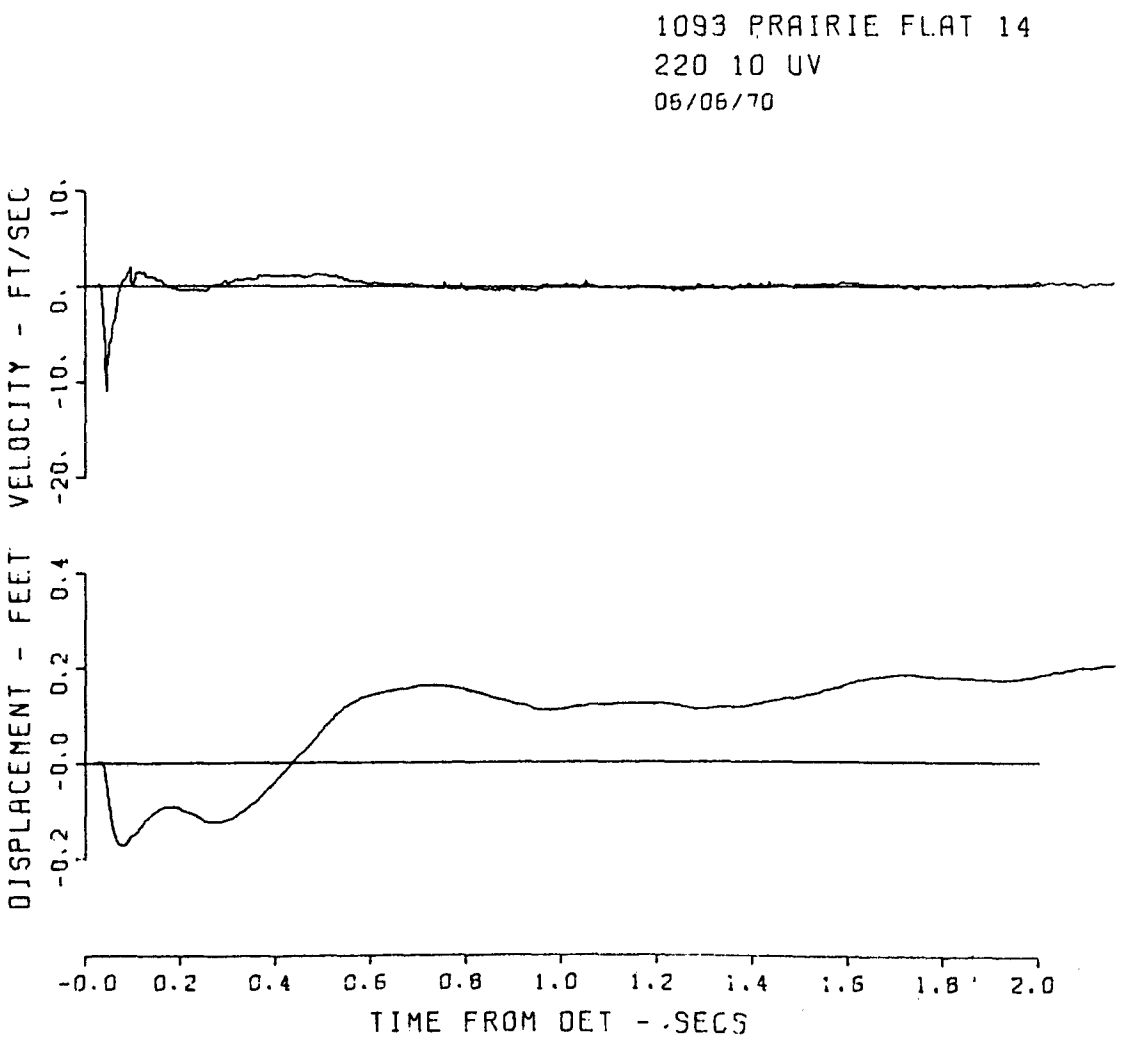

Figure A.30 Gage 1093 UV.

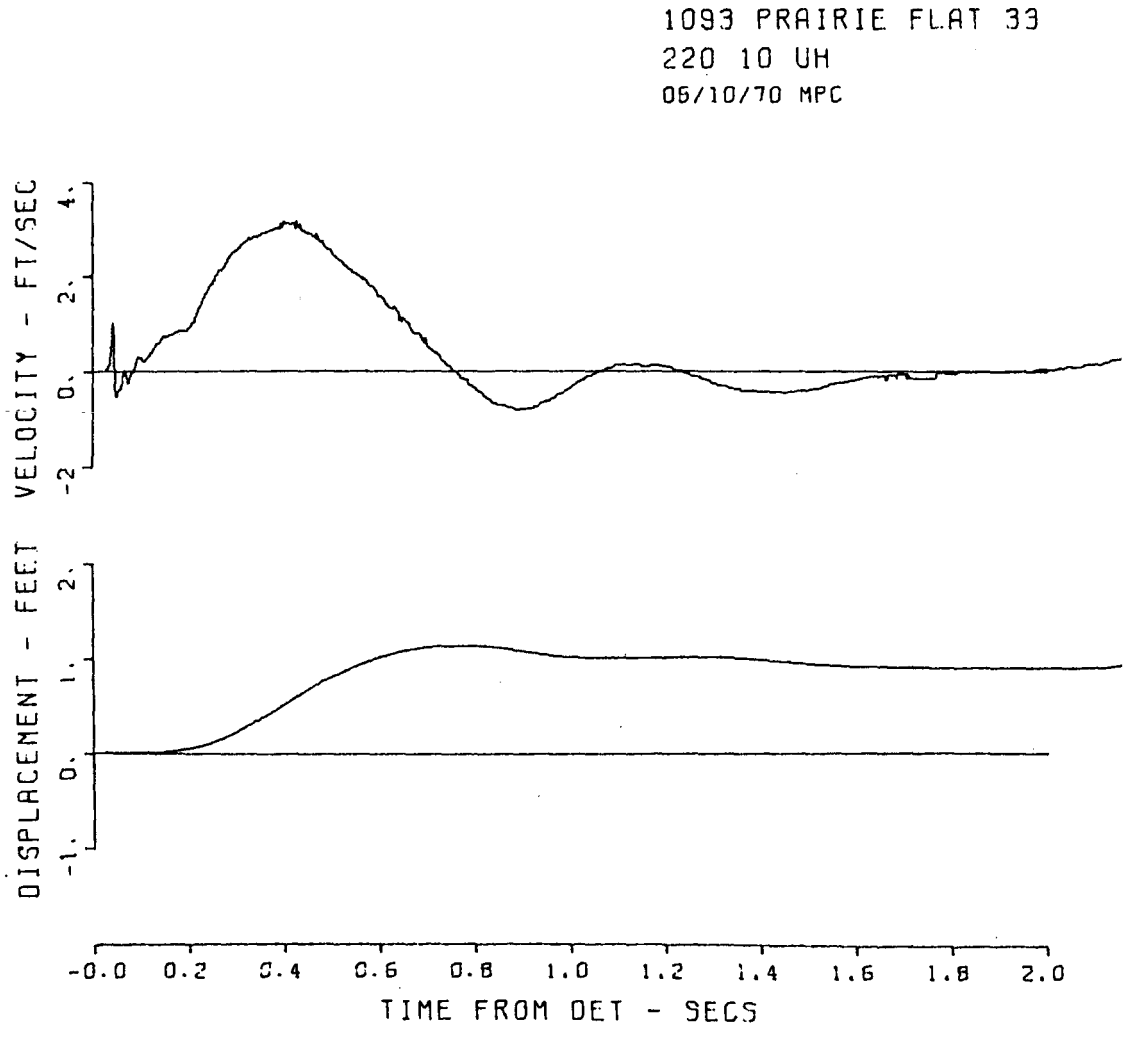

Figure A.31 Gage 1093 UH.

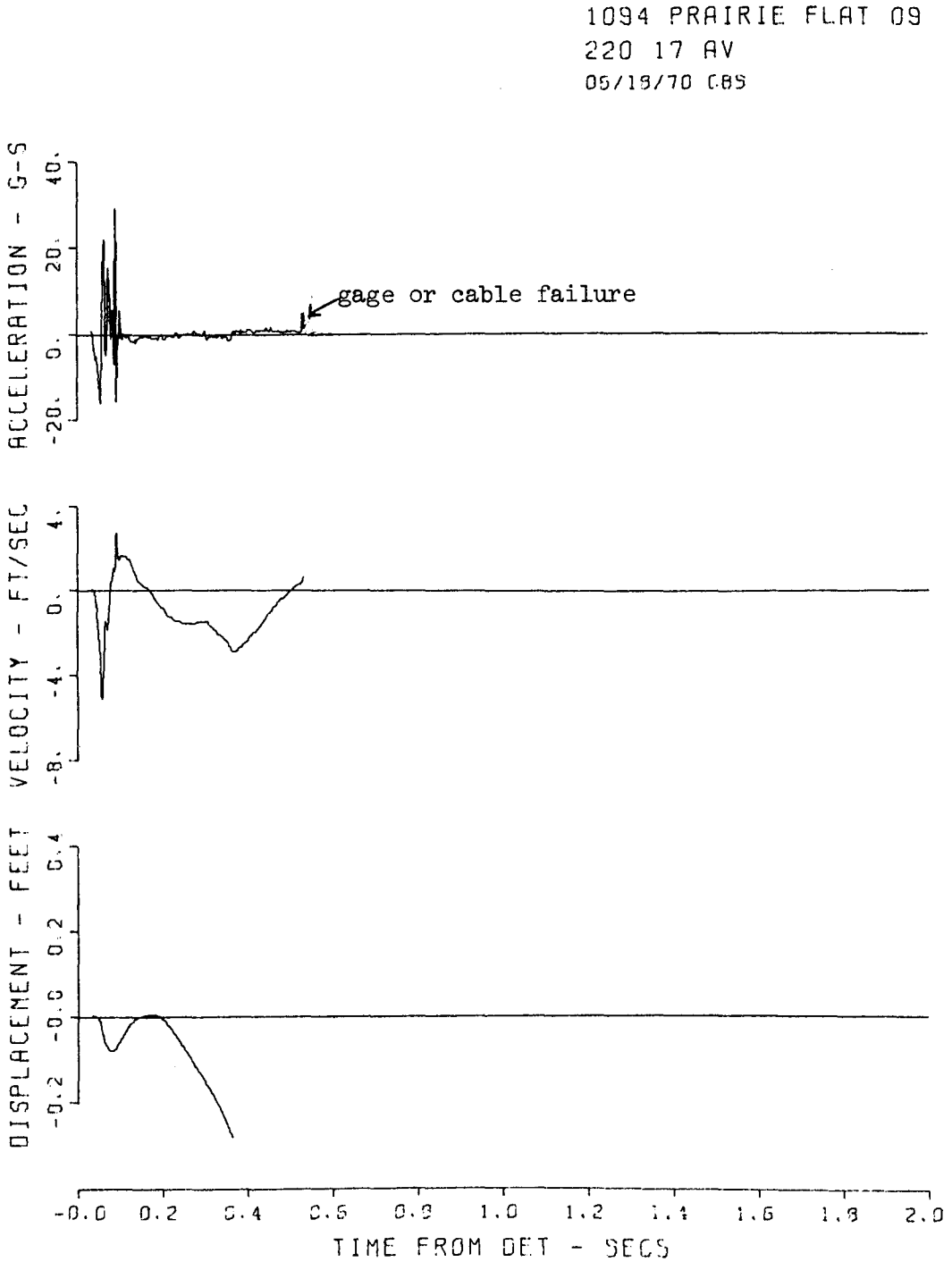

Figure A.32 Gage 1094 AV.

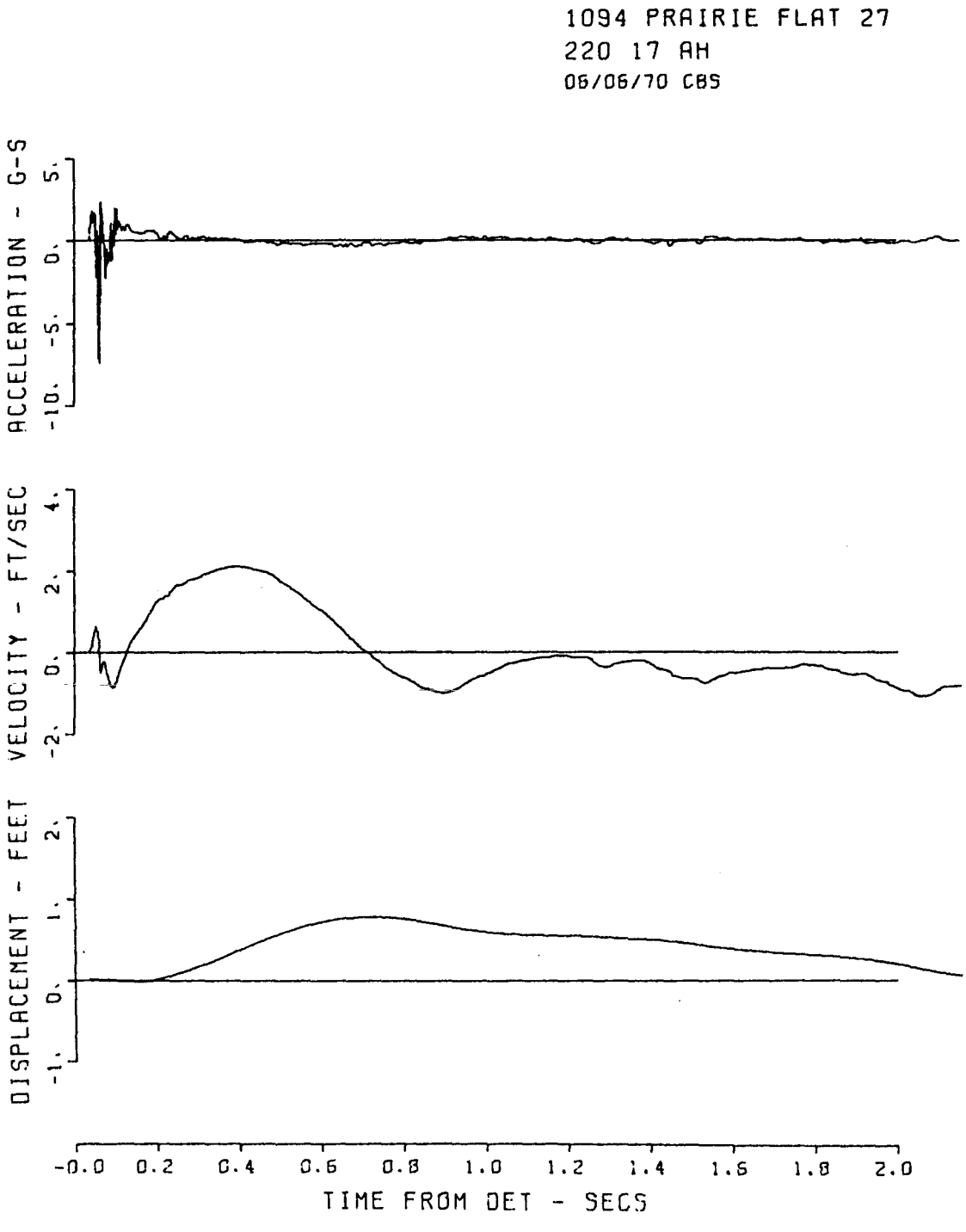

Figure A.33 Gage 1094 AH.

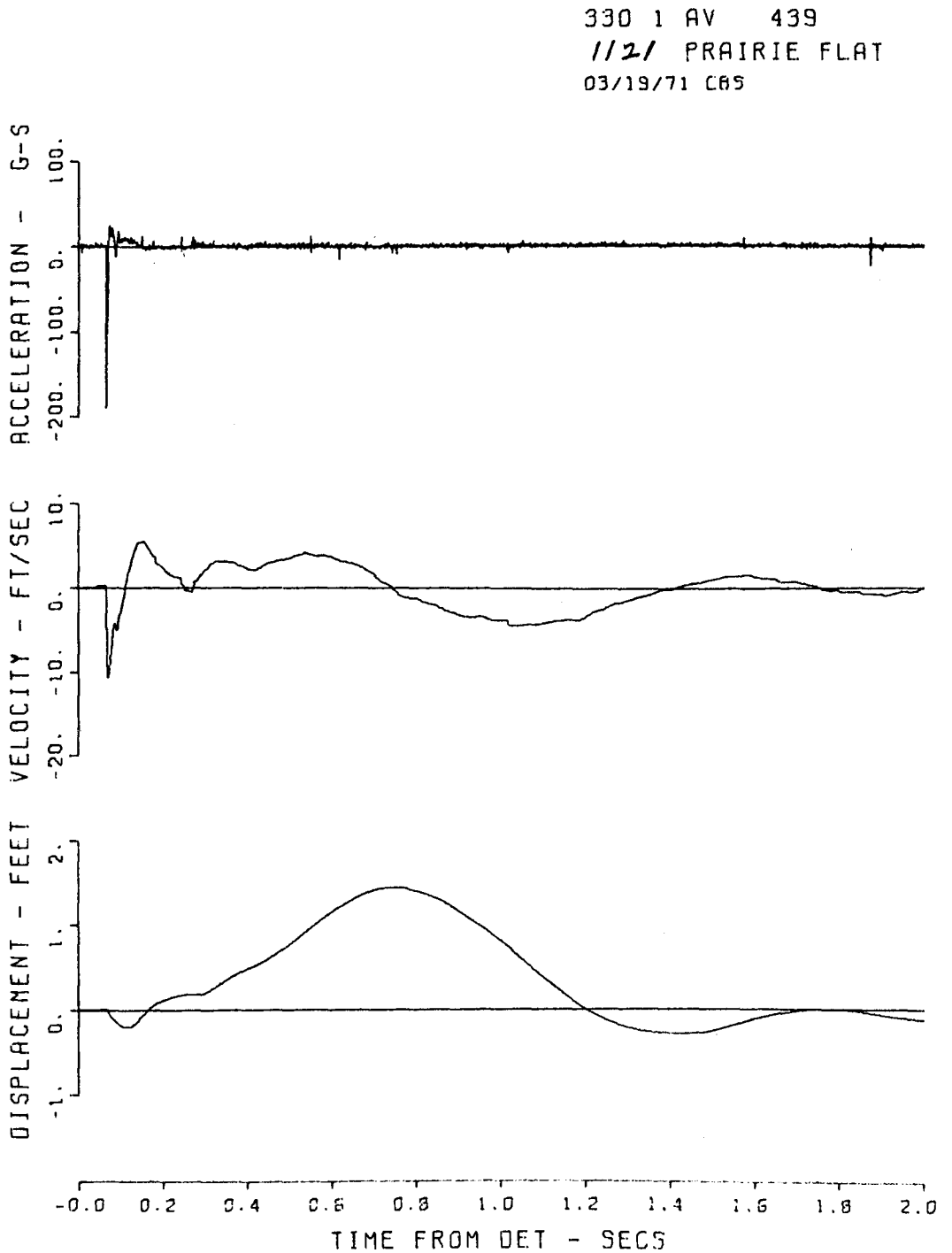

Figure A.34 Gage 1121 AV.

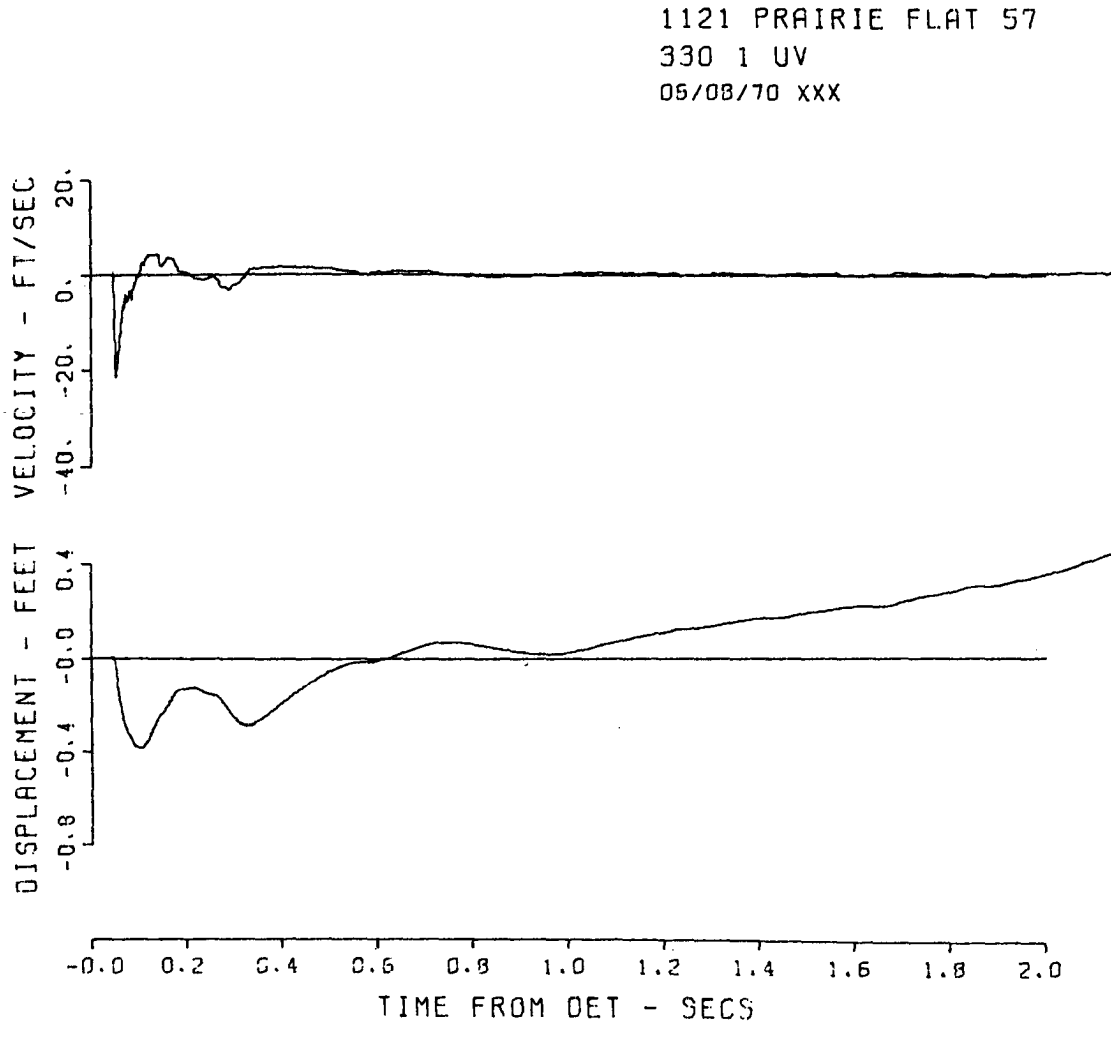

Figure A.35 Gage 1121 UV.

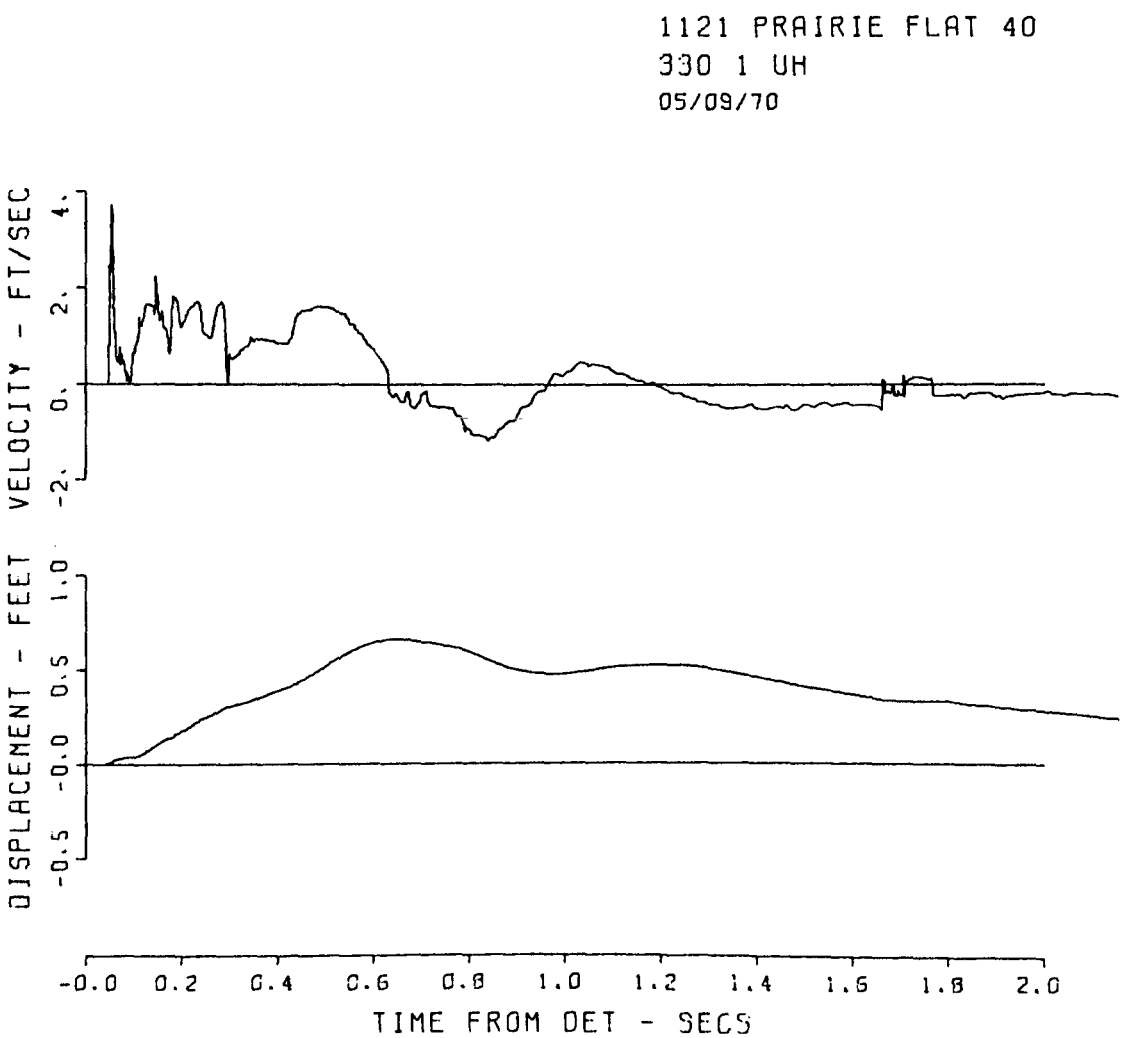

Figure A.36 Gage 1121 UH.

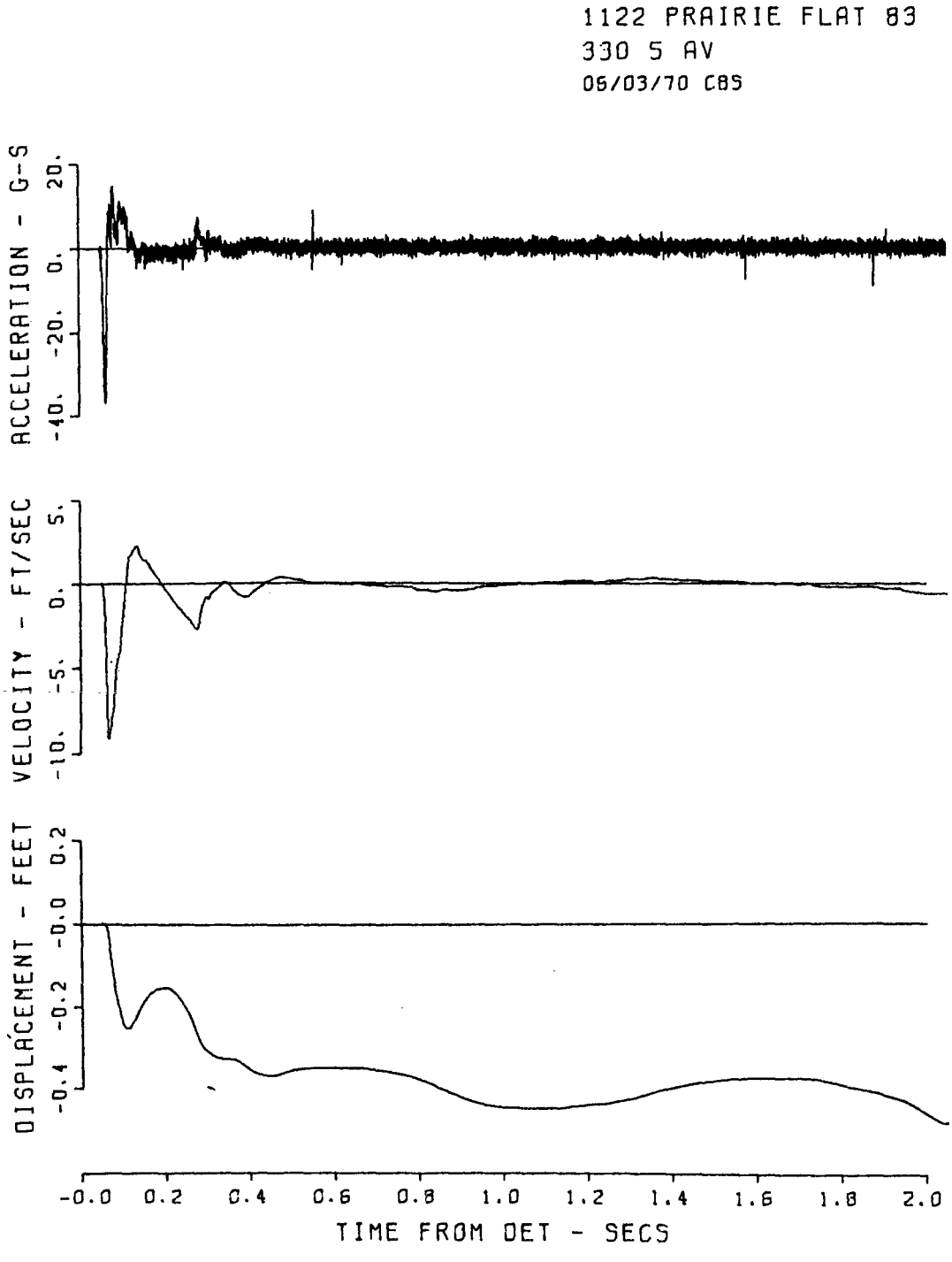

Figure A.37 Gage 1122 AV.

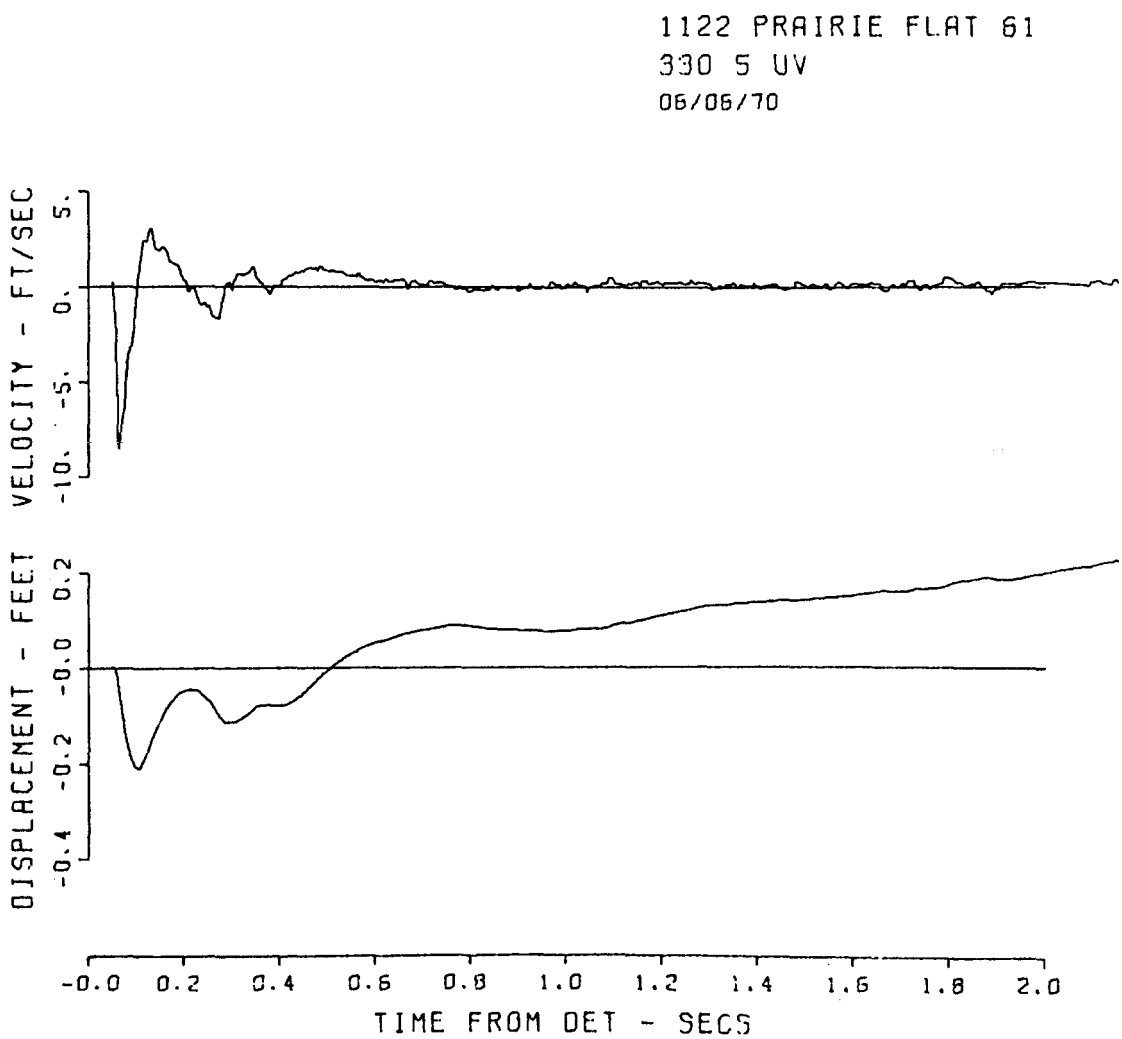

Figure A.38 Gage 1122 UV.

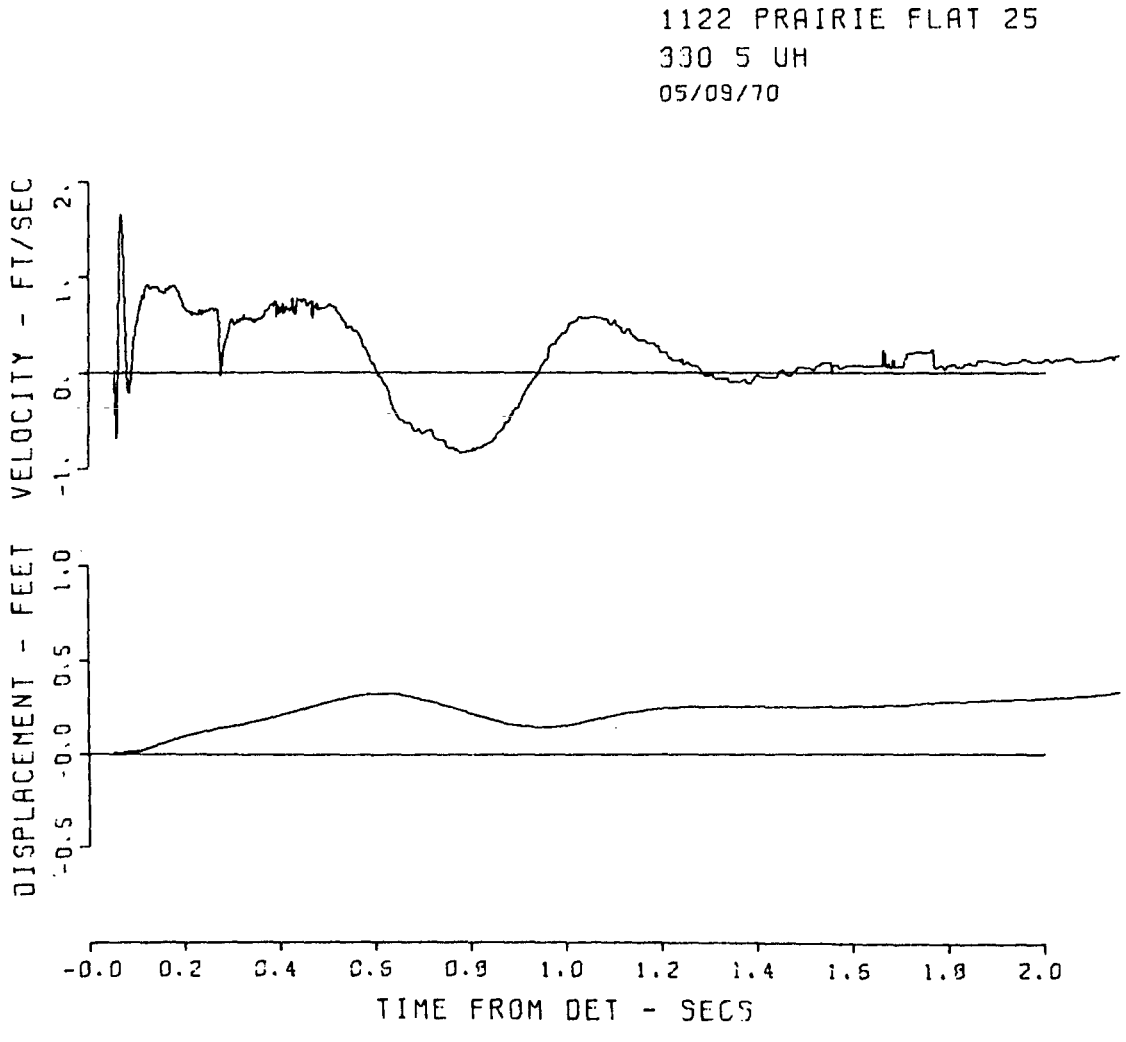

Figure A.39 Gage 1122 UH.

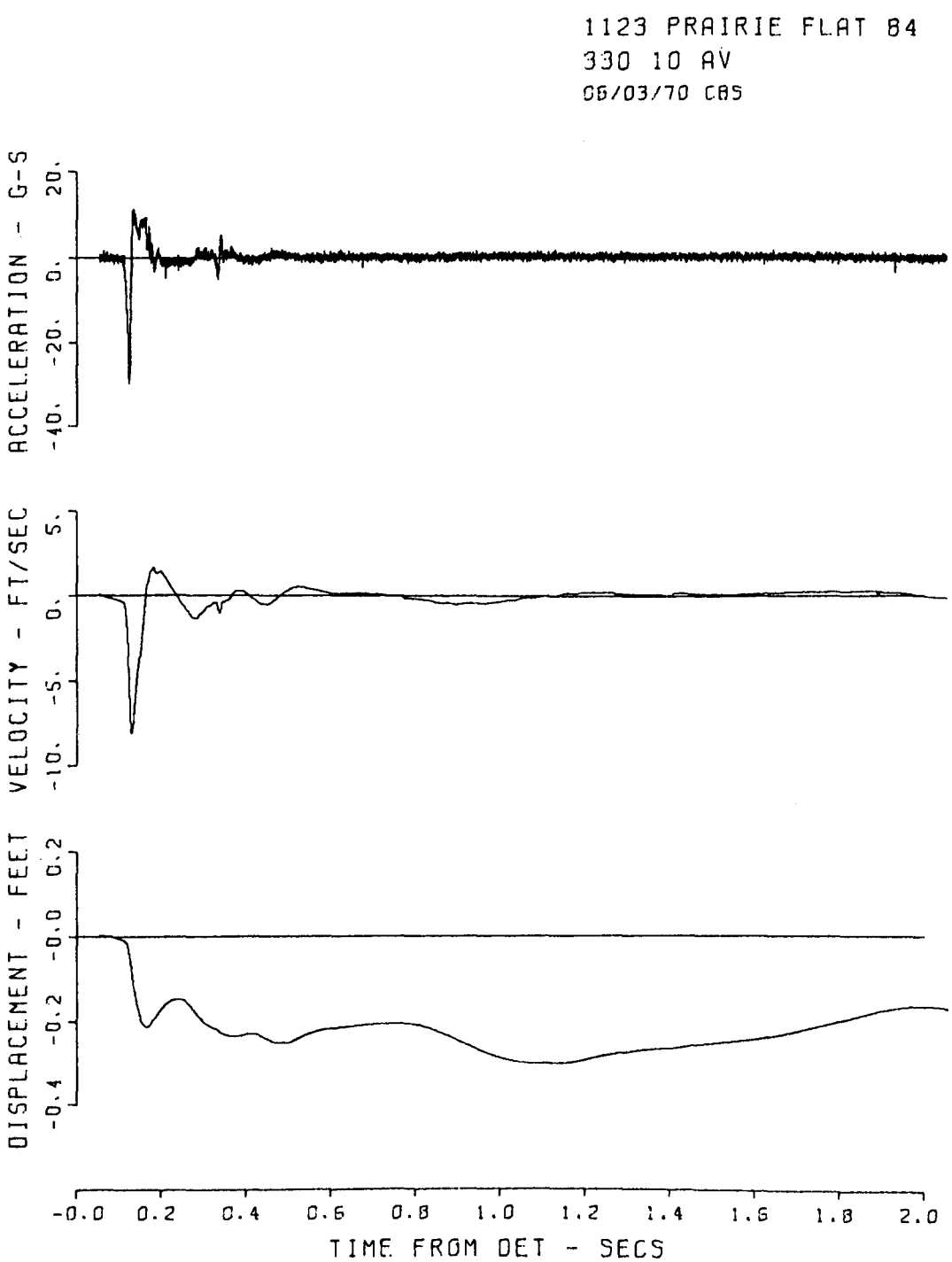

Figure A.40 Gage 1123 AV.

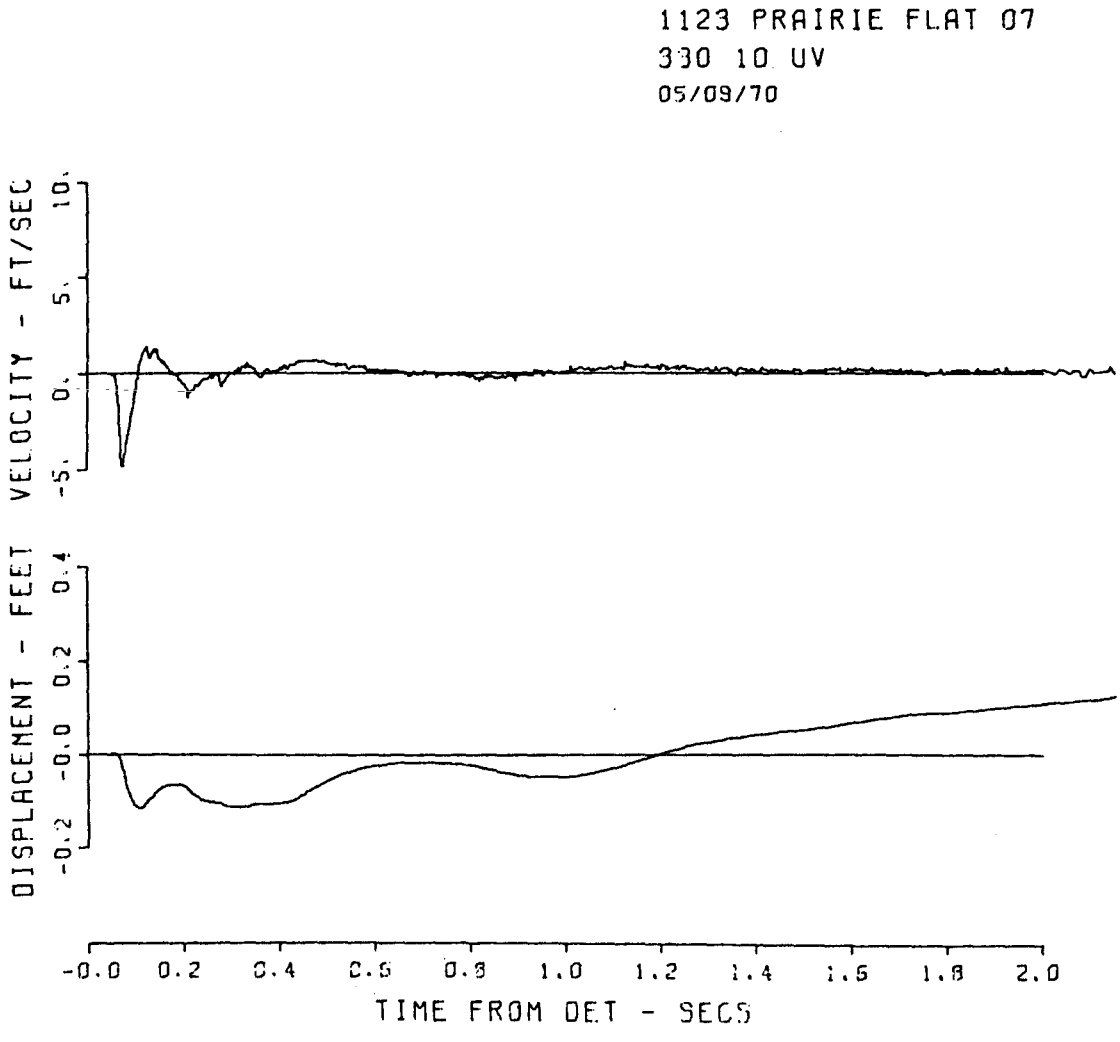

Figure A.41 Gage 1123 UV.

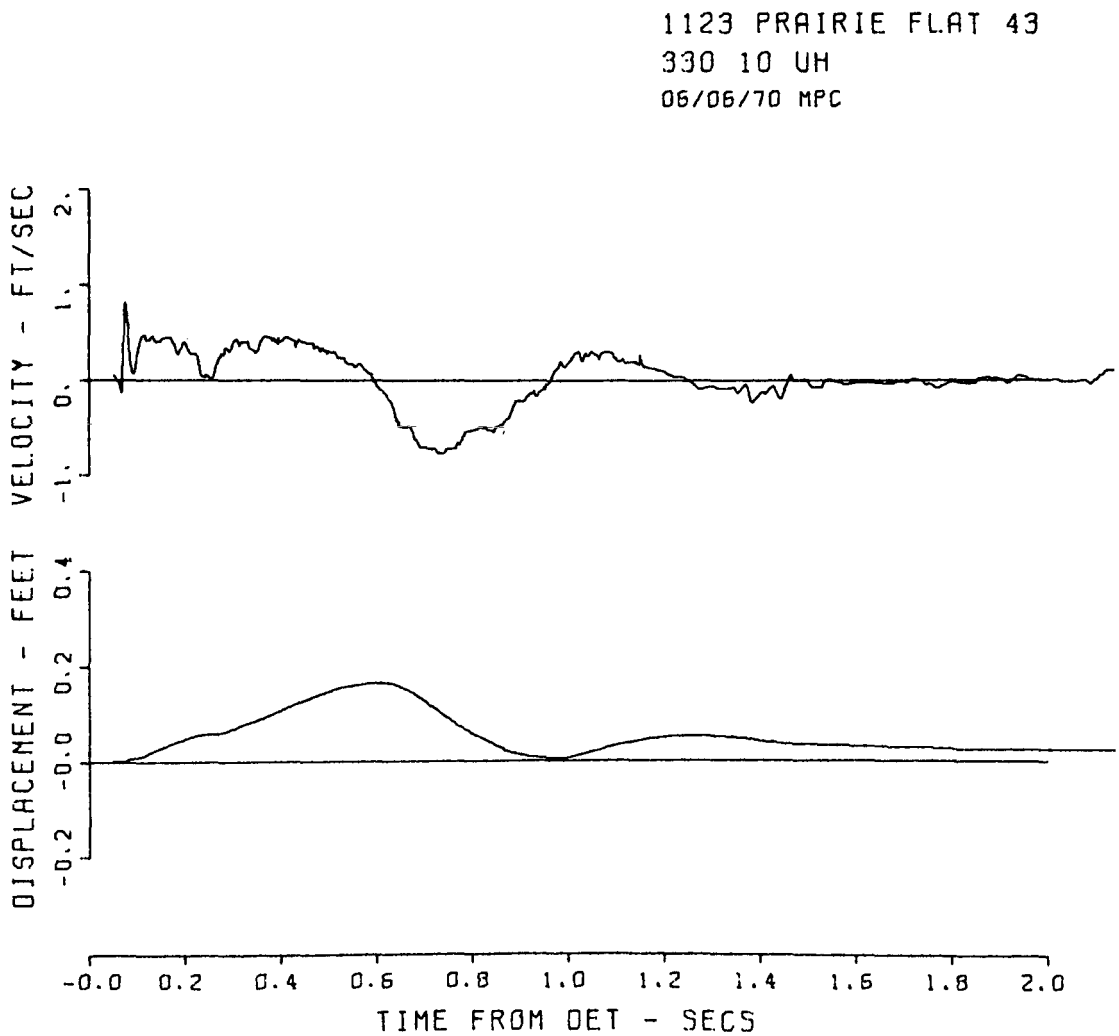

Figure A.42 Gage 1123 UH.

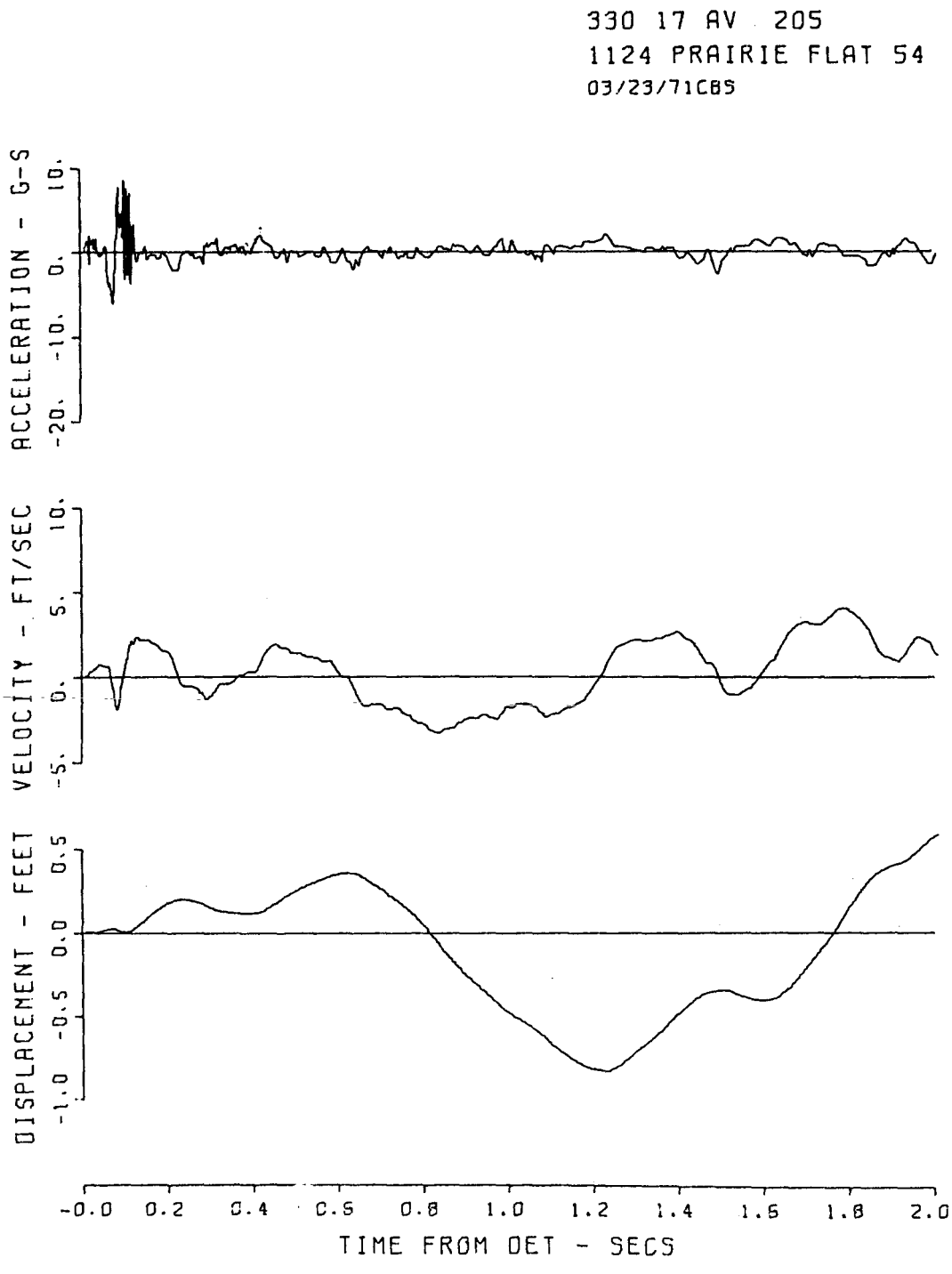

Figure A.43 Gage 1124 AV.

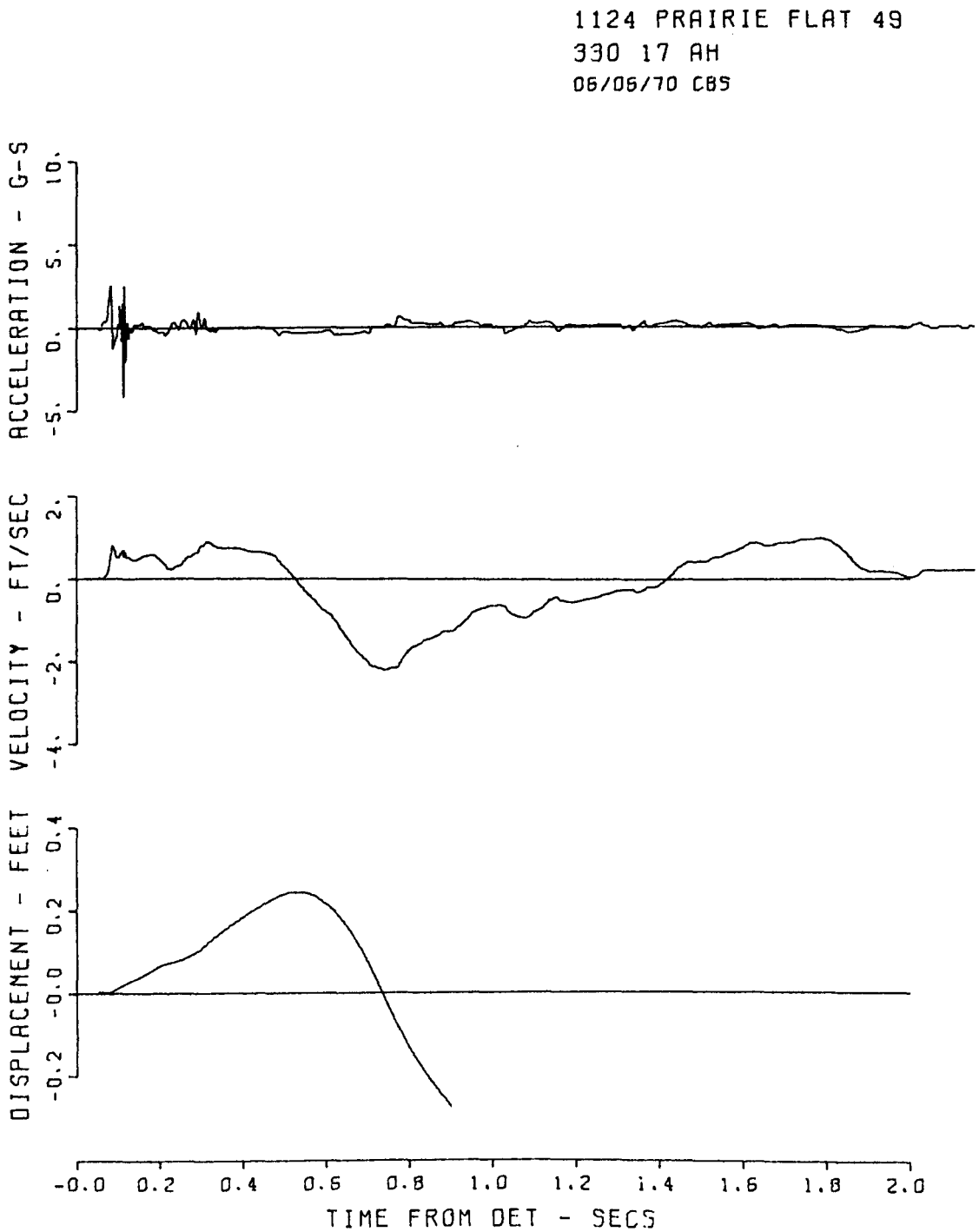

Figure A.44 Gage 1124 AH.

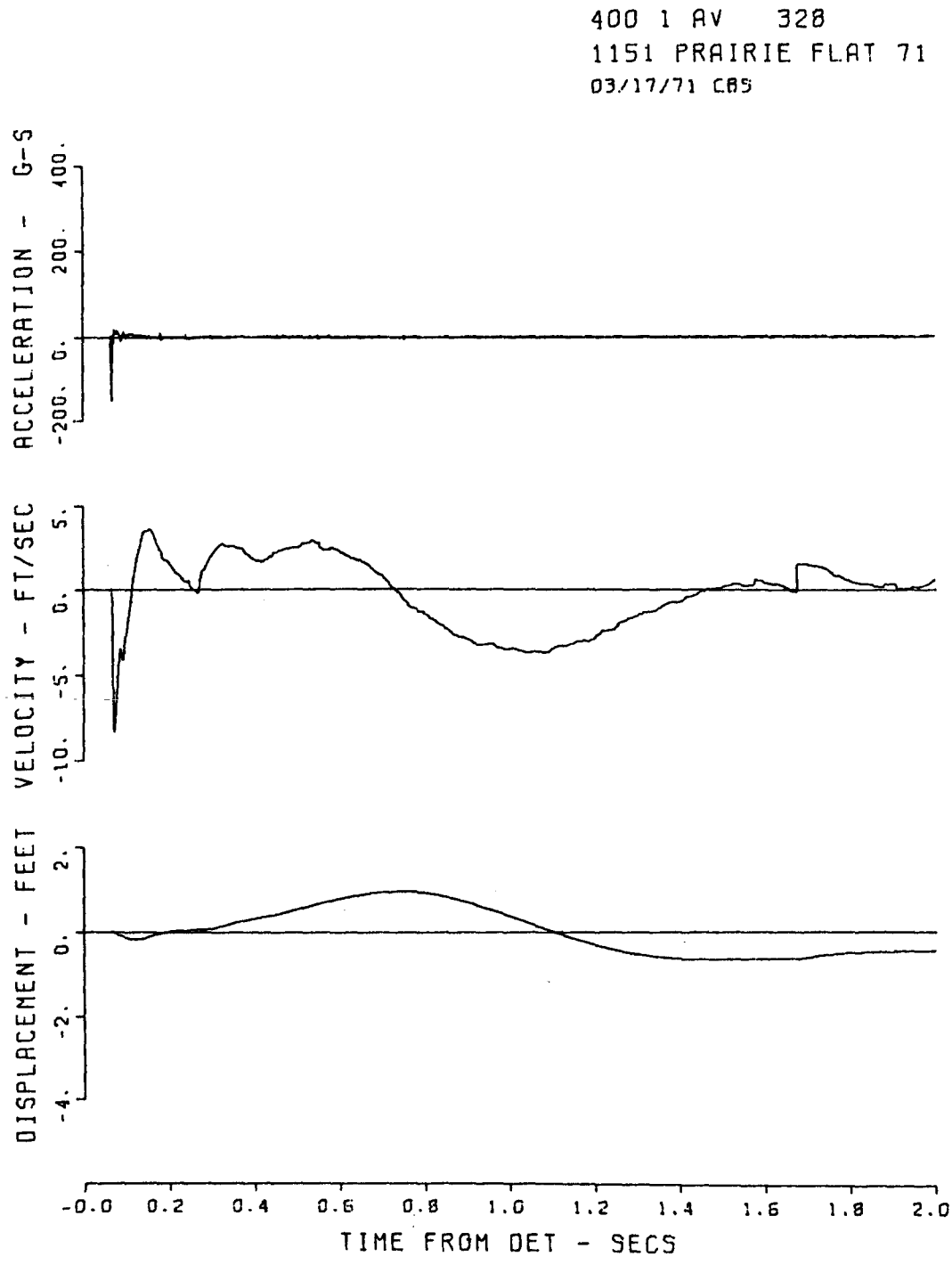

Figure A.45 Gage 1151 AV.

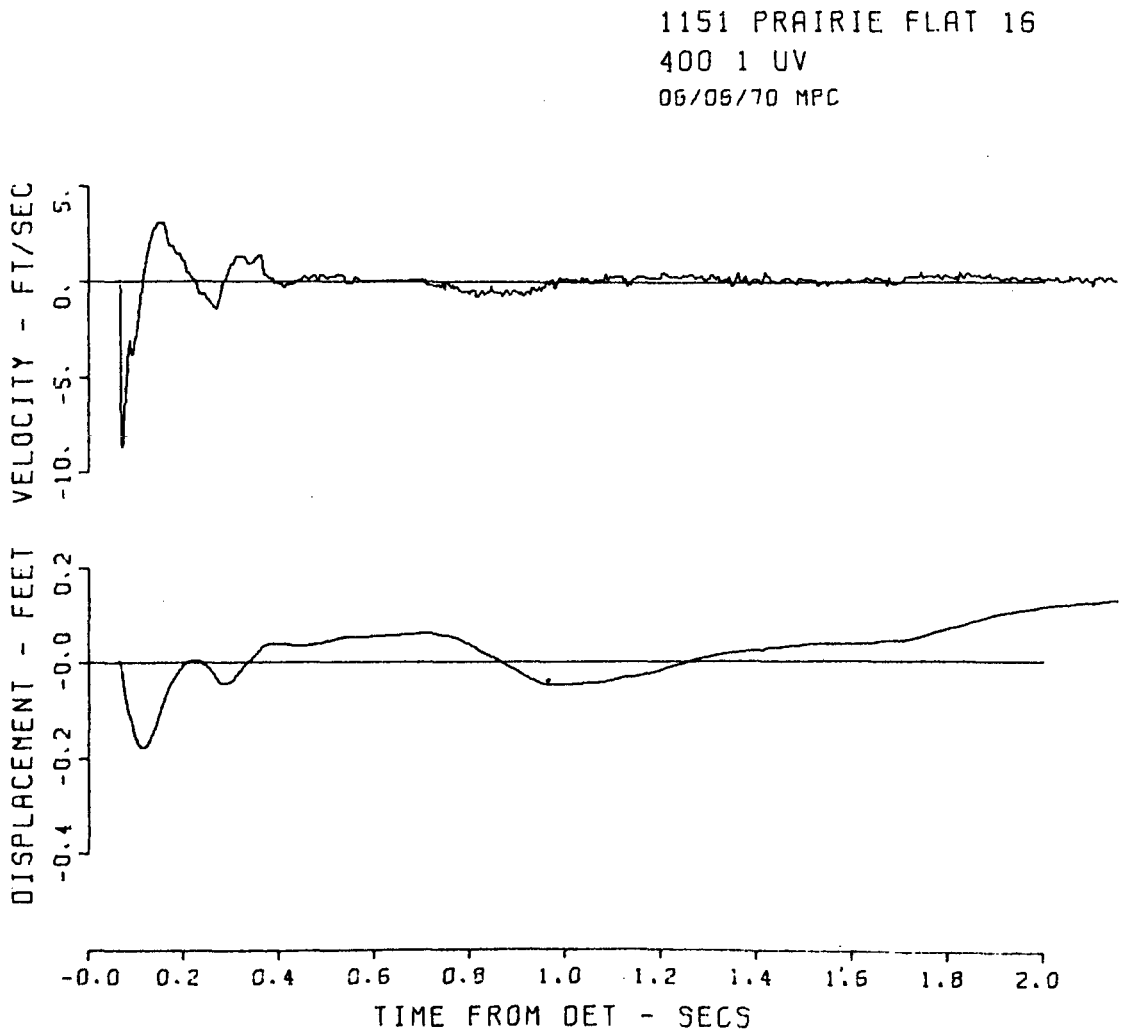

Figure A.46 Gage 1151 UV.

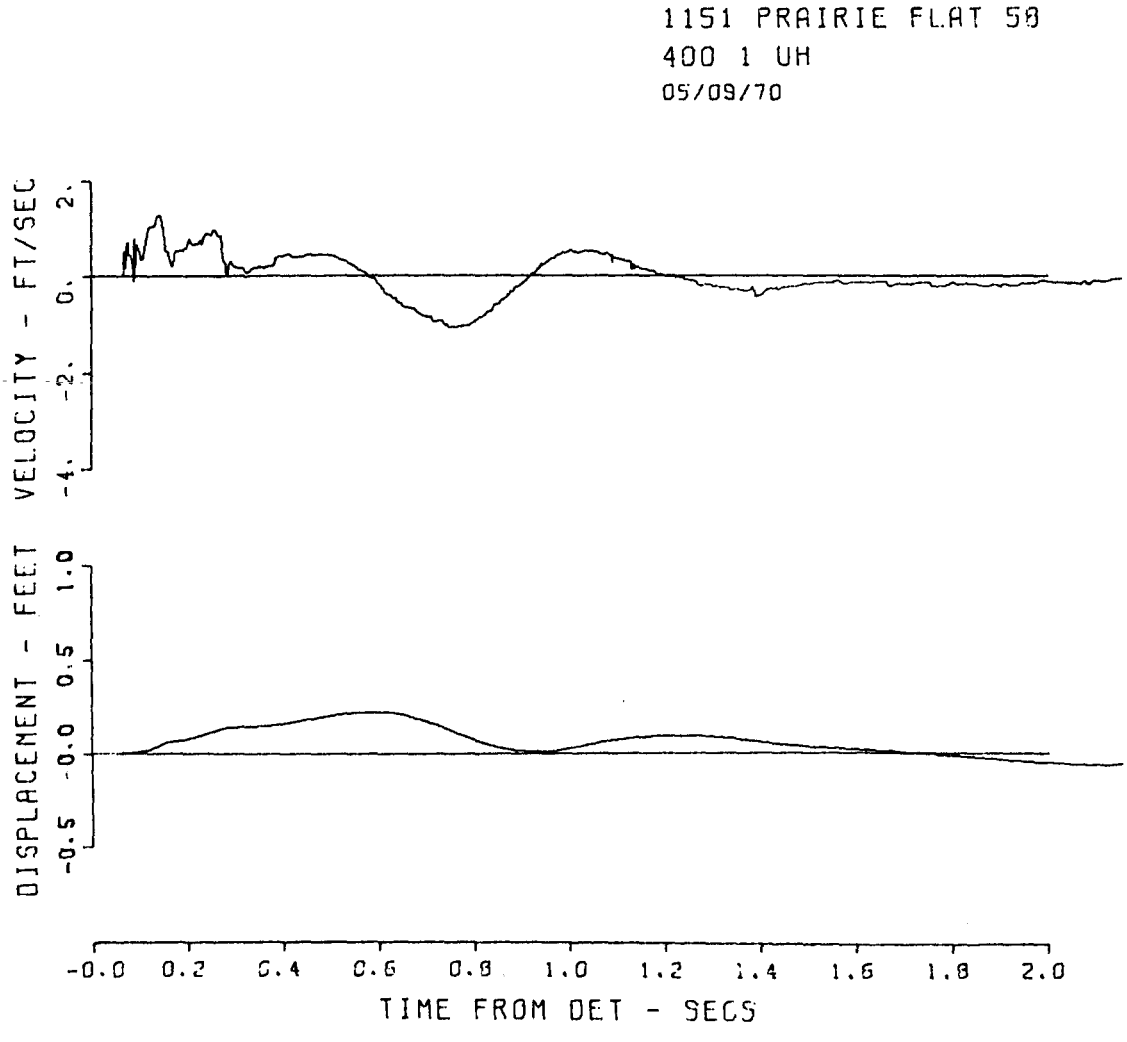

Figure A.47 Gage 1151 UH.

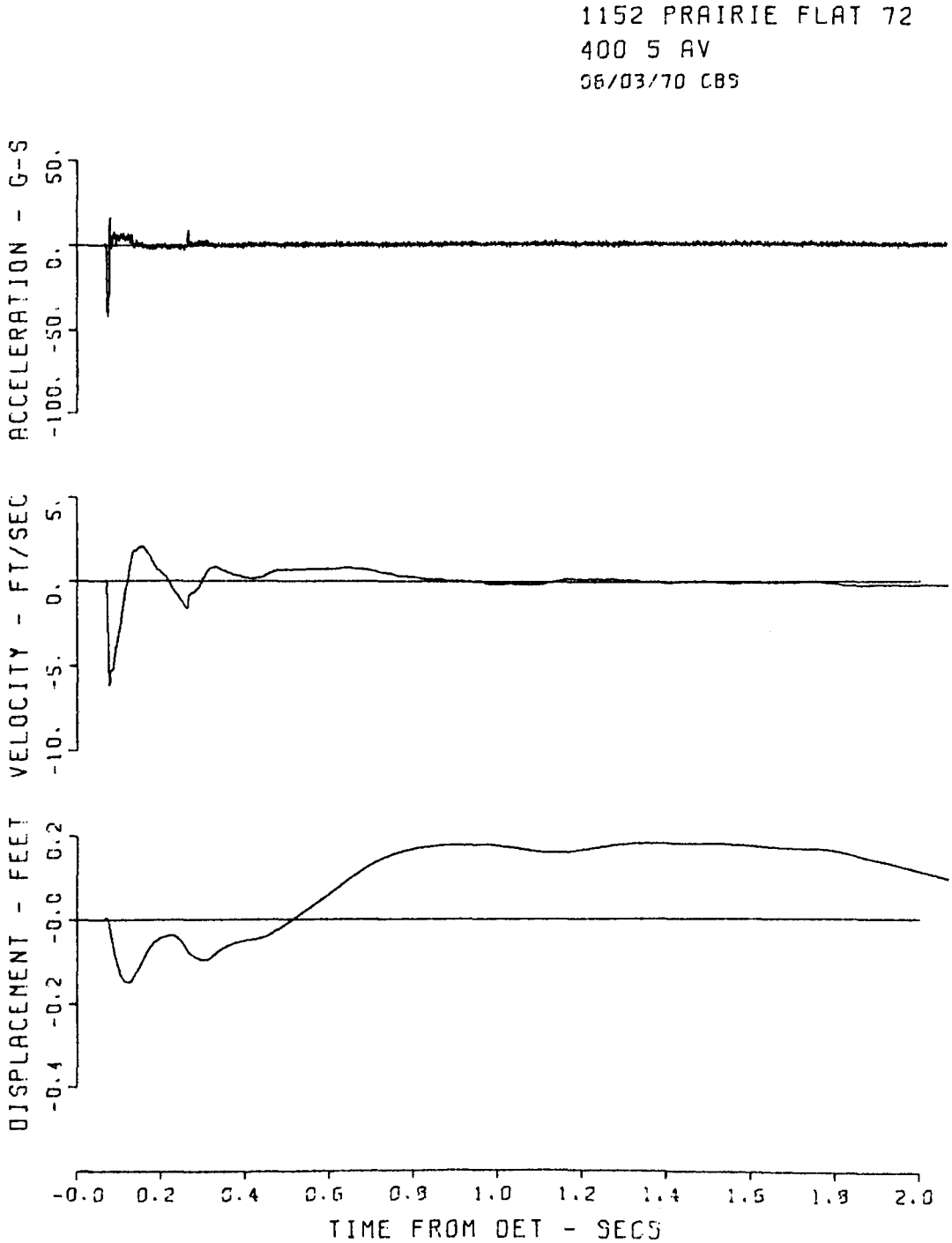

Figure A.48 Gage 1152 AV.

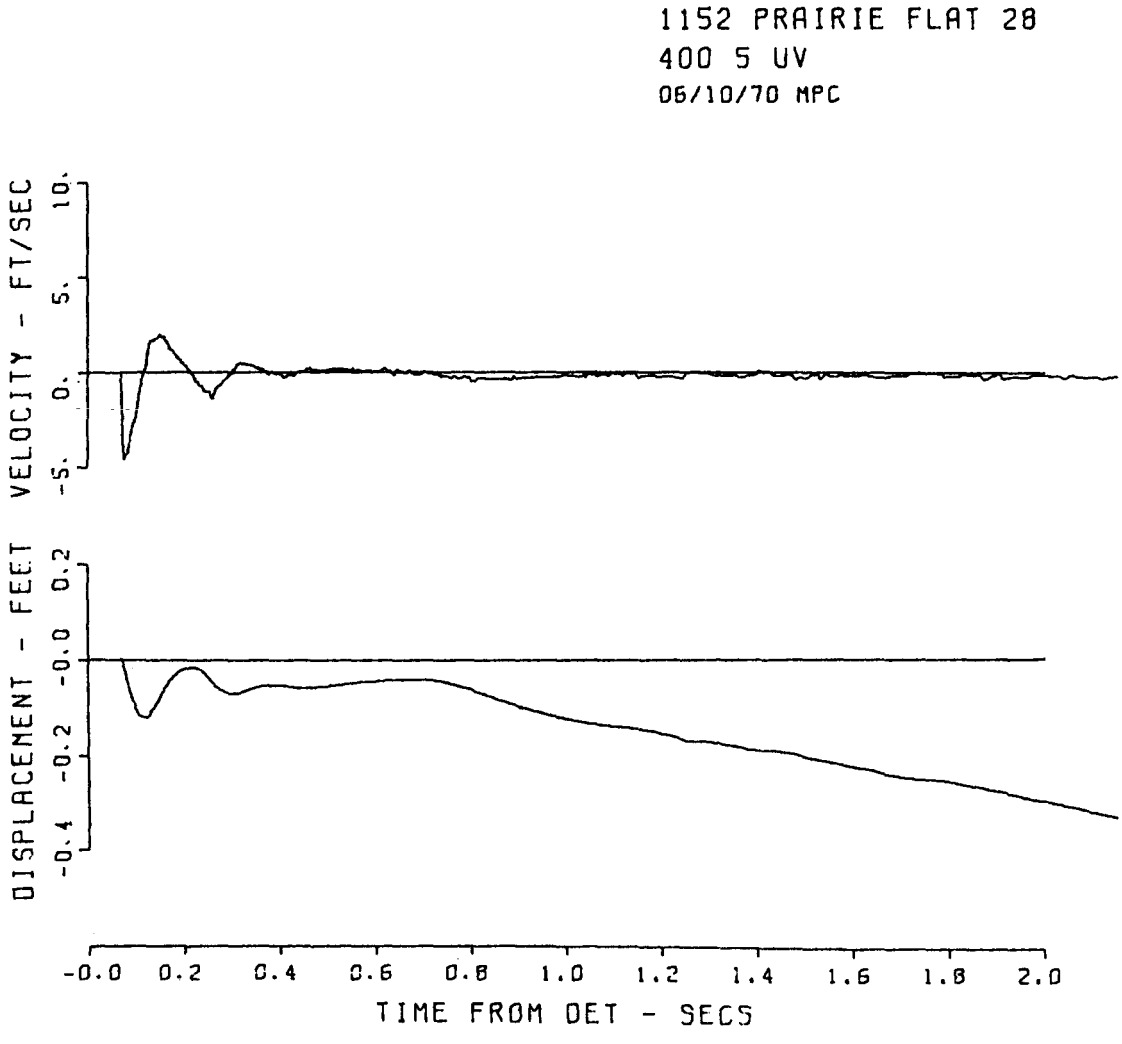

Figure A.49 Gage 1152 UV.

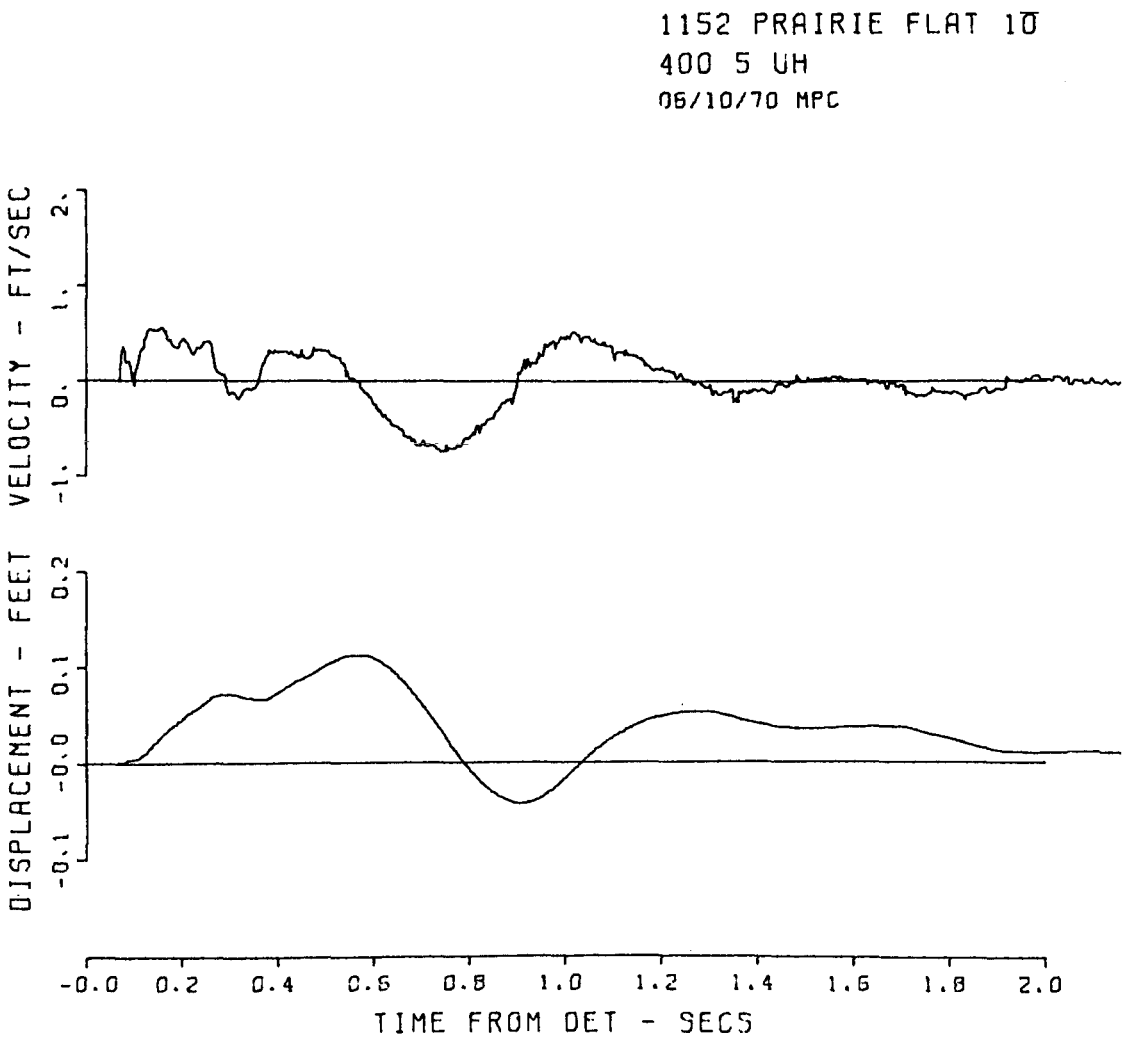

Figure A.50 Gage 1152 UH.

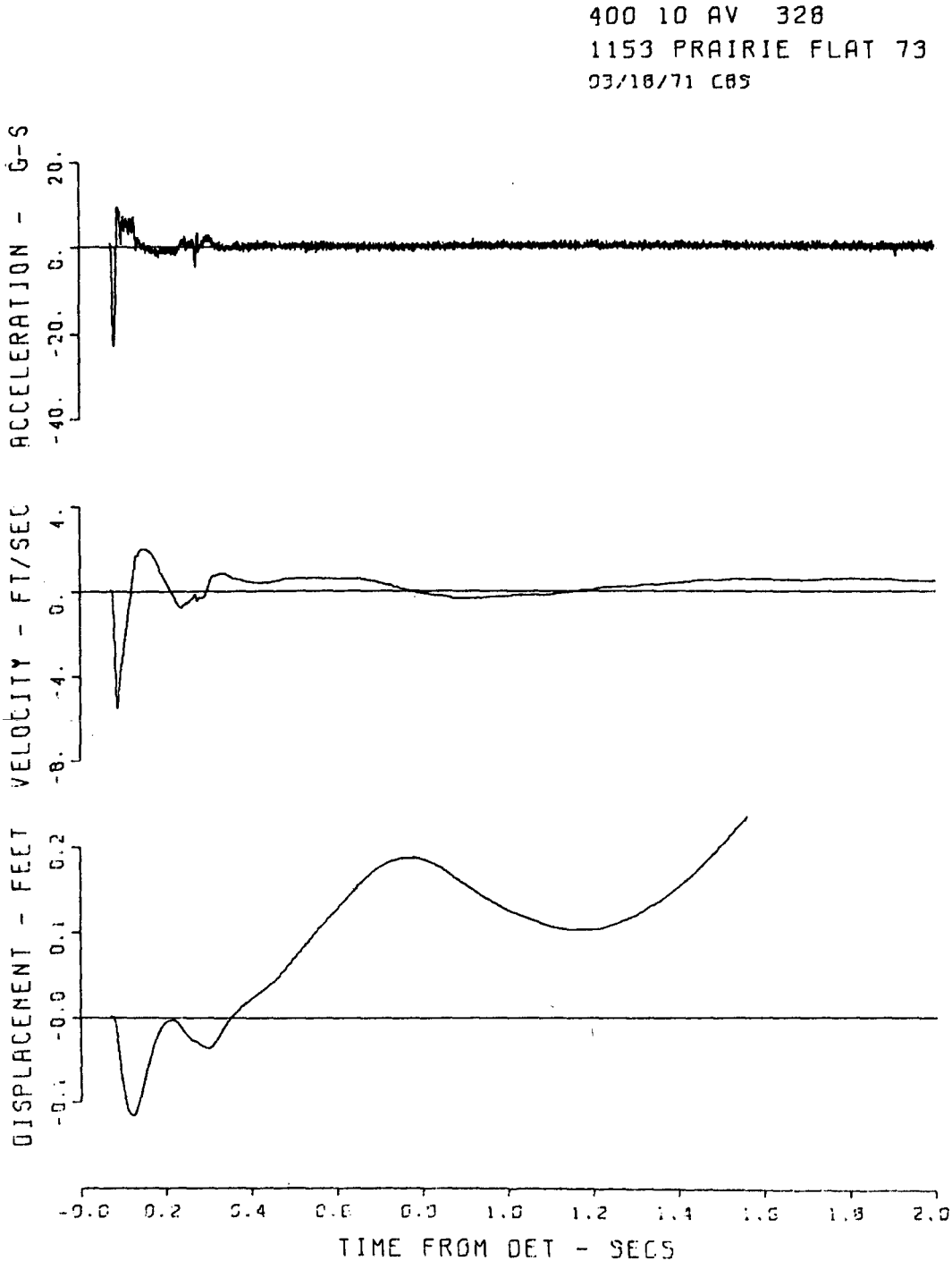

Figure A.51 Gage 1153 AV.

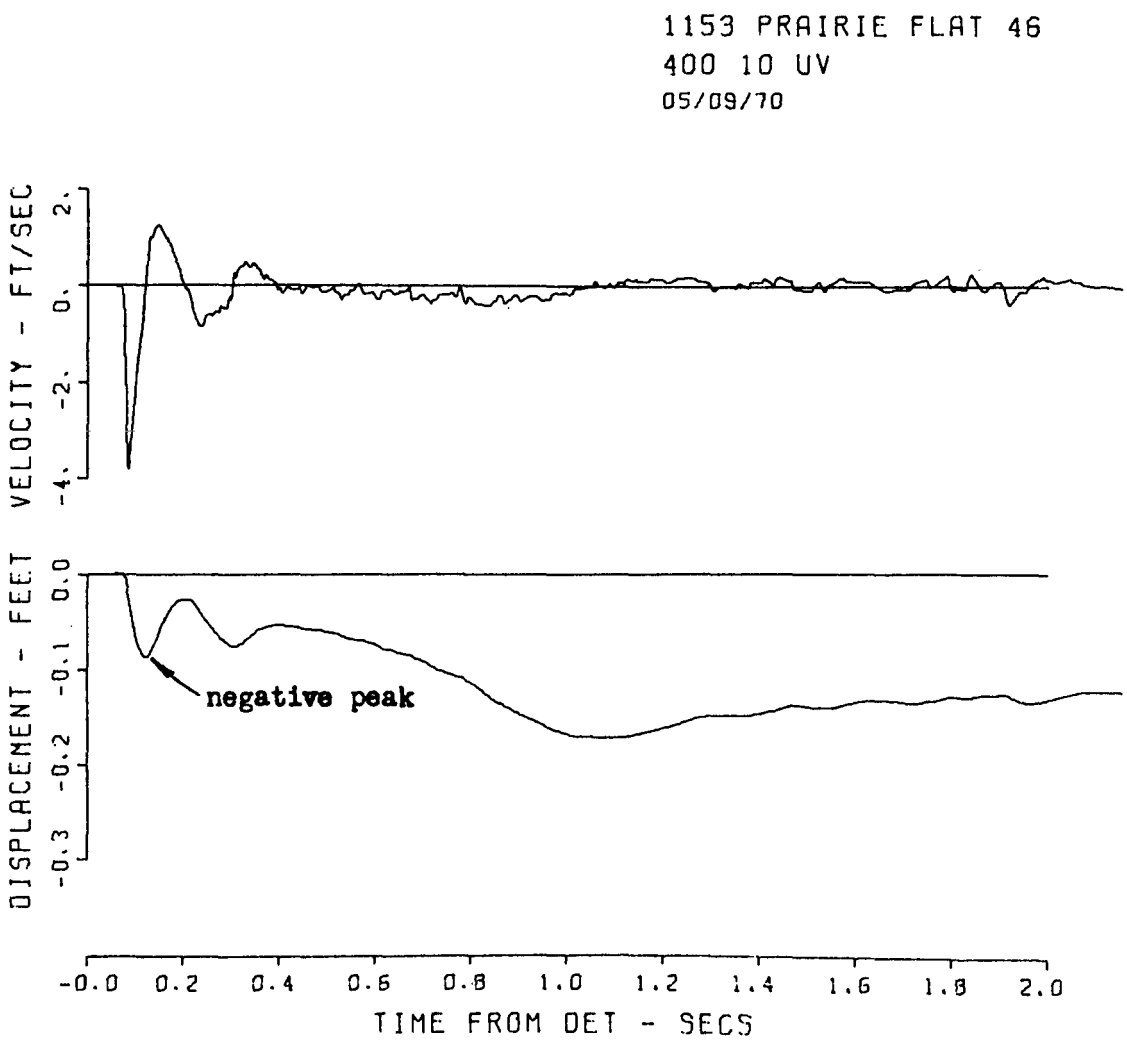

Figure A.52 Gage 1153 UV.

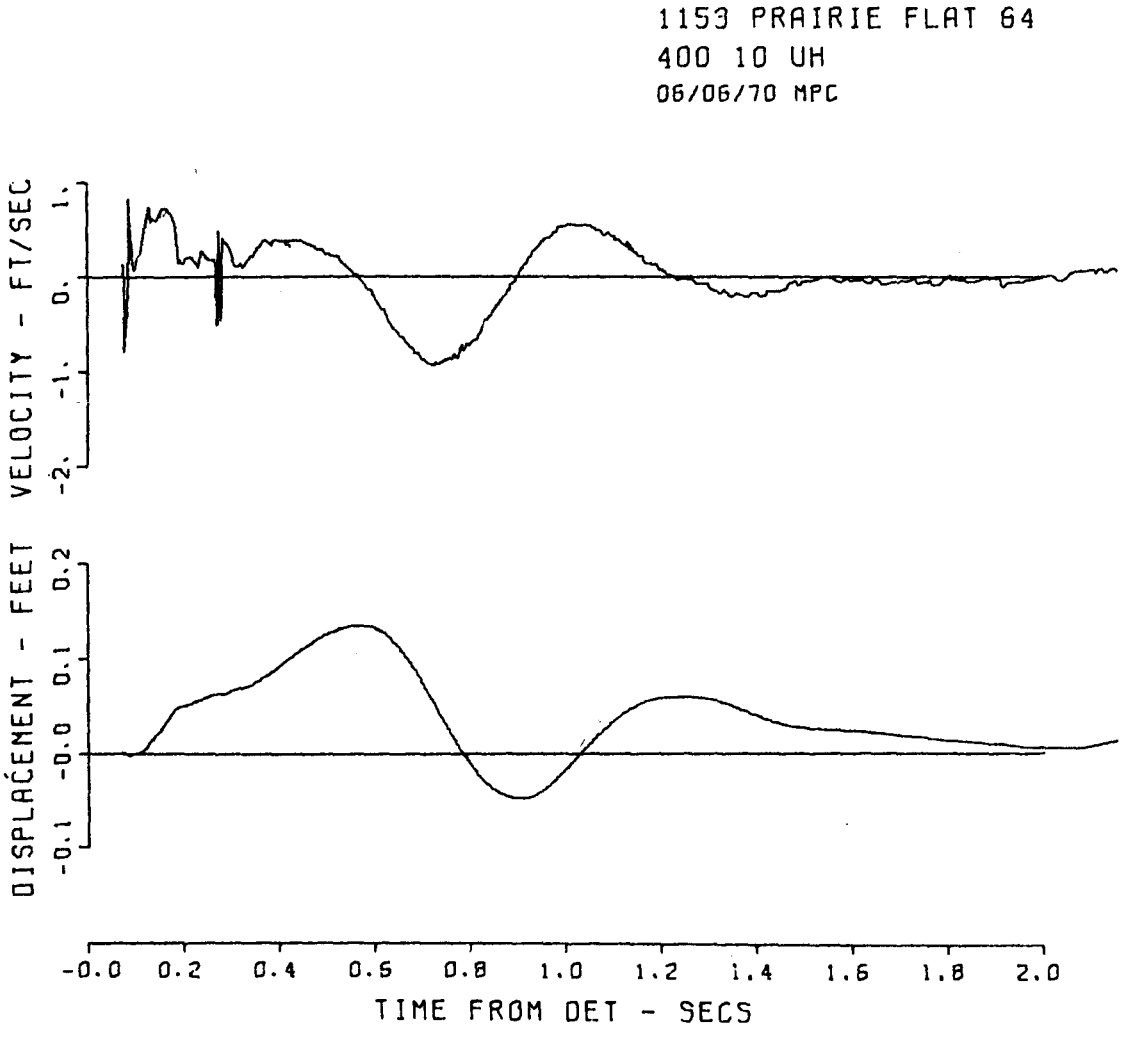

Figure A.53 Gage 1153 UH.

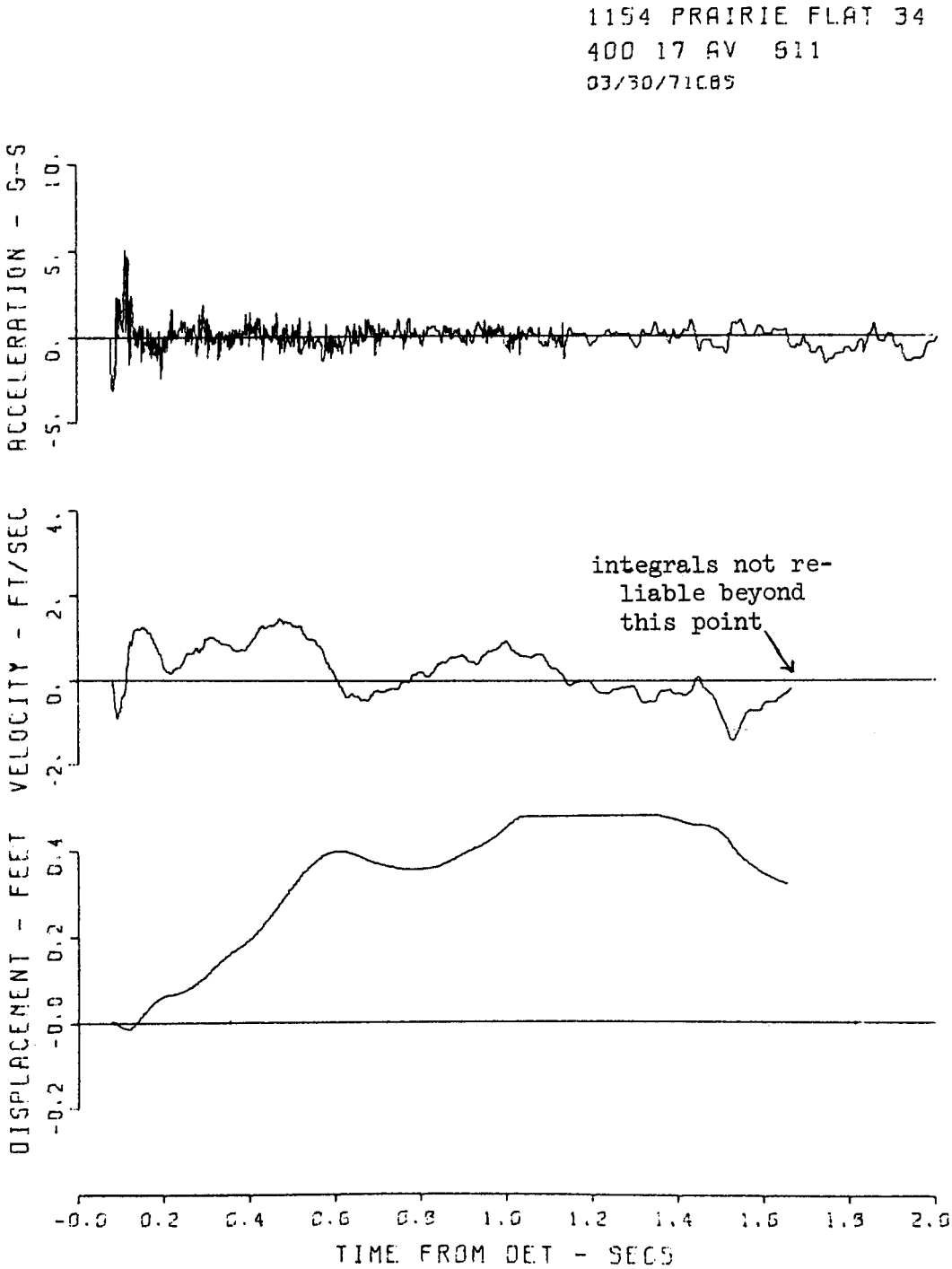

Figure A.54 Gage 1154 AV.

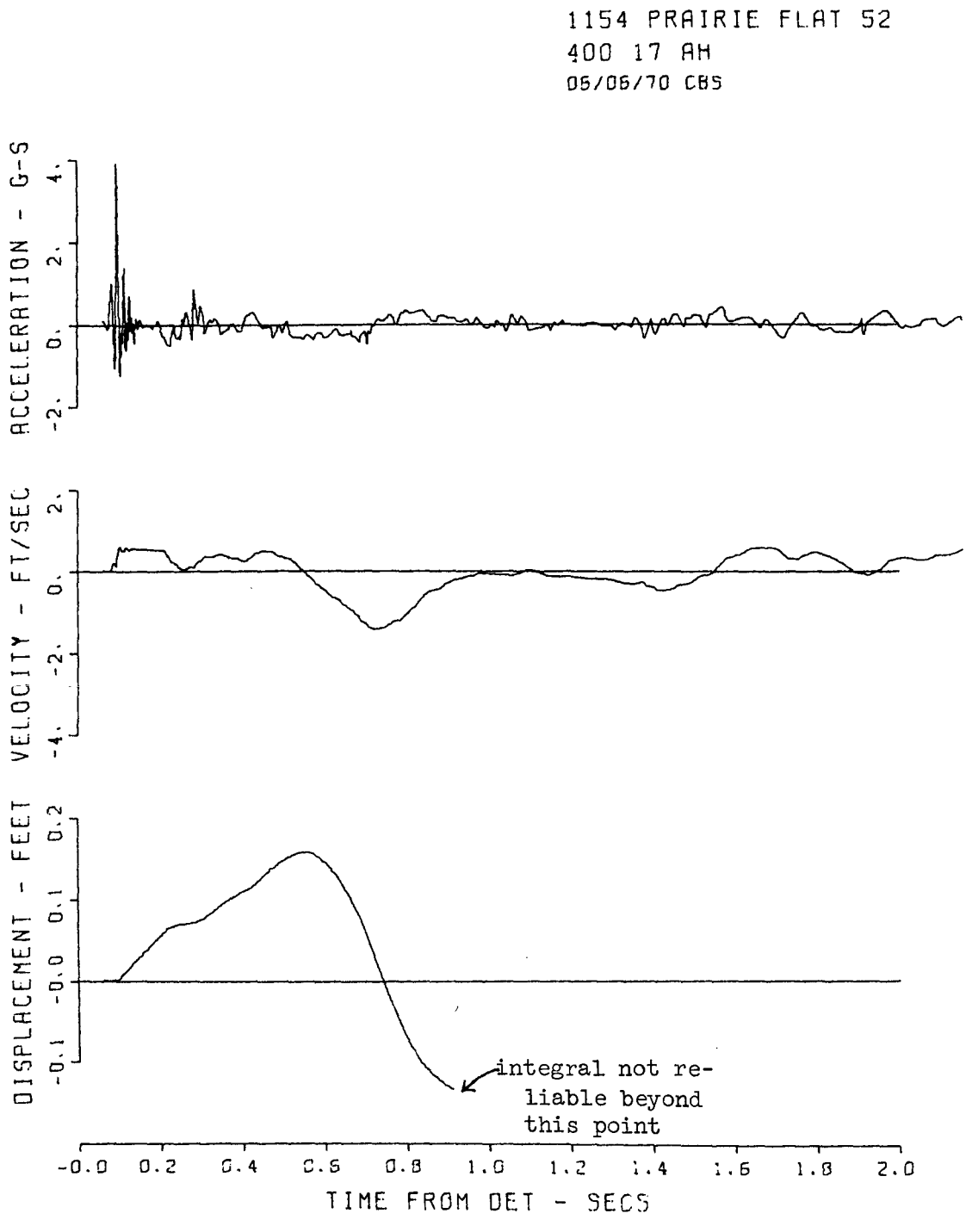

Figure A.55 Gage 1154 AH.

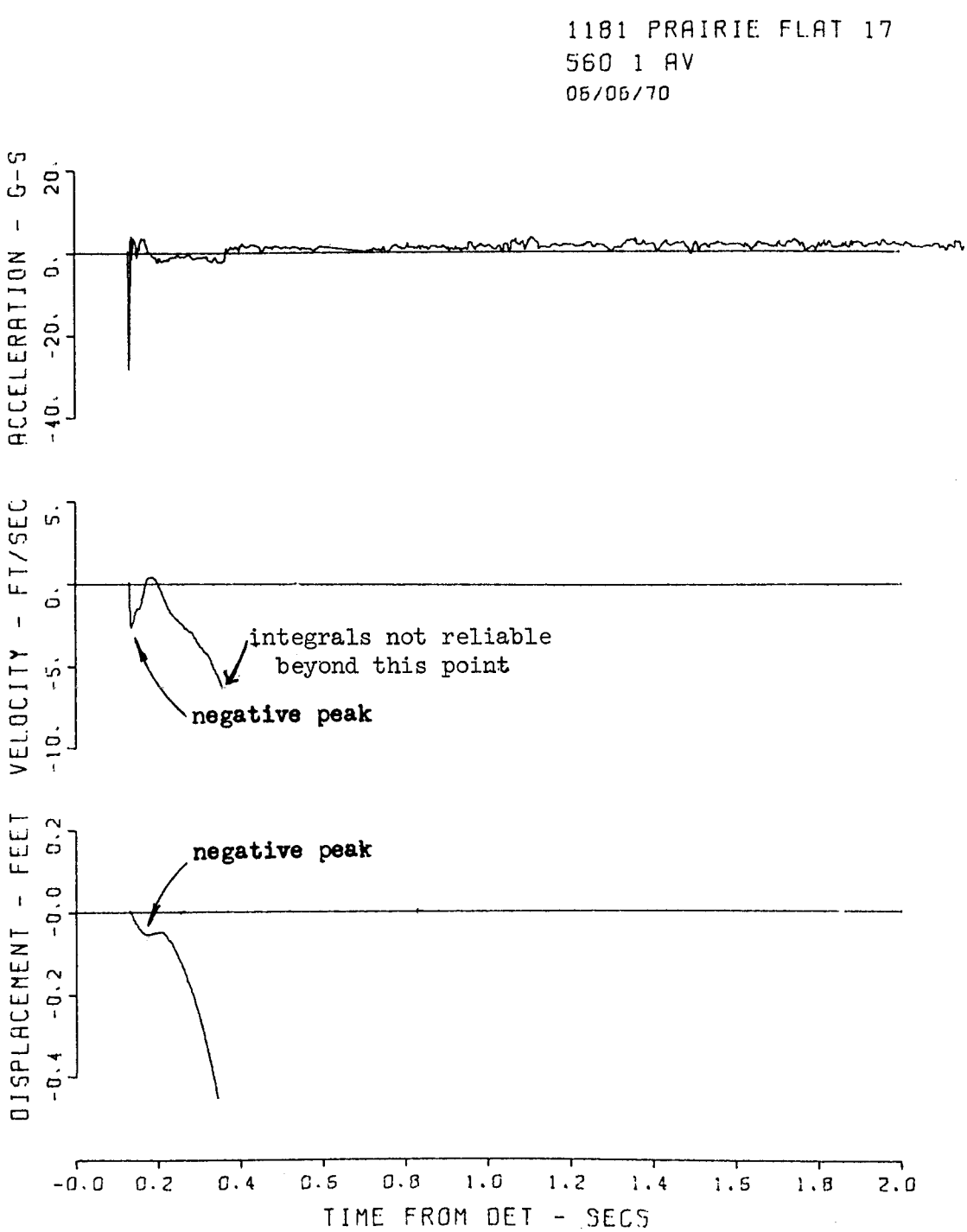

Figure A.56 Gage 1181 AV.

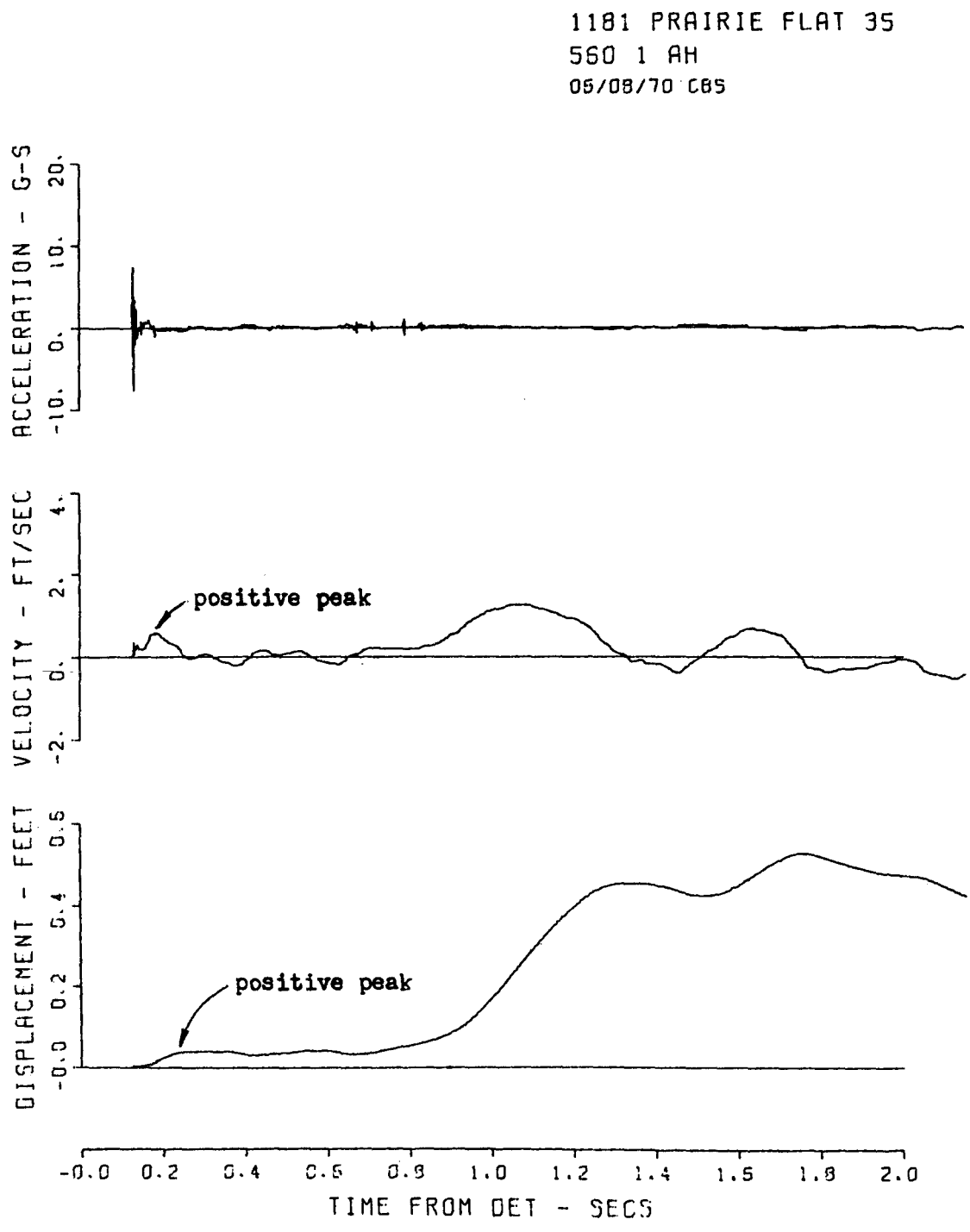

Figure A.57 Gage 1181 AH.

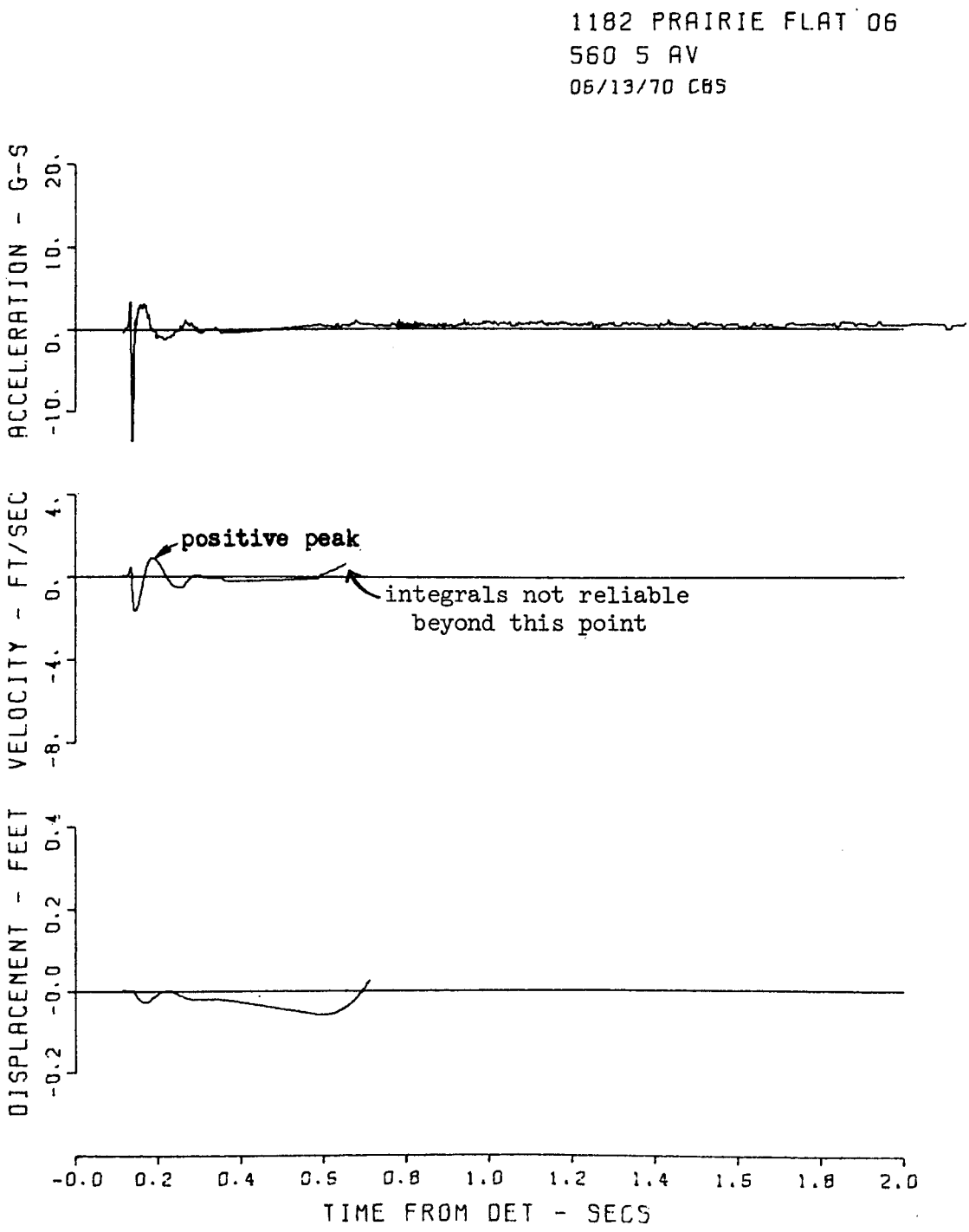

Figure A.58 Gage 1182 AV.

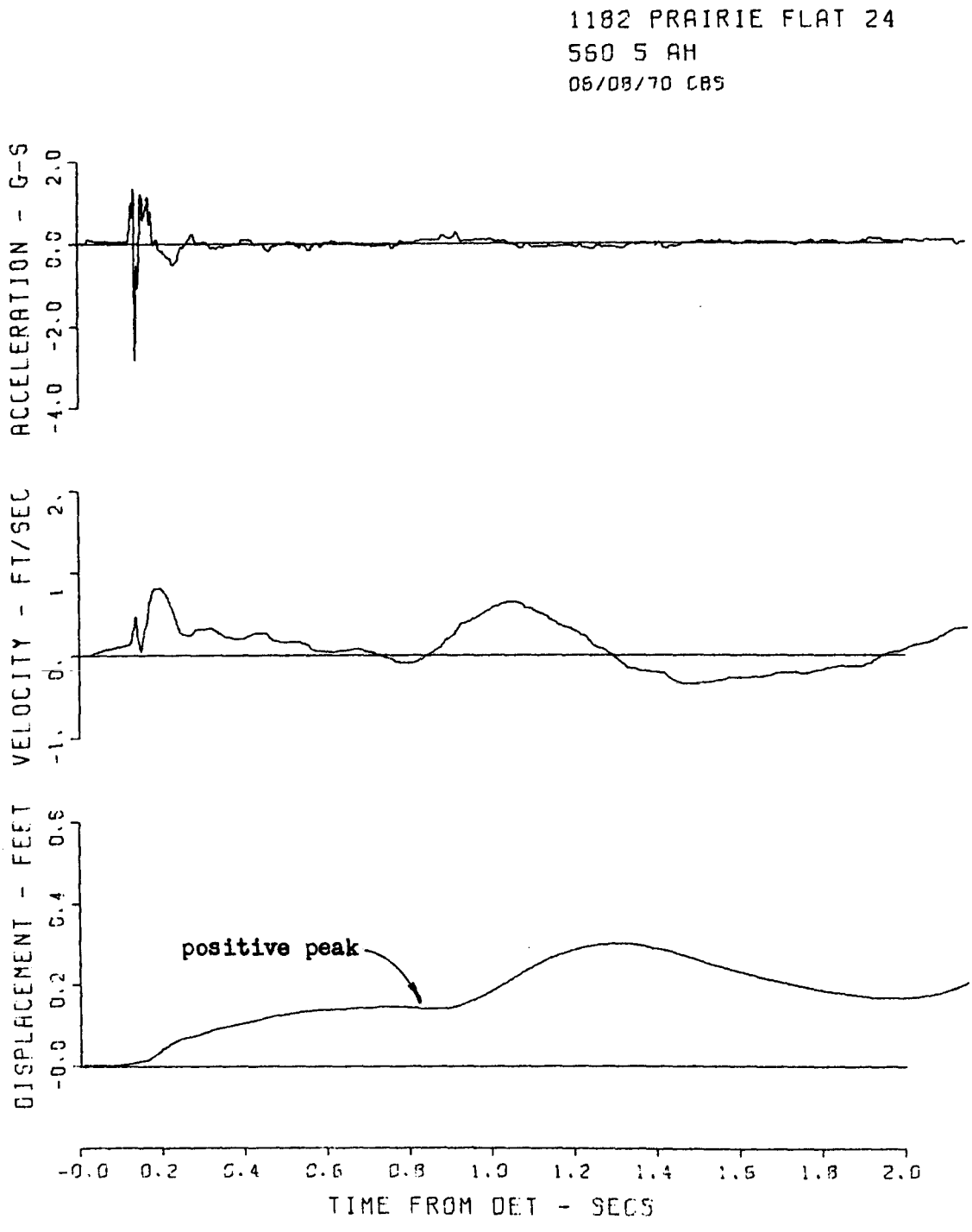

Figure A.59 Gage 1182 AH.

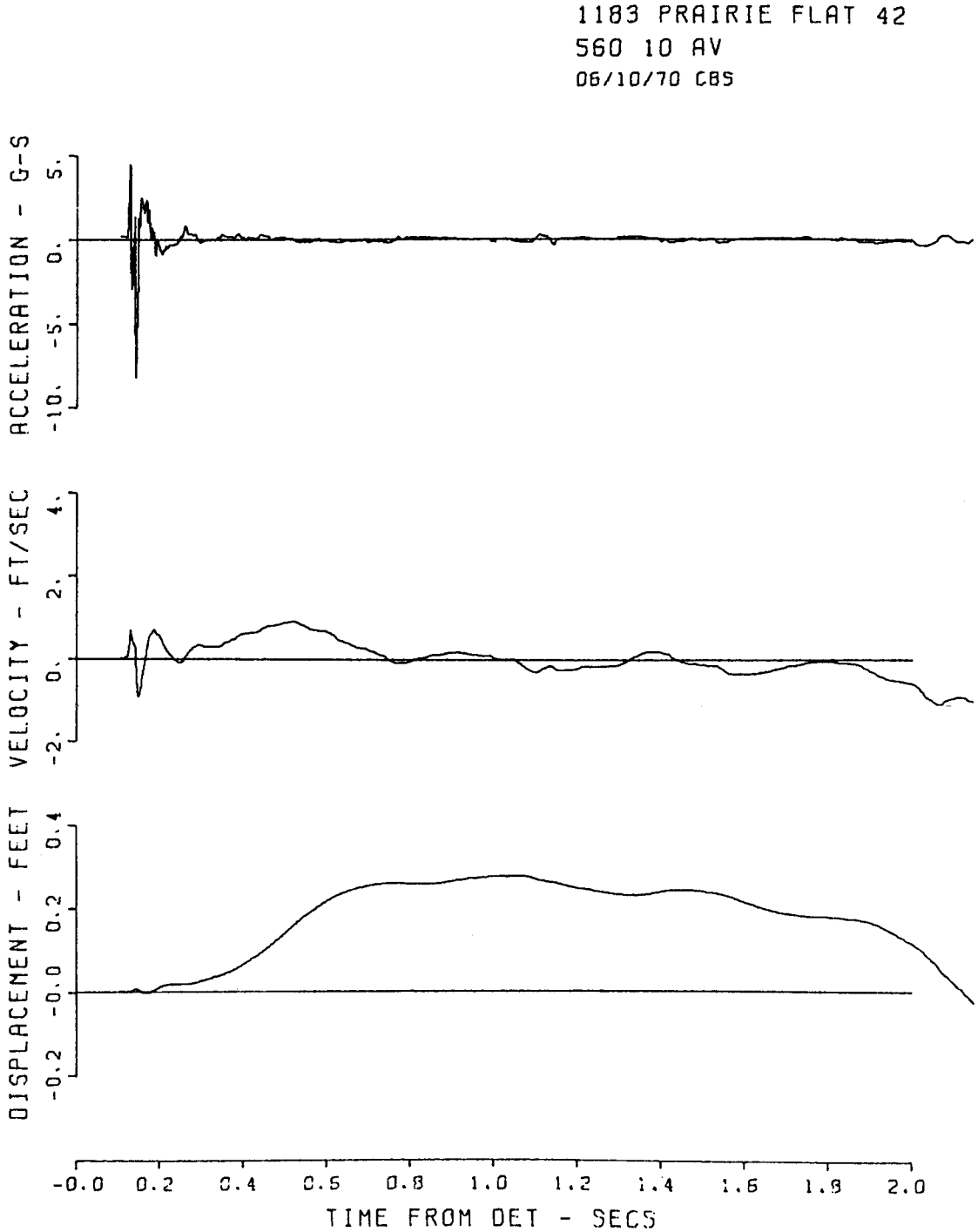

Figure A.60 Gage 1183 AV.

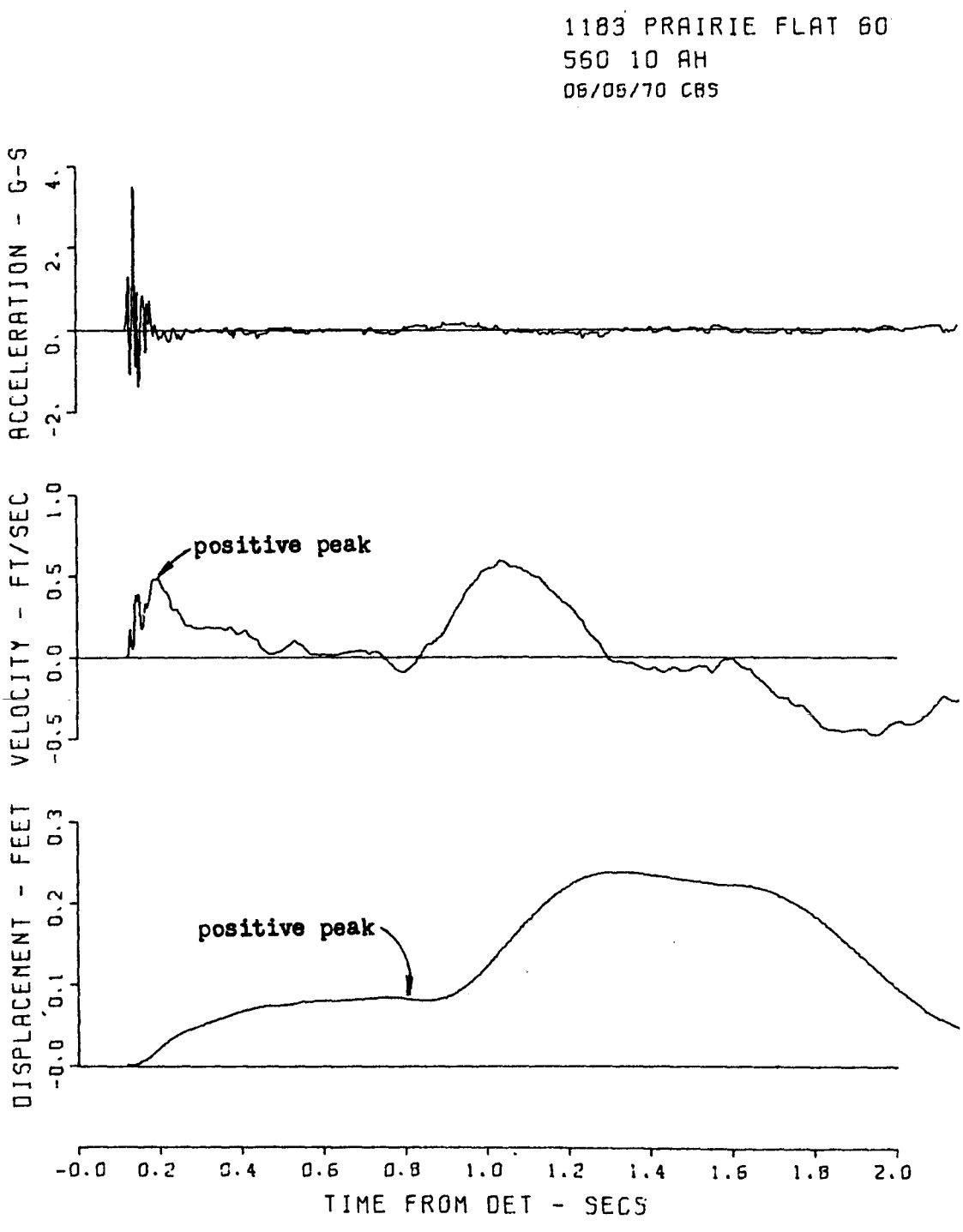

Figure A.61 Gage 1183 AH.

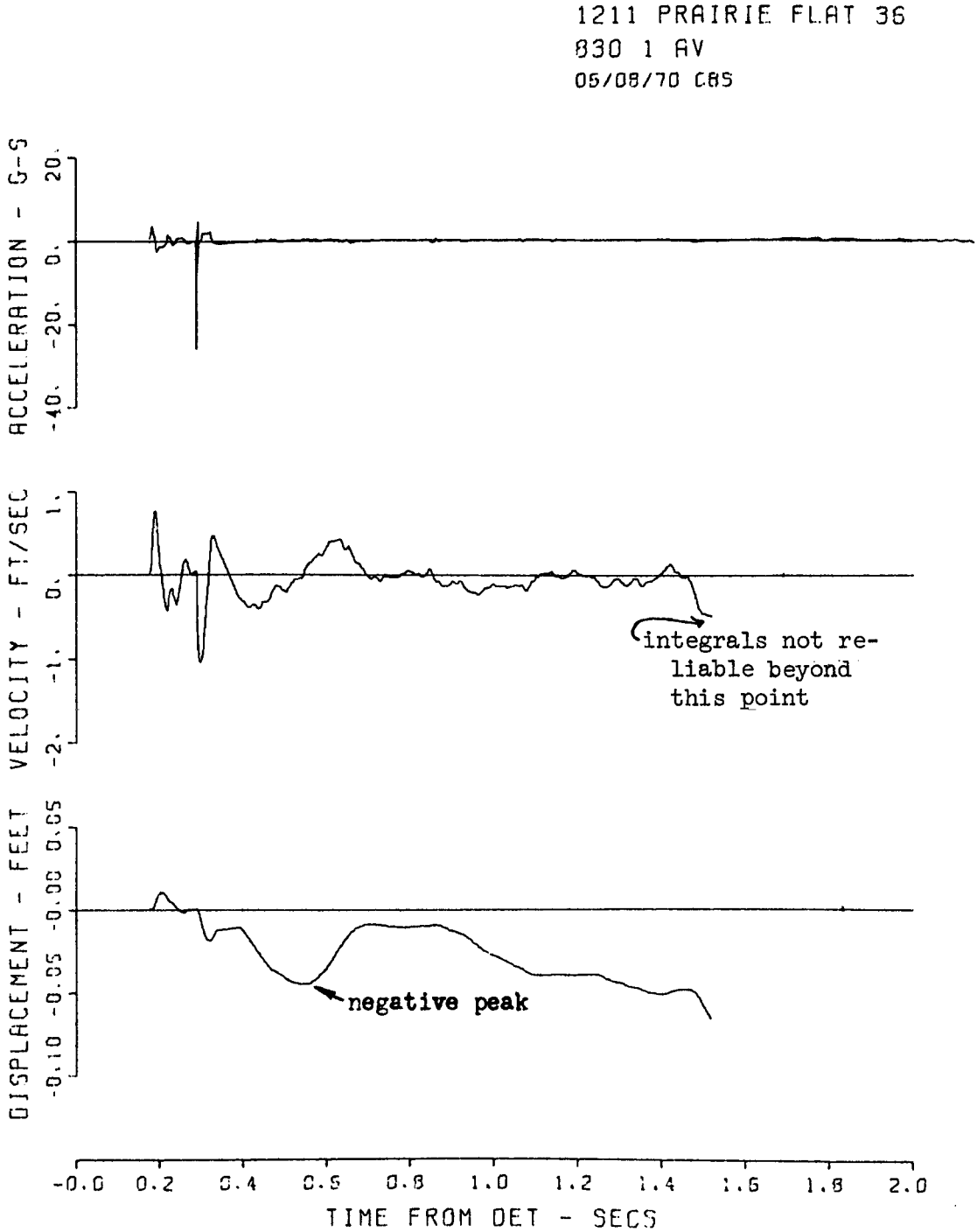

Figure A.62 Gage 1211 AV.

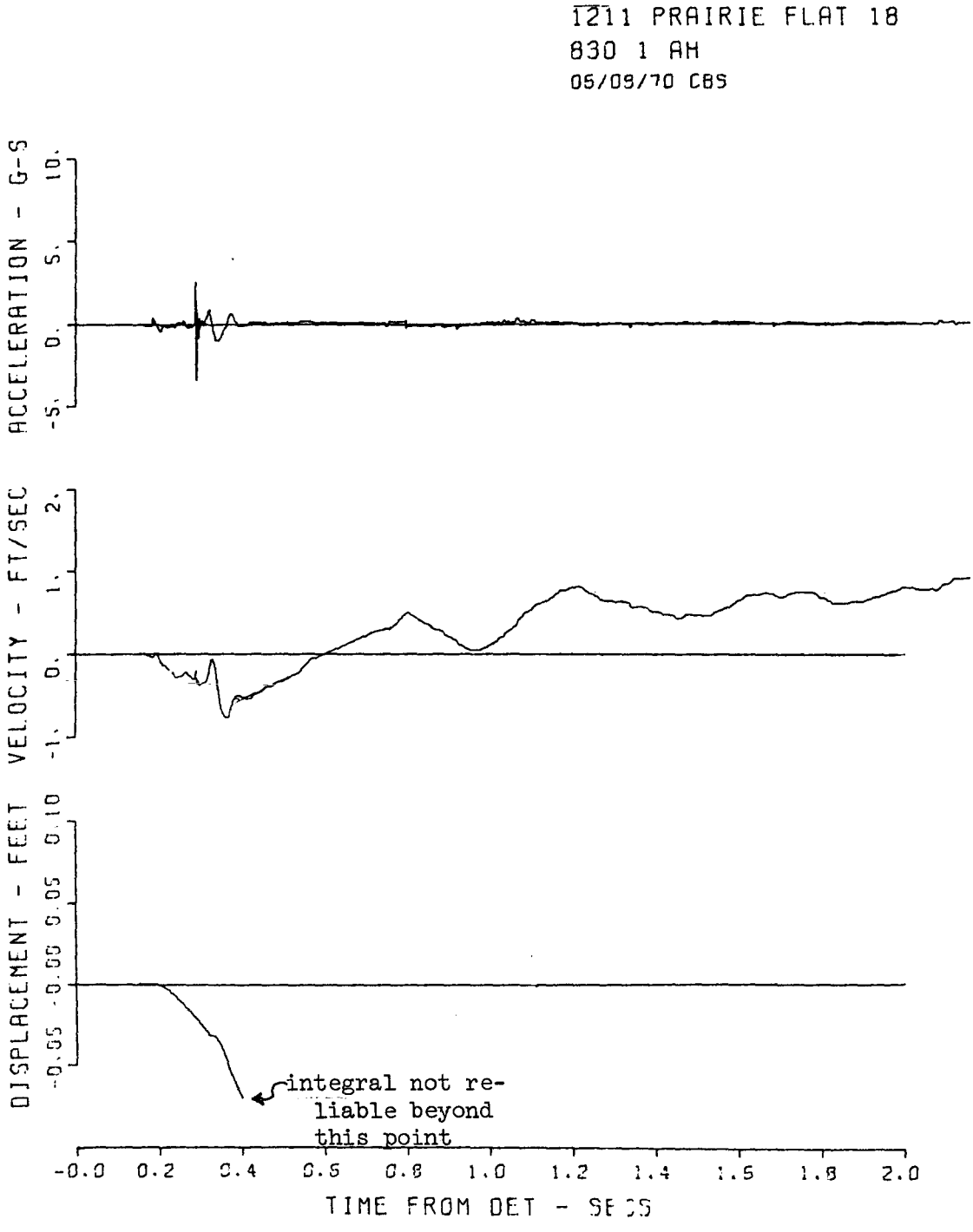

Figure A.63 Gage 1211 AH.

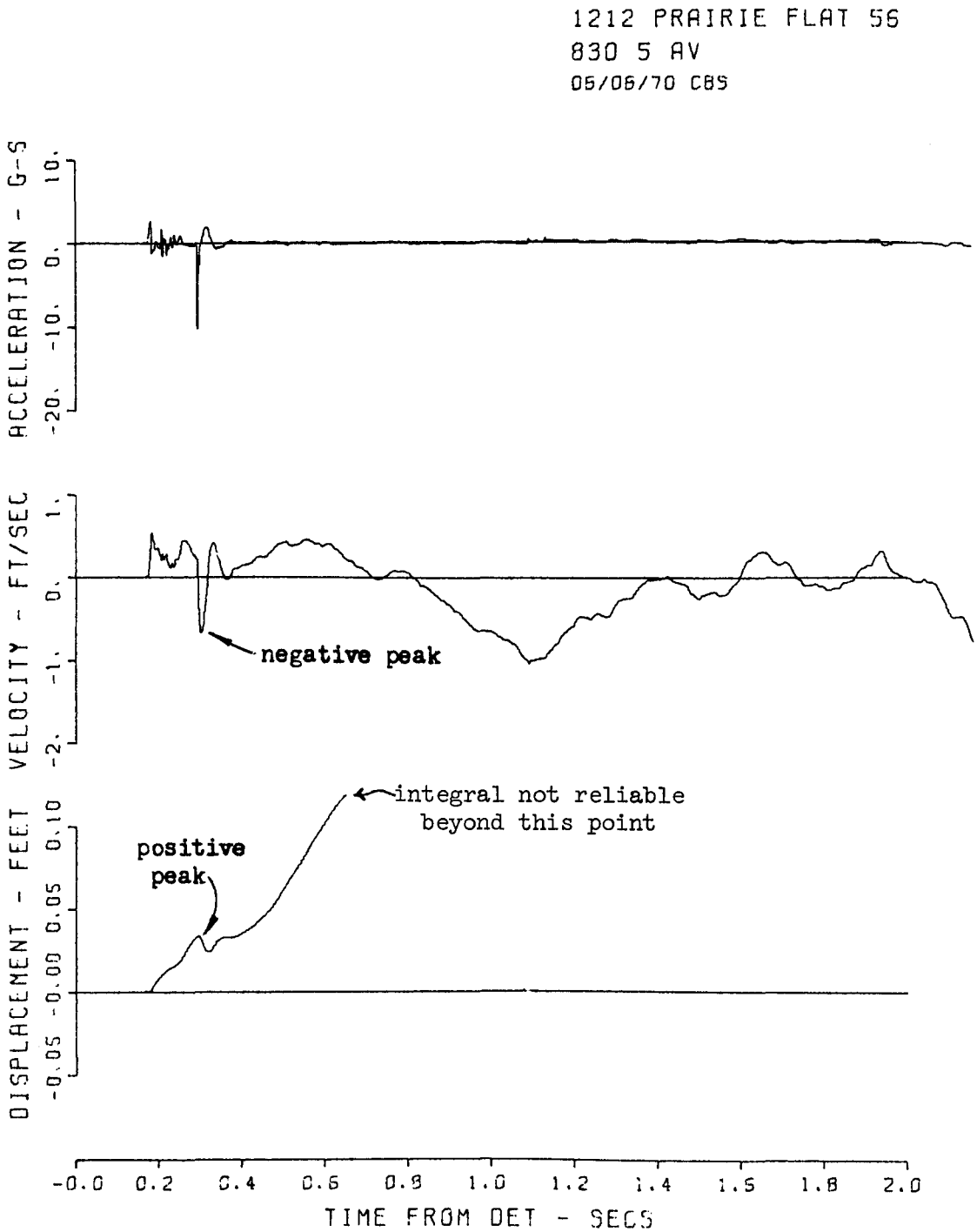

Figure A.64 Gage 1212 AV.

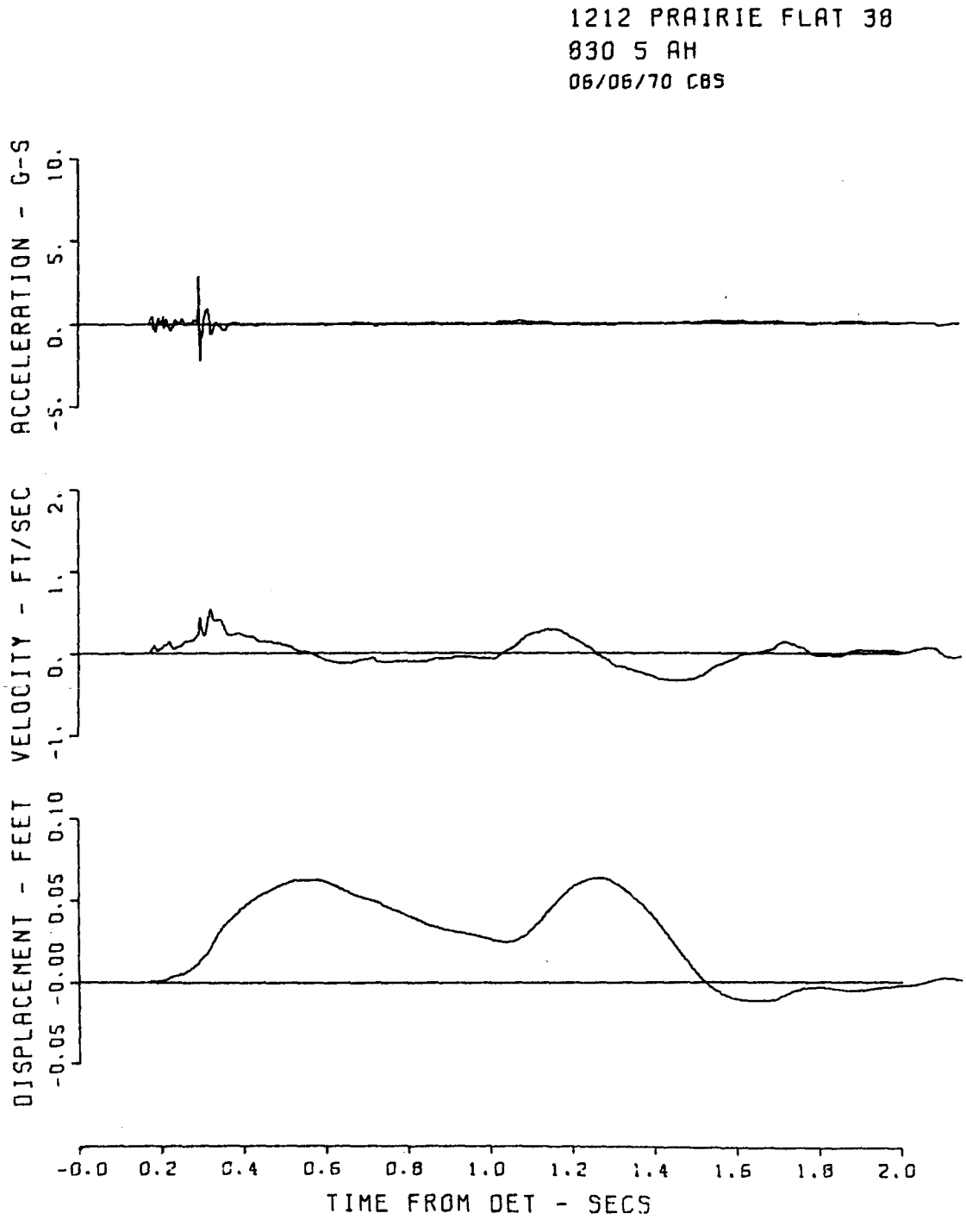

Figure A.65 Gage 1212 AH.

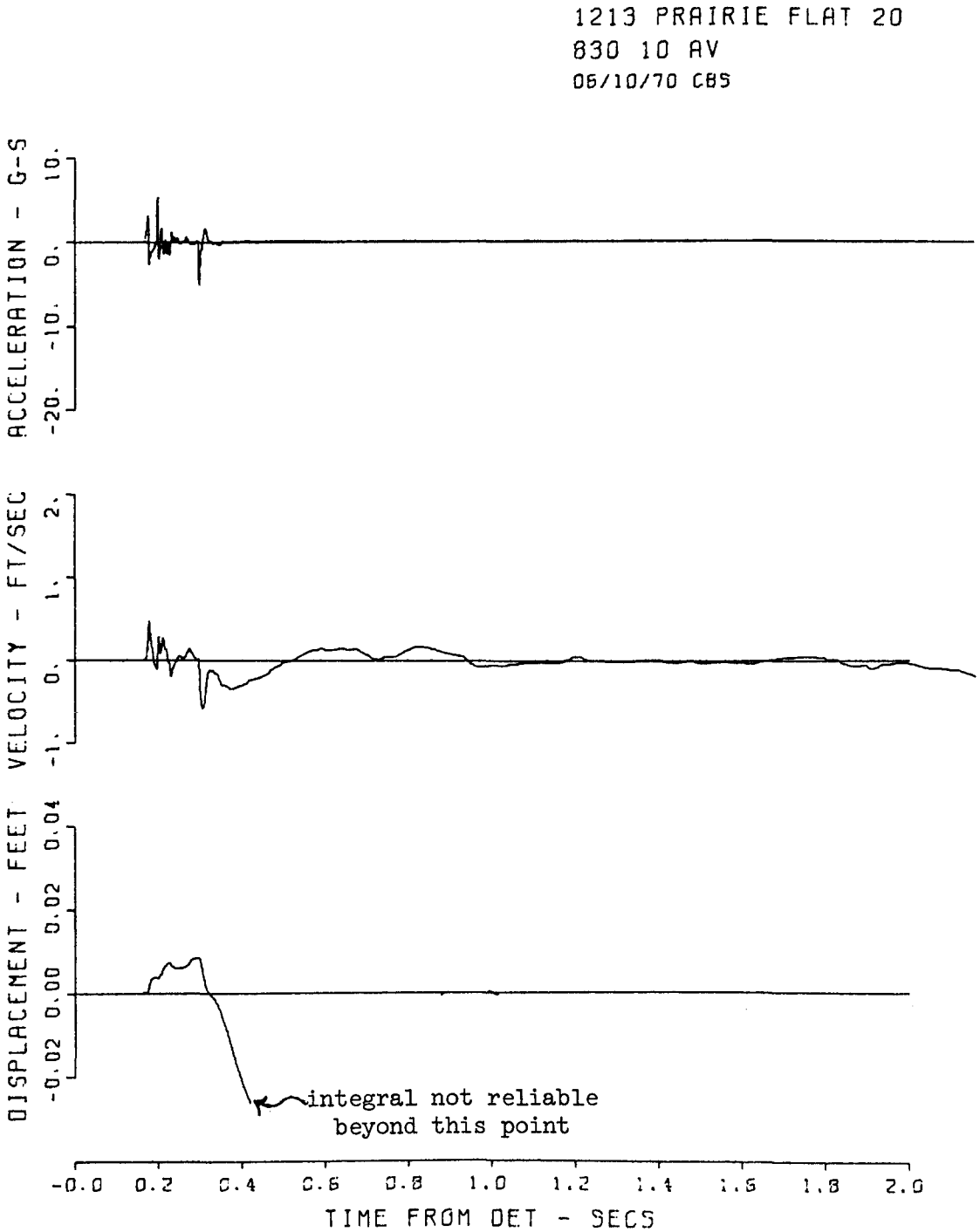

Figure A.66 Gage 1213 AV.

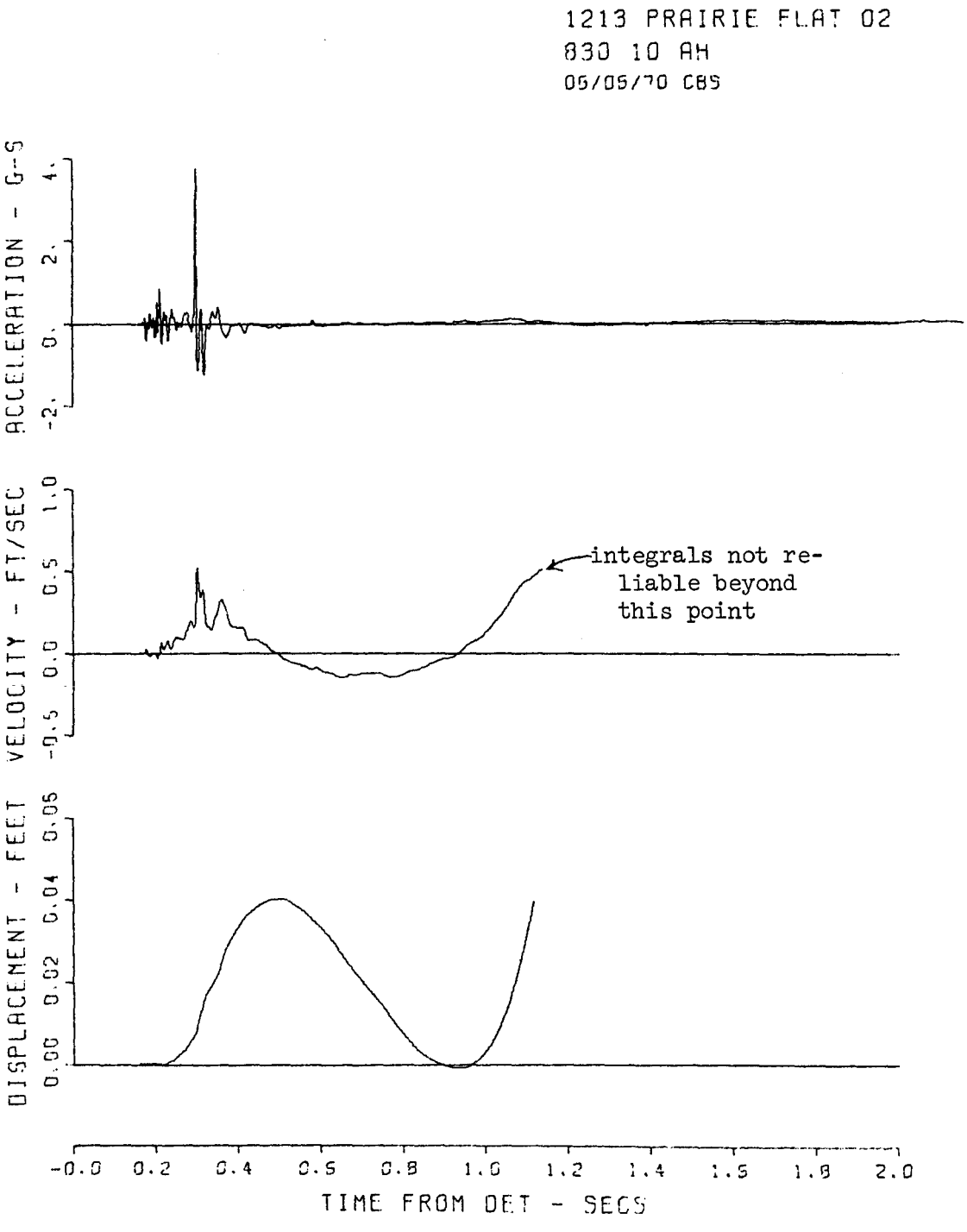

Figure A.67 Gage 1213 AH.

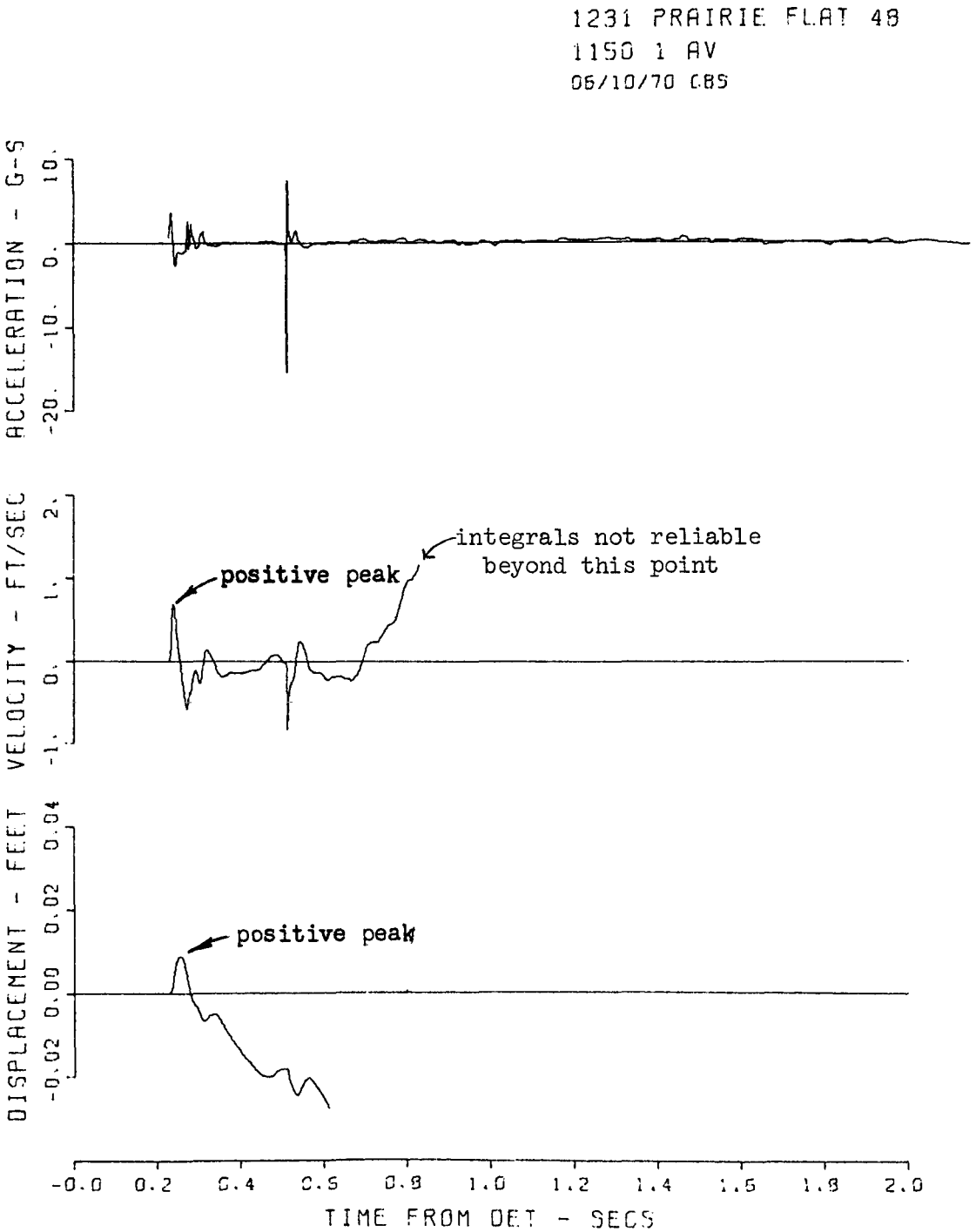

Figure A.68 Gage 1231 AV.

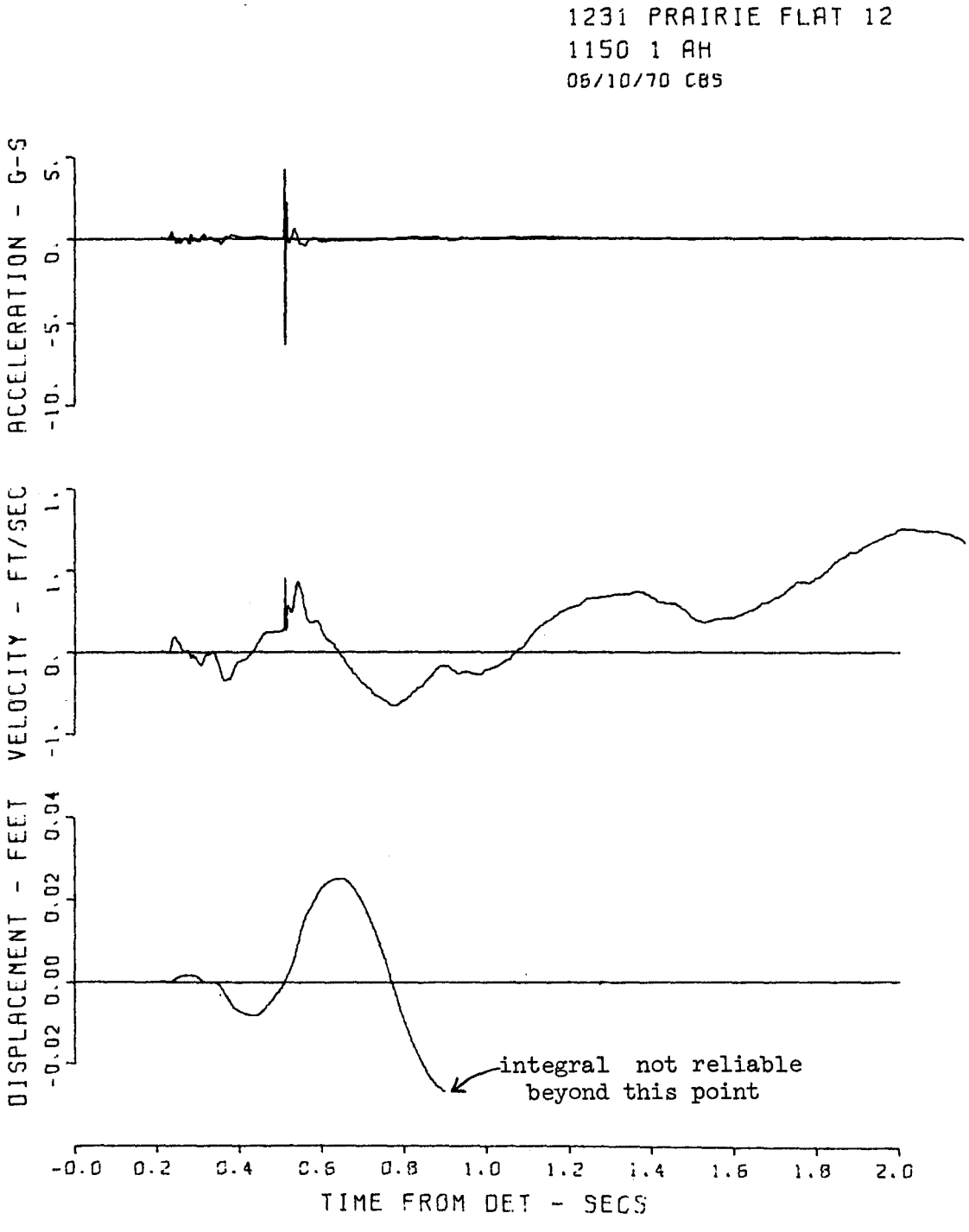

Figure A.69 Gage 1231 AH.

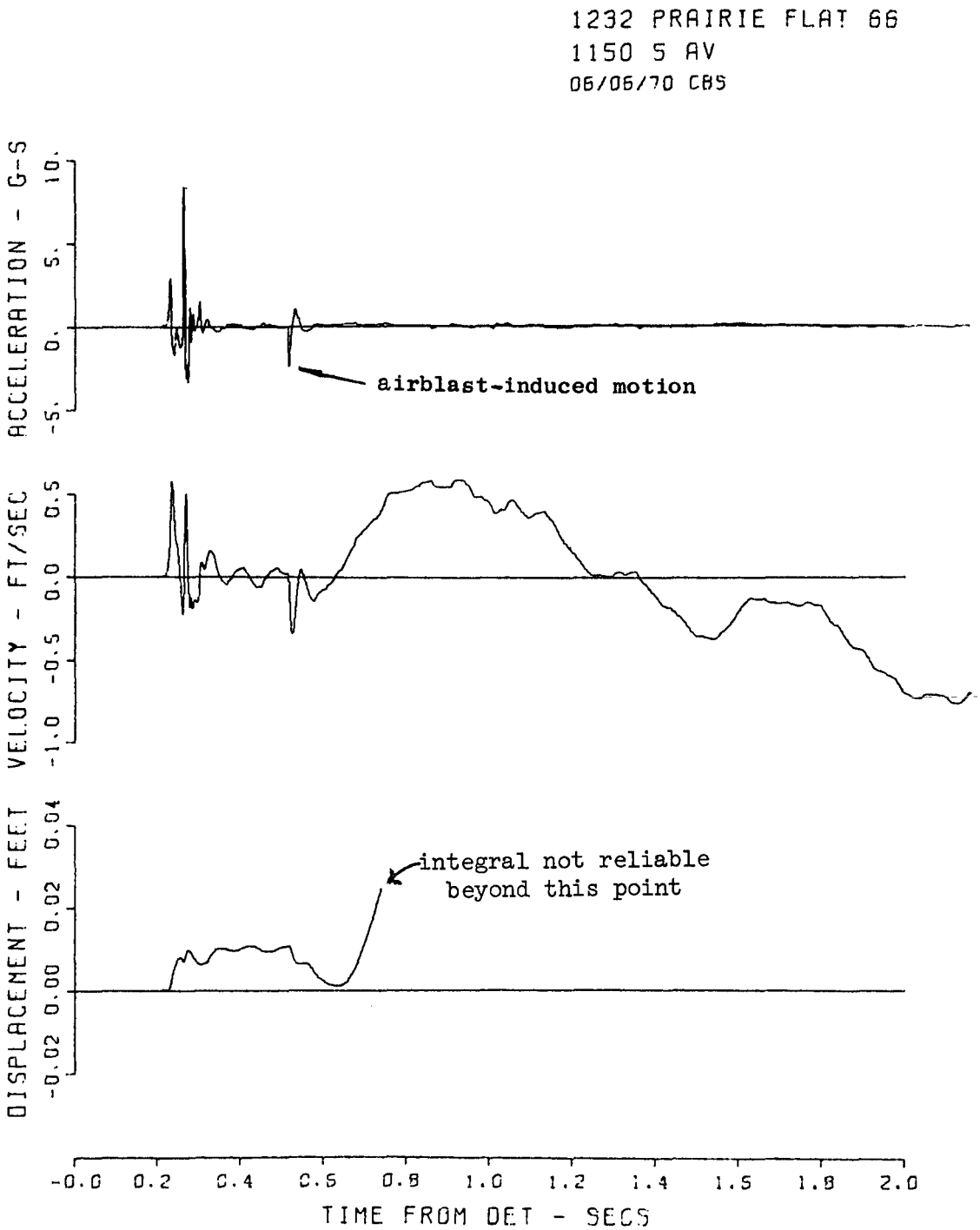

Figure A.70 Gage 1232 AV.

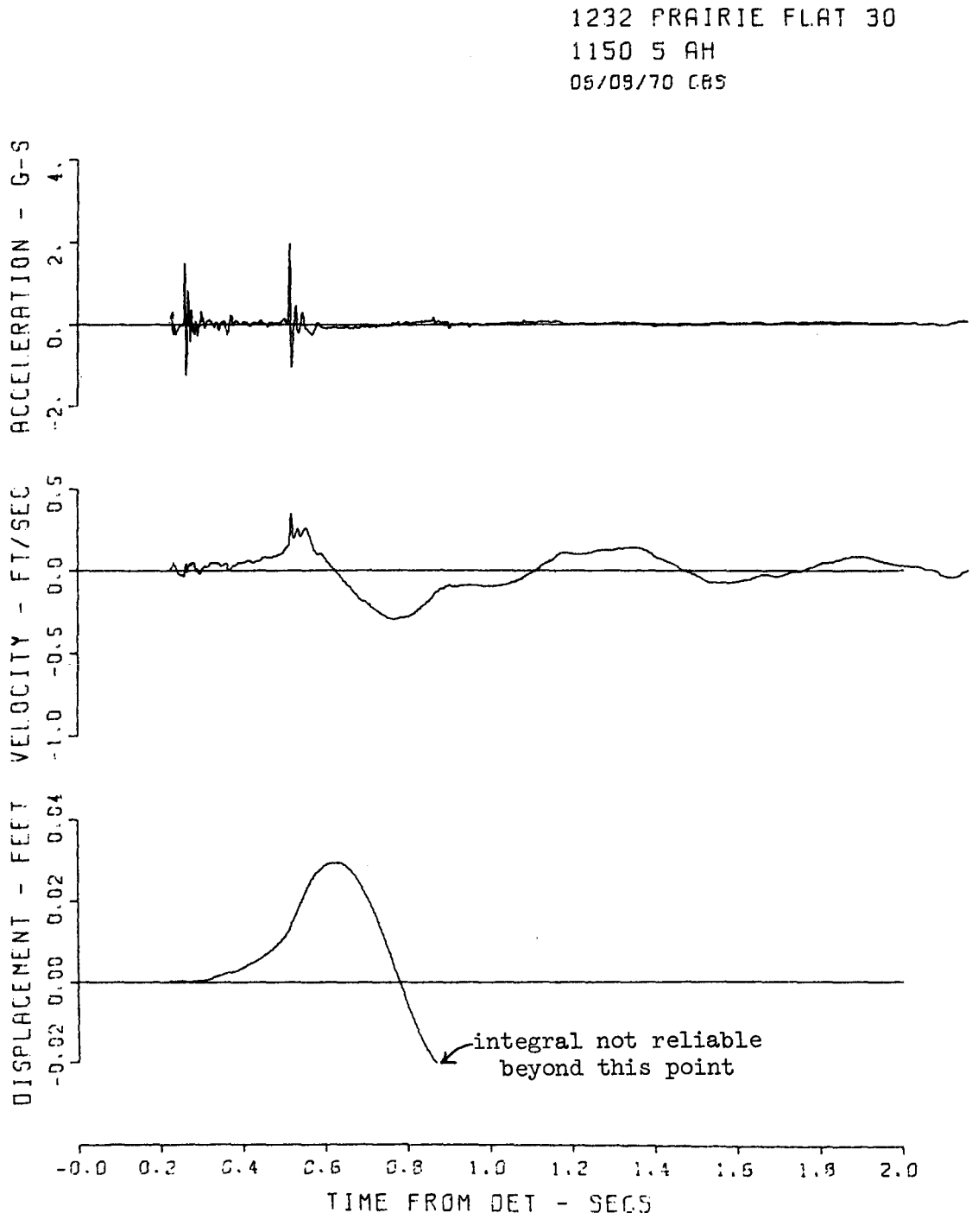

Figure A.71 Gage 1232 AH.

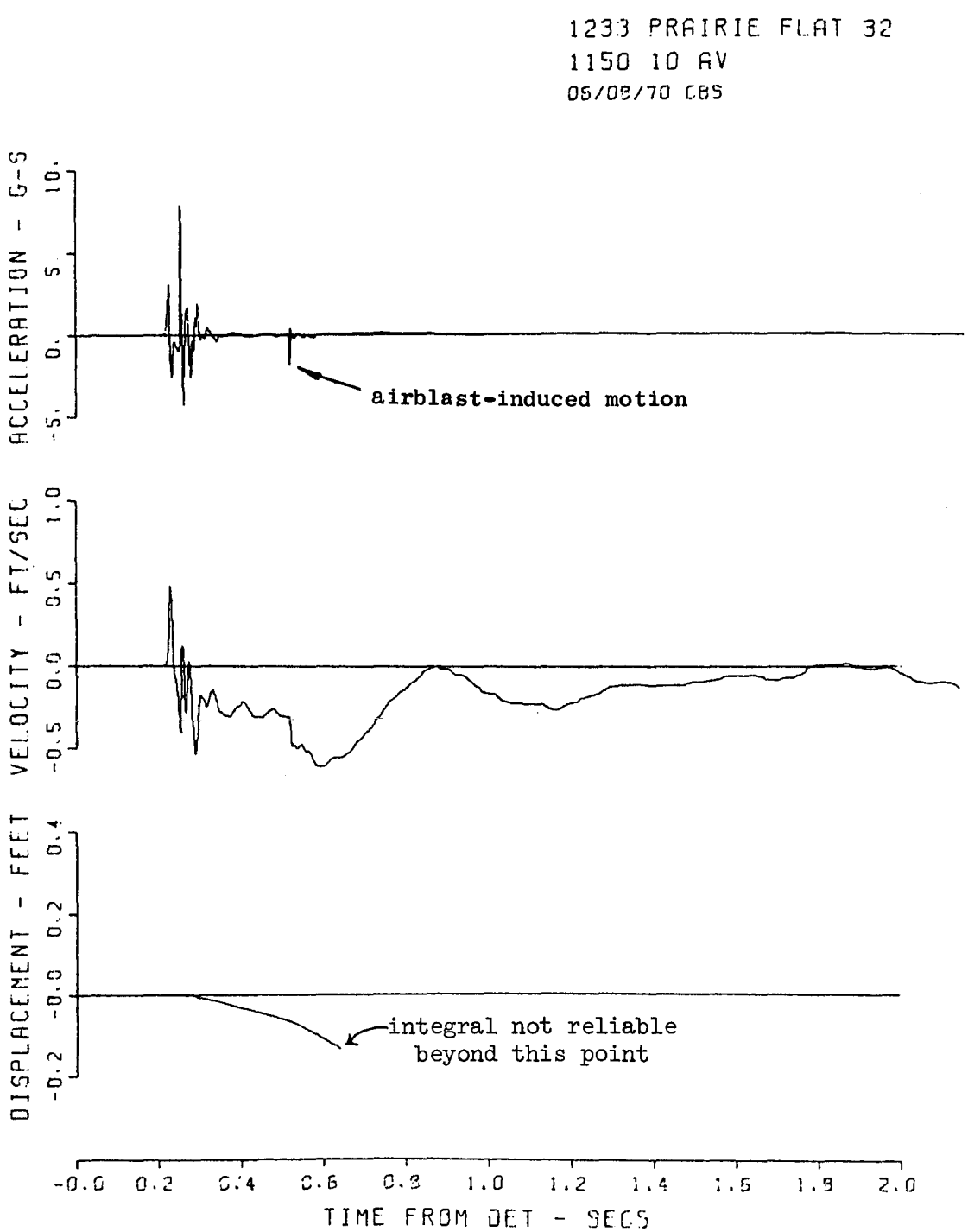

Figure A.72 Gage 1233 AV.

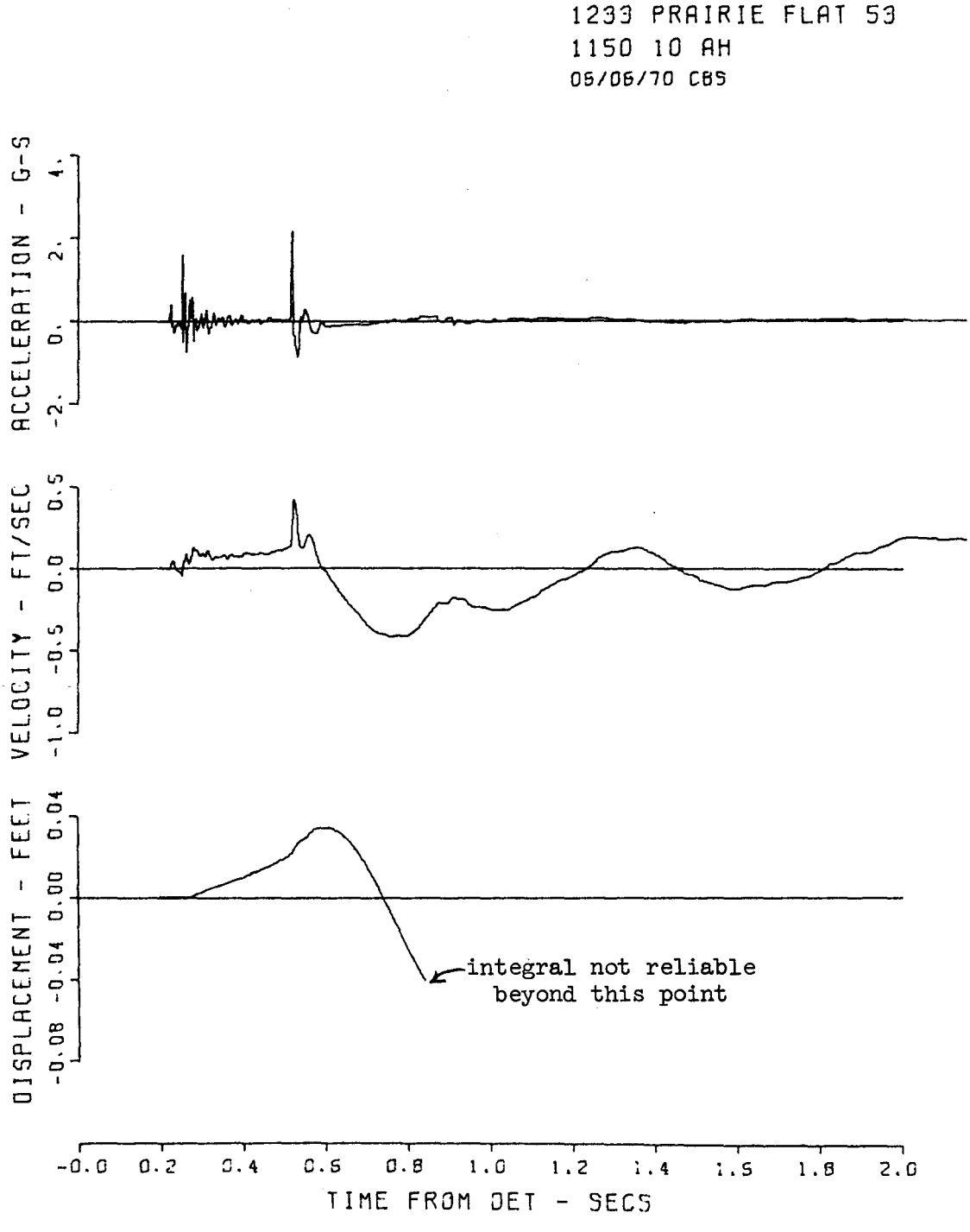

Figure A.73 Gage 1233 AH.

APPENDIX B

STRESS-TIME HISTORIES

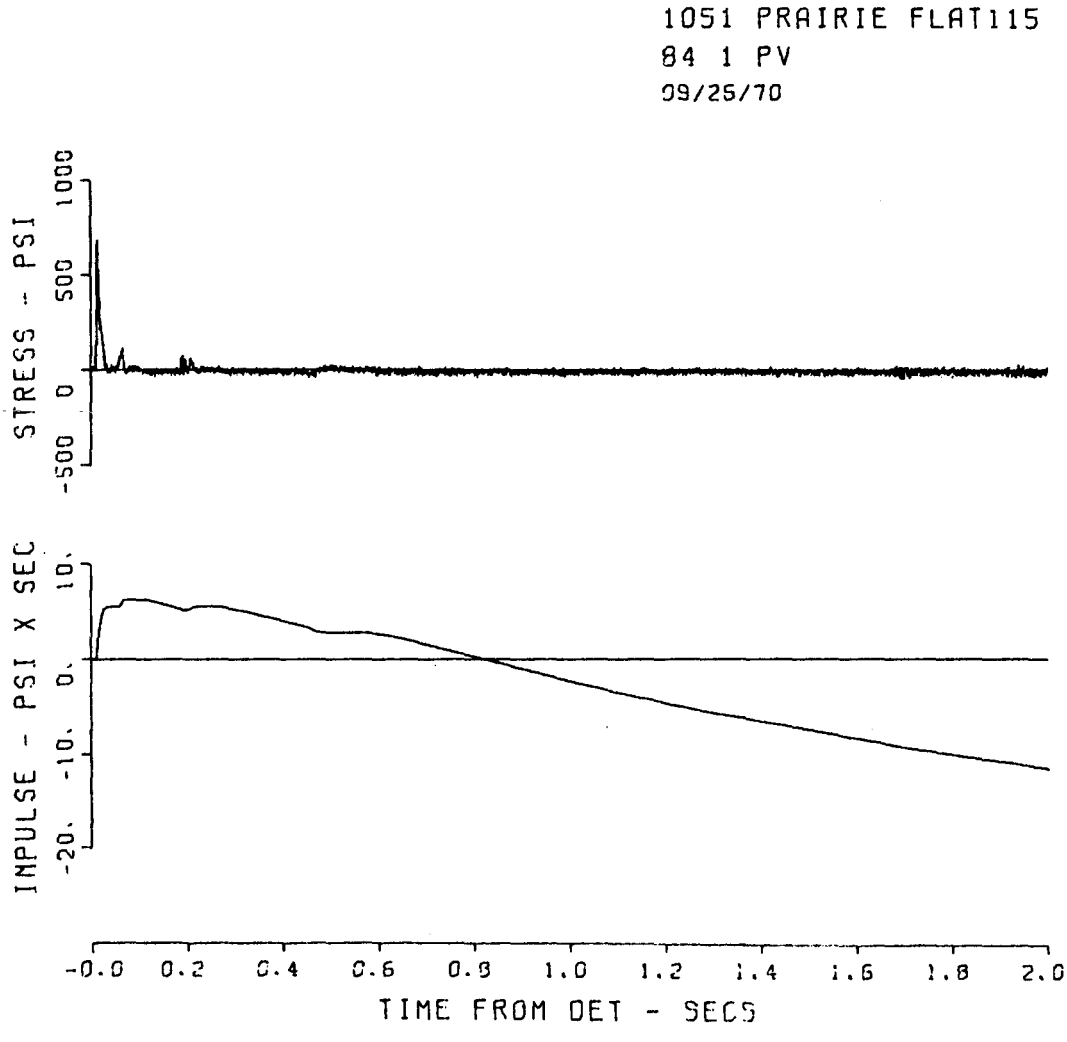

Figure B.1 Gage 1051 PV.

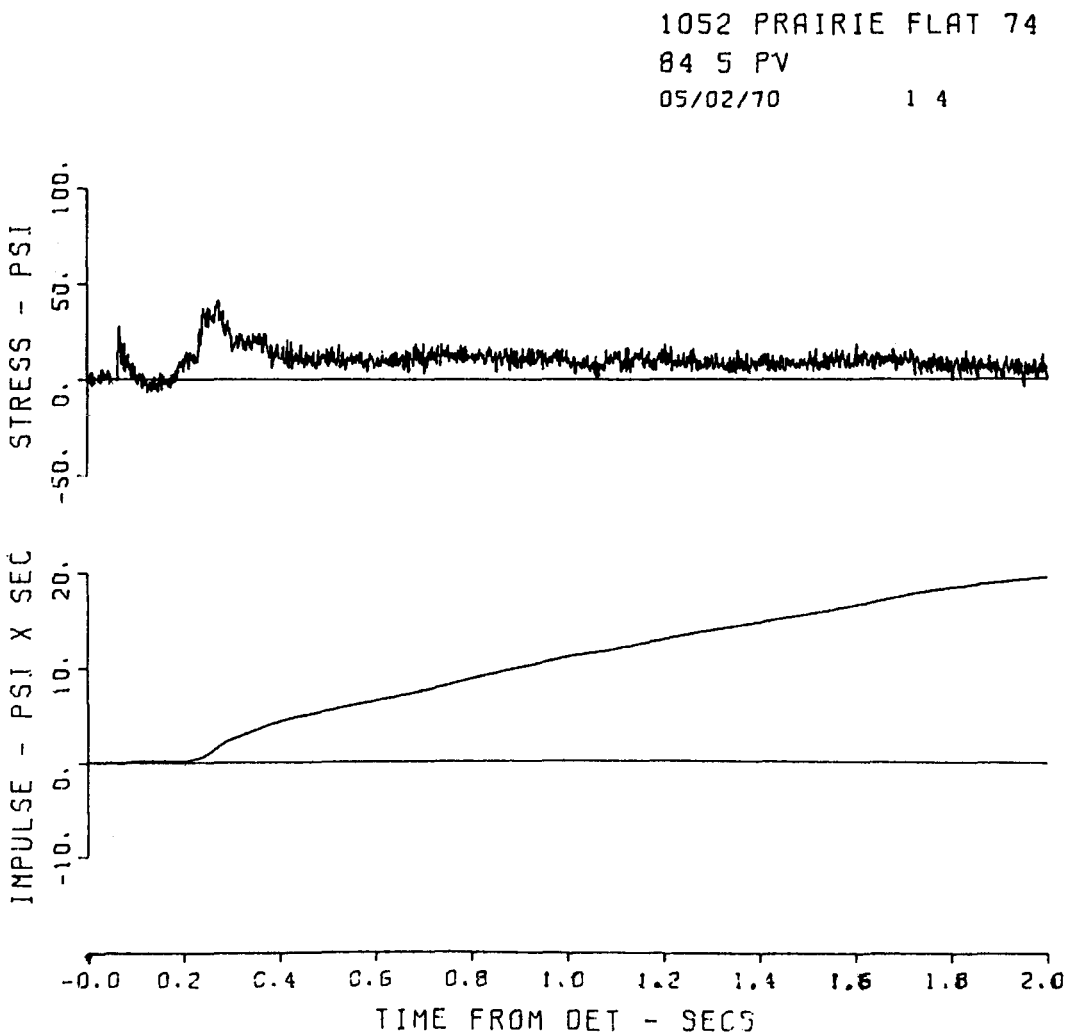

Figure B.2 Gage 1052 PV.

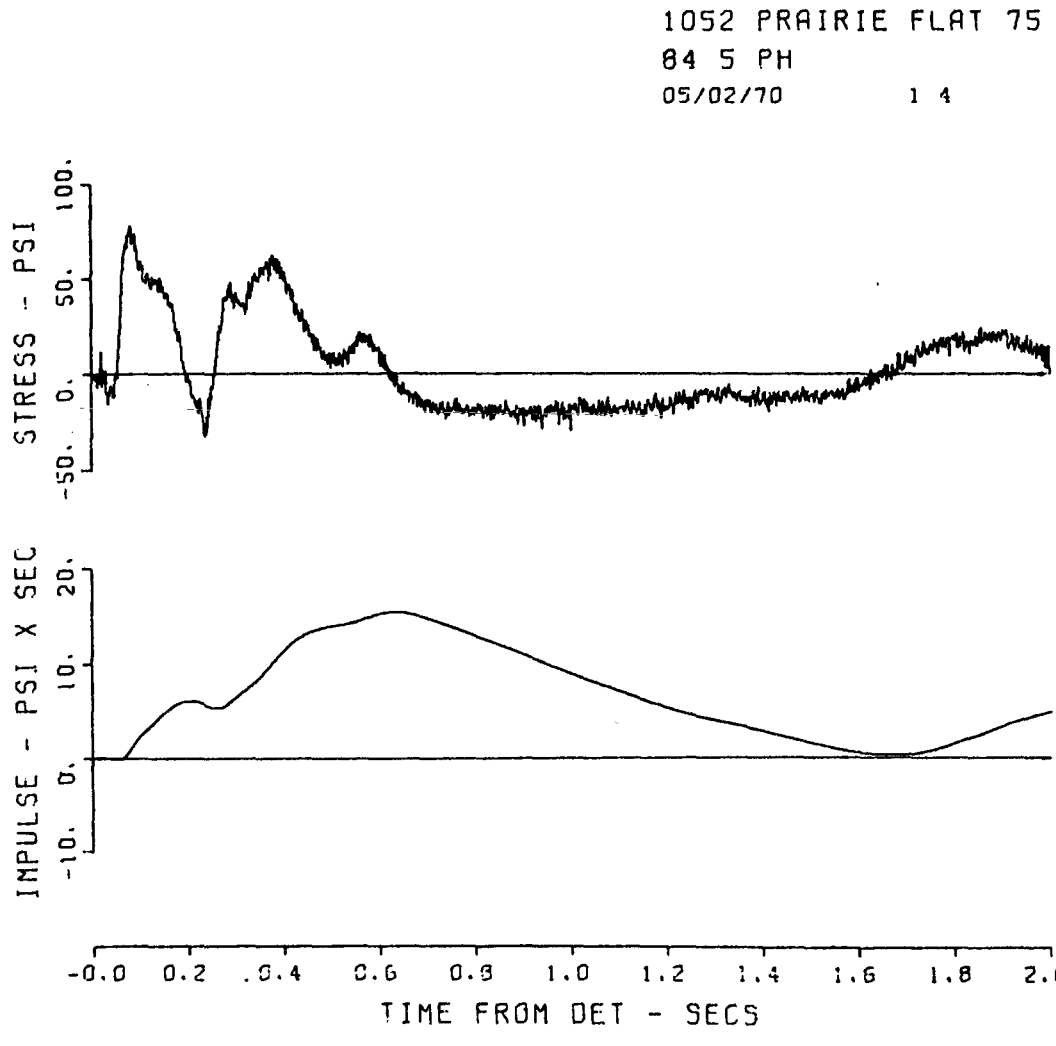

Figure B.3 Gage 1052 PH.

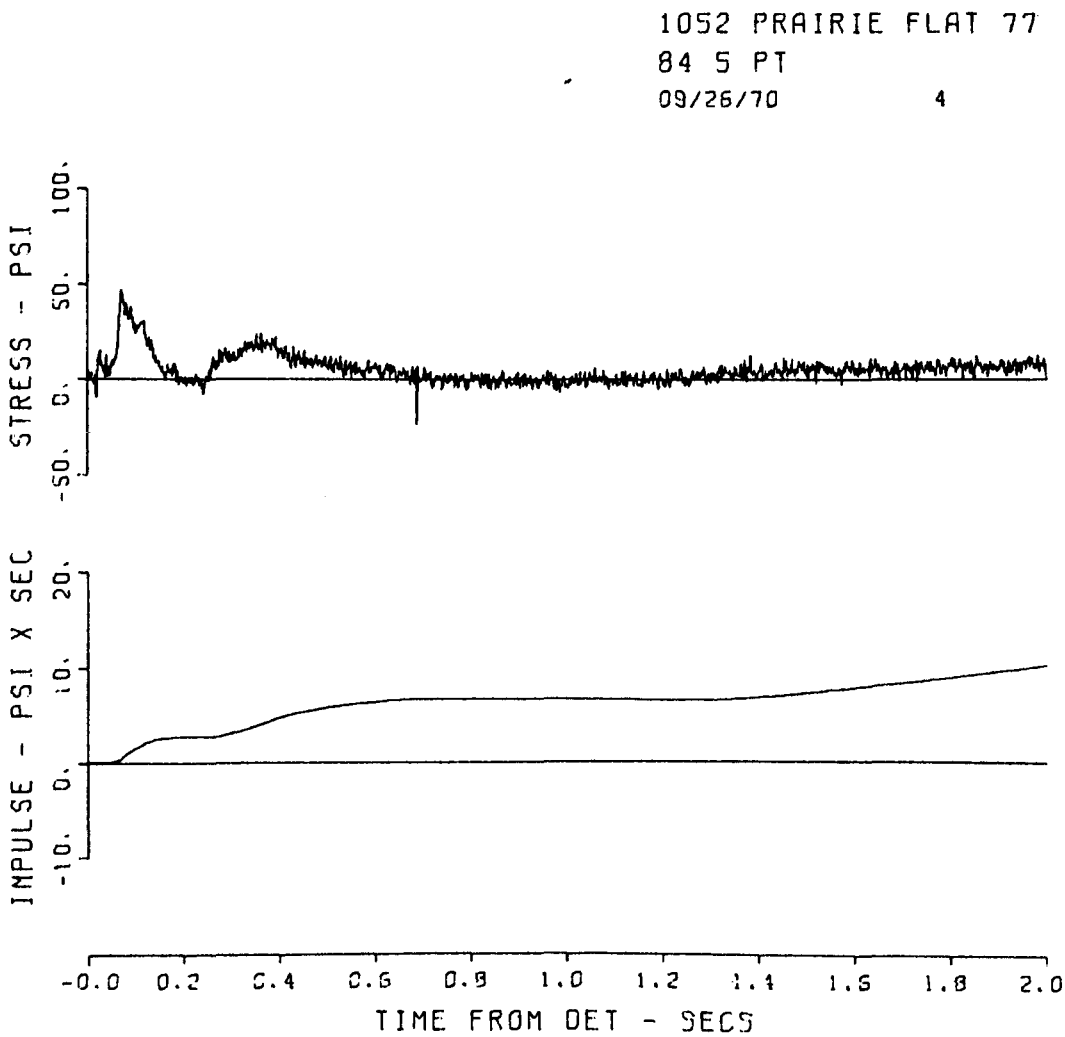

Figure B.4 Gage 1052 PT.

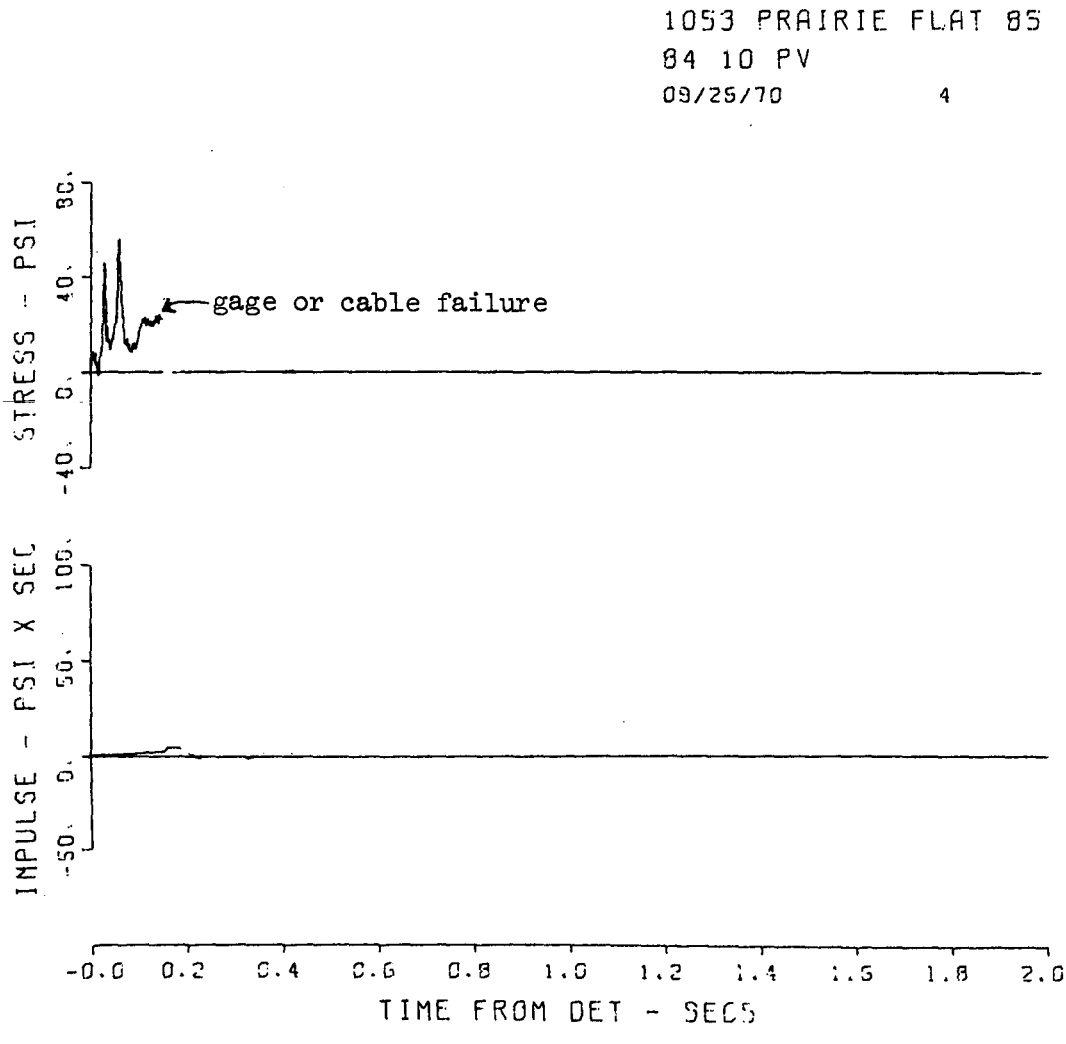

Figure B.5 Gage 1053 PV.

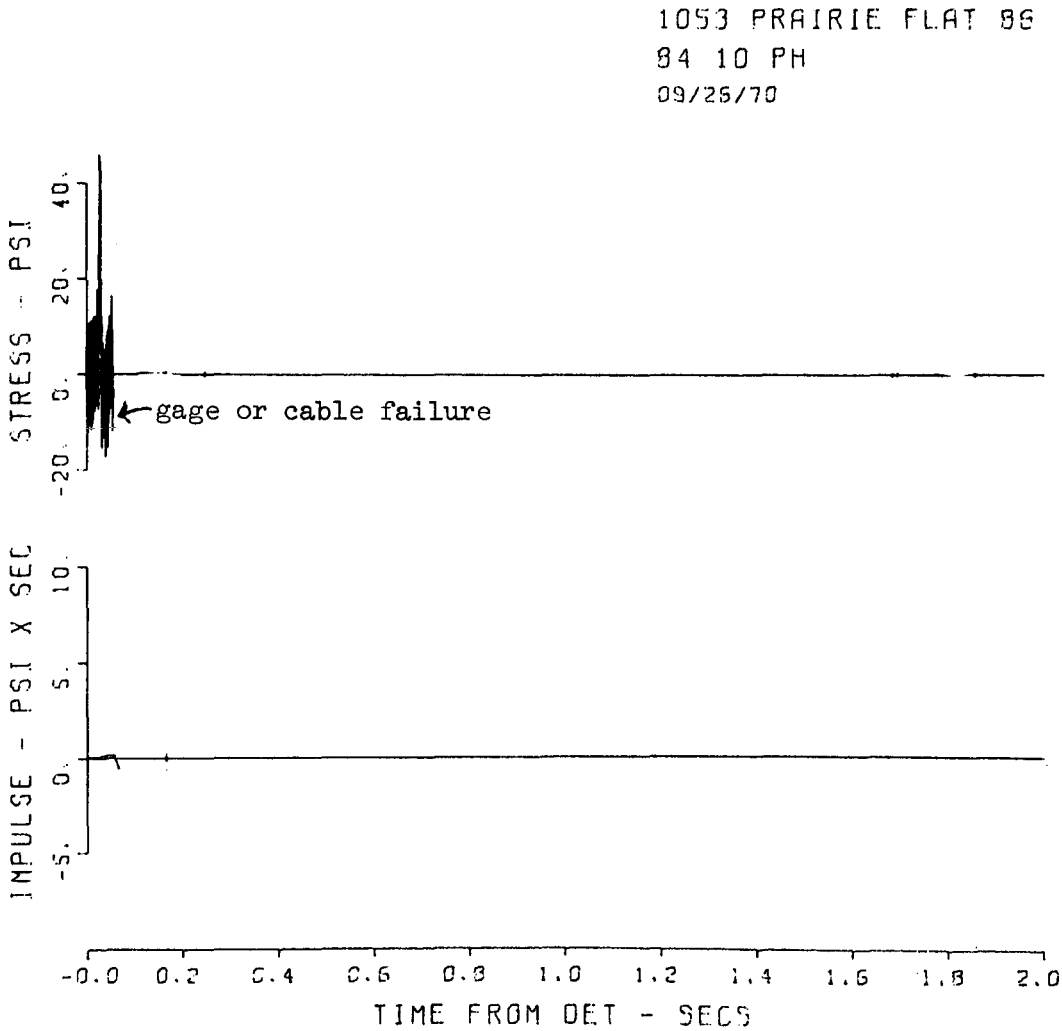

Figure B.6 Gage 1053 PH.

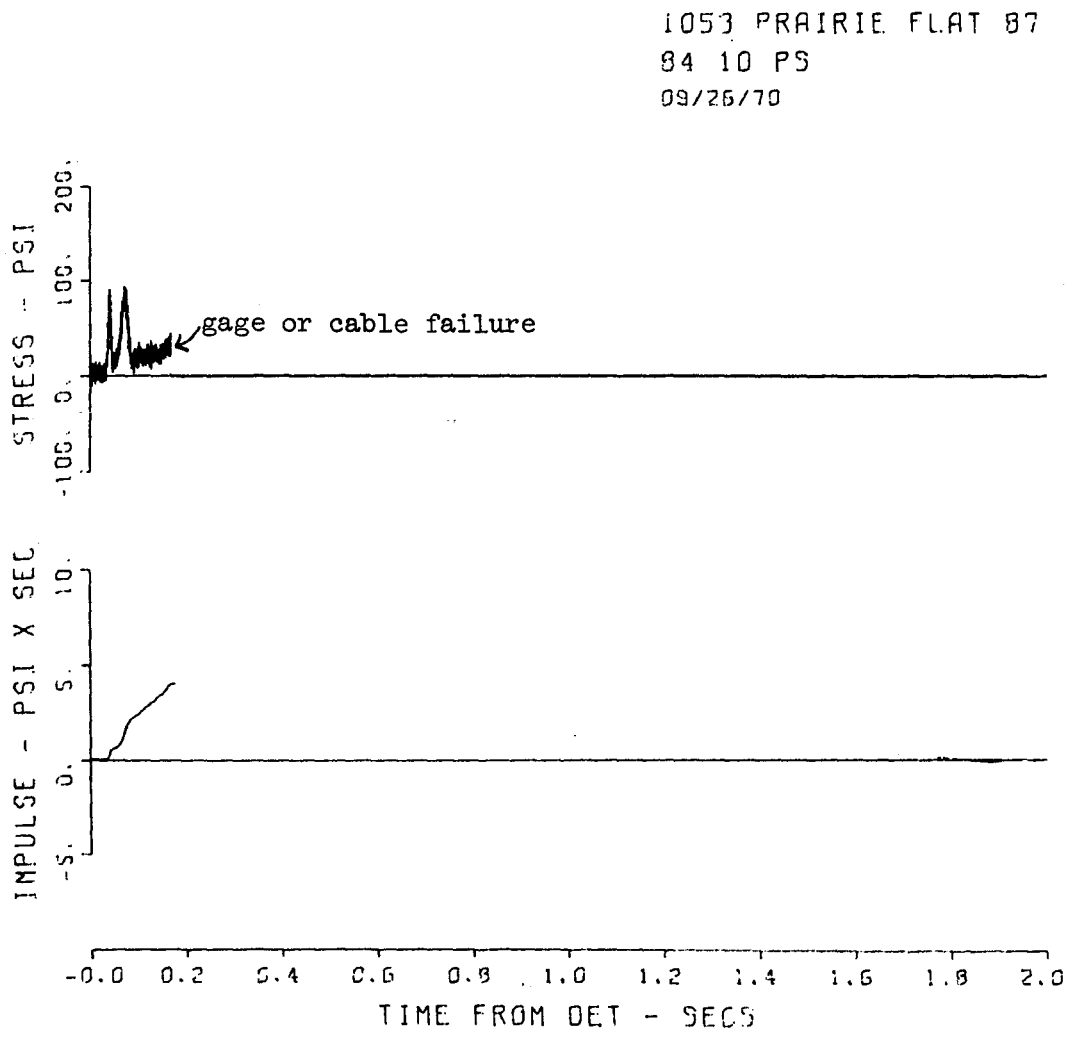

Figure B.7 Gage 1053 PS.

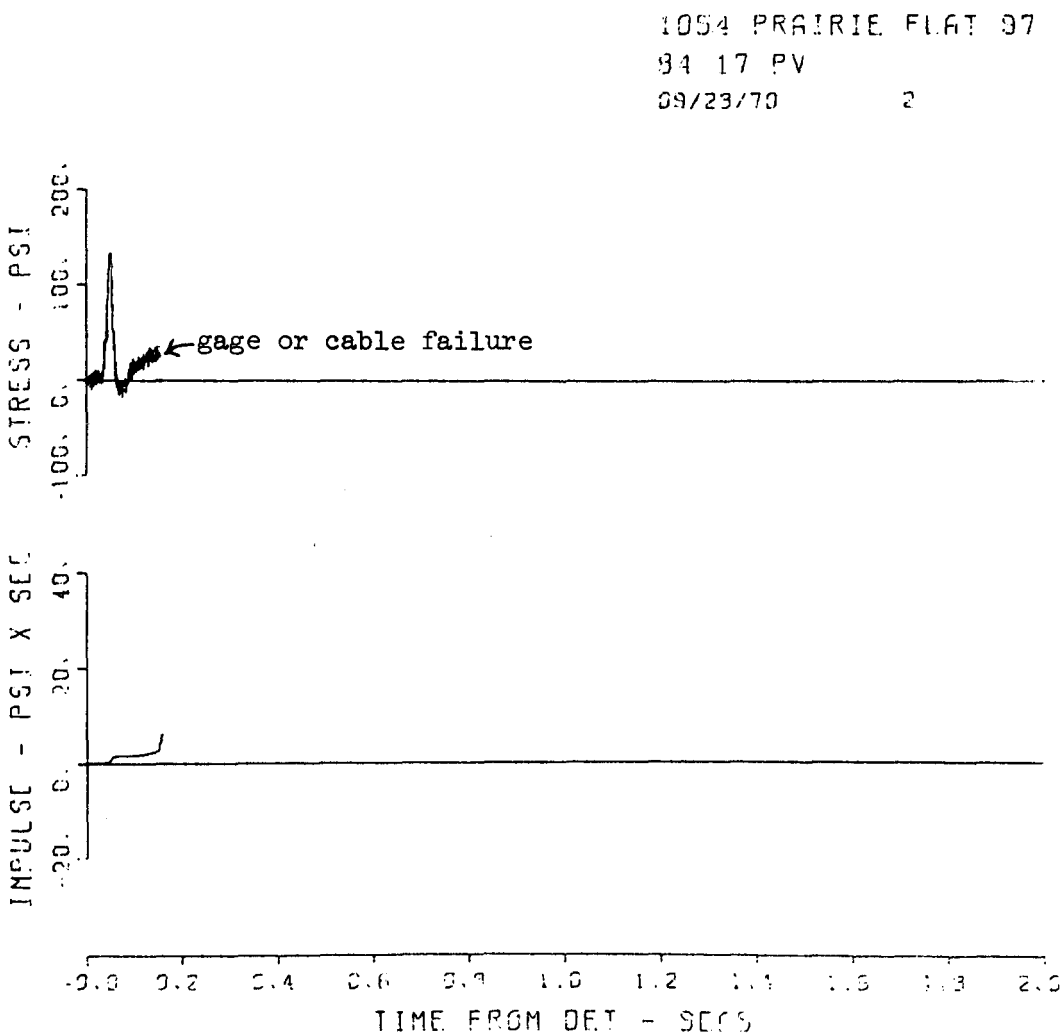

Figure B.8 Gage 1054 PV.

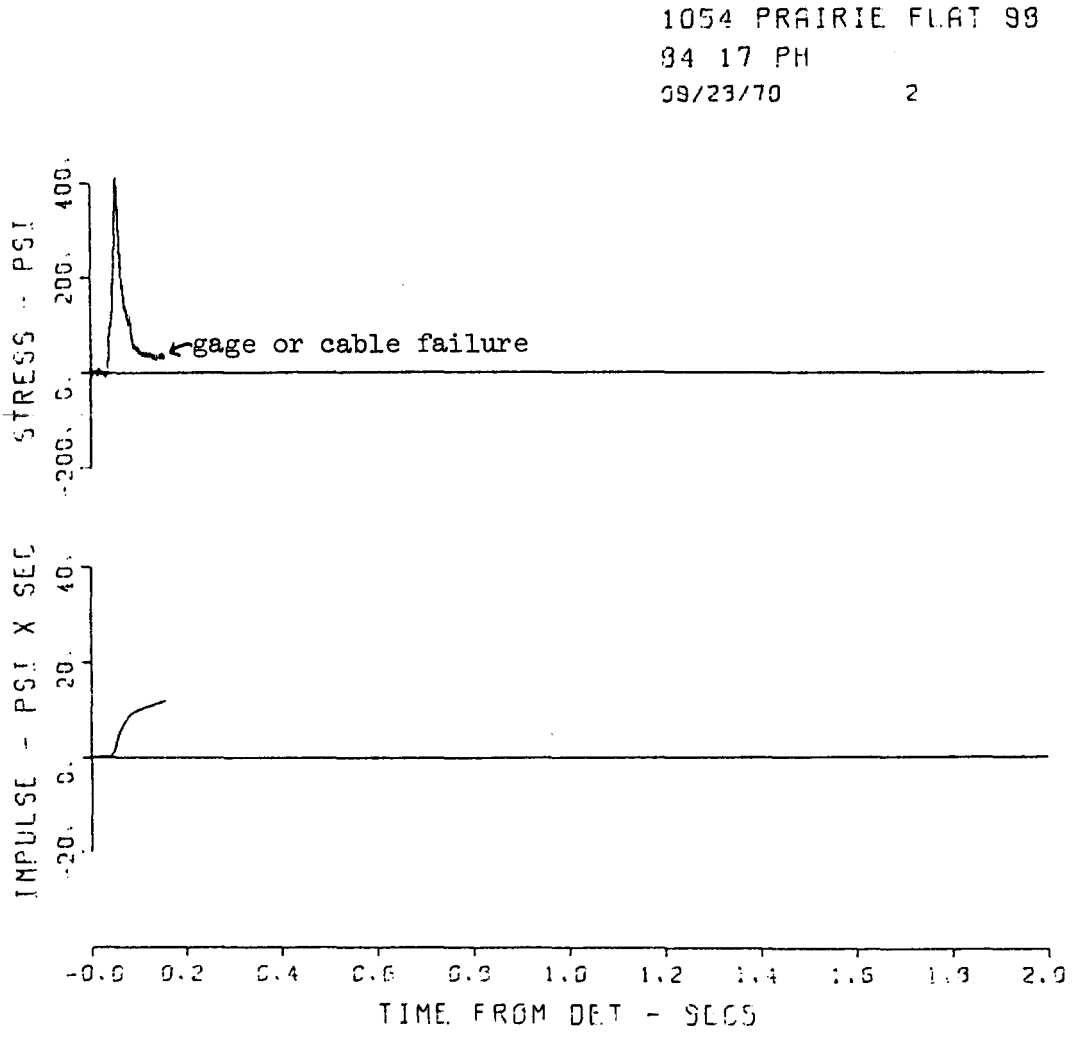

Figure B.9 Gage 1054 PH.

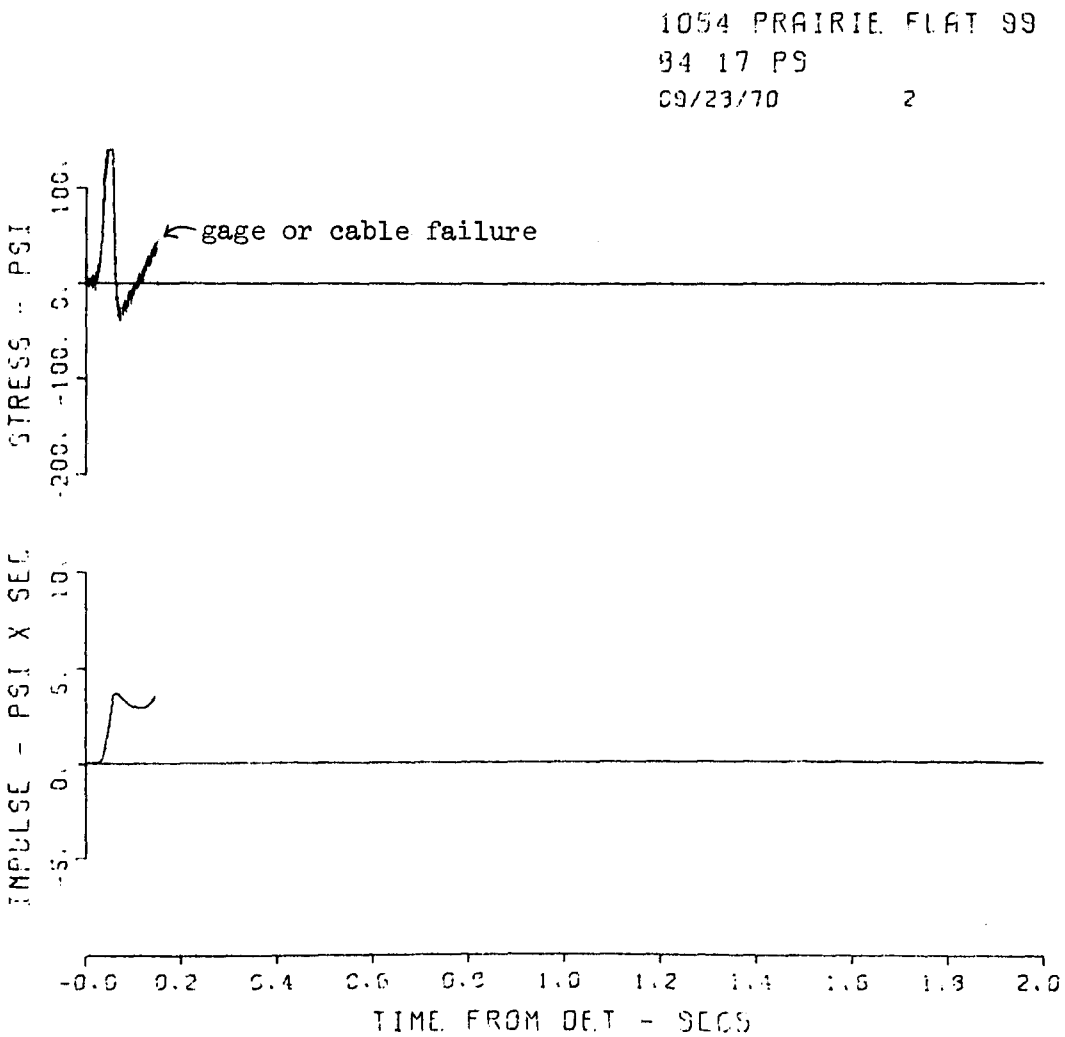

Figure B.10 Gage 1054 PS.

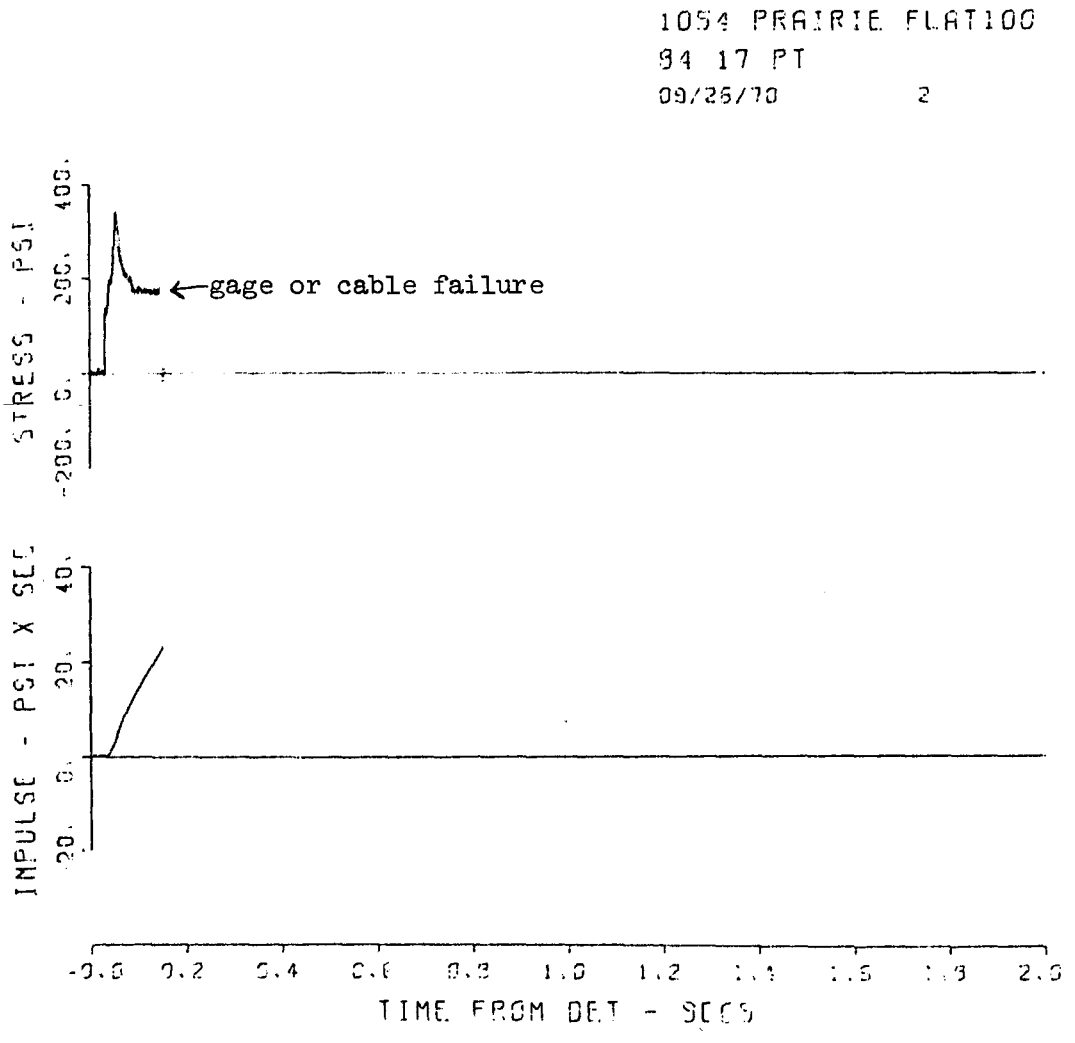

Figure B.11 Gage 1054 PT.

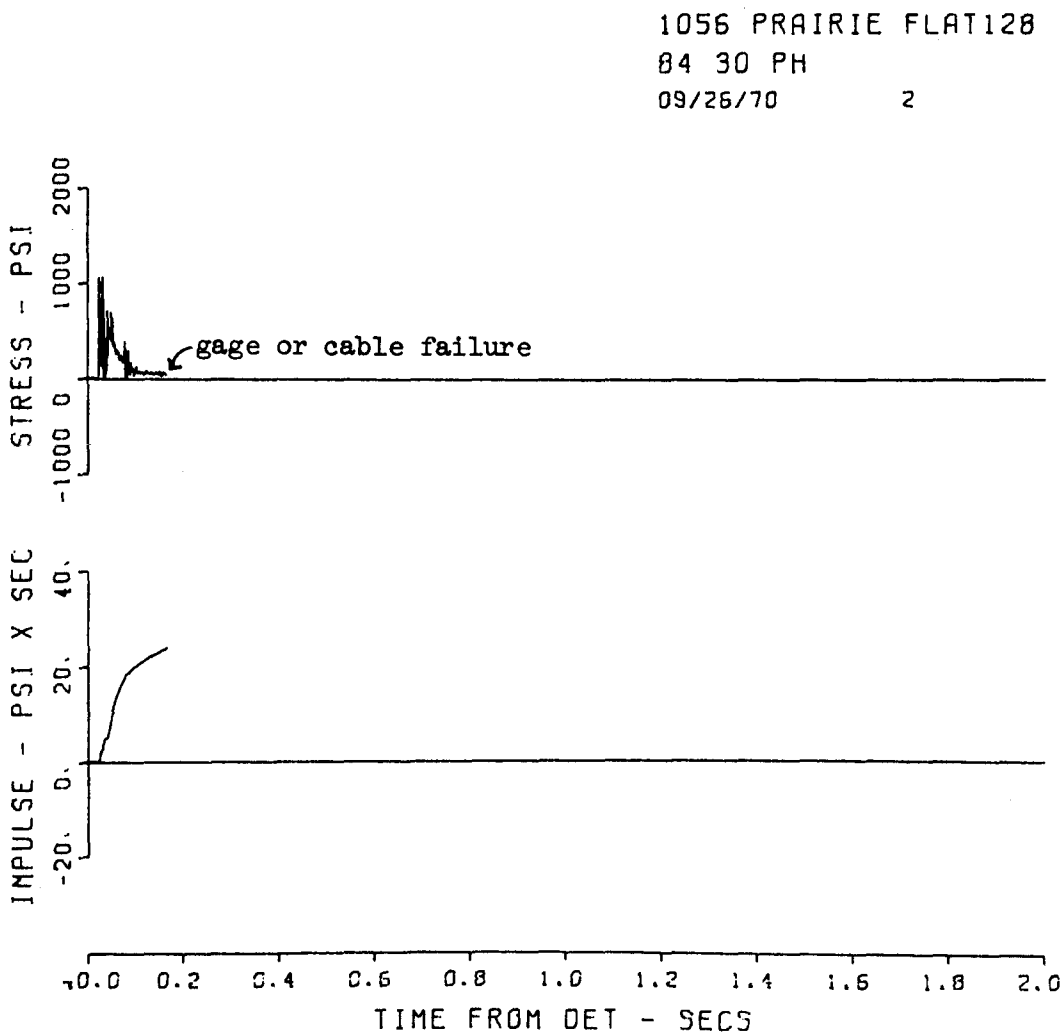

Figure B.12 Gage 1056 PH.

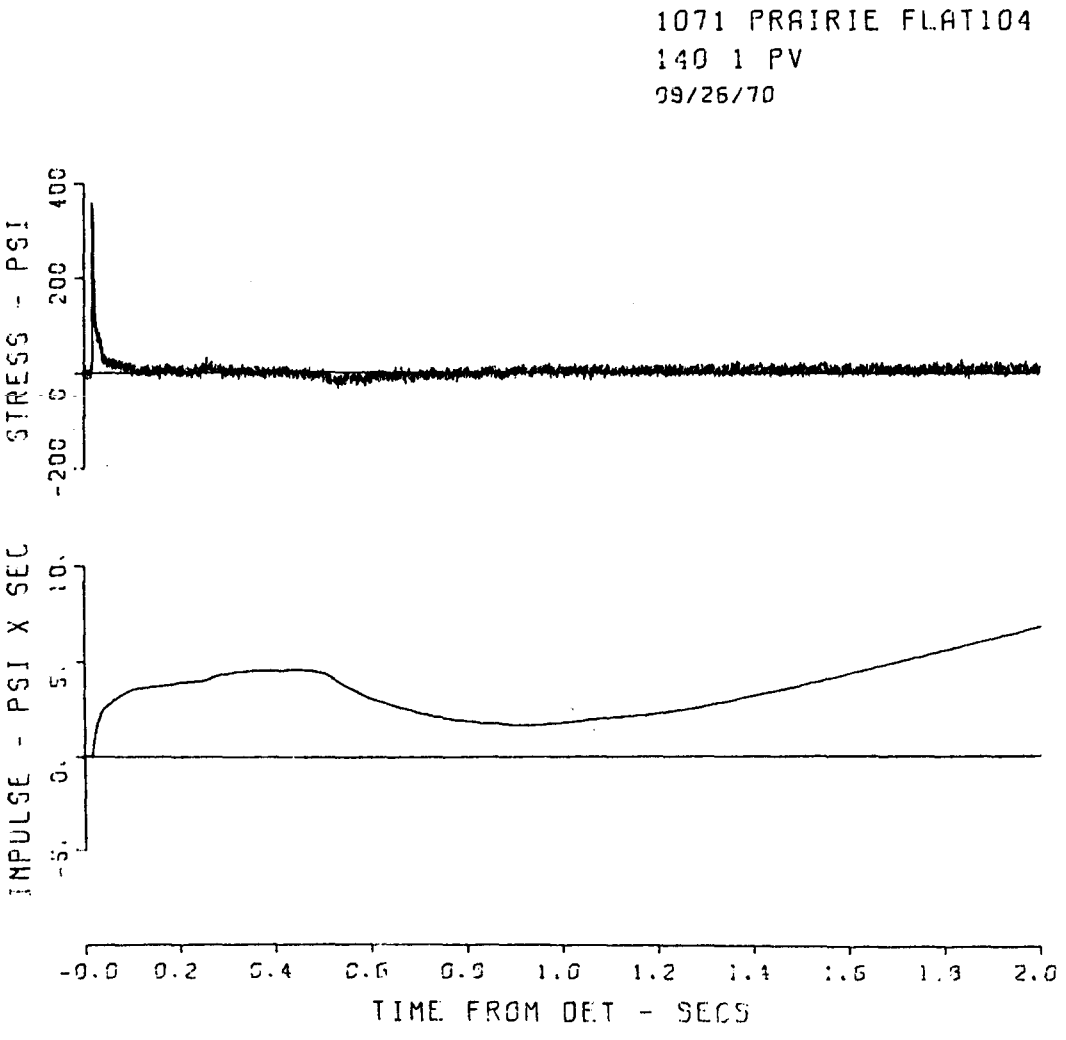

Figure B.13 Gage 1071 PV.

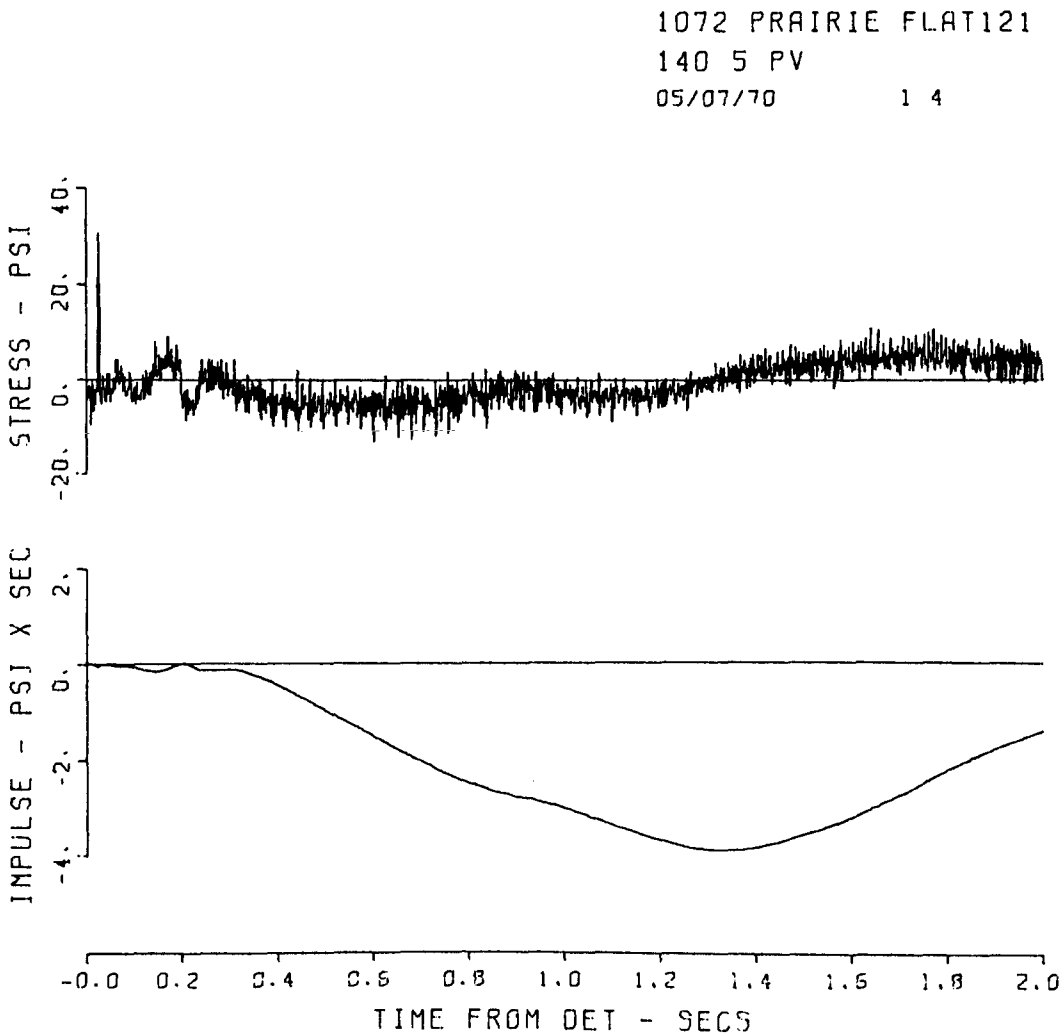

Figure B.14 Gage 1072 PV.

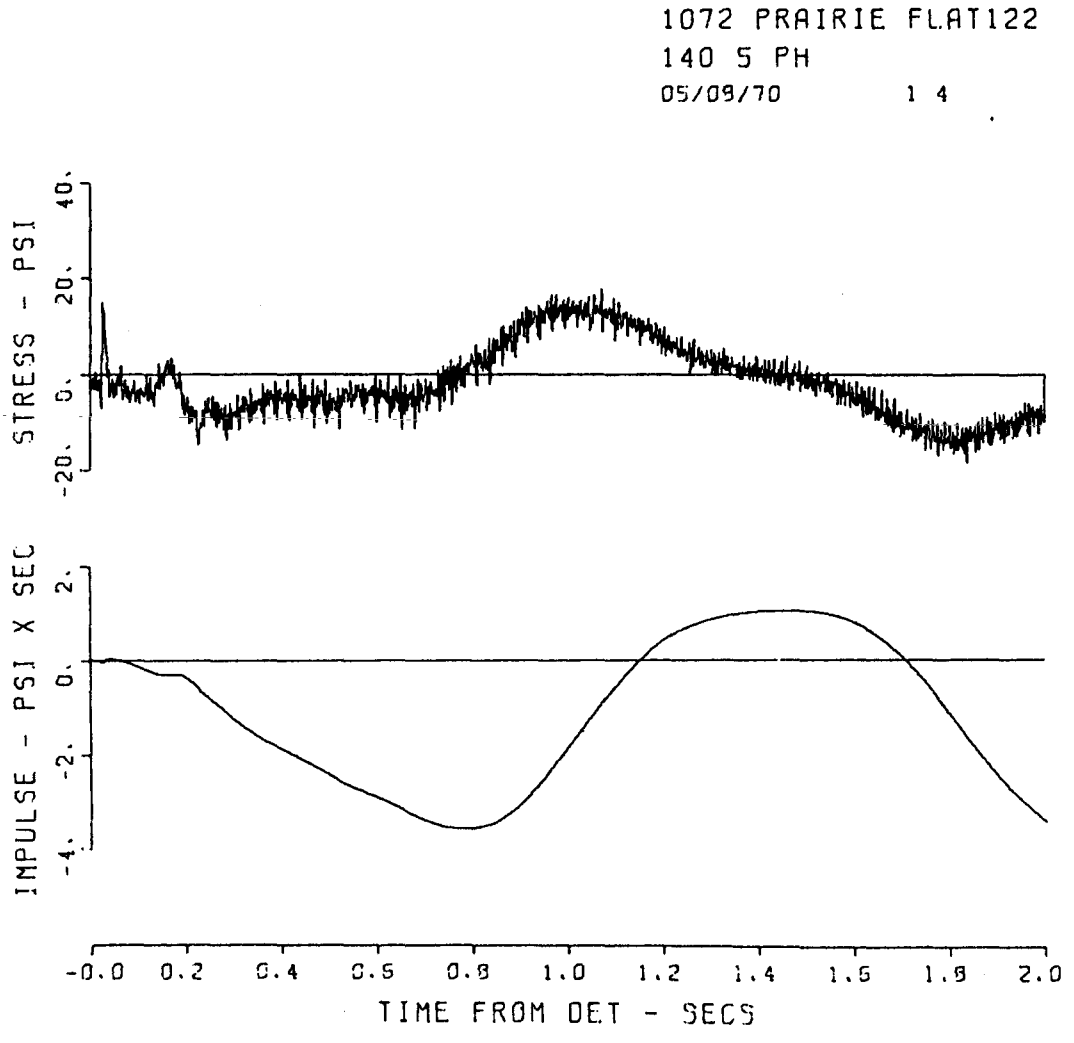

Figure B.15 Gage 1072 PH.

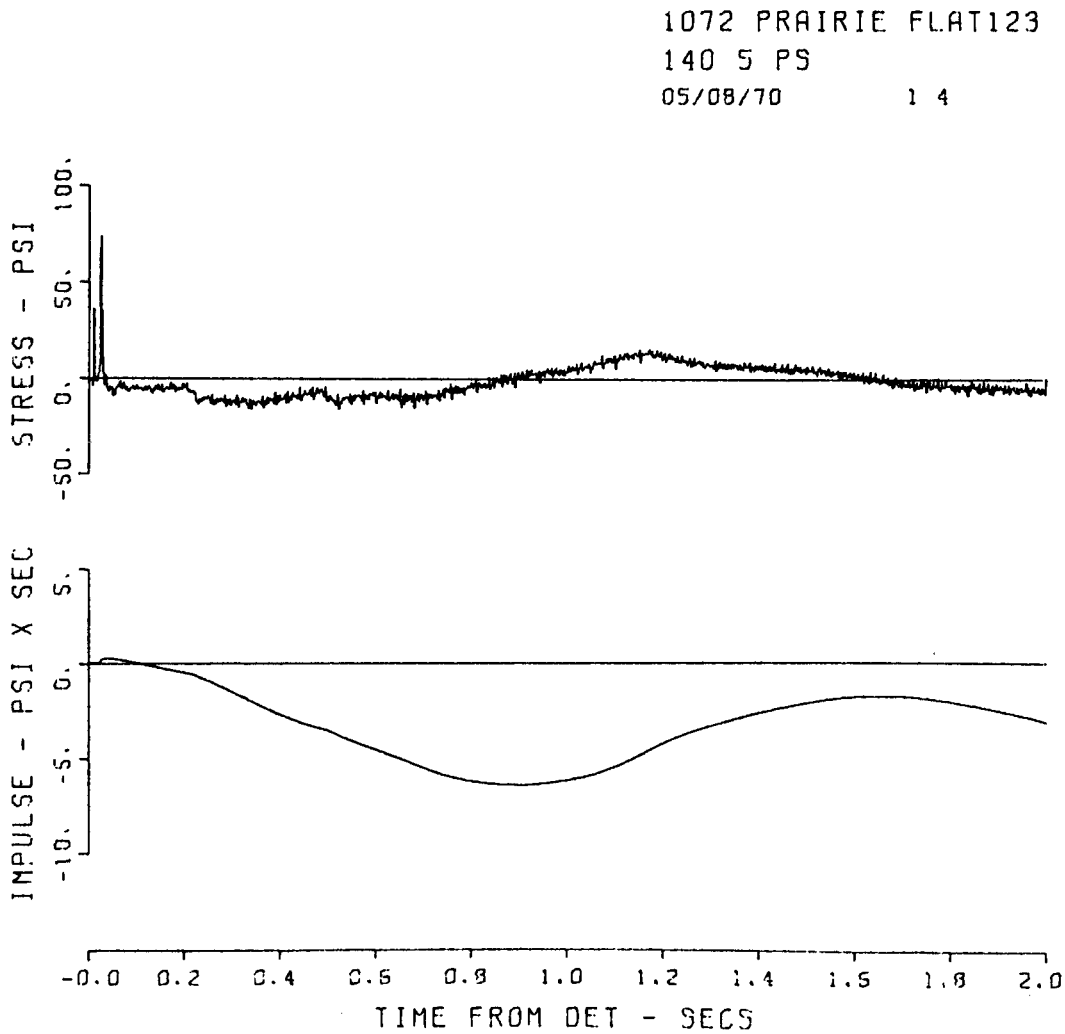

Figure B.16 Gage 1072 PS.

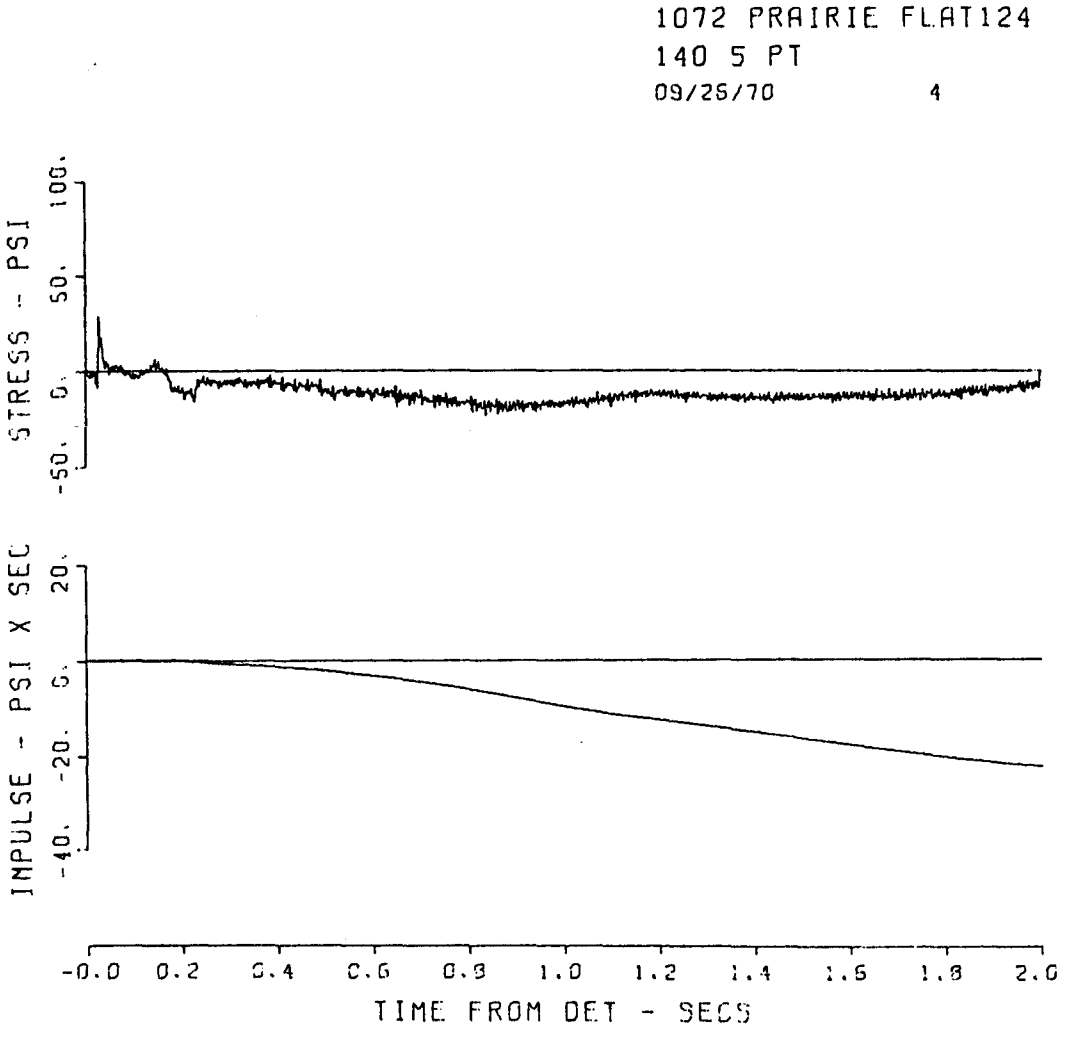

Figure B.17 Gage 1072 PT.

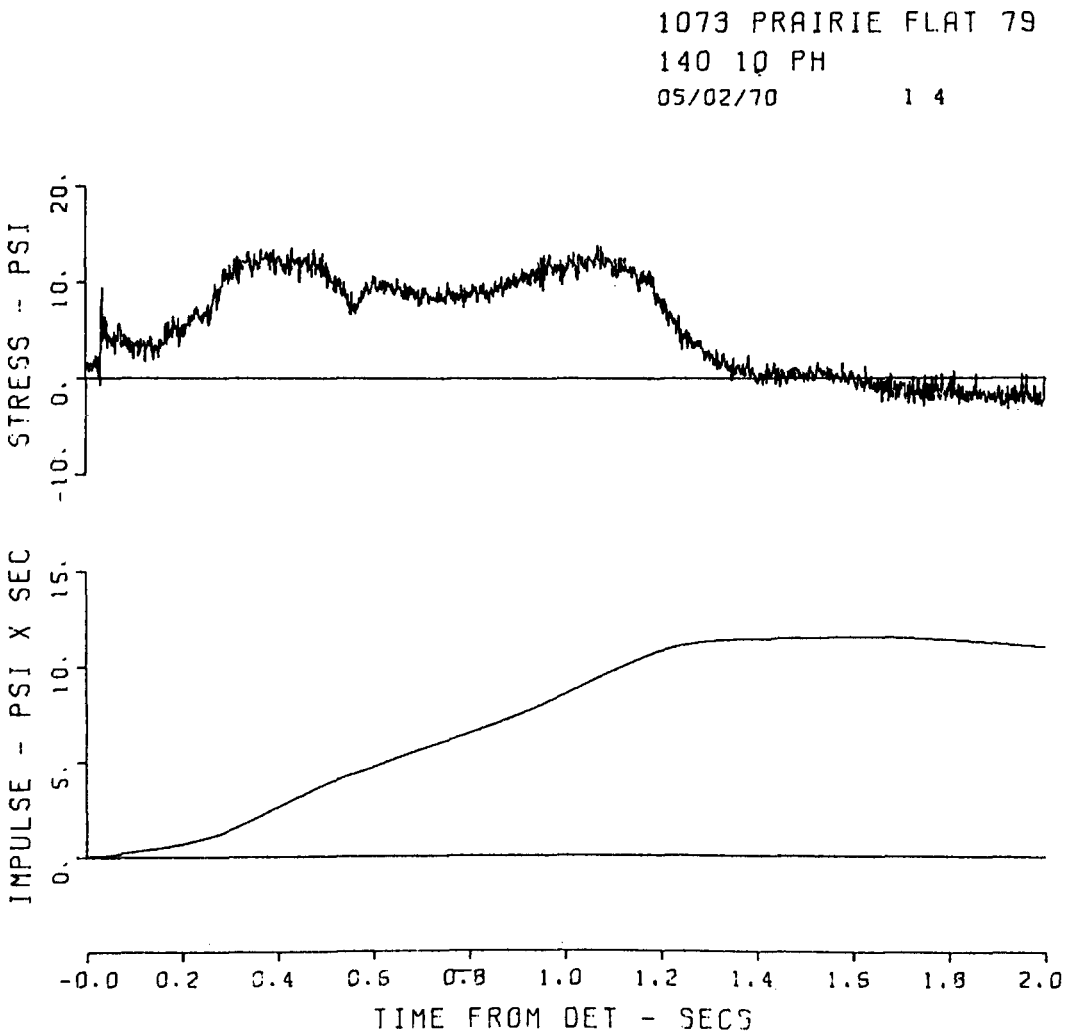

Figure B.18 Gage 1073 PH.

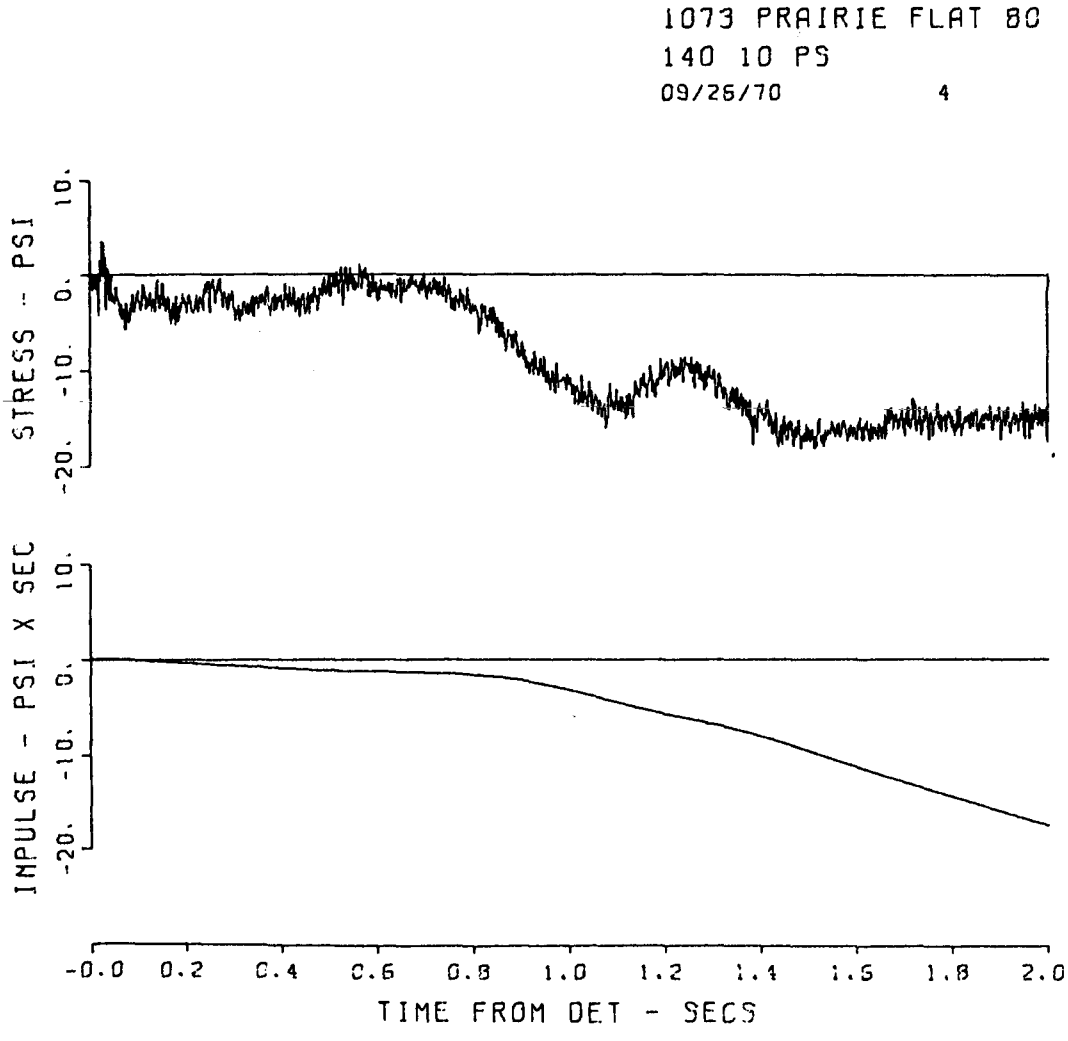

Figure B.19 Gage 1073 PS.

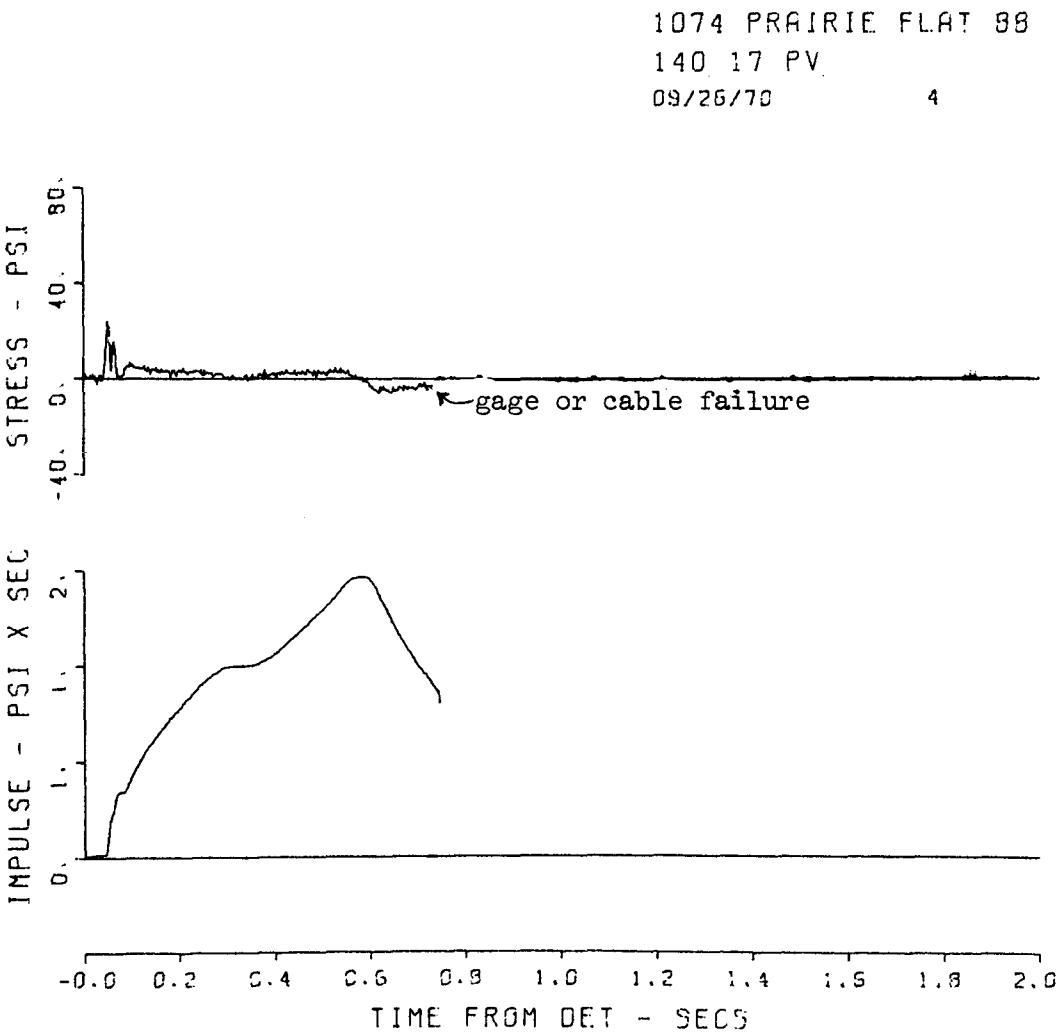

Figure B.20 Gage 1074 PV.

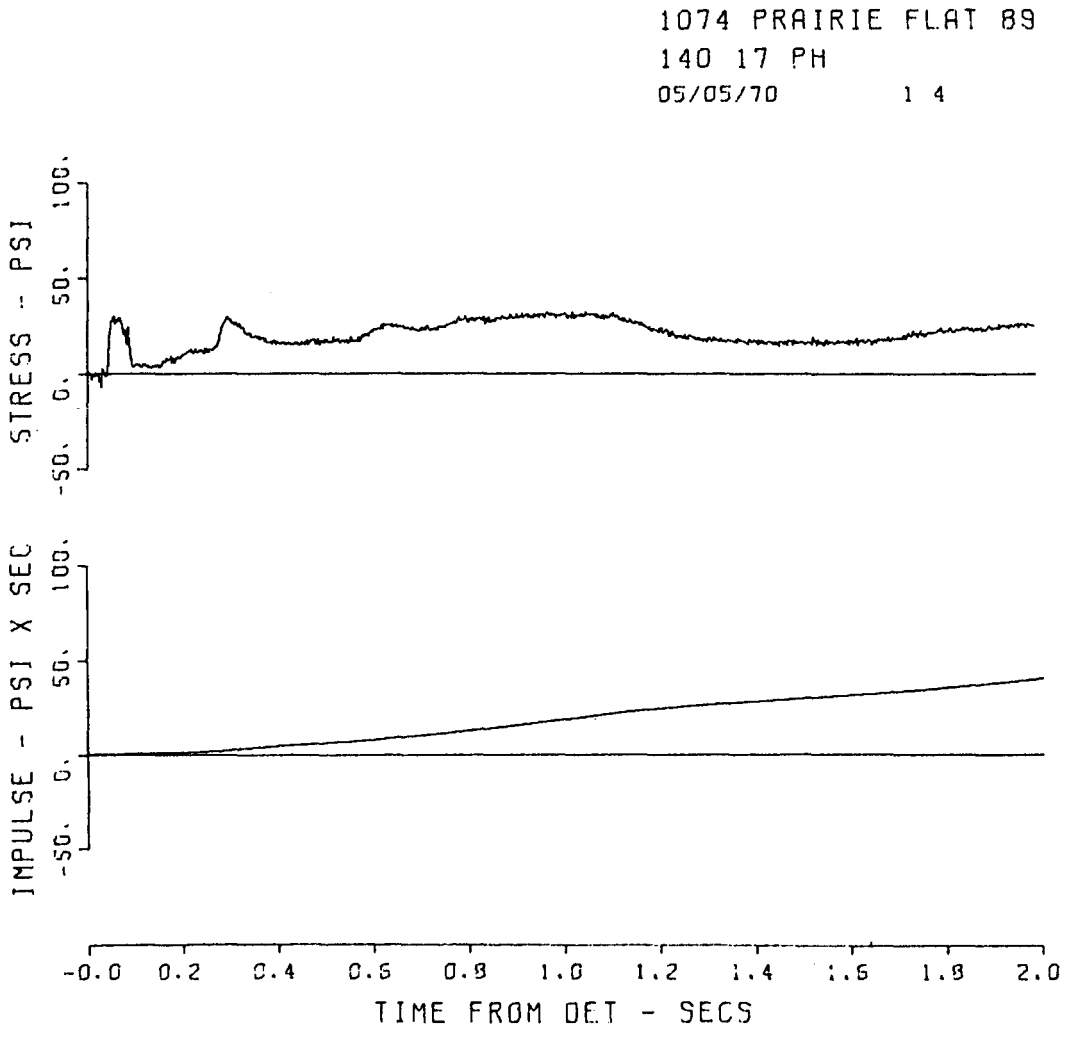

Figure B.21 Gage 1074 PH.

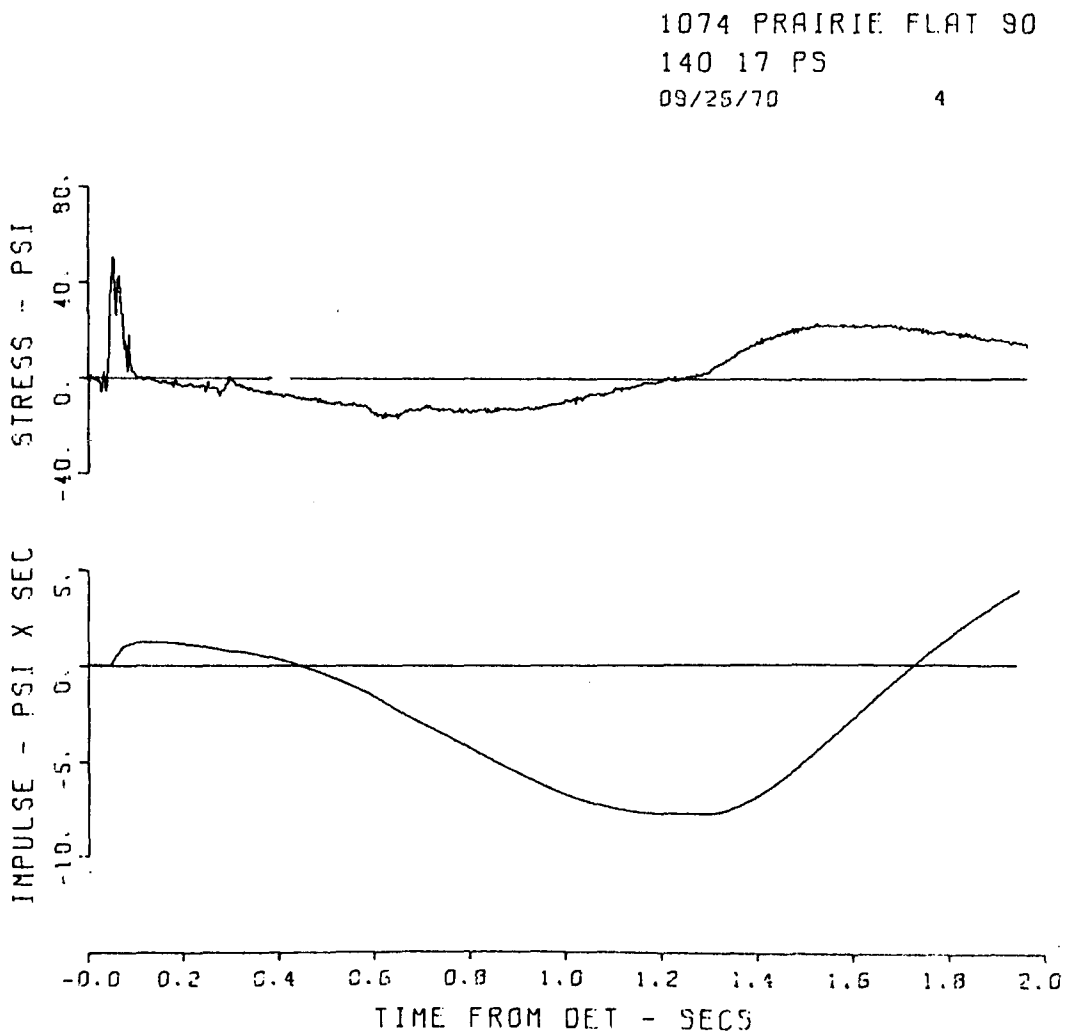

Figure B.22 Gage 1074 PS.

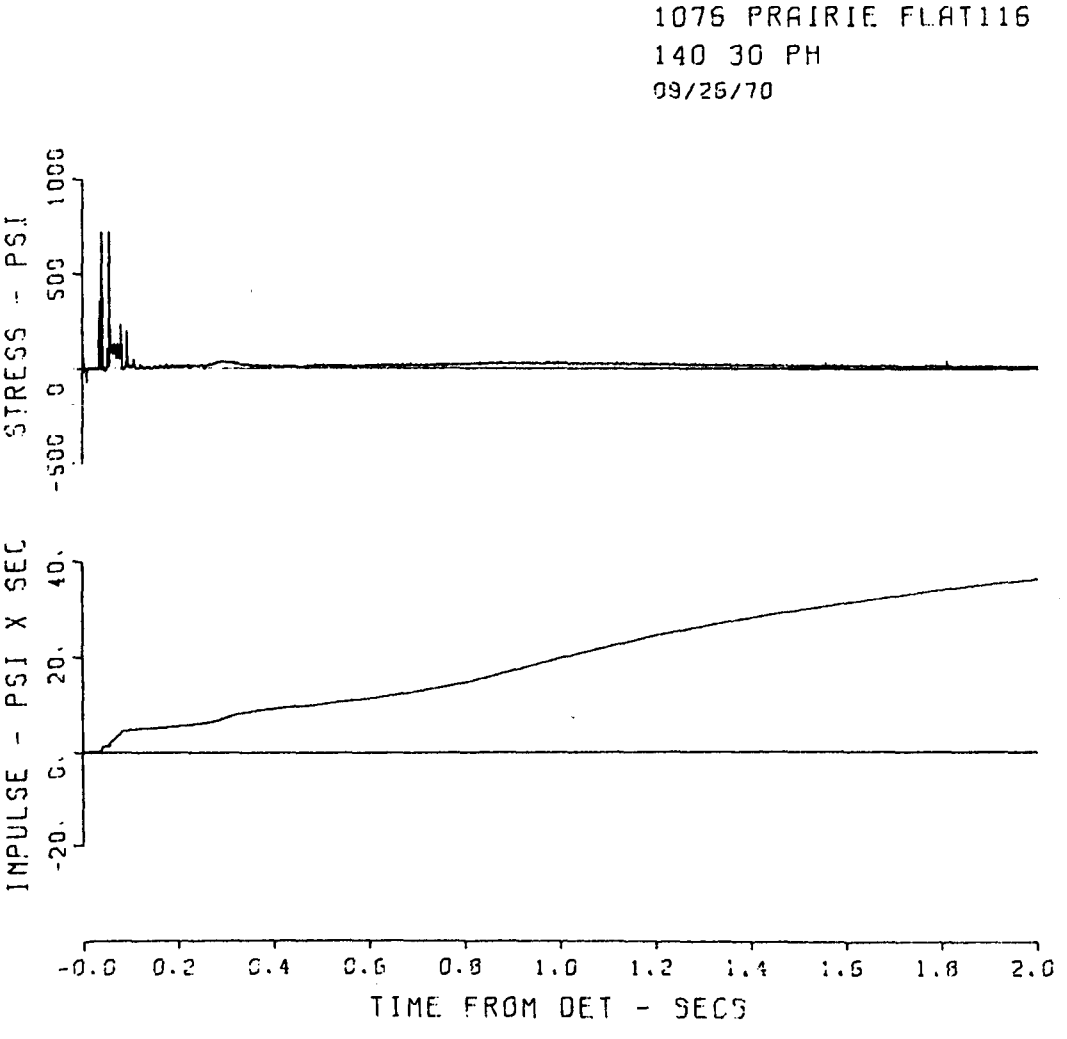

Figure B.23 Gage 1076 PH.

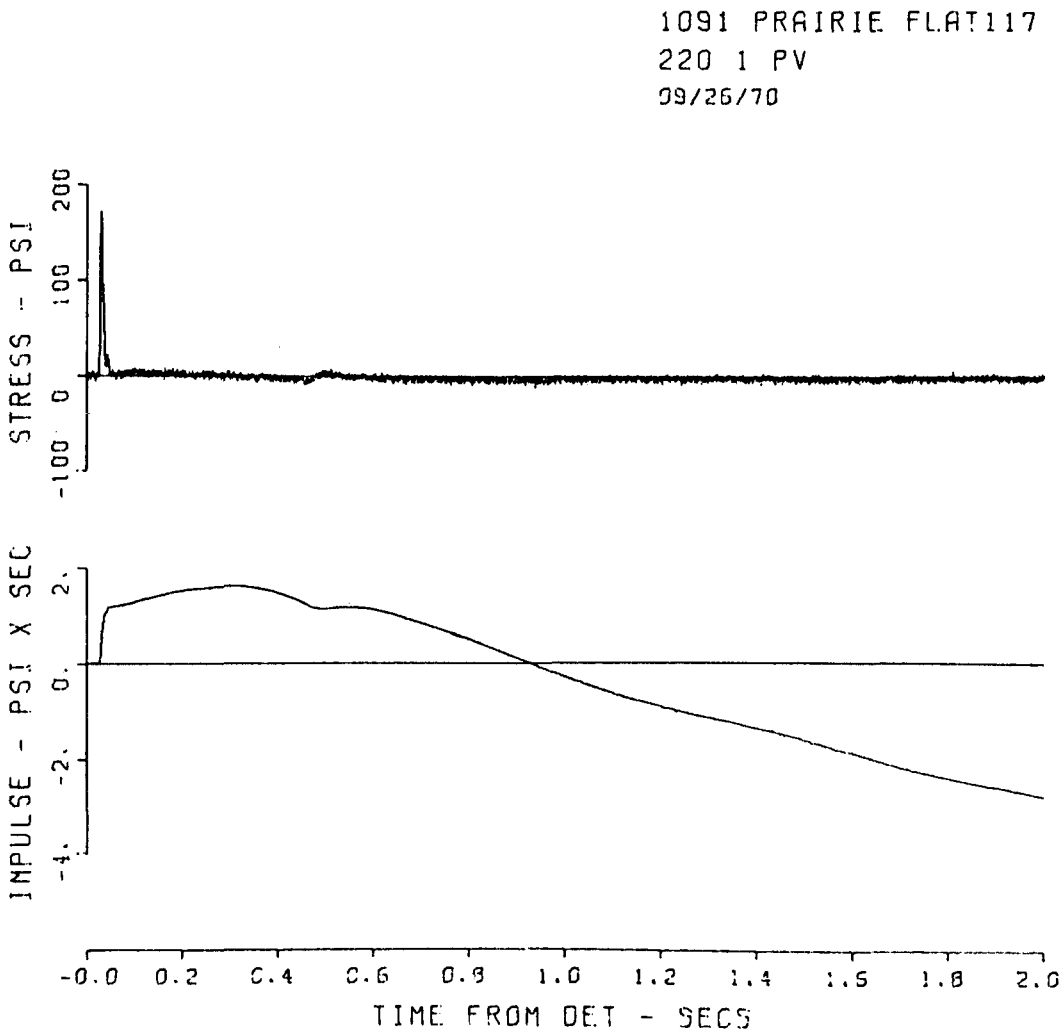

Figure B.24 Gage 1091 PV.

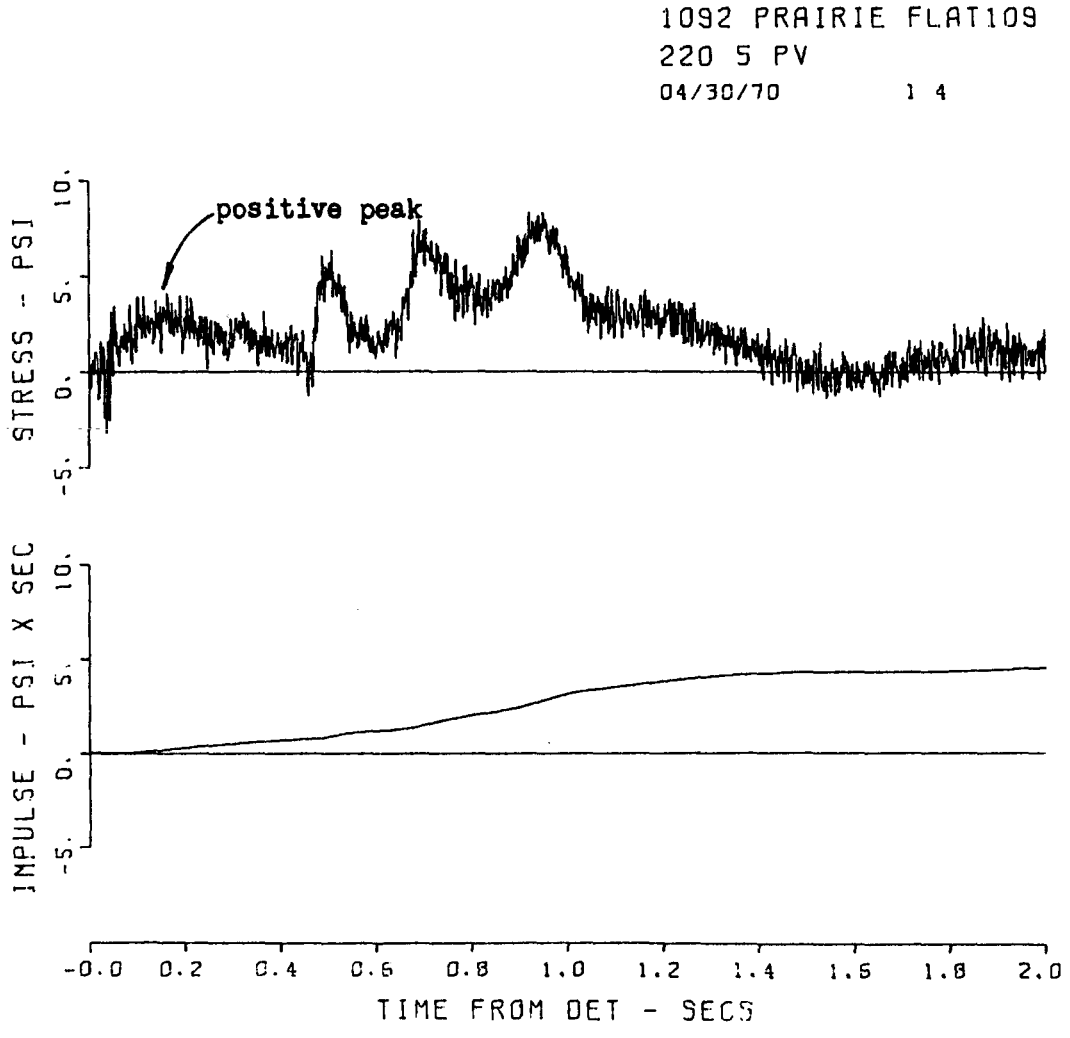

Figure B.25 Gage 1092 PV.

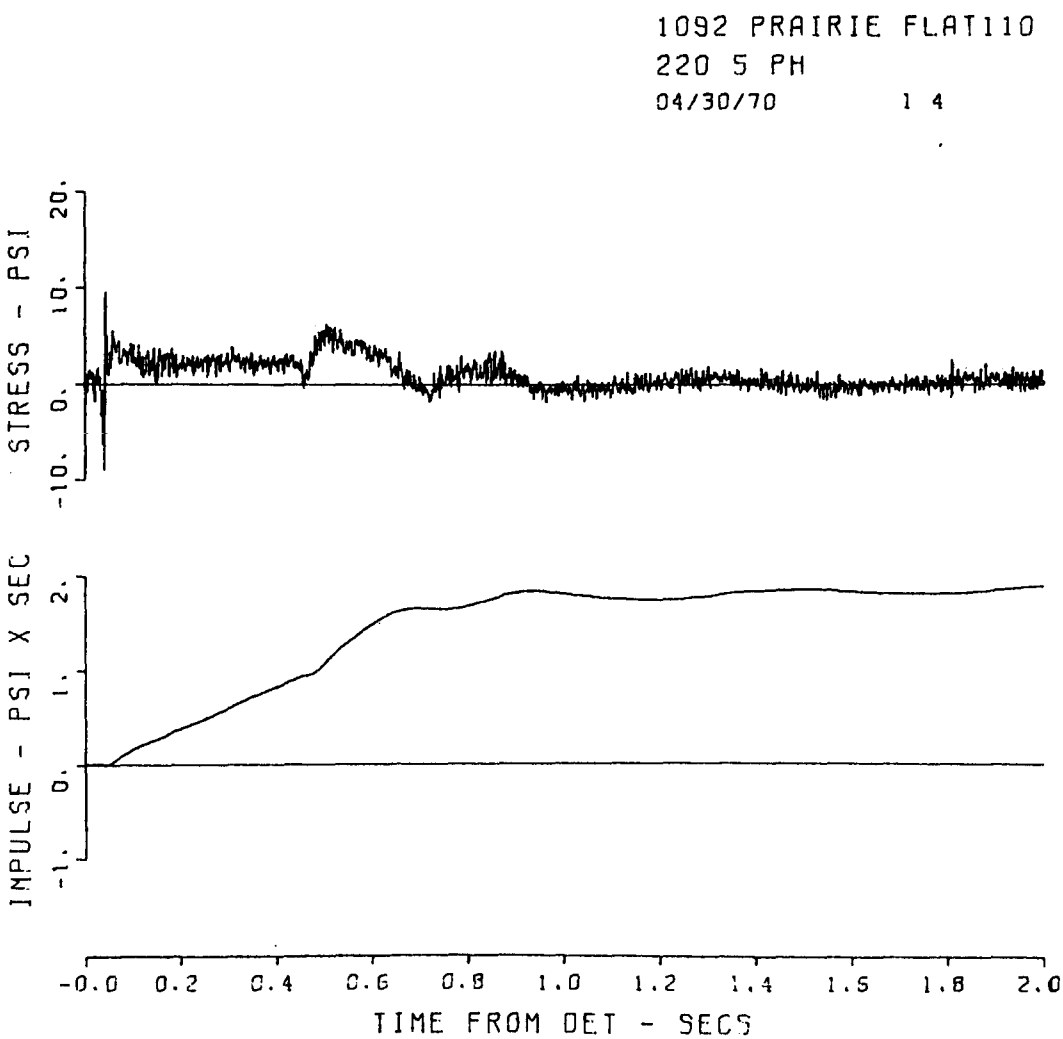

Figure B.26 Gage 1092 PH.

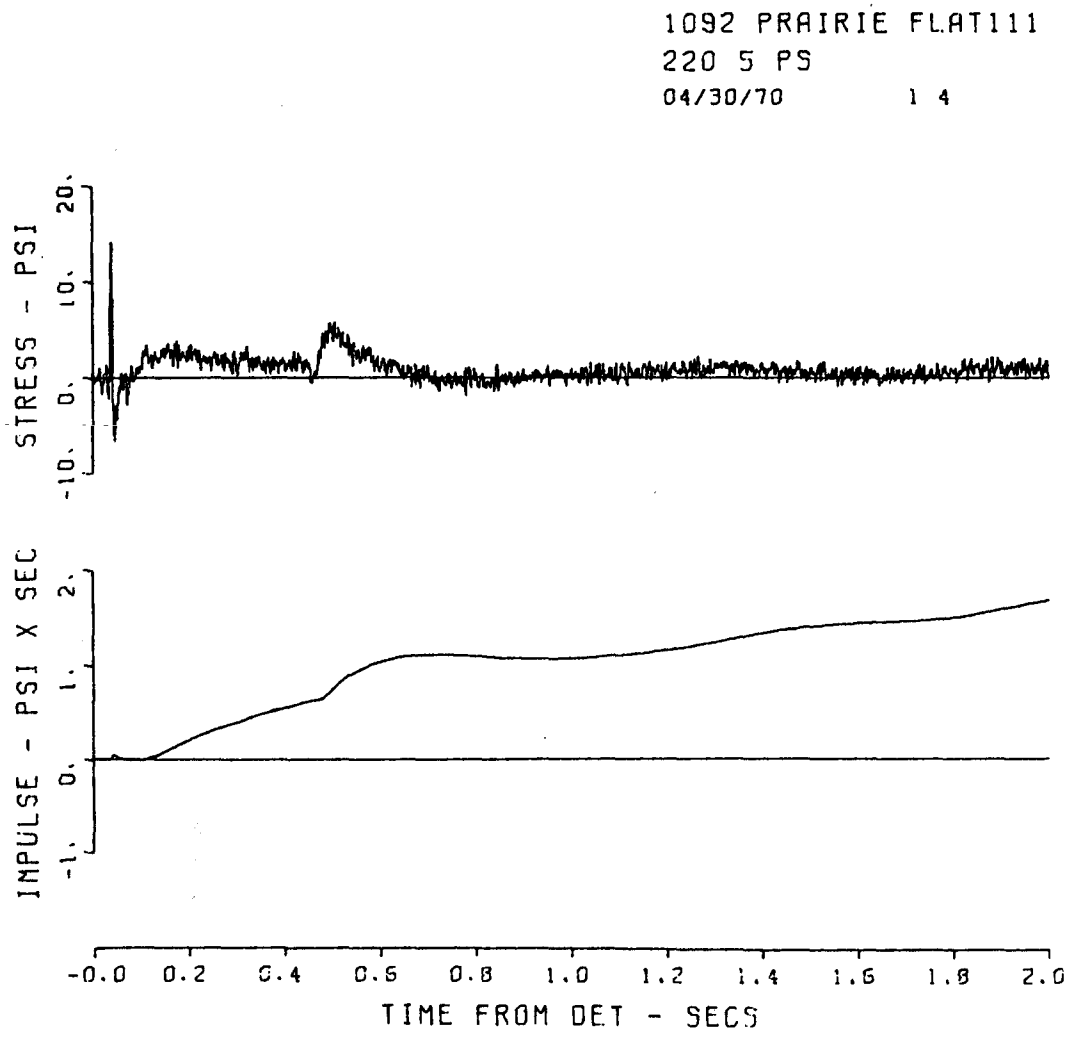

Figure B.27 Gage 1092 PS.

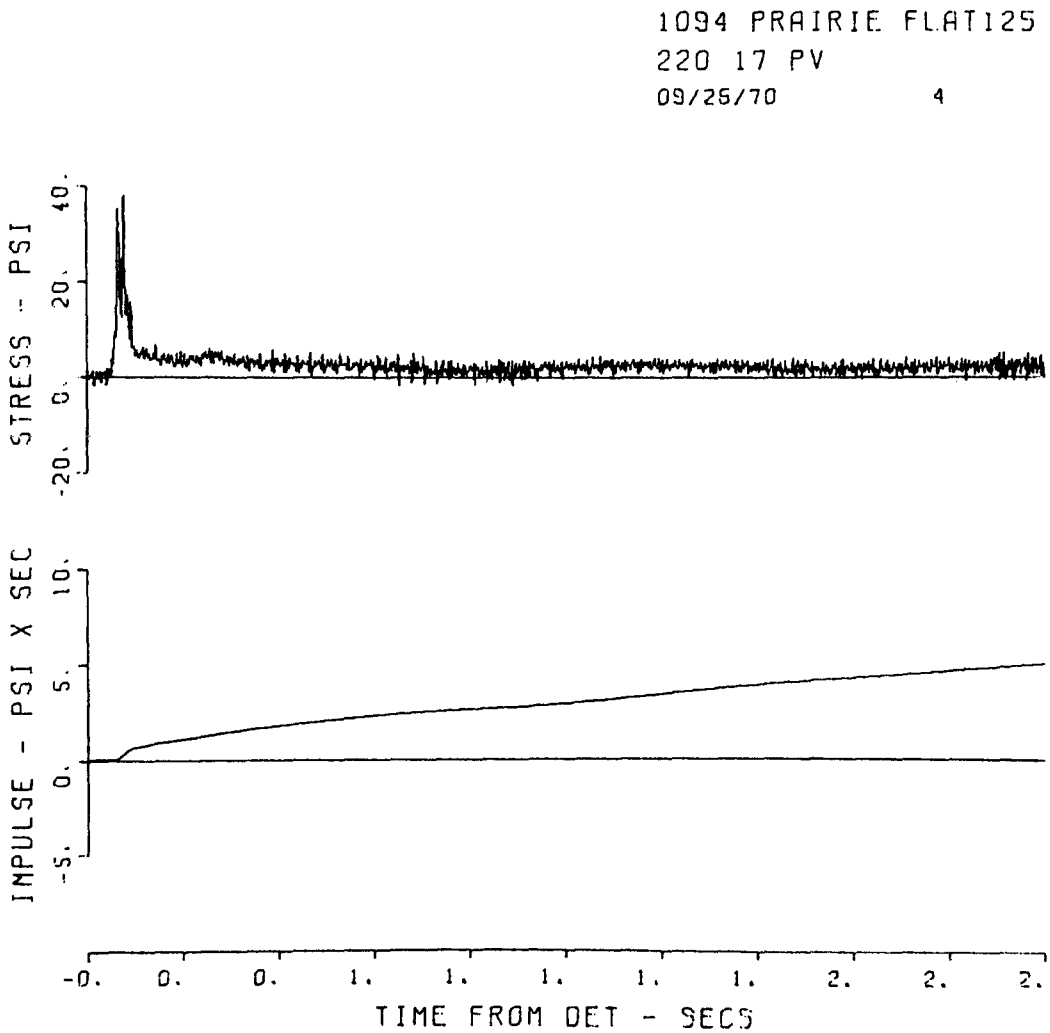

Figure B.28 Gage 1094 PV.

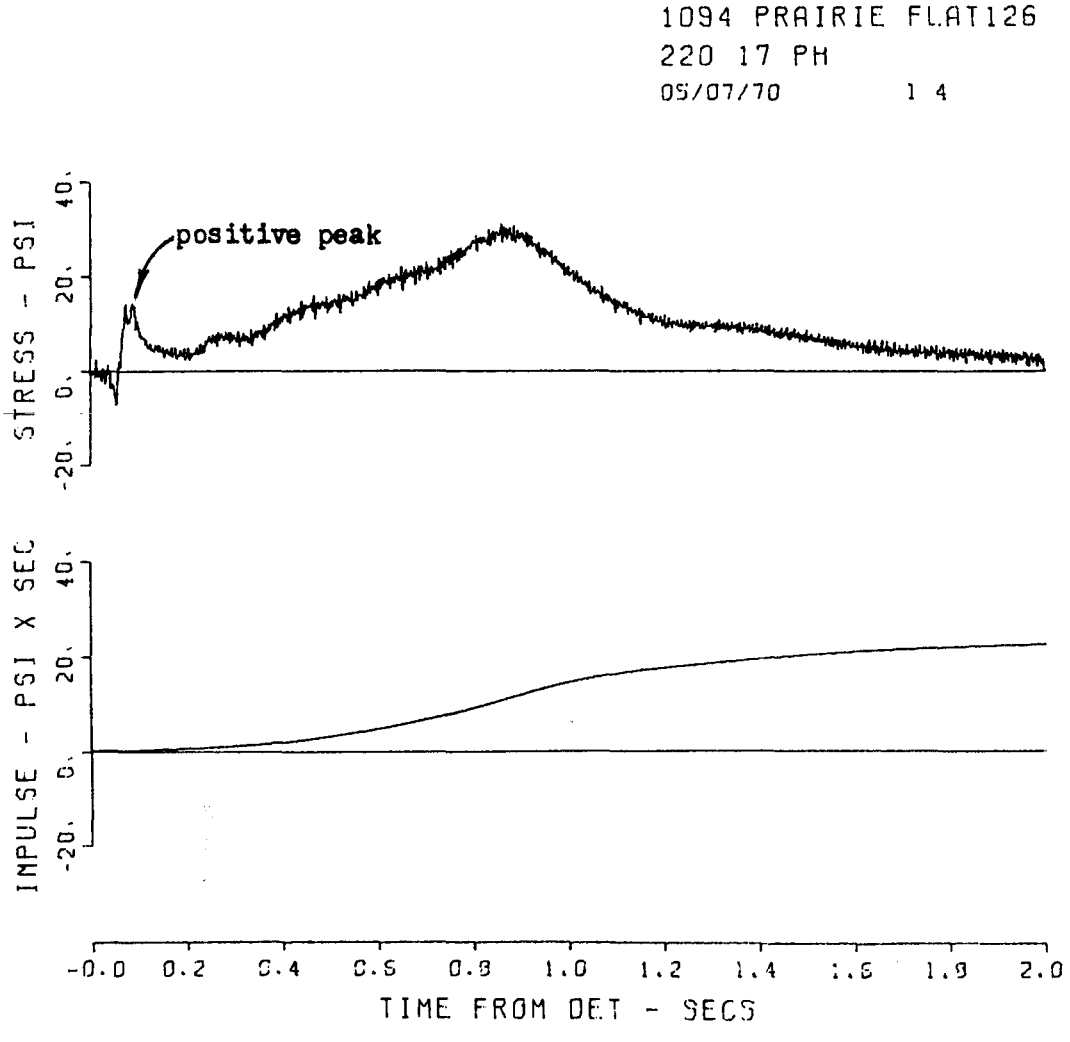

Figure B.29 Gage 1094 PH.

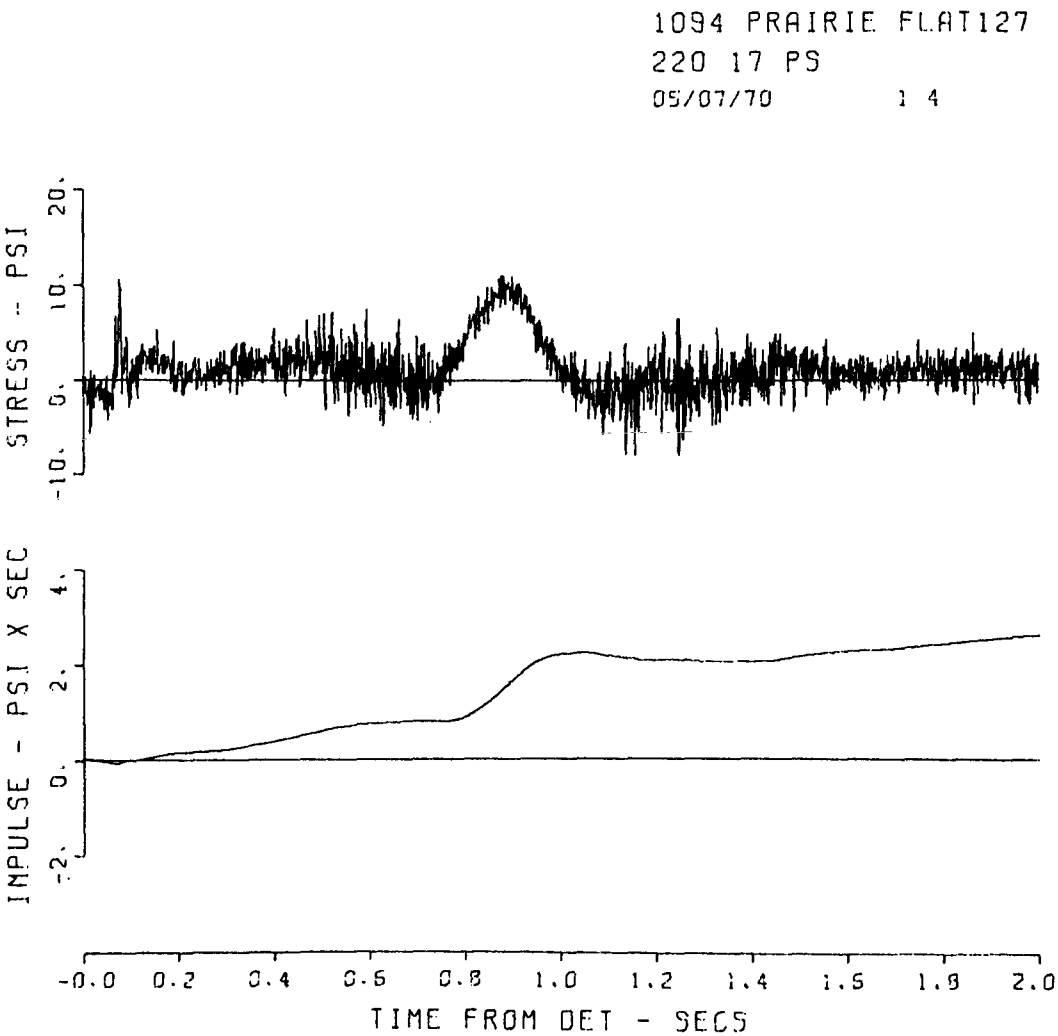

Figure B.30 Gage 1094 PS.

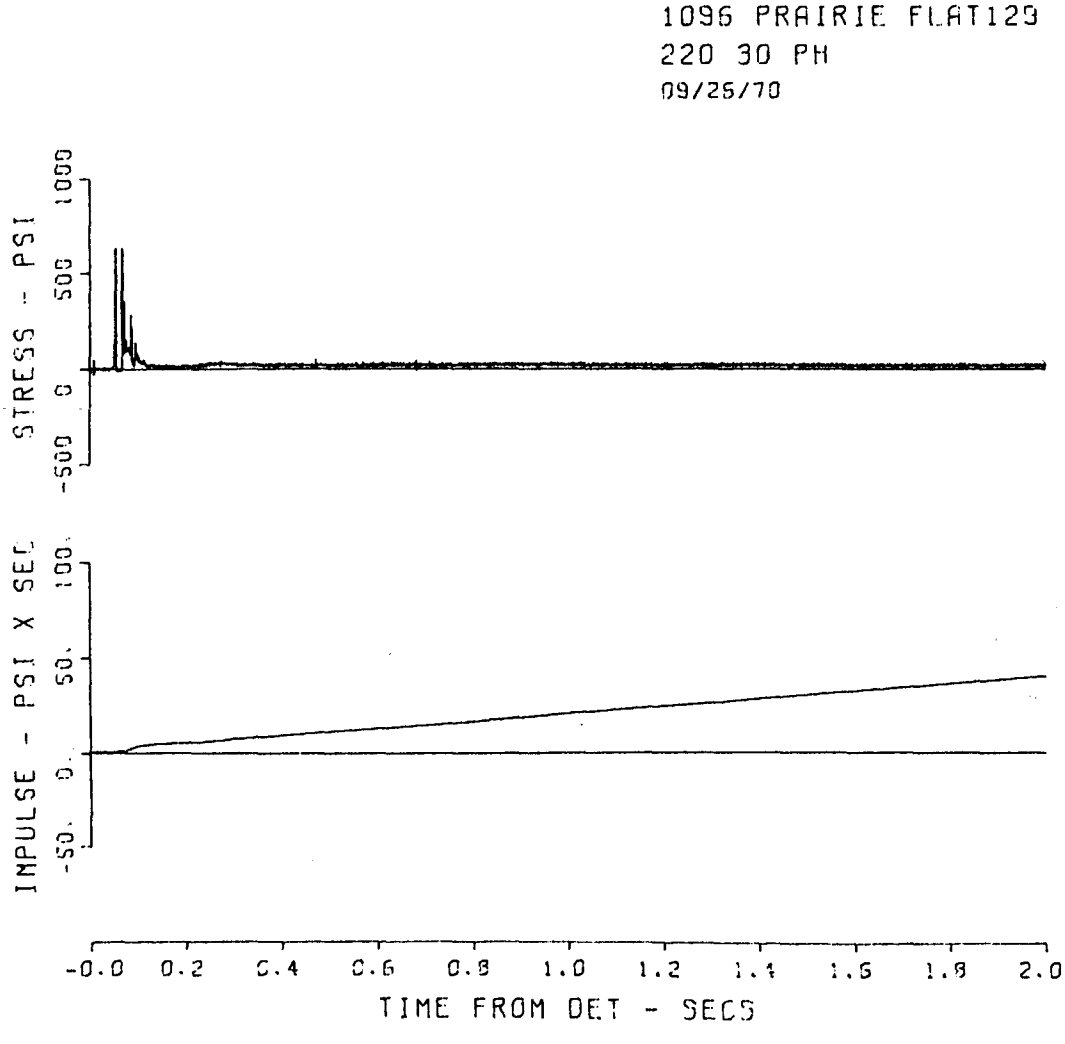

Figure B.31 Gage 1096 PH.

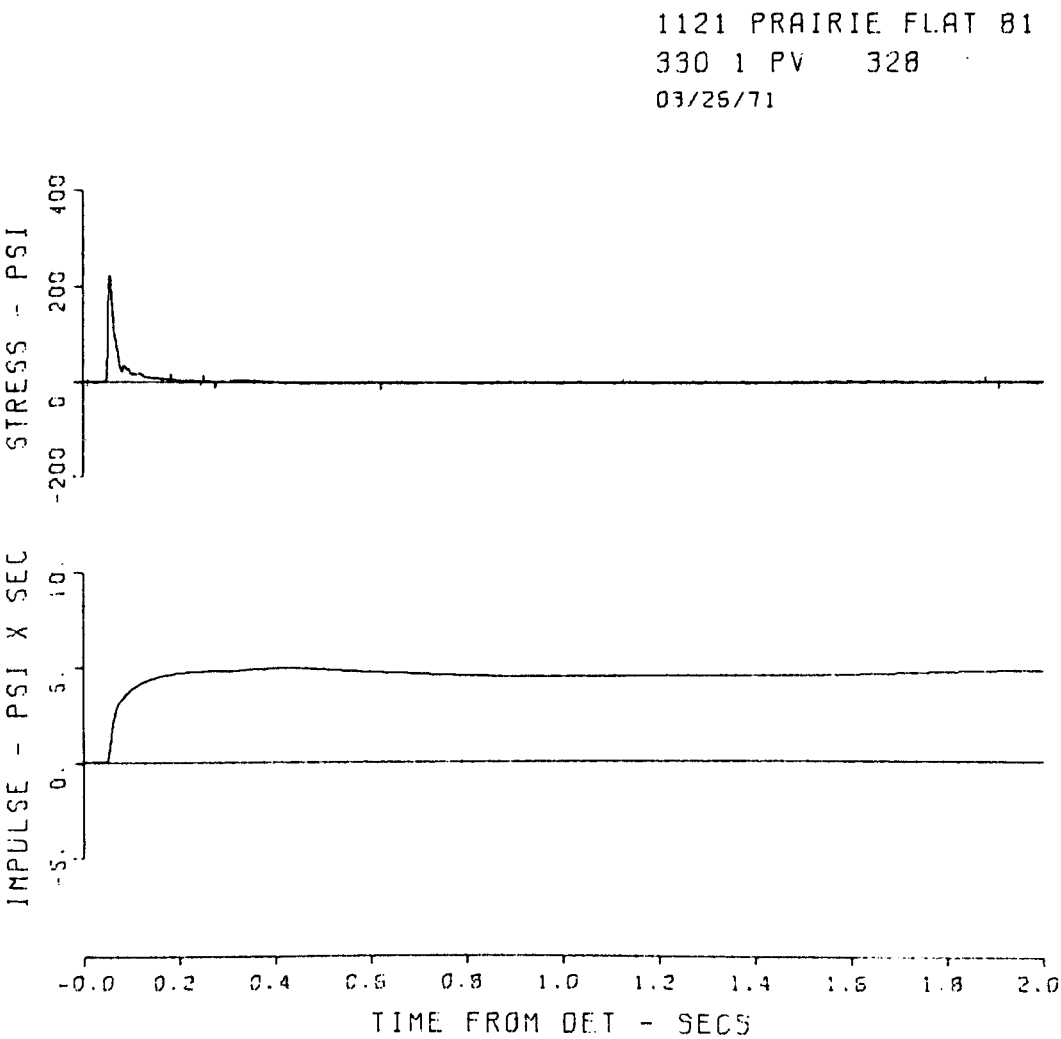

Figure B.32 Gage 1121 PV.

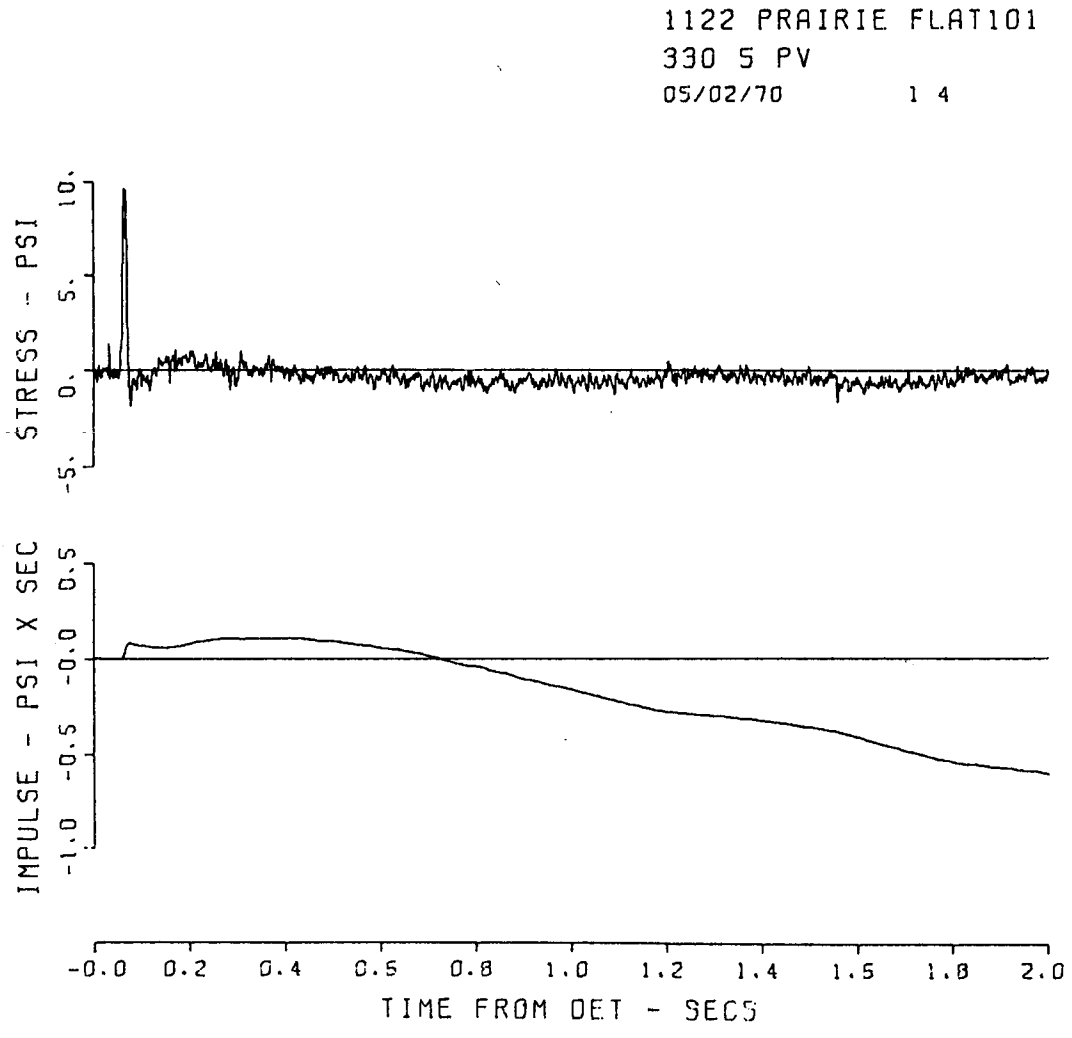

Figure B.33 Gage 1122 PV.

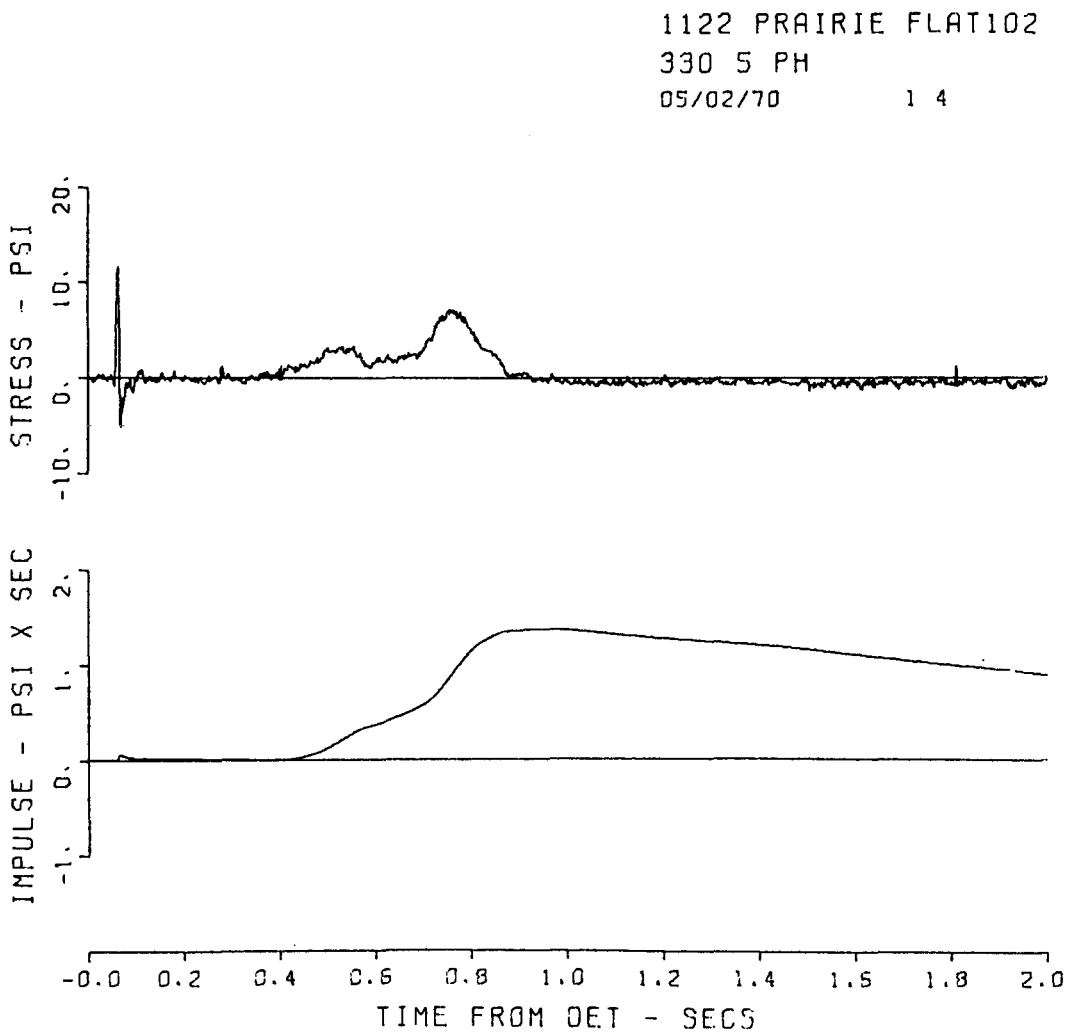

Figure B.34 Gage 1122 PH.

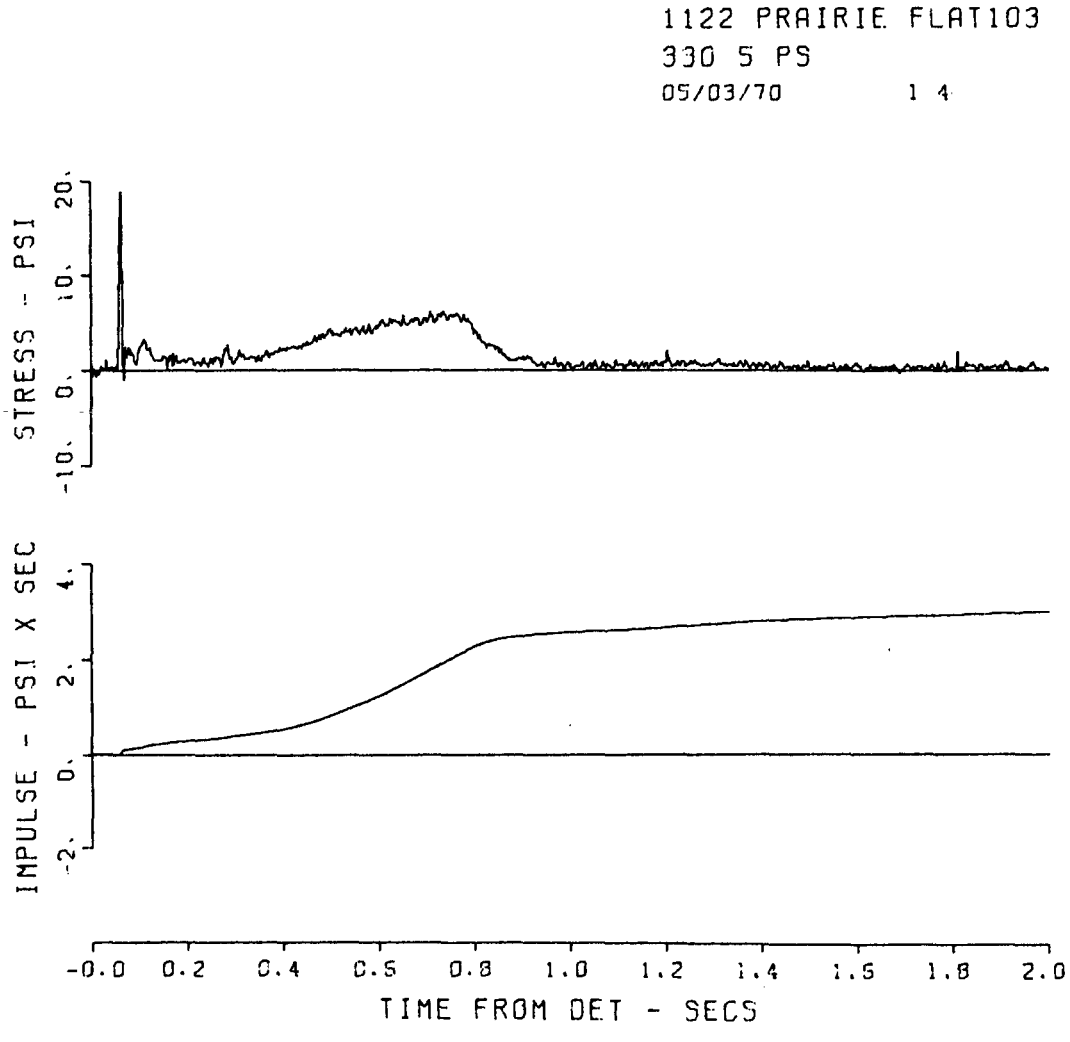

Figure B.35 Gage 1122 PS.

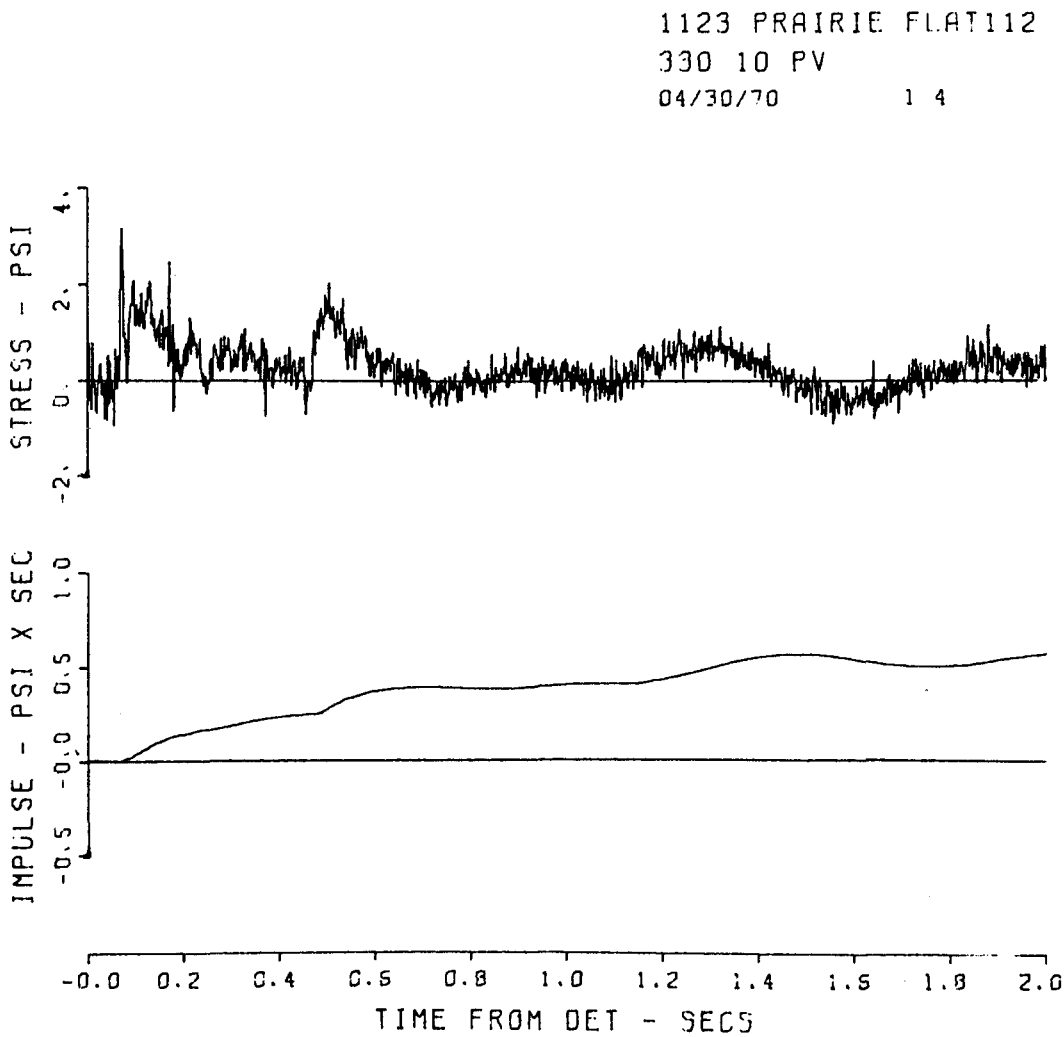

Figure B.36 Gage 1123 PV.

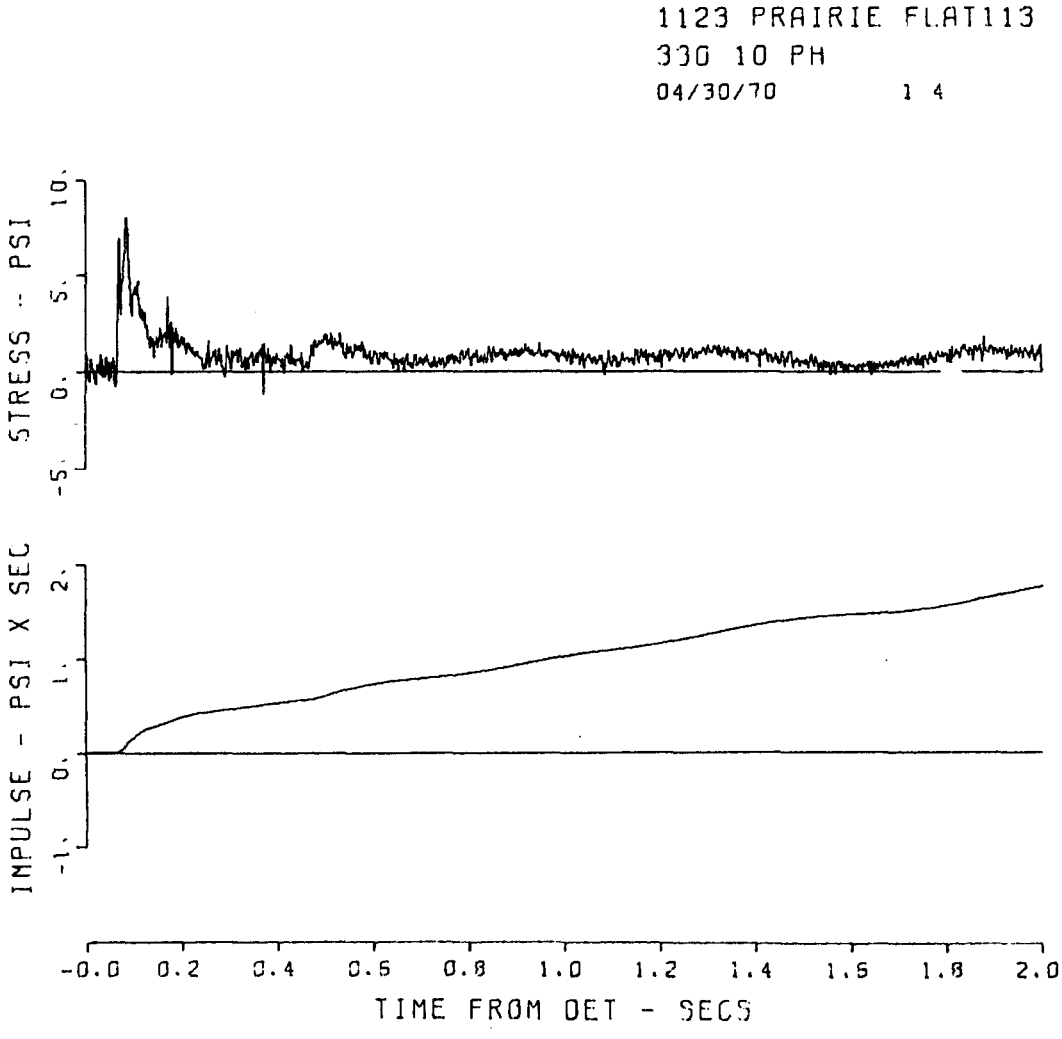

Figure B.37 Gage 1123 PH.

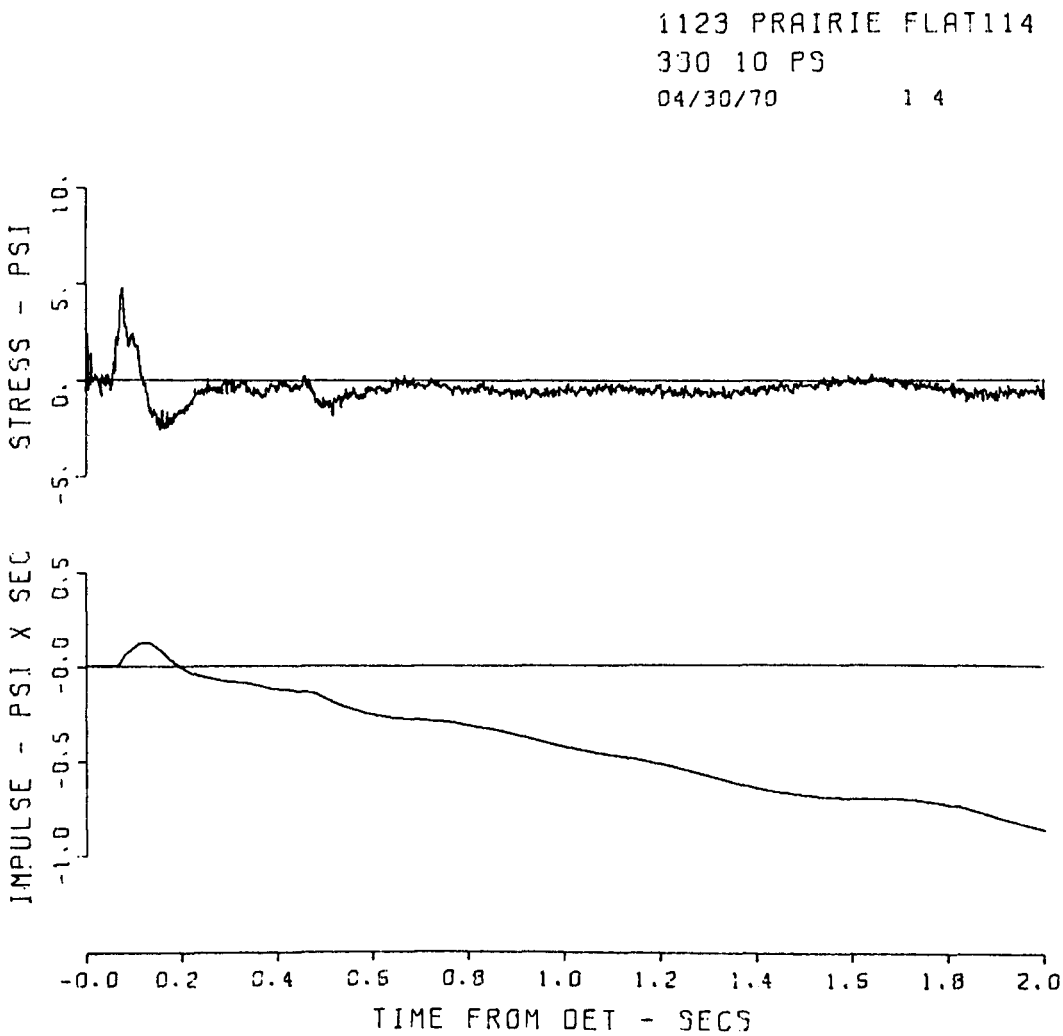

Figure B.38 Gage 1123 PS.

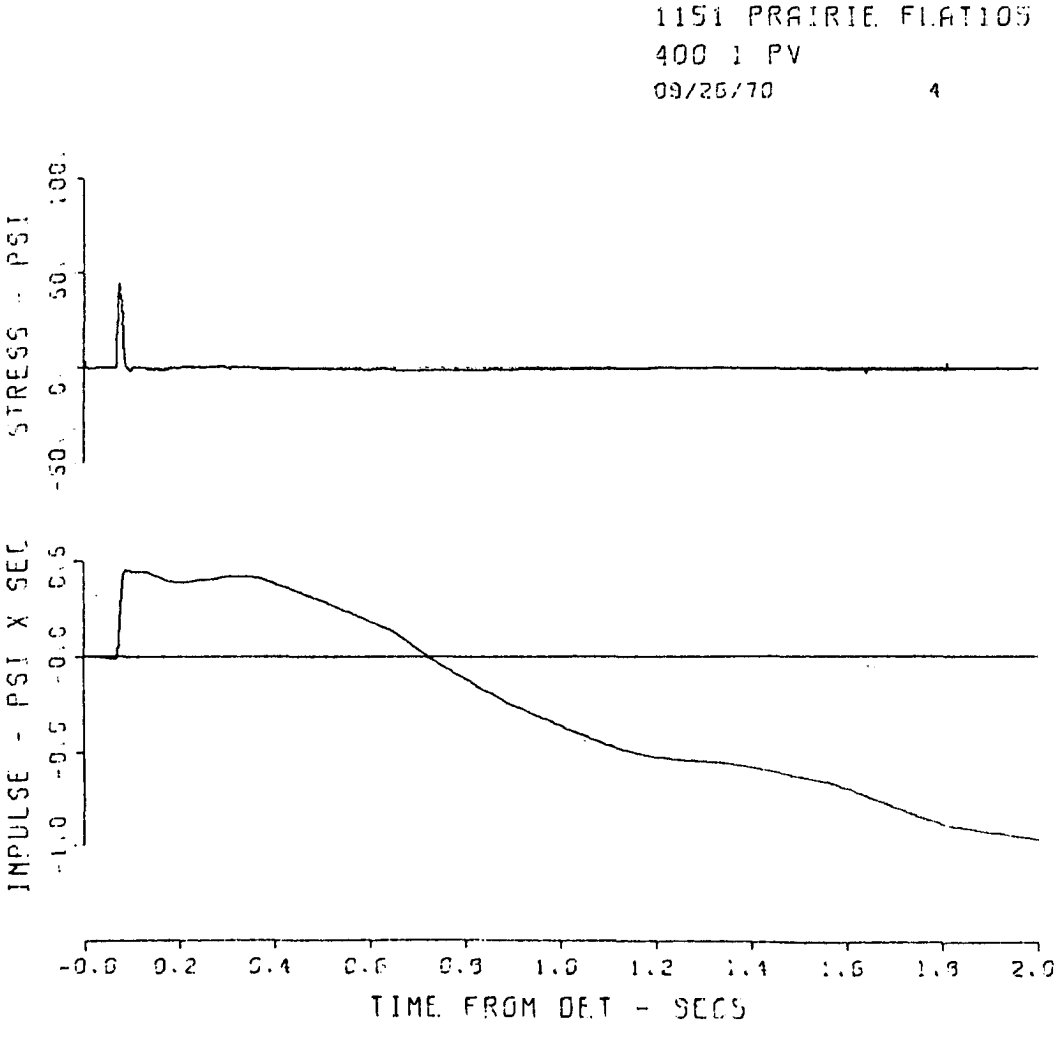

Figure B.39 Gage 1151 PV.

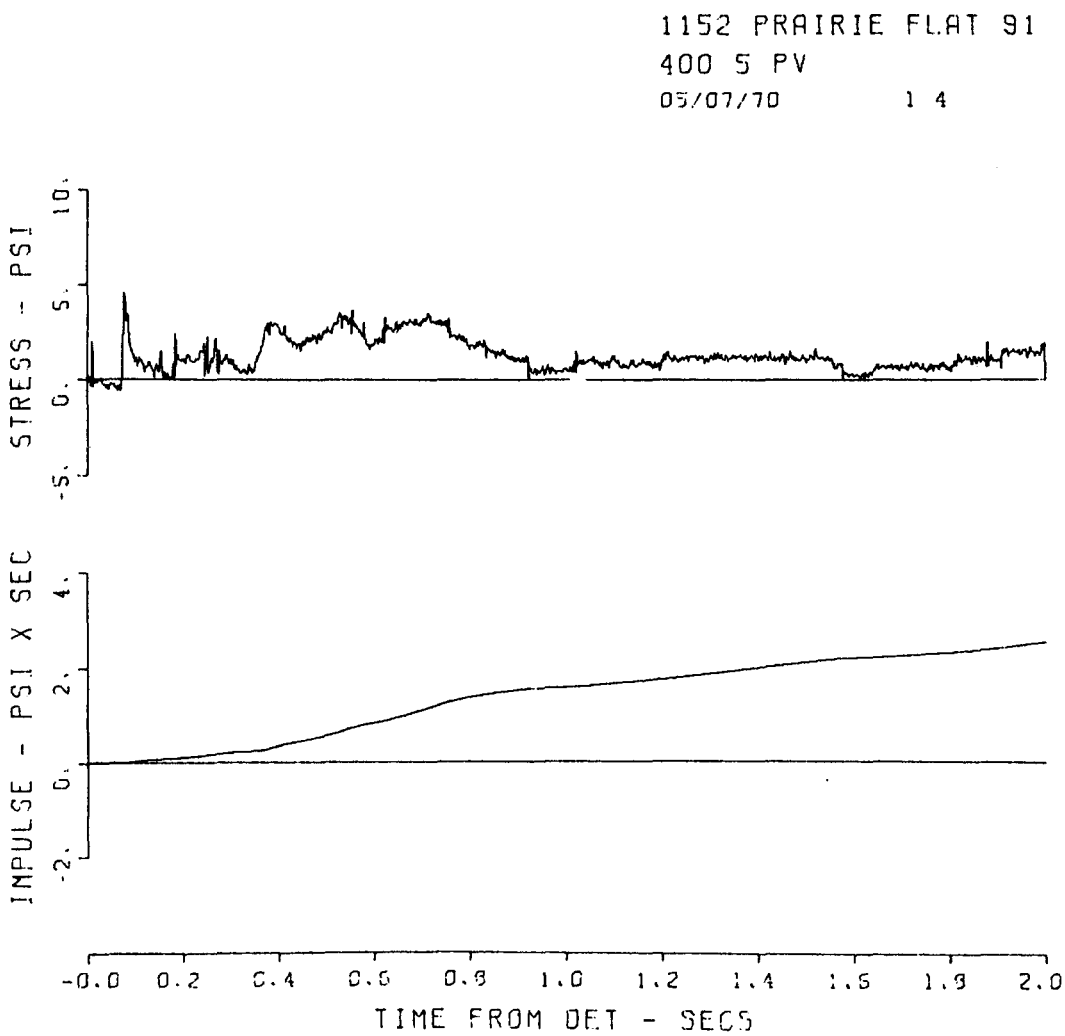

Figure B.40 Gage 1152 PV.

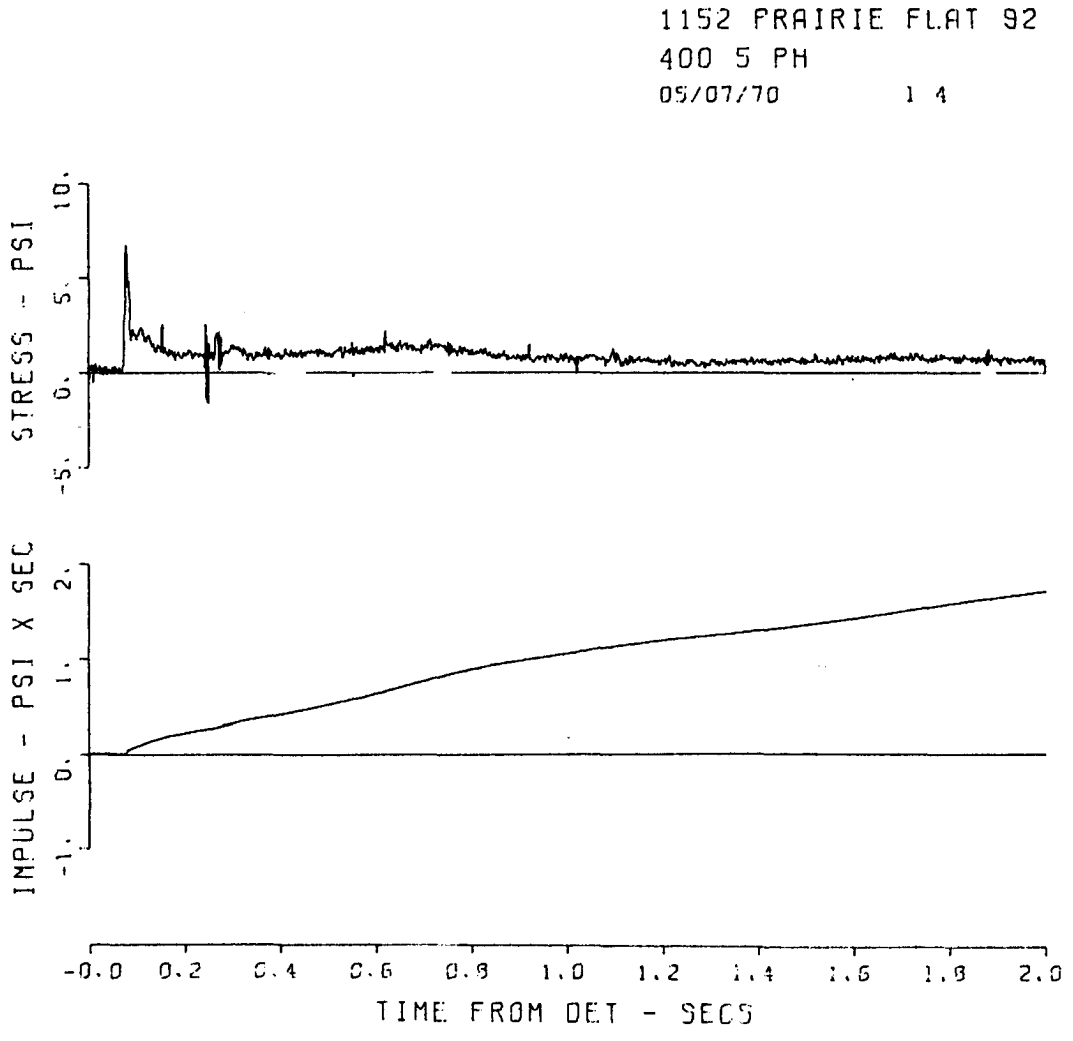

Figure B.41 Gage 1152 PH.

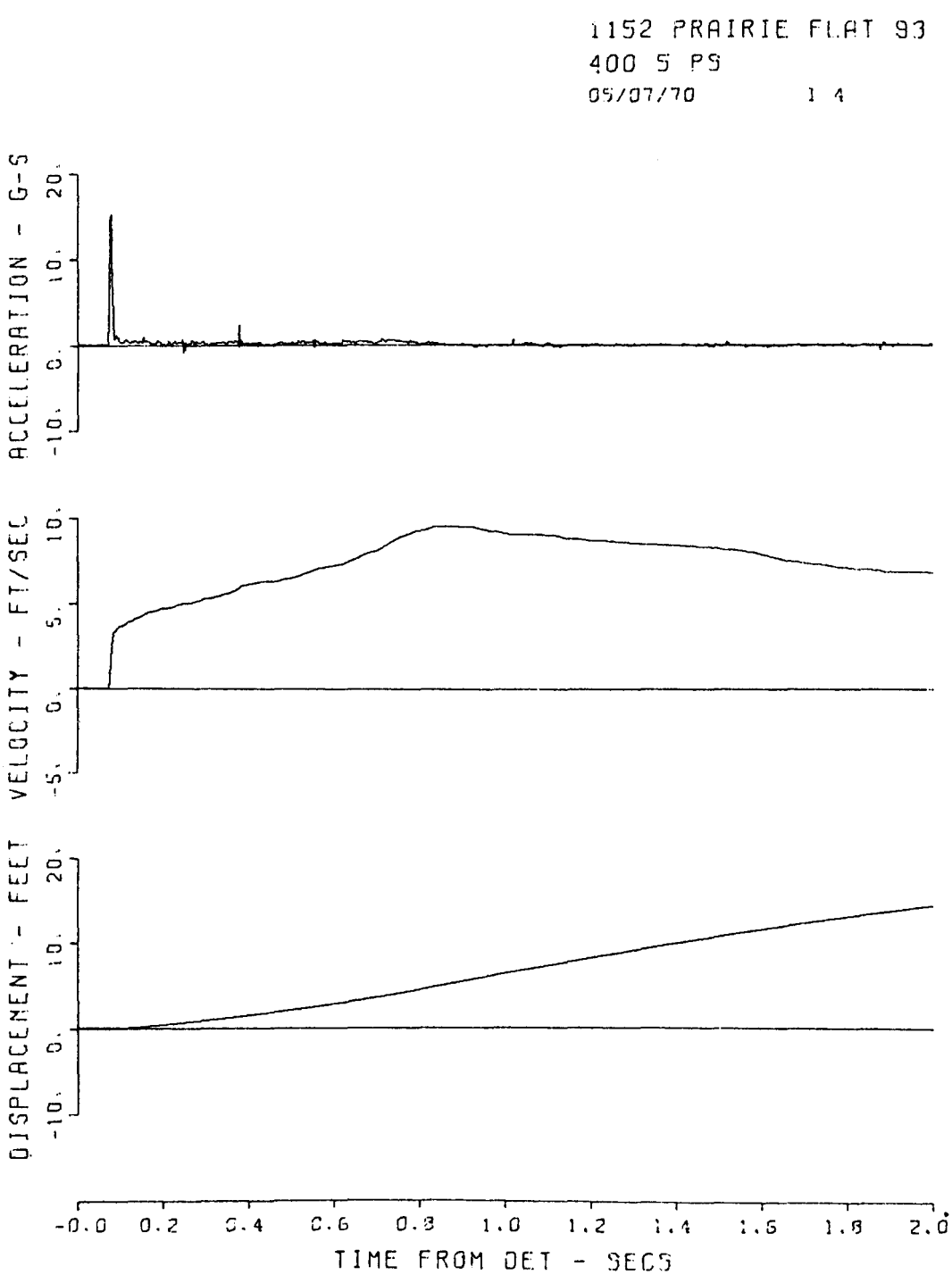

Figure B.42 Gage 1152 PS.

REFERENCES

1. J. H. Keefer, F. M. Sauer, and L. J. Cauthen, Jr.; "Technical and Administrative Information for Operation Prairie Flat"; DASIAC Special Report No. 69, 15 May 1968; DASA Information and Analysis Center, Santa Barbara, California; Unclassified.

2. W. R. Perret and V. L. Gentry; "Operation Upshot-Knothole, Project 1.4, Free-Field Measurements of Earth Stress, Strain, and Ground Motion"; WT-716, February 1955; Atomic Energy Commission, Oak Ridge, Tennessee; Unclassified.

3. A. J. Hendron, Jr.; "Correlation of Operation Snowball Ground Motions with Dynamic Properties of Test Site Soils"; Miscellaneous Paper No. 1-745, October 1965; U. S. Army Engineer Waterways Experiment Station, CE, Vicksburg, Mississippi; Unclassified.

4. J. L. Gatz; "Soil Survey and Support Activities, Operation Distant Plain Event 6"; Miscellaneous Paper No. 3-990, April 1968; U. S. Army Engineer Waterways Experiment Station, CE, Vicksburg, Mississippi; Unclassified.

5. J. G. Jackson, Jr., and J. E. Windham; "Preliminary Report, Operation Distant Plain, Event 6; Soil Property Investigation for Project 3.10, Soil Sampling and Testing"; December 1967; U. S. Army Engineer Waterways Experiment Station, CE, Vicksburg, Mississippi; Unclassified.

6. J. K. Ingram; "Development of a Free-Field Soil Stress Gage for Static and Dynamic Measurements"; Technical Report No. 1-814, February 1968; U. S. Army Engineer Waterways Experiment Station, CE, Vicksburg, Mississippi; Unclassified.

7. D. W. Murrell; "Distant Plain Events 6 and 1A, Project 3.02A, Earth Motion and Stress Measurements"; Technical Report N-70-14, September 1970; U. S. Army Engineer Waterways Experiment Station, CE, Vicksburg, Mississippi; Unclassified.

8. F. M. Sauer; "Operation Prairie Flat Symposium Report"; Vol. I, Part I, DASA 2377-1, DASIAC SR-92, January 1970; DASA Information and Analysis Center, Santa Barbara, California; Unclassified.

9. F. M. Sauer; "Summary Report on Distant Plain Events 6 and 1A Ground Motion Experiments"; DASA 2587, October 1970; Stanford Research Institute, Menlo Park, California; Unclassified.

DISTRIBUTION LIST FOR TECHNICAL REPORT N-72-2

Address	No. of Copies
Department of Defense	
Director, Defense Nuclear Agency, Washington, D. C. 20305	
ATTN: Technical Library (APTL)	2
STSP	1
OAOP	1
OPQR	1
SPLN	16
Commander, Test Command, Defense Nuclear Agency, Kirtland AFB, N. Mex. 87115	
ATTN: Document Control	2
Technical Library	1
FCTG-5	1
FCDV-1	1
Administrator, Defense Documentation Center, Cameron Station, Bldg. 5, Alexandria, Va. 22314	12
ATTN: Document Control	
Defense Intelligency Agency, Washington, D. C. 20301	
ATTN: DI-7B	1
DIA-AP8B-1	1
Assistant to the Secretary of Defense (Atomic Energy), Washington, D. C. 20301	1
ATTN: Class Rec. Library	
Director of Defense Research and Engineering, Washington, D. C. 20301	
ATTN: Asst. Director (Strategic Weapons)	1
Asst. Director (Nuclear Programs)	1
Director, Weapons Systems Evaluation Group, Washington, D. C. 20305	1
ATTN: Document Control	
Joint Strategic Target Planning Staff, Offutt AFB, Nebr. 68113	1
Commandant, Industrial College of The Armed Forces, Ft. McNair, Washington, D. C. 20315	1
ATTN: Document Control	

Address	No. of Copies
Department of Defense (Continued)	
Commandant, National War College, Fort Lesley J. McNair, Washington, D. C. 20315 ATTN: Class Rec. Library	1
Director of Defense Research and Engineering, Washington, D. C. 20301 ATTN: Asst. Director, Nuclear Programs	1
Chief, Livermore Division, Field Command DNA, Lawrence Radiation Laboratory, P. O. Box 808, Livermore, California 94550 ATTN: FCDV-3	1
Director, Defense Communications Agency, Washington, D. C. 20305 ATTN: NMCSSC	1
Department of the Army	
Chief of Engineers, Department of the Army, Washington, D. C. 20314	
ATTN: ENGMC-E	1
Director of Military Construction	1
Chief of Research and Development, Department of the Army, Washington, D. C. 30410 ATTN: Nuclear, Chemical-Biological Division	1
Commanding General, U. S. Army Engineer Center, Ft. Belvoir, Va. 22060 ATTN: Asst. Commandant Engineer School	1
Commanding Officer, U. S. Army Combat Developments Command, Institute of Nuclear Studies, Ft. Bliss, Tex. 79916 ATTN: Document Control	1
U. S. Army Engineer Waterways Experiment Station Explosive Excavation Research Office, Livermore California 94550 ATTN: Document Control	1
Division Engineer, U. S. Army Engineer Division, Ohio River, P. O. Box 1159, Cincinnati, Ohio 45201 ATTN: Document Control	1

Address	No. of Copies
Department of the Army (Continued)	
Division Engineer, U. S. Army Engineer Division, Huntsville, Box 1600, West Station, Huntsville, Ala. 35807	
ATTN: Mr. H. L. Solomonson	1
Mr. M. M. Dembo (HNDSE)	2
District Engineer, U. S. Army Engineer District, Omaha, 215 N. 17th Street, Omaha, Nebr. 68101	1
ATTN: Office of Administrative Services (MRD Library)	
Commanding General, Army Materiel Command, Bldg. T-7, Gravelly Point, Washington, D. C. 20315	2
ATTN: AMCPM-SM-EA (Mr. Powers)	
Commanding General, Army Test and Evaluation Command, Aberdeen Proving Ground, Maryland 21005	1
ATTN: Mr. B. Sisson	
Commanding Officer, Army Ballistic Research Laboratory, Aberdeen Proving Ground, Maryland 21005	12
ATTN: AMXBR-TB (J. H. Keefer)	
Commanding Officer, Army Terrestrial Sciences Center, P. O. Box 282, Hanover, New Hampshire 03755	1
ATTN: T. C. Vogel	
Commanding General, White Sands Missile Range, N. Mex. 88002	1
ATTN: Nuclear Effects Laboratory (Mr. Squires)	
Commandant, Army Command and General Staff College, Ft. Leavenworth, Kansas 66027	1
ATTN: Acquisitions, Library Division	
Director of Civil Defense, Department of the Army, Washington, D. C. 20310	1
ATTN: Mr. George Sisson	
Department of the Navy	
Chief of Naval Operations, Navy Department, Washington, D. C. 20350	
ATTN: OP-03EG	1
OP-75	1
Chief of Naval Research, Navy Department, Washington, D.C. 20390	1
ATTN: Code 418	

Address	No. of Copies
Department of the Navy (Continued)	
Commander, Naval Facilities Engineering Command, Headquarters, Washington, D. C. 20370	
ATTN: Code 04	1
Code 03	1
Director, Strategic Systems Projects Office, Navy Department, Washington, D. C. 20360	1
ATTN: NSP-272	
Commander, U. S. Naval Ordnance Laboratory, Silver Spring, Md. 20910	
ATTN: 241	1
243	1
240	1
Superintendent, U. S. Naval Postgraduate School, Monterey, Calif. 93940	1
ATTN: Technical Library	
Commanding Officer, U. S. Naval Civil Engineer Corps Officer School, U. S. Naval Construction Battalion Center, Port Hueneme, Calif. 93041	1
ATTN: Document Control	
Commanding Officer, Naval Applied Science Laboratory, Flushing and Washington Avenues, Brooklyn, N. Y. 11251	1
ATTN: W. L. Derksen	
Commanding Officer, Naval Civil Engineering Laboratory, Port Hueneme, Calif. 93041	10
ATTN: Code L51 (Dr. Shaw)	
Commander, Naval Ship Engineering Center, Center Building, Prince Georges Center, Hyattsville, Md. 20782	
ATTN: Code 6115, Y. Park	1
Code 6105	1
Commanding Officer and Director, Naval Ship Research and Development CTR, Washington, D. C. 2007	6
ATTN: Code 741 (E. T. Habib)	
Commander, Naval Weapons Center, China Lake, Calif. 93555	
ATTN: Code 3022	2

Address	No. of Copies
Department of the Air Force	
Headquarters, USAF, Washington, D. C. 20330	
ATTN: AFNINDE (Dissemination Req. Res. Br.)	1
AFOCE (Dir. of Civil Eng.)	1
AFRDQSN (Strat. and Def. Forces, Nuc Ord. Div)	1
AFRDDF (Missile Sys. Div., Dir. of Dev.)	1
Headquarters, Air Force Systems Command, Andrews AFB, Washington, D. C. 20331	
ATTN: SCS-7 (COL W. P. Wood)	1
DEE	1
Commander, Strategic Air Command, Offutt AFB, Nebr. 68113	
ATTN: OAI (Stinfo Section)	1
DPLBIC (LTC J. B. Tye)	1
AFSC STLO (SCTL-10), Air Force UPO, Los Angeles, Calif. 90045	
ATTN: RTSAL	1
Air Force Weapons Laboratory, Kirtland AFB, N. Mex. 87117	
ATTN: WLIL, Technical Library	1
WLDC (Dr. H. Cooper)	1
WLPM	1
Aerospace Defense Command, Ent AFB, Colo. 80912	
ATTN: ADLDC (DCS OF Plans)	1
ADLMD-W (Missile and Space Weapons Div.)	1
Space and Missile Systems Organization, Norton AFB, Calif. 92409	
ATTN: SMQHF	2
SMQN (MINUTEMAN Engineering Div.)	2
SMTSM-1	2
SMY	2
SMNP	2
SAFSP-6	2
Air Force Institute of Technology, AU, Wright-Patterson AFB, Ohio 45433	1
ATTN: Technical Library	

Address	No. of Copies

Department of the Air Force (Continued)

Air Force Special Weapons Center, AFSC, Kirtland AFB, New Mexico 87117 ATTN: STWU Tech. Operations	1
65715T Aeromedical Research Laboratory, AFSC, Holloman AFB, New Mexico 88330 ATTN: Capt. Klopfenstein	1
Rome Air Development Center, AFSC, Griffis AFB, N. Y. 13440 ATTN: Documents Library EMLAL-1	1
Rome Air Development Center, AFSC, Griffis AFB, N. Y. 13440 ATTN: EMEAM, R. Mair	2

Atomic Energy Commission

Sandia Corporation, P. O. Box 5800, Kirtland AFB, N. Mex. 87115 ATTN: Document Control for: Dr. M. L. Merritt (Org. No.9150) Mr. W. R. Perrett Library	 2 2 1
Atomic Energy Commission, Washington, D. C. 20545 ATTN: Division of Peaceful Nuclear Explosions	1
University of California, Lawrence Radiation Laboratory, Technical Information Div., P. O. Box 808, Livermore, California 94550 ATTN: Document Control for Technical Library	1
Los Alamos Scientific Laboratory, P. O. Box 1663, Los Alamos, N. Mex. 87544 ATTN: Document Control for LASL Library, Serials Librarian	1

Other Government Agencies

Bureau of Mines, Bldg. 20, Denver Federal Center, Denver, Colo. 80225 ATTN: Dr. L. A. Obert, Science Advisor, Mining Research	1
U. S. Geological Survey, Branch of Astrogeology (Dr. Roddy) 601 East Cedar Street, Flagstaff, Arizona 86001	1
National Aeronautics and Space Admin., Langley Research Center, Langley Station, Hampton, Virginia 23365 ATTN: Mr. H. Pierce	1

Address	No. of Copies
Civilian Contractors	
Aerospace Corporation, P. O. Box 95085, Los Angeles, Calif. 90045 ATTN: Technical Information Services	2
Aerospace Corporation, 1111 East Mill St., P. O. Box 1308, San Bernardino, Calif. 92408 ATTN: Dr. M. B. Watson Mr. W. Pfefferle Mr. Craig Smith	 1 1 1
Agbabian-Jacobsen Associates, 8939 South Sepulveda Blvd., Los Angeles, Calif. 90045 ATTN: Document Control	1
Analytic Services, Inc., 5613 Leesburg Pike, Falls Church, Va. 22041 ATTN: George Hesselbacher	1
Applied Theory, Inc., 1728 Olympic Blvd., Santa Monica, Calif. 90404 ATTN: Security Officer	1
Battelle Memorial Institute, 505 King Avenue, Columbus, Ohio 43201 ATTN: Mr. R. W. Klingesmith	1
Edgerton, Germeshausen & Grier, Inc., P. O. Box 227, Bedford, Mass. 01730 ATTN: Mr. D. F. Hansen, Document Control Center	1
Engineering Physics Company, 12721 Twinbrook Parkway, Rockville, Md. 28052 ATTN: Dr. Vincent J. Cushing	1
Environmental Research Corporation, 813 N. Royal Street, Alexandria, Va. 22314 ATTN: Mr. O. A. Israelson	1
General American Research Division, General American Transportation Corp., 7449 N. Natchez Ave., Niles, Ill. 60648 ATTN: Dr. G. L. Neidhardt	1
General Electric Company, TEMPO, 816 State Street, Santa Barbara, Calif. 93101 ATTN: Mr. W. Chan, DASA Information and Analysis Center	2

Address	No. of Copies
Civilian Contractors (Continued)	
General Motors Corporation, Manufacturing Development, Technical Center, Warren, Mich. 48090	
ATTN: Mr. W. Isbell	1
Dr. C. Maiden	1
General Research Corporation, P. O. Box 3587, Santa Barbara, Calif. 93105	1
ATTN: Dr. Benjamin Alexander	
General Research Corporation, 1501 Wilson Blvd., Arlington, Va. 22209	1
ATTN: Dr. W. Layson	
Gulf General Atomic, Inc., P. O. Box 1111, San Diego, Calif. 92112	1
ATTN: H. Dratz, Chief, Tech. Information Services	
IIT Research Institute, 10 West 35th Street, Chicago, Ill. 60616	
ATTN: Technical Library	1
Dr. E. Sevin	1
Institute for Defense Analyses, 400 Army-Navy Drive, Arlington, Va. 22202	2
ATTN: Technical Information Office	
Kaman Sciences Corp., Kaman Nuclear Division, Garden of the Gods Road, Colorado Springs, Colo. 80907	1
ATTN: Mr. Paul Ellis	
University of Illinois, Department of Civil Engineering, 1114 Civil Engineering Bldg., Urbana, Ill. 61801	
ATTN: Dr. Nathan M. Newmark	1
Prof. D. V. Deere	1
Prof. A. J. Hendron, Jr.	1
Physics International Company, 2700 Merced street, San Leandro, Calif. 94577	
ATTN: Dr. Charles Godfrey	1
Mr. F. M. Sauer	1

Address	No. of Copies
Civilian Contractors (Continued)	
The Rand Corporation, 1700 Main Street, Santa Monica, Calif. 90406	
ATTN: Library	1
Dr. A. L. Latter	1
Mr. W. B. Wright	1
Dr. Olen A. Nance	1
Dr. C. C. Mow	1
Research Analysis Corporation, McLean, Va. 22101	1
ATTN: Document Control Supervisor	
Systems, Science and Software, Inc., P. O. Box 1620, La Jolla, Calif. 92037	1
ATTN: Document Control	
URS Corporation, 1811 Trousdale Drive, Burlingame, Calif. 94010	
ATTN: Mr. Harold Mason	1
Mr. P. J. Morris	1
Paul Weidlinger, Consulting Engineer, 110 E. 59th St., New York, N. Y. 10022	1
ATTN: Dr. M. Baron	
Defence Research Establishment, Suffield, Ralston, Ralston, Alberta, Canada	
ATTN: Mr. J. S. Watson	1
Mr. R. Wyld	1
University of Denver, Denver Research Institute, University Park, Denver, Colo. 80210	1
ATTN: Mr. John Wisotski	
Eric H. Wang Civil Engineering Research Facility, P. O. Box 188, University Station, University of N. Mex. 87106	1
Mason and Hanger, Silas Mason Company, Inc., AEC Pantex Plant, Amarillo, Texas 79105	1
ATTN: Document Control for I. Akst	
Bell Telephone Labs., Inc., Whippany Road, Whippany, New Jersey 07981	
ATTN: W. Butler	1
G. Nevrincean	1
E. F. Witt	1

Address	No. of Copies

Civilian Contractors (Continued)

The Boeing Company, P. O. Box 3996, Seattle, Wash. 98124 ATTN: Glen Jones (Mail Stop BC-78)	3
Lovelace Foundation for Medical Education and Research, 5200 Gibson Blvd., S.E., Albuquerque, N. Mex. 87108 ATTN: Dr. Clayton White	1
Philco-Ford Corporation, Aeronutronics Division, 1001 E. Ball Road, Anaheim, California 92805 ATTN: A. Green, S. C. Bldg.	2
Shock Hydrodynamics, Inc., 15010 Ventura Blvd., Sherman Oaks, Calif. 91403 ATTN: Mr. Kreyenhagen	1
Stanford Research Institute, 333 Ravenswood Ave., Menlo Park, Calif. 94025	
ATTN: Dr. D. Grine	1
GO 37 External Reports	1
TRW Systems Group, San Bernardino Operations, P. O. Box 1310, 600 E. Mill St., San Bernardino, Calif. 92402 ATTN: F. Pieper	1
TRW Systems Group, One Space Park, Redondo Beach, Calif. 90278 ATTN: J. Carpenter	1
Lockheed Missiles and Space Co., A Division of Lockheed Aircraft Corp., P.O. Box 504, Sunnyvale, Calif. 94088 ATTN: Dr. R. Mayerutt, Palo Alto	1
Dr. Harold Brode, R&D Associates, P. O. Box 3580, Santa Monica, Calif. 90403	1

Unclassified

Security Classification

DOCUMENT CONTROL DATA - R & D

(Security classification of title, body of abstract and indexing annotation must be entered when the overall report is classified)

1. ORIGINATING ACTIVITY (Corporate author)	2a. REPORT SECURITY CLASSIFICATION
U. S. Army Engineer Waterways Experiment Station Vicksburg, Mississippi	Unclassified
	2b. GROUP

3. REPORT TITLE

OPERATION PRAIRIE FLAT; PROJECT LN 302: EARTH MOTION AND STRESS MEASUREMENTS

4. DESCRIPTIVE NOTES (Type of report and inclusive dates)

Final report

5. AUTHOR(S) (First name, middle initial, last name)

Donald W. Murrell

6. REPORT DATE	7a. TOTAL NO. OF PAGES	7b. NO. OF REFS
February 1972	180	9

8a. CONTRACT OR GRANT NO.	9a. ORIGINATOR'S REPORT NUMBER(S)
b. PROJECT NO.	Technical Report N-72-2
c.	9b. OTHER REPORT NO(S) (Any other numbers that may be assigned this report)
d.	

10. DISTRIBUTION STATEMENT

Approved for public release; distribution unlimited.

11. SUPPLEMENTARY NOTES	12. SPONSORING MILITARY ACTIVITY
	Defense Nuclear Agency Washington, D. C.

13. ABSTRACT The objectives of this study were to measure and interpret the earth motions and stresses produced by the Prairie Flat 500-ton TNT detonation. Acceleration, particle velocity, and soil stress gages were installed to measure the ground motions and stresses encompassed by the 2,000- to 10-psi predicted airblast overpressure region (84 to 1,150 feet from ground zero) and depths below the ground surface of 1.5 to 30 feet. Time histories of all successful measurements are included in Appendixes A and B. Ground shock arrival times indicated the occurrence of outrunning ground motion at a distance of about 560 feet, or the 35-psi pressure level. Peak vertical particle accelerations varied from 1,200 to 1.9 g's at the extremes of the instrumented region, attenuating sharply with both distance and depth. Peak acceleration to peak overpressure ratios, used as a basis for correlation, were observed to be both pressure and yield dependent, increasing with lower pressures and higher yields. Vertical particle velocities varied from 84 to 0.33 ft/sec over the area instrumented, also attenuating rapidly with distance and depth. Vertical velocities were also correlated on the basis of velocity to pressure ratios, and the ratios were again observed to be pressure and yield dependent. Peak horizontal velocities were found to vary from about 20 to 0.3 ft/sec over the same region, with little or no attenuation with depth. These velocities were compared with those obtained on Distant Plain Event 6 by means of cube-root scaling, and excellent comparability was noted. Both horizontal and vertical displacements were calculated from measured accelerations and velocities. Peak transient displacements were 20 feet upward and 20 feet outward at the 84-foot range and 1.5-foot depth. The upward displacement attenuated more rapidly with distance, so that at 400 feet it was only one-half of the outward displacement. Soil stress measurements were generally of poor quality from a signal-to-noise standpoint. Data at the 1.5- and 30-foot depths, where good measurements resulted, were exceptions. Vertical stresses at the 1.5-foot depth averaged 40 percent of the surface overpressure.

DD FORM 1 NOV 68 1473 REPLACES DD FORM 1473, 1 JAN 64, WHICH IS OBSOLETE FOR ARMY USE.

Unclassified

Security Classification

14. KEY WORDS	LINK A		LINK B		LINK C	
	ROLE	WT	ROLE	WT	ROLE	WT
Airblast waves						
Explosion effects						
Ground motion						
Prairie Flat (Operation)						
Stress measurement						